Design and Synthesis of Fluorescent Probes for Selective Detection of Thiols

A thesis

Submitted in partial fulfillment of the requirements

of the degree of

Doctor of Philosophy

By

Dnyaneshwar S. Kand

ID: 20093036

INDIAN INSTITUTE OF SCIENCE EDUCATION AND RESEARCH, PUNE

2014

This Thesis is dedicated to...

My Parents

And

My beloved family

For Their Constant Support,

Unconditional Love and Care.

भारतीय विज्ञान शिक्षा एवं अनुसंधान संस्थान, पुणे
INDIAN INSTITUTE OF SCIENCE EDUCATION AND RESEARCH (IISER), PUNE
(An Autonomous Institution, Ministry of Human Resource Development, Govt. of India)
900 NCL Innovation Park, Dr. Homi Bhabha Road, Pune 411008

Dr. Pinaki Talukdar
Assistant Professor
Department of Chemistry,
IISER Pune

CERTIFICATE

Certified that the work incorporated in the thesis entitled "***Design and Synthesis of Fluorescent probes for Selective Detection of Thiols"*** submitted by **Mr. Dnyaneshwar S. Kand** was carried out by the candidate, under my supervision. The work presented here or any part of it has not been included in any other thesis submitted previously for the award of any degree or diploma from any other university or institution.

Date: 8th July 2014, Pune

Dr. Pinaki Talukdar
(Research Supervisor)

Email: ptalukdar@iiserpune.ac.in • Ph: +91-20-25908098 • Fax: +91-20-25908186

DECLARATION

I declare that, this written submission represents my ideas in my own words and where others' ideas have been included; I have adequately cited and referenced the original sources. I also declare that I have adhered to all principles of academic honesty and integrity and have not misrepresented or fabricated or falsified any idea / data / fact/ source in my submission. I understand that violation of the above will be cause for disciplinary action by the Institute and can also evoke penal action from the sources which have thus not been properly cited or from whom proper permission has not been taken when needed.

Date: 8th July 2014, Pune

Mr. Dnyaneshwar S. Kand

ID: 20093036

Acknowledgements

First and foremost, I would like to express my deepest and sincerest gratitude to my advisor Dr. Pinaki Talukdar (PT), who cordially accepted me into his research group and trusted in my intellectual capacity. I would like to thank him for leading me towards the most beautiful scientific truth with his guidance, time and encouragement. It is my great fortune to work in his group, and explore the most attractive field in chemistry under his guidance. I believe this experience will be unforgettable for my whole life.

I sincerely thank Director, Prof. K. N. Ganesh for giving me an opportunity to work in well equipped labs and state of art research facility provided by the IISER-Pune.

I am also very grateful to my committee members, Dr. Gangadhar J. Sanjayan and Dr. Harinath Chakrapani, for agreeing to serve on my advisory committee and for influencing my intellectual development. I really appreciate their precious time, valuable suggestions and continual support.

I am deeply grateful to the entire Department of Chemistry at IISER Pune, all the faculty members and staff for being extremely helpful.

My thanks goes to all the members in PT group, thanks all of you for your friendship and help. A heartfelt "Thank you" goes out to Tanmoy Saha, Arundhati Roy, Prashant Mandal and Sopan Shinde for their helps, encouragements and discussions during this study. I am grateful to Deepali Jadhav and Pooja Lunawat for taking NMR spectra. I deeply thank to Swati Dixit, Swati Hegde, Archana Jogdand for recording MALDI, HRMS, X-ray crystal data, and Mayuresh for administrative and official support.

I would like to acknowledge the financial assistance from CSIR and IISER-Pune for my entire research work and graduate research fellowship.

Speaking of friendships, I am forever grateful to my friends Anupam Sawant (Alex), Maroti Pawar, Sanjog Nagarkar, Prakash Sultane, Dr. Amar Mohite, Shekhar Shinde, Dr. Sachin Mali, Nitin Bansode, Dr. Arvind Gupta, Arun Tanpure, Pramod Sabale, Sushil Benke, Balu Navale, Gopalkrishna and Kiran Badgami. Thank you all for your friendship, stimulating advice, constructive criticism and positive outlook that played a pivotal role in shaping my life during these past five years. I would also like to thank my friends outside the lab, who have helped me and make these past five years so enjoyable, including Navnath Walke, Dr. Jalindar Padwal, Bhaskar Kasar, Vishwas Choudhari and Balasaheb Jadhav. All

the days, late nights and the frustrations when I thought I would never get to this page, you guys were always there to encourage me and believe in my vision.

I would like to thank my parents and my family. I am indebted to my parents for giving endless support, unconditional love and encouragement. I owe much to them for their help to overcome difficulties I have encountered.

Finally, my deepest appreciation and love are devoted to my dear wife, Reshma. I am grateful to her for everything she made for us to have such a beautiful life. It's been an incredible journey and I am so grateful to all of the amazing people that have helped me along the way. Infact, the phrase "Thank you" can never capture the gratitude I want to express.

Dnyaneshwar S. Kand

Synopsis

The thesis entitled "***Design and Synthesis of Fluorescent Probes for Selective Detection of Thiols***" comprises of five chapters.

Thiols represent a class of organic compounds characterized by having sulfhydryl functional (-SH) group. Thiols are also referred as mercaptans (Latin '*mercurium captans'* meaning 'capturing mercury') because of strong affinity and ability of the thiolate group to form stable bonds with mercury compounds. Thiols are widely present in natural products, used in drug molecules, and have shown great potentials in organic/bio-organic synthesis, material science and biological chemistry. Various thiol substrates have been used in protein and peptide chemistry, the transition metal catalyzed synthesis of S-heterocyclic compounds and sulfides, and other C-S coupling reactions. Interestingly, thiols exert both useful and adverse effects on human health. Aliphatic thiols are found in several biologically important molecules. These thiols are known as biothiols. Cysteine (Cys), Homocysteine (Hcy) and Glutathione (GSH) are three major Low Molecular Weight (LMW) biothiols having similar structures which are associated with a wide range of biological functions (Figure 1). These LMW biothiols-containing compounds play important roles in various biochemical and pharmacological processes because they are oxidized easily and moreover can be rapidly regenerated.

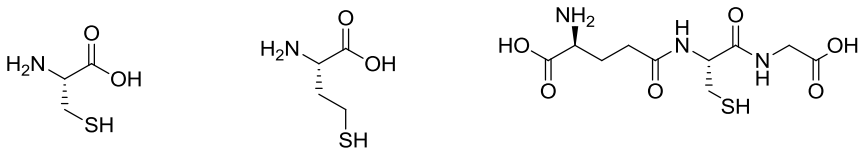

Figure 1: Structures of Cysteine (Cys), Homocysteine (Hcy) and Glutathione (GSH).

Chapter 1 of this dissertation is about introduction of thiols. It involves classification and importance of thiols. Various reaction based approaches used for developing fluorescent probes for selective and sensitive detection of thiols were also discussed in this chapter.

Classification of Thiols

Thiols are broadly classified as aliphatic thiols and aromatic thiols (Figure 2). Aliphatic thiols are sulfur analogs of aliphatic alcohols while thiophenols are sulfur analogs of phenols. Hydrogen sulfide can be considered as unsubstituted thiol.

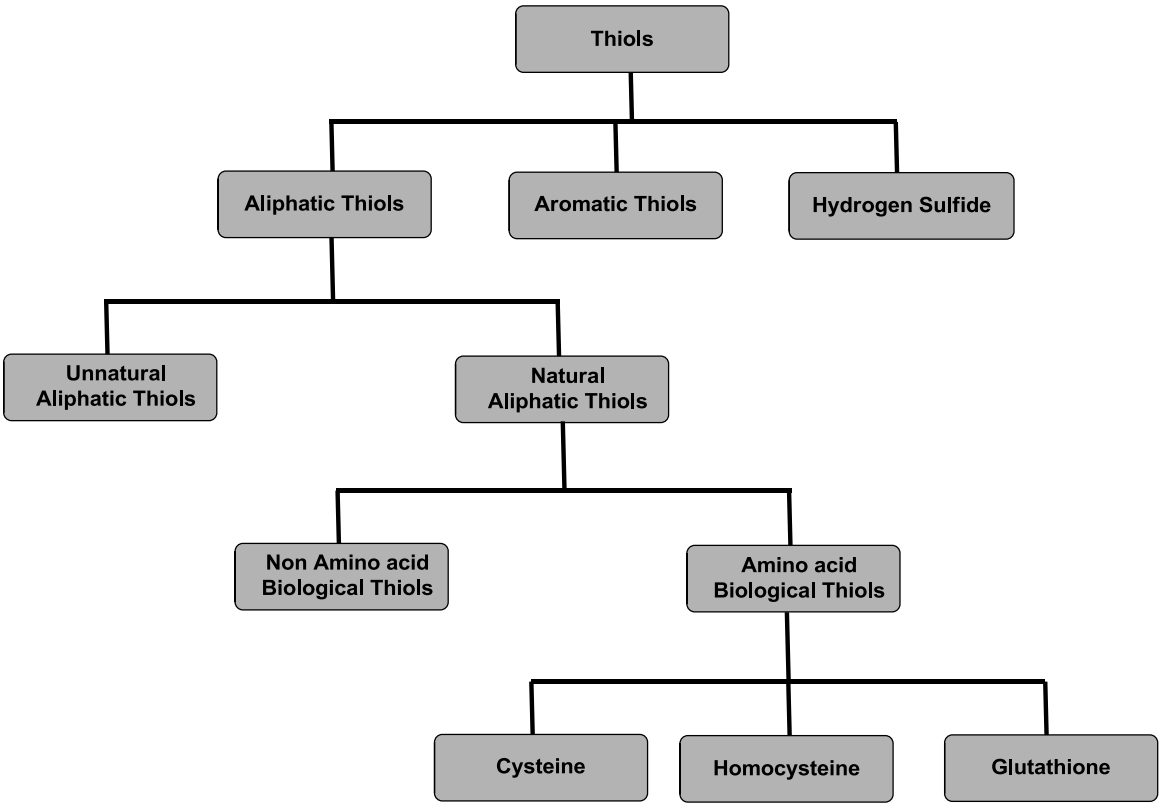

Figure 2: Classification of thiols.

Methods for the detection of Thiols

Considering biological, clinical, and environmental importance of thiols there has been increasing interest to design and develop analytical techniques and methodologies for their detection. Reported instrumental methods for the detection of thiol levels includes high performance liquid chromatography (HPLC), capillary electrophoresis, mass spectrometry (MS), and electrochemical methods. However, these methods generally have some limitations, e.g., high equipment costs, sample processing, and run times, which make them impractical for real time analysis in biological systems and samples.

Fluorescent probes for Thiols

To overcome the limitations of these instrumental methods, the development of fluorescence based probes for detection of thiols gained the attraction and has become an active research area in recent years. Due to their simplicity, low detection limits and capability to perform real time analysis in living systems and biological samples, fluorescent based methods have been widely explored. Most of the fluorescent probes for thiols utilize two characteristic properties of thiols: their strong nucleophilicity and their high binding affinity for metal ions. Recently, the highly selective reactions of thiols in appropriately designed molecular systems have enabled their quantification in biological, abiotic as well as natural environments.

Chapter 2 discusses design, synthesis, characterization and photophysical studies of the fluorescence *Off-On* probes for selective detection of biological thiols. Furthermore applications of these probes in live cell imaging were also demonstrated.

Section A: Cys, Hcy and GSH are three major biothiols which play vital role in the various physiological processes. Each of these biothiols is associated with specific cellular function and alterations in the levels of the same are thus linked to particular diseases. Therefore selective and sensitive detection technique discriminating amongst these biothiols is necessary. In this aspect, fluorescence based methods have shown promising outcome and gained their importance.

Selection of appropriate pair of the fluorophore and quencher is a key in the design of good fluorescent probe which would show remarkable differences in the fluorescence properties upon sensing thiols. Fluorescence properties of probes are also influenced by position and distance between fluorophore and quencher.

Our aim was to develop the fluorescent probes for the selective detection of biothiols. We hypothesized that the discrimination amongst the biothiols can be achieved by varying the position of the quencher on the fluorophore. Many synthetic methodologies are reported for the synthesis of chromenoquinolines. However, the photophysical properties of the chromenoquinolines were not explored. In our group we synthesized various substituted chromenoquinolines and studied their photophysical properties. Owing to easy scalable synthesis, good yields and fluorescence properties of chromenoquinolines, we selected chromenoquinolines as fluorophore. Maleimide is well explored thiol

recognizing unit widely used in the synthesis of thiol selective fluorescent probes. Therefore, maleimide was selected as a quencher.

In section A of chapter 2, we reported three chromenoquinoline-based probes **4**, **5** and **6** in which the position of the maleimide moiety is varied at position (Figure 3). Probes **4** and **6** were predictable to provide better quenching compared to **5** due to the higher electron density at C-2 and C-4 positions and therefore, expected to exhibit better *Off-On* response upon thiol sensing. The probe **6** on the other hand is crucial as the steric crowding at the groove of the chromenoquinoline is expected to contribute in either selectivity by reducing the rate of Michael addition reaction or enhancing the sensitivity, especially with sterically hindered thiols. Bulkier thiols are presumed to favour the more orthogonal spatial orientation of the resulting succinimide moiety relative to the chromenoquinoline fluorophore and this is expected to decrease the fluorescence quenching by the succinimide moiety. The present work describes the design, theoretical calculations, synthesis, photophysical properties and thiol sensing abilities of these probes in living cell.

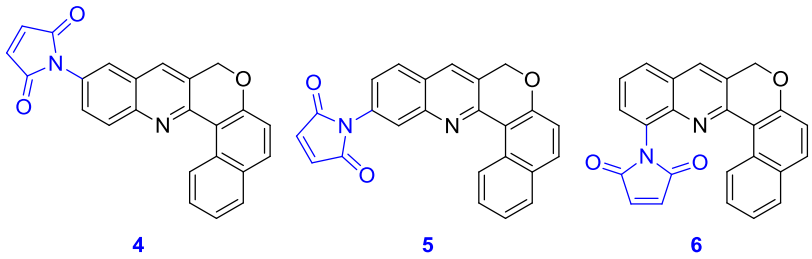

Figure 3: Proposed structures of fluorescent turn-*On* probes **4**, **5** and **6** for selective detection of thiols.

Section B: Among diverse fluorescence-based approaches, thiol mediated Michael addition on maleimide, aromatic nucleophilic substitution reactions (SNAr) on 2,4-Dinitrophenylsulfonyl (DNs) have been used for developing thiol probes. However, the selectivity of these probes could not be predicted prior to experimental evaluation. More predictive approach for selective Cys sensing involves the formation of thiazolidine from aldehyde. Involvement of both –SH and $–NH_2$ groups contribute to better selectivity although, Hcy is reported to compete in the sensing process by forming thiazinane product. Recently, an alternate two-step strategy has been reported by Yang and co-workers which involves the addition (rate = k_1) of thiol on the nonfluorescent species **7** leading to thiol-conjugate **7(*S*)** as a kinetically controlled product (Figure 4A). Subsequent conversion of **7(*S*)** to thermodynamically controlled amine-conjugate **7(*N*)** is characterized

as S-N Smiles rearrangement. The rate k_2 of the rearrangement is determined by the covalent-length of the spacer between the sulfur and the nitrogen atoms. The rearrangement is more feasible for Cys because, it involves cyclic five-membered transition state. For Hcy, the rearrangement would proceed at slower rate due to formation of a cyclic six-membered transition state. Corresponding rearrangement involving GSH would not be feasible due to the formation of a cyclic ten-membered transition state. According to this two-step strategy, the *Off-On* response of probe **7** to either of Cys, Hcy and GSH can be dictated by rate, k_2 of each rearrangement reaction and fluorescent properties of **7(*S*)** and **7(*N*)** species formed.

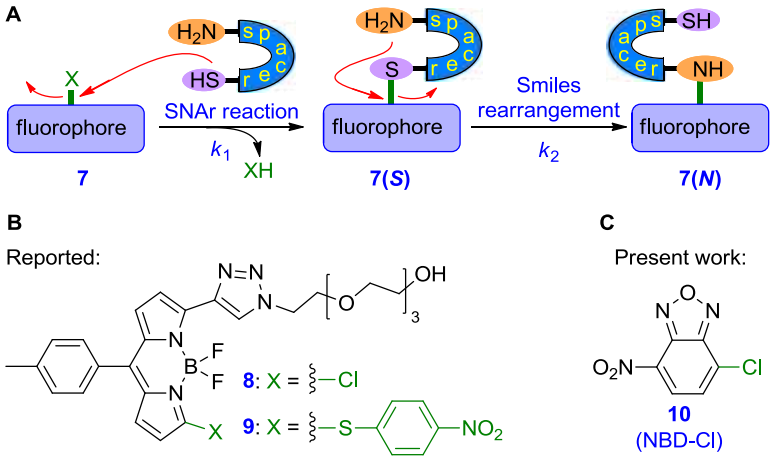

Figure 4: Schematic diagram for illustrating the two-step thiol sensing process by **7** (**A**). Structures of BODIPY-based *Off-On* thiol probes **8** and **9** (**B**). Structure of NBD-based *Off-On* Cys sensing probe **10** (**C**).

In section B of chapter 2, we reported the ability of NBD-chloride **10** in selective and sensitive detection of Cys relying on the two-step SNAr reaction and S-N Smiles rearrangement (Figure 4C). Probe **10** is commonly used as an efficient probe for selective labeling of thiols, such as free thiols and sulfhydryl groups in proteins because of the feasibility of thiol-conjugation under physiological conditions compared to more basic and elevated temperature conditions for amine-conjugation. In 1983, Houk *et. al.* during the labeling native actin protein, observed a very slow conversion of NBD-thiol conjugate of cysteine-residue into a NBD-amine conjugate triggered by a neighbouring lysine-residue. In 2012, Botta and coworkers also reported a similar S-N rearrangement during the acylation of 4-(2-aminoethylthio)-7-nitrobenzofuran under basic conditions. A plausible mechanism of the process was provided by them based on the S-N Smiles rearrangement. We realized the importance of the rearrangement in establishing **10** as more specific

fluorescent probe for either Cys or *N*-terminal Cys containing peptides/proteins compared to other biothiols (Hcy, GSH and proteins) under physiological conditions. Formation of NBD-amine conjugates with expected longer absorption wavelength and stronger emission would contribute to better sensitivity during labelling.

Section C: Eukaryotic cells contain various compartments and cell organelles such as nucleus, mitochondria, endoplasmic reticulum, lysosomes, *etc*. Each cell organelle is associated with specific function/s essential for life. *e.g.* Lysosomes have intracompartmental pHs of 4.0–6.0 and it contain approximately 50 different degradative enzymes that are active at acidic pH. The lysosome membrane constitutes a physiological barrier between the lysosome matrix and the surrounding cytoplasm. The membrane's impermeability ensures the retention of both the lysosomal enzymes and their substrates within the lysosomes. It is believed that GSH may be involved in stabilizing lysosome membranes. Thiols facilitate intralysosomal proteolysis by reducing disulphide bonds. For example, Cys is an effective stimulator of albumin degradation in liver lysosomes. For better understanding of the role of lysosomal thiols it is important to develop fluorescent probes capable of targeting lysosomes.

In section C of chapter 2, we report the design, synthesis of lysosome targeting fluorescence turn-*on* probe **11** (Figure 5) and its biothiol sensing properties in the organelle. To obtain a photostable water soluble fluorescent thiol probe, excitable in the visible region and applicable for live-cell imaging, boron-dipyrromethene (BODIPY) was selected as the fluorophore. The necessary molecular decorations for thiol recognition and lysosome targeting were incorporated via 2,4-dinitrobenzenesulfonyl (DNs) group and morpholine ring, respectively. As BODIPY-based chemosensors operate by perturbing the reduction potential of the *meso*-substituent, the DNs group was attached to aryl group at *meso*-position. Moreover, a phenyl ring at 5-position was considered for extended conjugation and thereby, exciting at longer wavelengths while maintaining high quantum yield.

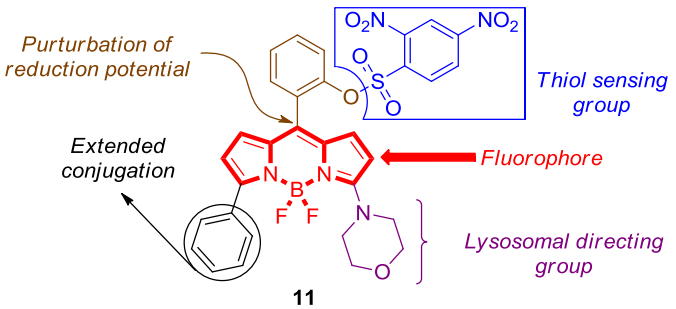

Figure 5: Structure of the liposomal targeting probe **11**.

Chapter 3 describes the rational design, synthesis, characterization and photophysical studies of the fluorescence *Off-On* probes for selective detection of thiophenols.

In chapter 3, we report the design and synthesis of new fluorescent probes **12 – 15** which are applied for selective and rapid detection of aromatic thiols (Figure 6). In the design of probe **12**, boron-dipyrromethene (BODIPY) was selected as the fluorophore due to its intense absorption in visible light, relatively high molar extinction coefficient (ε) and stability against light and chemicals. 2,4-Dinitrobenzenesulfoyl (DNs) group which is an established quencher in the design of the thiol sensitive probes was selected in our design. Thiol-mediated cleavage of the resulting sulfonyl group through S_NAr process releases the fluorophore resulting in the *turn-on* of fluorescence. The arenesulphonamide was selected over arenesulfonate in the probe design due to better reactivity towards thiols compared to oxygen and nitrogen nucleophiles.

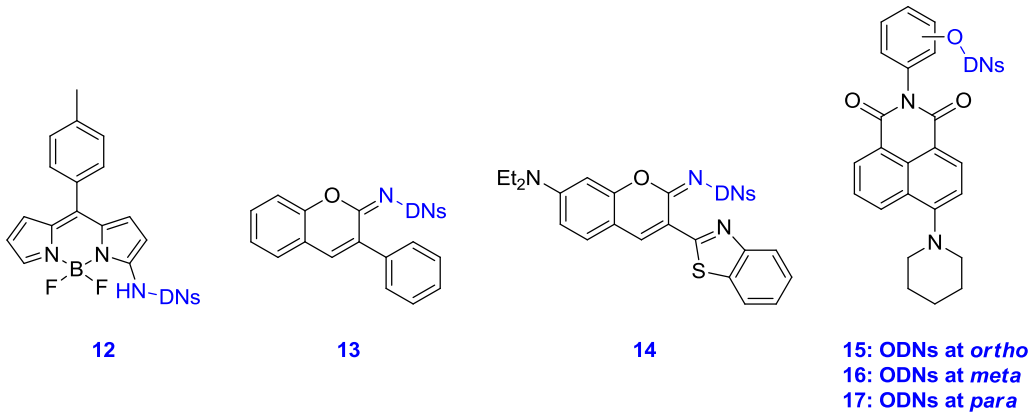

Figure 6: Structures of proposed probes **12 – 17** for selective detection of thiophenols.

For probes **13** and **14** iminocoumarin was selected as fluorophore (Figure 6). We speculate that a photoinduced electron transfer (PET) pathway from iminocoumarin to DNs moiety is responsible for the fluorescence *Off*-state in these probes. Free imimocoumarins **13a** and **14a** can be released as strongly fluorescent species from these probes via the thiolate (PhS^-) mediated cleavage of DNs moiety.

For probe **15** 4-aminoinaphthalimide was selected as electron donor and Dinitronenzenesulfonyl (DNs) group as electron acceptor moiety. Based on the position of quencher on fluorophore three isomers *i.e. ortho, meta* and *para* probes were synthesized. In the PET process, the distance of DNs moiety from fluorophore will greatly affect the quenching ability of DNs and *ortho* substituted probe will exhibit better properties in sensing process compared to *meta* and *para* substituted isomers.

The correlation diagram demonstrates a decrease in t_R value of probe toward PhSH upon increase in pK_{aH} of released fluorophore (Figure 7). Among probes **12** – **15**, probe **12** with pK_{aH} of 2.84 shows slower response towards PhSH with response time (t_R) 12 min. For probe **13** with pK_{aH} of 5.22 response time t_R was found to be 5.5 min. Probe **14** with pK_{aH} of 5.75 shows rapid response towards PhSH with t_R = 1.5 min. Probe **15** with pK_{aH} of 8.25 shows fastest response towards PhSH with t_R < 1 min.

A

Fluorophore	t_R (min)	pK_{aH}	Fluorophore	t_R (min)	pK_{aH}
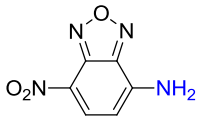 **18a**	17	-1.62	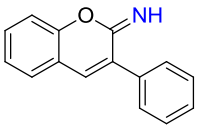 **13a**	5.5	5.22
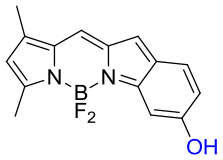 **19a**	20	-5.71	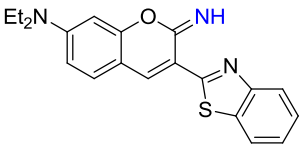 **14a**	1.5	5.75
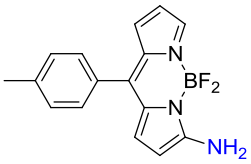 12a	12	2.84	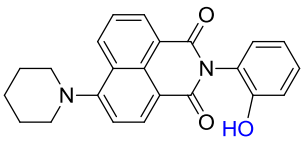 **15a**	<1.0	8.25

B

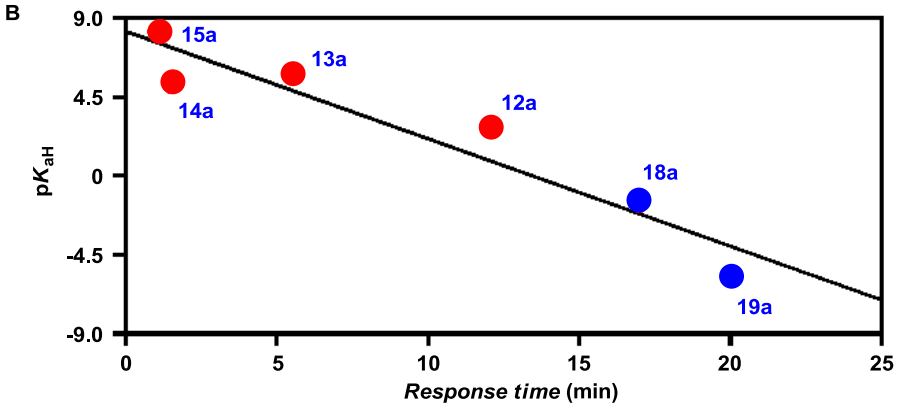

Figure 7: (**A**) t_R, pK_{aH} values and (**B**) correlation diagram of t_R values of probes **12** – **15**, **18** and **19** with pK_{aH} of **12a** – **15a**, **18a** and **19a**.

Chapter 4 reports on the design, synthesis, characterization and photophysical studies of the fluorescence *Off-On* probe for selective detection of hydrogen sulfide. Application of the probe in live cell imaging was demonstrated.

Hydrogen sulfide (H_2S) has traditionally been known as a toxic chemical species in biological systems. However emerging studies have challenged this view and recognized the importance of H_2S as one of the three gasotransmitters. Considering the complex biological roles of H_2S along with its volatile and reactive nature, the accurate detection of H_2S is necessary in order to monitor its production and consumption in biological systems. The methods for selective detection and quantification of the H_2S are important in the areas of diagnostics and therapeutics. Monitoring of H_2S levels using traditional methods such as, gas chromatography, electrochemical methods and polarographic methods require multistep sample preparation, which limits their use in live systems for real time analysis. Owing to high sensitivity and the ability of fluorescent methods to conduct analysis in live systems, fluorescent probes offer promising approach for the detection of H_2S.

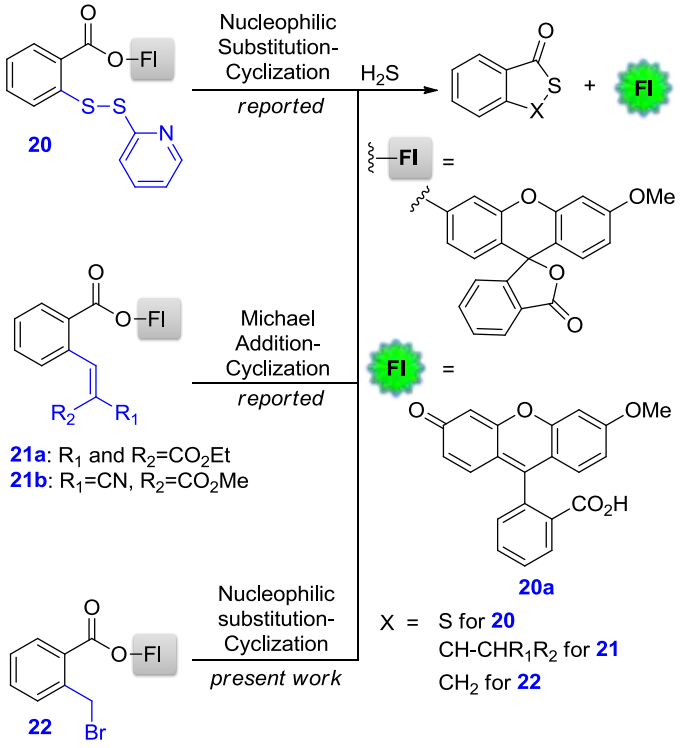

Figure 8: Reported reaction based fluorescence *turn-On* probes **20** – **22** for H_2S sensing.

In probe **20**, 2-pyridinyl disulfide and an ester group was employed as two electrophilic sites for reaction of H_2S. Probe **21** was based on Michael addition followed by cyclization to release active fluorophore (Figure 8).

Fluorescence *Off-On* probes **20** and **21** exhibited long response times, ranging from 30 to 60 min and may not be suitable for monitoring the intracellular level of the species due to high fluctuations in endogenous free H_2S concentration.

In this chapter, we reported nucleophilic substitution-cyclization reaction based probe **22** for fast, highly selective and sensitive detection H_2S. We believed that other nucleophiles including biological thols such as Cysteine (Cys), Homocysteine (Hcy) and Glutathione (GSH) could also undergo nucleophilic substitution at benzylic position to substitute bromide. However, absence of the reactive intermediate limits the possibility of second nucleophilic attack to release fluorophore.

Chapter 5 reports the experimental procedures, characterization and spectral data of the compounds reported in first four chapters.

List of Publications:

1. Kand, D.; Kalle, A. M.; Varma, S. J.; Talukdar, P. *Chem. Commun.* **2012**, *48*, 2722.
2. Kand, D.; Mishra, P. K.; Saha, T.; Lahiri, M.; Talukdar, P. *Analyst* **2012**, *137*, 3921.
3. Kand, D.; Kalle, A. M.; Talukdar, P. *Org. Biomol. Chem.* **2013**, *11*, 1691.
4. Saha, T.; Kand, D.; Talukdar, P. *Org. Biomol. Chem.* **2013**, *11*, 8166.
5. Kand, D.; Mandal, P.; Talukdar, P. *Dyes and Pigments* **2014**, *106*, 25.
6. Kand, D.; Saha, T.; Talukdar, P. *Sensors and Actuators B: Chemical*, **2014**, *196*, 440.
7. Kand, D.; Chauhan, D. P.; Lahiri, M.; Talukdar, P. *Chem. Commun.* **2013**, *49*, 3591.
8. Gening, M. L.; Tsvetkov, Y. E.; Titov, D. V.; Gerbst, A. G.; Yudina, O. N.; Grachev, A. A.; Shashkov, A. S.; Vidal, S.; Imberty, A.; Saha, T.; Kand, D.; Talukdar, P.; Pier, G. B.; Nifantiev, N. E. *Pure Appl. Chem.* **2013,** *85*, 1879.
9. Roy, A.; Datar, A.; Kand, D.; Saha, T.; Talukdar, P. *Org. Biomol. Chem.* **2014**, *12*, 2143.
10. Roy, A.; Kand, D.; Saha, T.; Talukdar, P. *Chem. Commun.* **2014**, *50*, 5510.
11. Roy, A.; Kand, D.; Saha, T.; Talukdar, P. *RSC Adv.* **2014**, *4*, 33890.
12. Kand, D.; Mandal, P.; Saha, T.; Talukdar, P. *RSC Adv.* **2014**, *4*, 59579.
13. Saha, T.; Kand, D.; Talukdar, P. *RSC Adv.* **2015**, *5*, 1438 .

Table of contents

Chapter 1: Introduction

1.1 Introduction of Thiols 1

1.2 Classification of Thiols 1

1.3 Redox process and disulfide linkage 2

1.4 Importance of Thiols 4

1.4.1 Aliphatic Thiols 4

1.4.2 Biothiols (Cys, Hcy, GSH) 4

1.4.3 Aromatic Thiols 6

1.4.4 Hydrogen Sulfide (H_2S) 7

1.5 Methods for the detection of Thiols 7

1.6 Fluorescent probes for Thiols 7

1.6.1 Classification of fluorescent probes for thiols based on fluorescence response 8

1.6.2 Design principles and Sensing Mechanism of turn-On probes 12

1.7 Types of probes according to mechanism of reaction with thiols 15

1.7.1 Thiol mediated cleavage of sulfonamide and sulfonate esters 16

1.7.2 Michael addition of thiols 16

1.7.3 Michael addition to α, β-unsaturated compounds 17

1.7.4 Michael addition/cyclization to α, β-unsaturated carbonyl compounds 18

1.7.5 Cyclization with aldehydes 19

1.7.6 Cleavage of disulfide bonds by thiols 19

1.7.7 Nucleophilic substitution by thiols 20

1.8 Fluorescent probes for Hydrogen Sulfide 21

1.9 Research Outlook 24

1.10 References 25

Chapter 2: Design and Synthesis of Fluorescence *Off-On* Probes for Biological Thiols

Section 2A: Chromenoquinoline Based Fluorescence *Off-On* Probes for Biological Thiols

2A.1 Introduction 29

2A.2 Results and discussion 30

2A.2.1 Theoretical calculations 30
2A.2.2 Synthesis 31
2A.2.3 Photophysical studies 34
2A.2.4 Thiol sensing 37
2A.2.5 Cell imaging 45

2A.3 Summary and conclusions 46

2A.4 References 47

Section 2B: NBD Chloride as Fluorescence *Off-On* Probe for Selective Detection of Cysteine and Homocysteine over Glutathione

2B.1 Introduction 48

2B.2 Results and discussion 50

2B.2.1 Theoretical calculations 50
2B.2.2 Synthesis 53
2B.2.3 Thiol sensing 54
2B.2.4 1H NMR titration 59
2B.2.5 Cell imaging 60

2B.3 Summary and conclusions 61

2B.4 References 61

Section 2C: BODIPY based Fluorescence *Off-On* probes for Detection of Biological Thiols in Lysosomes

2C.1 Introduction 64

2C.2 Results and discussion 65

2C.2.1 Synthesis 65
2C.2.2 Photophysical studies 66
2C.2.3 Thiol sensing 67
2C.2.4 1H NMR titration 70
2C.2.5 Cell imaging 73
2C.2.6 MTT cell viability assay 75

2C.3 Summary and conclusions 75

2C.4 References 76

Chapter 3: Design and Synthesis of Fluorescence *Off-On* Probes for Rapid Detection of Aromatic Thiols

3.1 Introduction 77

3.2 Results and discussion 79

3.2.1 Theoretical calculations 81
3.2.2 Synthesis 93
3.2.3 Photophysical studies and thiol sensing 95
3.2.4 Cell imaging 112

3.3 Summary and conclusions 114

3.4 References 115

Chapter 4: Cascade Reaction Based Fluorescence turn-*On* Probe for Selective Detection of Hydrogen Sulfide

4.1 Introduction 116

4.2 Review of literature 116

4.3 Results and discussion 117

4.3.1 Synthesis 117
4.3.2 Photophysical studies and Hydrogen Sulfide sensing 118
4.3.3 1H NMR titration 122
4.3.4 Cell imaging 124

4.4 Summary and conclusions 125

4.5 References 125

Chapter 5: Experimental procedures

5.1 Methods and materials 127

5.1.1 General methods 127
5.1.2 Physical measurements 127
5.1.3 Live cell imaging 128
5.1.4 Procedures 128

5.2 Experimental section 131

5.3 Crystal structure parameters 150

5.4 NMR data 158

5.5 HPLC purity 195

5.6 References 196

Note: Cell imaging studies presented in the thesis were carried out by either Dr. Arunasree Marasanapalli Kalle from University of Hyderabad or Mr. Tanmoy Saha of Dr. Pinaki Talukdar group. These images are given in thesis as representation of data. Author does not claim any credit for these cell imaging studies.

List of Symbols and Abbreviations

Cys	Cysteine
Hcy	Homocysteine
GSH	Glutathione
DNs	2, 4-Dinitrobenzenesulfonyl
HPLC	High Performance Liquid Chromatography
MALDI	Matrix Assisted Laser Desorption Ionization
NBD-Cl	7-Chloro-4-nitrobenz-2-oxa-1,3-diazole
Boc	*tert*-Butoxycarbonyl
^{1}H NMR	Proton nuclear magnetic resonance spectroscopy
^{13}C NMR	Carbon-13 nuclear magnetic resonance spectroscopy
HR-MS	High resolution mass spectrometry
XRD	X-ray diffraction
ORTEP	Oak ridge thermal ellipsoid plot
TLC	Thin-layer chromatography
TMS	Tetramethylsilane
Brine	Saturated aqueous sodium chloride
t_R	Response time
H_2S	Hydrogen Sulfide
h	Hour
min	Minute
A	Absorbance
mg	Milligram(s)
mmol	Millimole(s)
μM	Micromolar
μL	Microlitre
mL	Millilitre
mol	Mole(s)
DL	Detection limit
M.p.	Melting point
α	Alpha
β	Beta
br	Broad singlet

m	Multiplet
s	Singlet
d	Doublet
dd	Doublet of doublet
t	Triplet
ϕ	Quantum yield
^{o}C	Degree Celsius
rt	Room temperature
δ	Chemical shift
calcd.	Calculated
cm^{-1}	Reciprocal centimetres
Hz	Hertz
MHz	Mega Hertz
IR	Infrared spectroscopy
J	Coupling constant
$CaCl_2$	Calcium chloride
$CDCl_3$	Deuterated chloroform
$CHCl_3$	Chloroform
CH_2Cl_2	Methylene chloride
CCl_4	Carbon tetrachloride
DMF	*N*,*N* –Dimethylformamide
DMSO	Dimethyl sulfoxide
D_2O	Deuterated water
THF	Tetrahydrofuran
Na_2SO_4	Sodium sulphate
DMAP	4-Dimethylaminopyridine
DDQ	2,3-Dichloro-5,6-dicyano-*p*-benzoquinone
CTAB	Cetyl trimethylammonium bromide
HEPES	(4-(2-Hydroxyethyl)-1-piperazineethanesulfonic acid

Chapter 1

Introduction

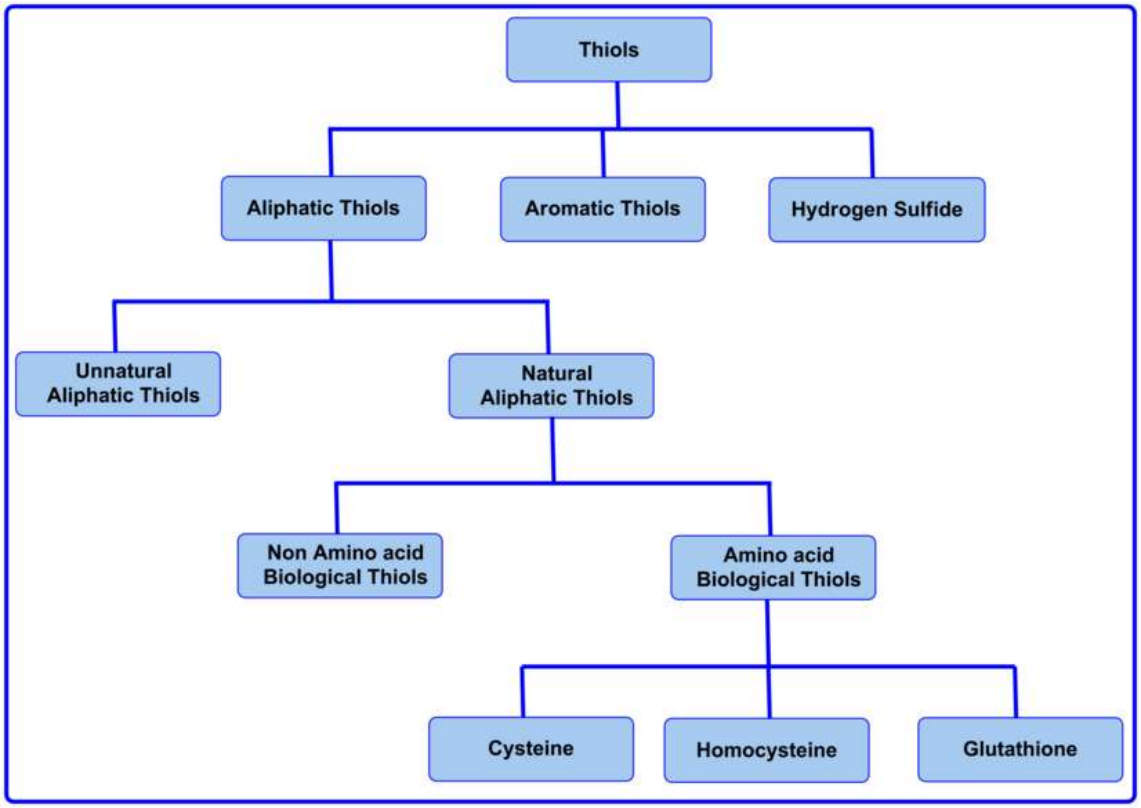

1.1 Introduction of Thiols

Thiols represent a class of organic compounds characterized by having sulfhydryl functional (-SH) group. Thiols are also referred as mercaptans (Latin '*mercurium captans'* meaning 'capturing mercury') due to strong affinity and ability of the thiolate group towards mercury compounds. Aliphatic thiols are sulfur analogs of aliphatic alcohols while aromatic thiols are sulfur analogs of phenols. Therefore aromatic thiols are also termed as thiophenols. Physical and chemical properties of thiols differ significantly from those of alcohols. Thiols are less polar than their corresponding alcohol analogs as hydrogen bonding is either absent or weak in thiols. Thiols have low melting and boiling points compared to alcohols of same carbon numbers. Thiols are more nucleophilic than their oxygen analogs because 3*p* valence electrons on sulphur are less tightly held compared to 2*p* electrons on oxygen.

Thiols are widely present in natural products, used in drug molecules. Interestingly, thiols exert both useful and adverse effects on human health. They have shown great potentials in organic/bio-organic synthesis, material science and biological chemistry.[1] Various thiol substrates have been used in protein and peptide chemistry,[2] the transition metal catalyzed synthesis of S-heterocyclic compounds and sulfides,[3] and other C-S coupling reactions.[4] Oxidation of thiols results in the formation of disulfide (-S-S-) linkages. S-S cross links are used to make strong polymers such as latex and synthetic rubber.

1.2 Classification of Thiols

Thiols are broadly classified into aliphatic thiols and aromatic thiols while hydrogen sulfide is unsubstituted thiol[5](Figure 1.1).

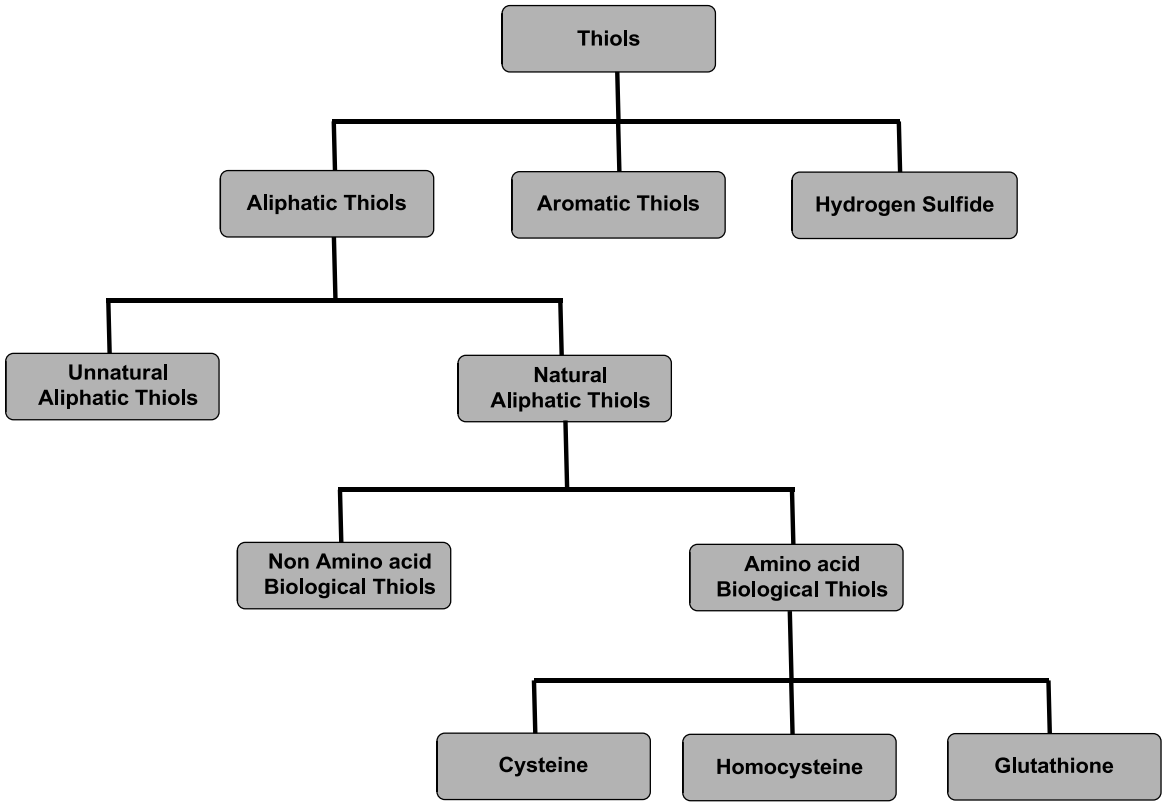

Figure 1.1: Classification of thiols.

1.3 Redox process and disulfide linkage

Thiols are easily oxidized to form disulfide (sulfur-sulfur) linkages and because they are oxidized easily and moreover can be rapidly regenerated (Figure 1.2).[6]

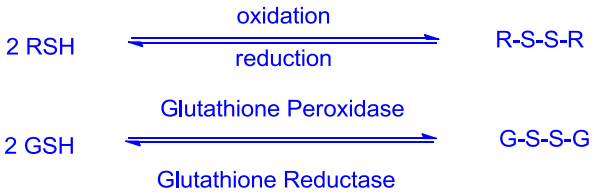

Figure 1.2: The interconversion between thiols and disulfide groups for maintaining intracellular redox potential.

Biothiols are important in maintaining redox homeostasis in proteins, cells and organism through the equilibrium of reduced free thiols and oxidized disulfides.[7] Disulfide linkages between two cysteine residues are responsible for the three-dimensional structure of many proteins (Figure 1.3). The interconversion between thiols and disulfide groups is a redox reaction: the thiol is the reduced state, and the disulfide is the oxidized state. The

redox agent that mediates the formation and degradation of disulfide bridges in most proteins is glutathione.

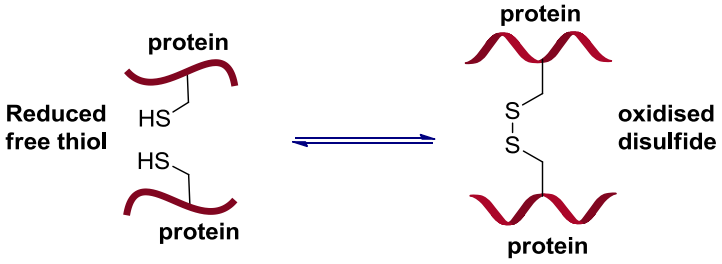

Figure 1.3: Redox process between thiols and disulfide groups in proteins.

Lipoic acid (LA) **1** is an example of biomolecule which contains two sulfur atoms (at C6 and C8) connected by a disulfide bond (Figure 1.4). It is considered to be in oxidized form although either sulfur atom can exist in higher oxidation states. The carbon atom at C6 is chiral and the molecule can exists as two enantiomers (*R*)-(+)-lipoic acid (RLA) and (*S*)-(-)-lipoic acid. Only the (*R*)-(+)-enantiomer exists in nature and is an essential cofactor of four mitochondrial enzyme complexes. Endogenously synthesized RLA is essential for aerobic metabolism. Fungi also produce unusual disulfide containing compounds like. Mycotoxin sporidesmin **2**.

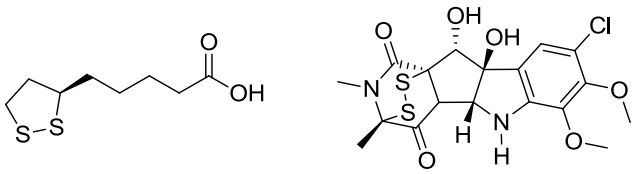

1
Lipoic acid

2
Mycotoxin sporidesmin

Figure 1.4: Structures of Lipoic acid (LA) **1** and Mycotoxin sporidesmin **2**.

In the biochemistry lab, proteins are often maintained in their reduced state by incubation in buffer containing an excess concentration of *β*-mercaptoethanol (BME) **3** or dithiothreitol (DTT) **4** (Figure 1.5). BME functions in a similar manner to that of GSH, whereas DTT has two thiol groups, forms an intramolecular disulfide in its oxidized form.

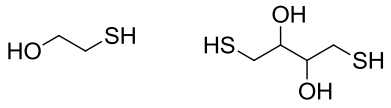

3
***β*-mercaptoethanol**
(BME)

4
Dithiothreitol
(DTT)

Figure 1.5: Structures of reducing agents *β*-mercaptoethanol (BME) **3** and dithiothreitol (DTT) **4**.

1.4 Importance of Thiols

1.4.1 Aliphatic Thiols

Aliphatic thiols are used as lubricant additives and chain-propagating agents in polymerization reactions. They have distinct strong and unpleasant odour. Therefore, aliphatic thiols such as ethanethiol **5**, *tert*-butylthiol **6** and tetrahydrothiophene **7** are used as odorants in the detection of leakage of Liquid Petroleum Gas (LPG) and natural gas which are odorless in their pure form (Figure 1.6). Some aliphatic thiols are present in eatables and have less-offensive odours and flavours. Freshly chopped onions emit propanethiol **8** which is lachrymator. 1-Propene-3-thiol **9**, 3, 3-di-(1-propenyl) disulfide **10** and ajoene **11** are partially responsible for the odour and flavour of garlic. Because of the potent organoleptic properties of thiols and disulphides and their natural occurrence in foodstuffs, synthetic compounds of these types find wide application as food flavours. Several aliphatic thiols and disulphides are also approved for their use in food. British anti-Lewisite (BAL; 2,3-dimercaptopropanol) **12** is most commonly used as a chelator (remove a heavy metal from the body) in the treatment of poisoning from arsenic, mercury, lead, gold, etc.

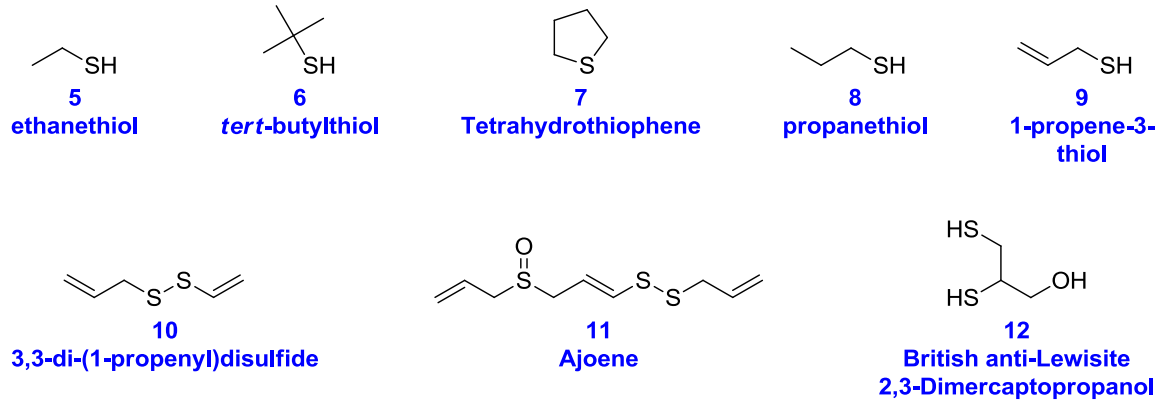

Figure 1.6: Aliphatic thiols with various applications in industry, food and medicine.

1.4.2 Biothiols (Cys, Hcy, GSH)

Aliphatic thiol group is present in several biologically important molecules which are commonly known as biothiols. Cysteine (Cys) **13**, homocysteine (Hcy) **14** and glutathione (GSH) **15** are three major Low Molecular Weight (LMW) biothiols having similar structures which are associated with a wide range of biological functions[8] (Figure

1.7). These biothiols play important roles in various biochemical and pharmacological processes.

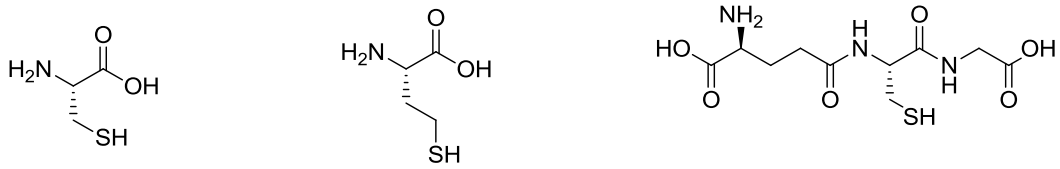

13 ***L*-Cysteine (Cys)** **14** ***L*-Homocysteine (Hcy)** **15** **Glutathione (GSH)**

Figure 1.7: Structures of Cysteine (Cys) **13**, Homocysteine (Hcy) **14** and Glutathione (GSH) **15**.

Thiols are also found in many proteins which occur in mammalian tissues.[9] Albumin is the most abundant protein in human plasma which is more than 50% of the total plasma protein. Most of thiol groups present over albumin are considered as major *in vivo* plasma antioxidants.[9]

Glutathione (GSH):

GSH is a tripeptide which found in most plants, microorganisms, and all mammalian tissues. It is most abundant non-proteinogenic intracellular thiol (1 – 10 mM)[7a] and in human plasma its concentration varies in the range of 0.2 – 4 μM.[10] Eukaryotic cells have three major reservoirs of GSH *i.e.* cytosol (90%), mitochondria (10%) and small percentage in the endoplasmic reticulum.[11] Intracellular GSH exists in thiol-reduced (GSH) and disulfide oxidized (GSSG) forms.

GSH is referred as 'master antioxidant' as it protects cells from oxidative damage by trapping free radicals that damage DNA and RNA.[12] GSH is also associated with various cellular functions such as storage and transport of cysteine,[13] intracellular signal transduction and gene regulation.[14]

Cysteine (Cys):

Cysteine (Cys) is involved in metabolic processes, detoxification, protein synthesis, *etc*.[15] Cys also plays crucial roles in structure and function of proteins [6].[16] Cys is required for glutathione synthesis. Cys is only thiol containing amino acid in proteins which is major thiol in plasma and its concentration is in the range of 8 – 10 μM.[17] Cystine (CysS-SCys disulfide) concentration in plasma is higher (40 μM) than that of Cys [18] Low

molecular weight compounds such as coenzyme A, lipoic acid, ergothioneine are derived from cysteine which play varied and important roles in cellular biochemistry.

Abnormal levels of Cys are linked with many human diseases such as liver damage, loss of muscle and fat, slow growth in children, edema, hair depigmentation, lethargy, and skin lesions.[19] Cys is extremely unstable extracellularly and rapidly auto-oxidizes to cystine, in a process producing potentially toxic oxygen free radicals.[13]

Homocysteine (Hcy):

Hcy is a key intermediate formed during the biosynthesis of Cys from the amino acid methionine.[20] At elevated levels in plasma, Hcy is a risk factor for disorders including Alzheimer's,[21] cardiovascular diseases (CVD),[22] folate and cobalamin (vitamin B_{12}) deficiency,[23] neural tube defects, inflammatory bowel disease, and osteoporosis.[24] Alterations in the intracellular biothiols levels have been associated with various diseases including psoriasis, cancer, leucocyte loss, and AIDS.[2a,25]

Therefore, selective and sensitive detection of intracellular and plasma levels of biothiols may help in early diagnosis and prevent the onset of such diseases.

1.4.3 Aromatic thiols

Aromatic thiols are widely used chemical intermediates in pharmaceutical, pesticide, polymers and amber dyes industries.[26] Aromatic thiols are largely produced from oil and coal refineries, plastic and rubber industries[27] and waste deposit fields.[28] In spite of their wide synthetic utility, aromatic thiols are the class of hazardous, highly toxic and pollutant chemicals.[29] Presence of thiophenols in water and soil are reported to cause damage to natural habitats.[30] Studies reveal that LC_{50} (a dose required to kill half the members of a tested population) of thiophenols is 0.01 – 0.4 mM for fish.[30] Exposure to aromatic thiols leads to headache, nausea, and vomiting by targeting central nervous system (CNS), kidney, and liver.[31]

As aromatic thiols are more toxic compared to aliphatic ones, the simple detection technique that can selectively differentiate toxic thiophenols and biologically important thiols is of great significance in the fields of chemical, biological and environmental sciences.

1.4.4 Hydrogen sulfide (H_2S)

Hydrogen sulfide (H_2S) has traditionally been known as a toxic chemical species in biological systems.[32] However, emerging studies have challenged this view and recognized the importance of H_2S as one of the three gasotransmitters[33] along with nitric oxide (NO)[34] and carbon monoxide (CO)[35] being other two. H_2S is produced naturally during geological and microbial activities.[32] H_2S is synthesized in the cell enzymatically as well as non enzymatically. Endogenous H_2S in mammalian systems is produced by involving three enzymes: cystathionine β-synthase (CBS, mainly localized in brain and liver),[36] cystathionine γ-lyase (CSE, mainly localized in liver)[37] and cysteine aminotransferase/3-mercaptopyruvate sulfurtransferase (CAT/3MST, mainly localized in vascular endothelium and brain).[38] H_2S is a potent antioxidant, anti-inflammatory molecule with potent cardio protective and neuroprotective effects.[39] Overexposure to same leads to unconsciousness, brain damage, olfactory paralysis or even death.[40] The understanding of molecular mechanism of H_2S, its physiological and pathological functions are still ongoing. Therefore selective detection and quantification of the H_2S may have therapeutic and diagnostic relevance.

1.5 Methods for the detection of thiols

Considering biological, clinical, and environmental importance of various thiols, there has been increasing interest to develop analytical techniques and methodologies for their detection. Reported instrumental methods for the detection of thiol levels includes high performance liquid chromatography (HPLC),[41] capillary electrophoresis,[42] Mass spectrometry (MS),[43] and electrochemical methods.[44] However, these methods generally have limitations, such as high equipment costs, sample processing, and long run times. As a result real time analysis in biological systems and samples using these techniques are generally impractical.[45] Differentiation amongst the biothiols is another challenging task for traditional methods due to close resemblance in structures and reactivities of biothiols.

1.6 Fluorescent probes for thiols

To overcome the limitations of these traditional methods, development of fluorescence based probes for detection of thiols has become an active research area in recent years.[7a,45-46] Due to their simplicity, low detection limits and applicability to carry

out real time analysis in various biological samples, fluorescent based methods have been widely explored.[8a] Most of the fluorescent probes for thiol utilize two characteristic properties of thiol group: (a) strong nucleophilicity and (b) high binding affinity for metal ions.[7a] Highly selective reactions of thiols in appropriately designed molecular systems have enabled their quantification in biological, abiotic as well as natural environments.[45]

1.6.1. Classification of fluorescent probes for thiol detection

Many fluorescent probes are reported for selective detection of thiols. Various reaction mechanisms were also adopted for the selective sensing of thiols. Based on the nature of fluorescence response upon thiol sensing, these fluorescent probes can be broadly classified in four types (Figure 1.7):

(a) Ratiometric probes
(b) Förster resonance energy transfer (FRET) based probes
(c) Fluorescence turn-*Off* probes
(d) Fluorescence turn-*On* probes

(a) Ratiometric probes

Ratiometric effects can be produced by either spectral shift or variation of relative intensities of two or more wavelengths. In the case of spectral shifts, the ratio of intensities at two wavelengths of the spectrum is recorded. In the case of fluorescence intensity changes at two wavelengths (without spectral shifts), relative fluorescence intensities are recorded. In ratiometric probe, fluorescence intensity at one wavelength decreases linearly with consistent increase in fluorescence intensity at other wavelength. Ratiometric probes offer an advantage of measuring the fluorescence intensity at two different wavelengths thus provide in build correction for quantification. For example, Ghosh *et. al.* reported one of the first ratiometric NIR probe **16** for selective detection of aminothiols (Fig. 1.8 B).[47] Song *et. al.* reported ratiometric fluorescent probe **17** in which selective sensing of Cys resulted decrease in emission intensity at 590 nm gradually with increase in emission intensity at 485 nm (Figure 1.8 C).[48] In ratiometric probes, it is generally difficult to predict the spectral shifts during sensing of the analyte. When wavelength shifts in emission spectrum are not significant, these probes are not preferred for in *vivo* applications.

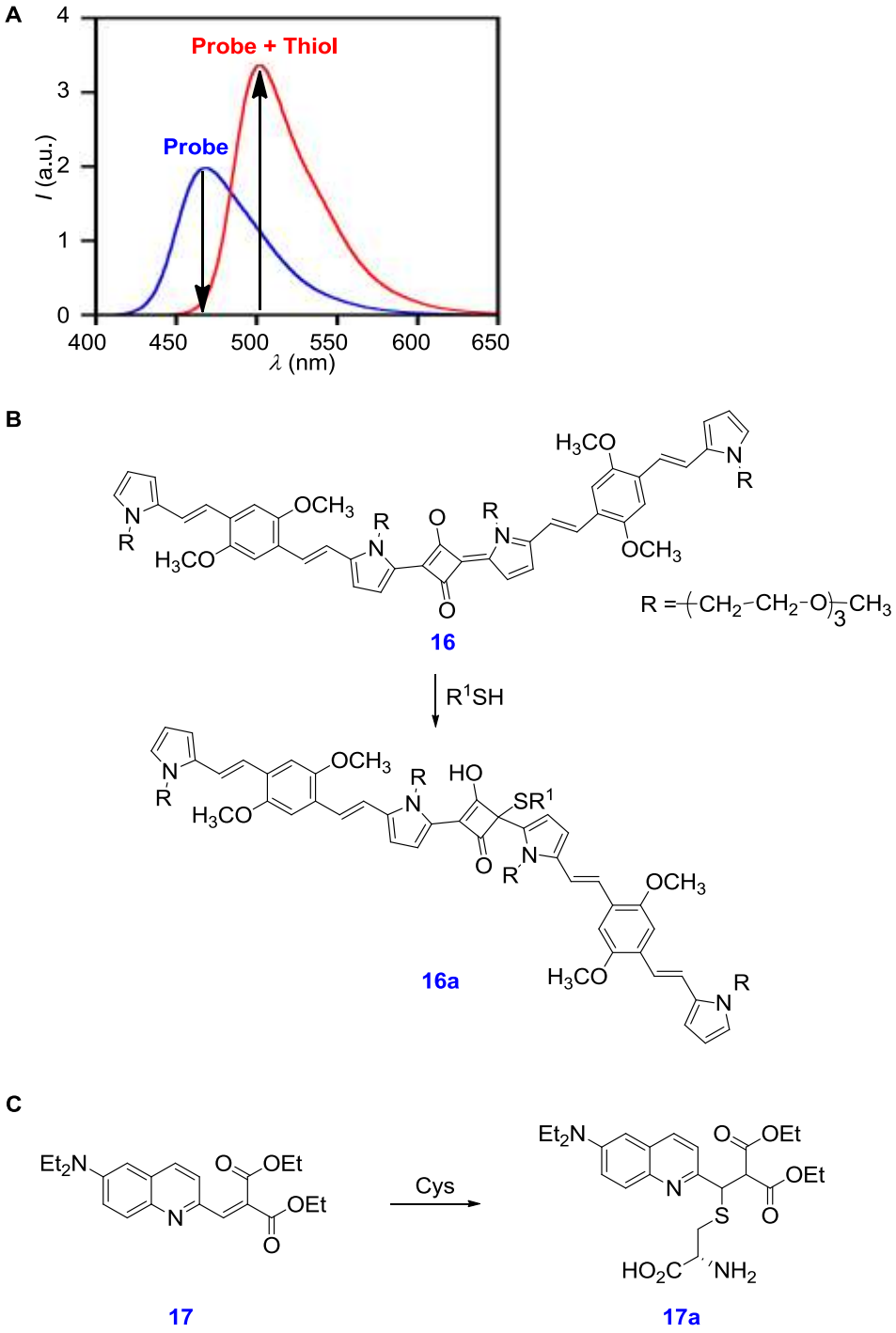

Figure 1.8: (**A**) Representative emission diagram and (**B** and **C**) examples for ratiometric fluorescent thiol probes.

(b) Förster resonance energy transfer (FRET) based probes

In FRET based probes, two fluorophores *i.e.* acceptor and donor are linked by small covalent spacer. FRET-based probes are normally composed of two chromophores;

hence, their synthesis is more complicated compared to that of single-chromophore probes. The efficiency of FRET based probes largely depends on through-space energy transfer efficiencies which indeed depend on several factors, including (i) spectral overlap of the donor emission with the acceptor absorption (ii) distance between the donor and the acceptor (iii) the orientation factors and (iv) the effectiveness of alternative de-excitation modes.[49] Yuan *et. al.* reported FRET based probe **18** in which BODIPY was used as FRET donor while Rhodamine was used as FRET acceptor (Figure 1.9).[50]

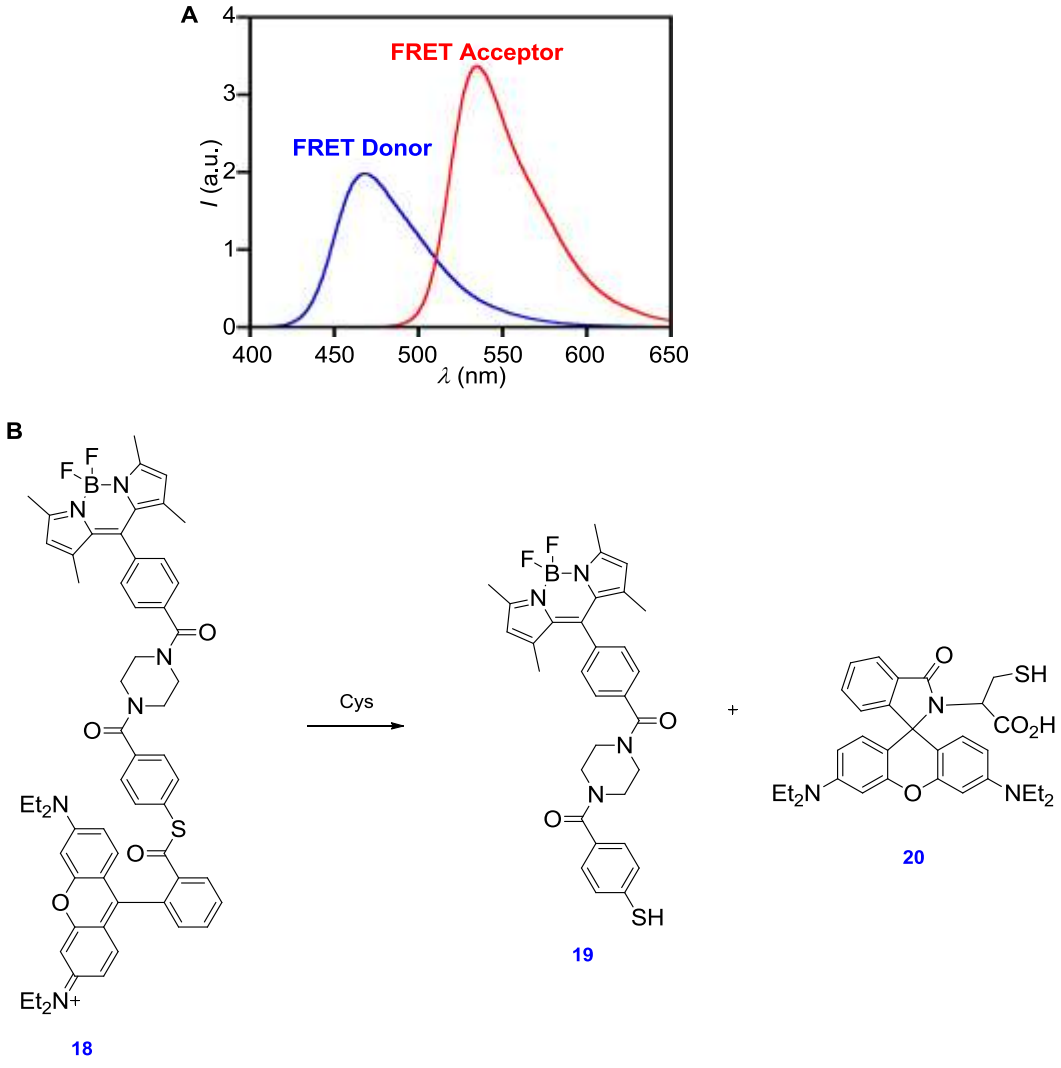

Figure 1.9: (**A**) Representative emission diagram and (**B**) example for FRET based fluorescent thiol probe.

(c) Fluorescence turn-*Off* probes

In fluorescence turn- *Off* probes, fluorescence intensity decreases upon sensing of analyte. Therefore, these probes are not suitable for quantitative detection of analytes/species of interest because fluorescence quenching can also be non selective process. Das *et. al.* reported fluorescence turn-*Off* **21** for sensing of thiols (Figure 1.10).[51]

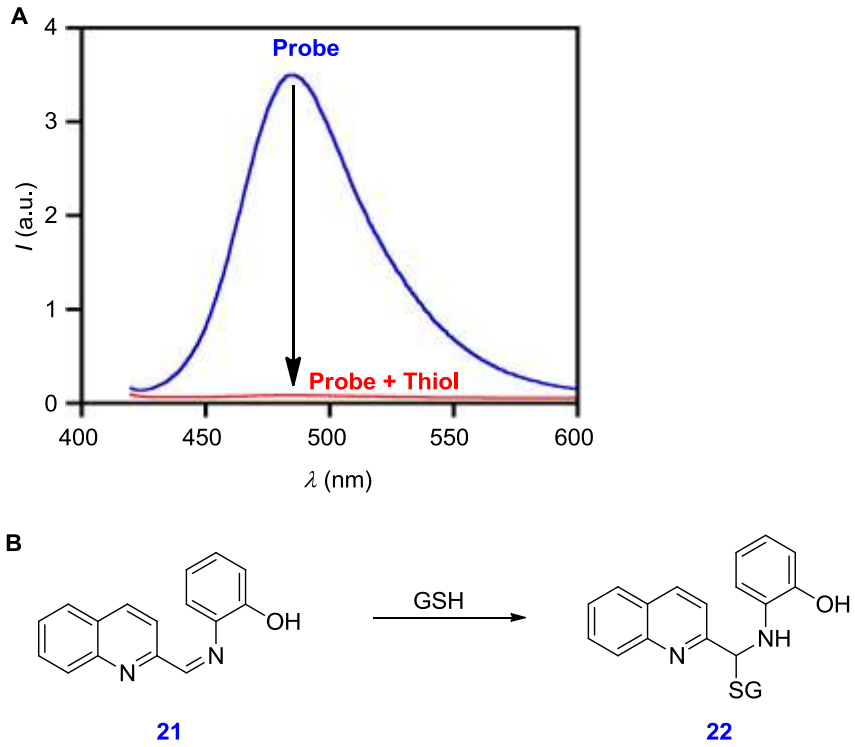

Figure 1.10: (**A**) Representative emission diagram and (**B**) example of fluorescence turn-*off* thiol probe.

(d) Fluorescence turn-*On* probes

In fluorescence turn-*On* probes fluorescence intensity increases upon sensing of analyte. These probes are preferred, because lower background fluorescence provides higher accuracy and if the fluorescence change is proportional to the concentration of analyte, the amount of analyte/species can be quantified. Moreover, fluorescence turn-*On* probes are widely used in live cell imaging because formation of fluorescent product from non-fluorescent probe occurs in the sensing event. Nagano *et. al.* reported photoinduced electron transfer (PET) based fluorescence turn-*On* probe **23** for selective sensing of thiols.[52] Wang *et. al.* reported intramolecular charge transfer (ICT) based fluorescence turn-*On* probe **25** for selective sensing of thiophenol (Figure 1.11).[31a]

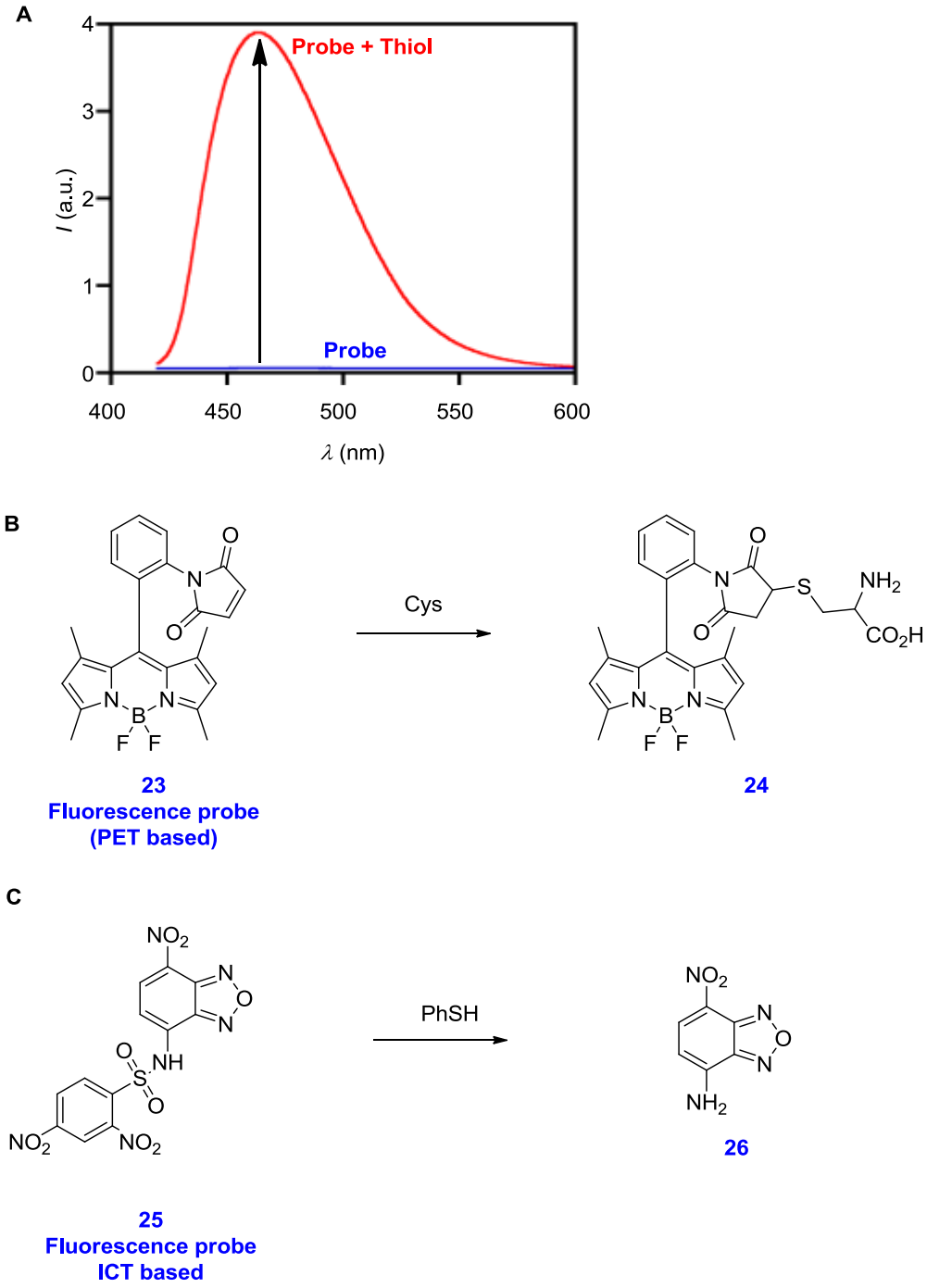

Figure 1.11: (**A**) Representative emission diagram; (**B**) and (**C**) examples of fluorescence turn-*on* thiol probe.

1.6.2. Design principles and Sensing Mechanism of turn-*On* probes

In the design of a fluorescence turn-*On* probe, a fluorophore is attached to a suitable moiety (quencher) capable of reacting selectively with thiols (Figure 1.12). This state is termed as "Fluorescence-*Off*" state of the probe. Reaction with thiol results in the

strong fluorescence of the resultant species. This state is termed as "Fluorescence-*On*" state of the probe. One strategy of sensing involves thiol mediated cleavage of the quencher releasing free fluorophore (path a). Alternately, chemical reaction of thiol with quencher leads to destruction of its quenching ability (path b). In both processes formation of strong fluorescent product leads to "Fluorescence-*On*" state.

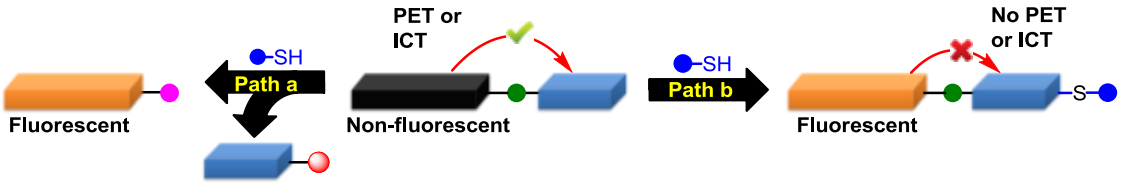

Figure 1.12: Schematic diagram illustrating fluorescence turn-*On* pathways upon selective detection of thiols.

The fluorescence of the probe was quenched by various pathways. Amongst these, photoinduced electron transfer (PET) and intramolecular charge transfer (ICT) are most extensively studied pathways.

1.6.2a Photoinduced electron transfer (PET)

Photoinduced electron transfer (PET) is often the pathway of fluorescence quenching. The PET is classified as either reductive PET or oxidative PET depending upon the direction of flow of electron between fluorophore and quencher.[53] The Oxidative PET process occurs when a fluorophore is attached to an electron deficient quencher. Maleimide and dinitrobenzenesulfonyl are frequently used electron deficient thiol recognising moieties. Oxidative PET is expected pathway for quenching of fluorescence in these probes. This mechanism is also termed as "donor-excited photoinduced electron transfer, (d-PeT)." Oxidative PET can be represented according to Equation (1):

$$^{1}F^{*} + Q \rightarrow F^{\bullet+} + Q^{\bullet-} \qquad \text{(Equation 1)}$$

where $^{1}F^{*}$ (F = fluorophore) denotes the singlet-excited fluorophore and Q (Q = Quencher) stands for the electron-deficient quencher. In oxidative PET, the fluorophore is oxidised whereas the quencher is reduced.

When the fluorophore serves as the electron donor, the LUMO (lowest unoccupied molecular orbital) of the fluorophore should be higher than the LUMO of the quencher so that an electron from the fluorophore can be transferred to the quencher and fill its

unoccupied LUMO (Figure 1.13). This opens a nonluminescent deactivation channel to the excited fluorophore, fluorescence quenching occurs and the probe becomes nonfluorescent or weakly fluorescent (i.e., the sensor is in the fluorescence '*Off*' state).

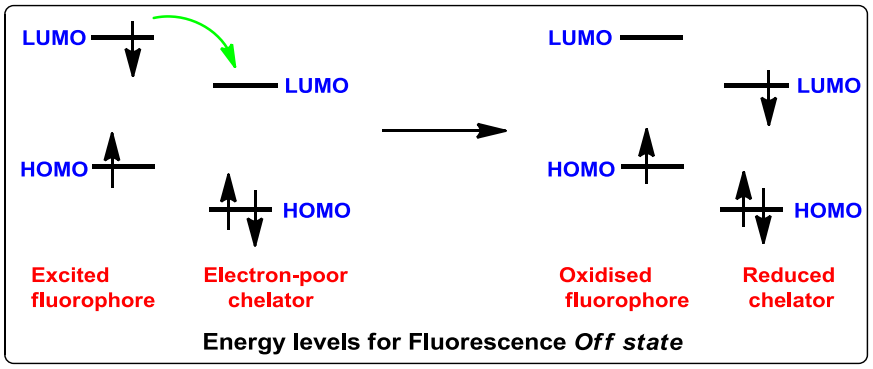

Figure 1.13: Molecular orbital (MO) diagram illustrating the Oxidative PET for fluorescent probe in '*Off*' state.

Sensing of thiol higher the LUMO so that electron transfer from the attached fluorophore is slowed down (or even switched *Off*) and fluorescence is turned '*On*' (Figure 1.14). For example, in case of probe **19,** the fluorescence of the unreacted probe was strongly quenched due to PET mechanism where in excited state BODIPY fluorophore was electron donor and the maleimide moiety was an electron acceptor.

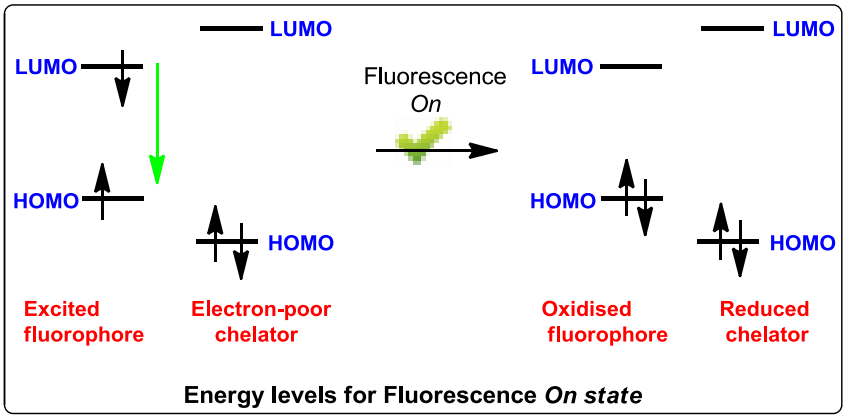

Figure 1.14: Molecular orbital (MO) diagram illustrating the Oxidative PET for fluorescent probe in '*On*' state.

1.6.2b Intramolecular charge transfer (ICT)

Intramolecular charge transfer (ICT) is also an electron transfer process. ICT process occurs within the same electronic system or between systems with a high level of electronic conjugation between the partners. The electronic states achieved in this reaction

are not 'charge-separated' but 'charge-polarized' states. Still, they are the localized states with distinct energy minima.

Fluorophore in which an electron donating (such as amino, methoxy) group is conjugated to an electron withdrawing group undergoes intramolecular charge transfer from the donor to the acceptor upon photo excitation.[53] The most important distinction between PET and ICT based probes lies in the different fluorescence response upon analyte sensing. PET probes display fluorescence enhancement or quenching without significant spectral shifts. Therefore the terms '*Off–On*' and '*On–Off*' are often used for probes involving PET pathways. The absence of spectral shift upon sensing the analyte rules out ratiometric measurements at two different wavelengths. In contrast, probes in which ICT was involved show clear fluorescence band shifts upon analyte sensing. Therefore ratiometric measurements are possible for ICT based probes. For example, ICT based probe **20** is non-fluorescent due to the masking of electron donating amine by dinitrobenzenesulfonyl group, which blocks the ICT process.[31a] Thiophenol mediated cleavage of the dinitrobenzenesulfonyl group restored the ICT pathway and resulted in strong fluorescence.

1.7 Types of probes according to mechanism of reaction with thiols

Various quenchers such as maleimide, 2, 4-dinitrobenzenesulphonyl (DNs), α, β-unsaturated compounds, *etc.* have been reported as specific reaction sites for selective sensing of thiols. Depending on the reaction site employed in the design, fluorescence turn-*On* probes can be classified as:

1.7.1 Probes based on thiol mediated cleavage of sulfonamide and sulfonate esters

1.7.2 Probes based on Michael addition to maleimides

1.7.3 Probes based on Michael addition to α,β-unsaturated compounds

1.7.4 Probes based on Michael addition/cyclization to α,β-unsaturated carbonyl compounds

1.7.5 Probes based on cyclization of thiols with aldehydes

1.7.6 Probes based on cleavage of disulfide bonds by thiols

1.7.7 Probes based on nucleophilic substitution by thiols

1.7.1 Probes based on thiol mediated cleavage of sulfonamide and sulfonate esters

Aromatic nucleophilic substitution (SNAr) of sulfonate esters and amides has been used for the development of fluorescent turn-*On* probes for the detection of thiols. Thiol mediated cleavage of sulfonate ester or sulfonamide releases the active fluorophore with the formation of sulphur dioxide (Figure 1.15). First example of thiol specific fluorescent probe **27** using 2, 4-dinitrobenzenesulfonyl group as quencher was reported by Maeda *et. al*. in 2005.[54] Probe **27** undergoes biothiols mediated cleavage of DNs to release fluorophore. Biothiols did not react with probes **28** and **29**. These probes undergo thiophenol mediated cleavage of DNs to release fluorophore and thereby discriminate thiophenol from aliphatic thiols.[31a,55]

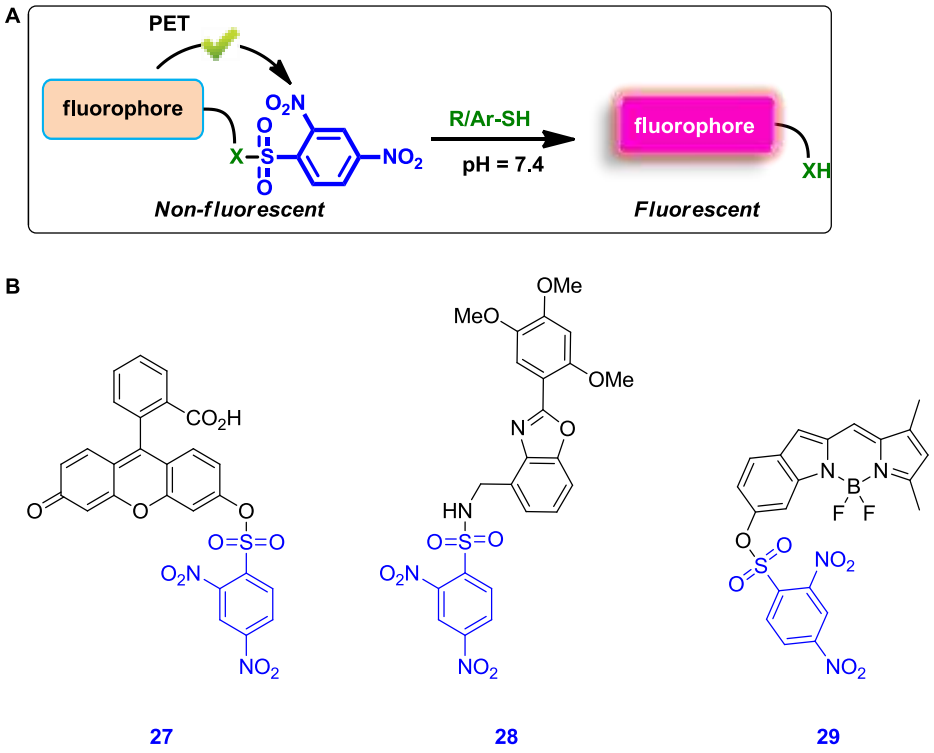

Figure 1.15: (**A**) Schematic diagram illustrating fluorescence turn-*On* mechanism of DNs bearing probes and (**B**) Structures of fluorescent probes **27 – 29** for selective detection of thiols.

1.7.2 Probes based on Michael addition of thiols to maleimide

Maleimide is an excellent functional group used for labelling of proteins through thiol group. Michael addition of thiols across double bond of maleimide results in the formation of thioether formation. Amines are inert towards maleimide under physiological

conditions. This feature was used in the development of *Off-On* fluorescent probes for selective detection of biothiols (Figure 1.16).

In 1970, Kanaoka reported pioneering work regarding fluorescence turn-*On* probe **30** for thiols in which maleimide moiety was utilized as reaction site for thiols (Figure 1.16).[56] Since then many fluorescent probes including **31 – 33** for selective detection of biothiols were reported based on this strategy.[57]

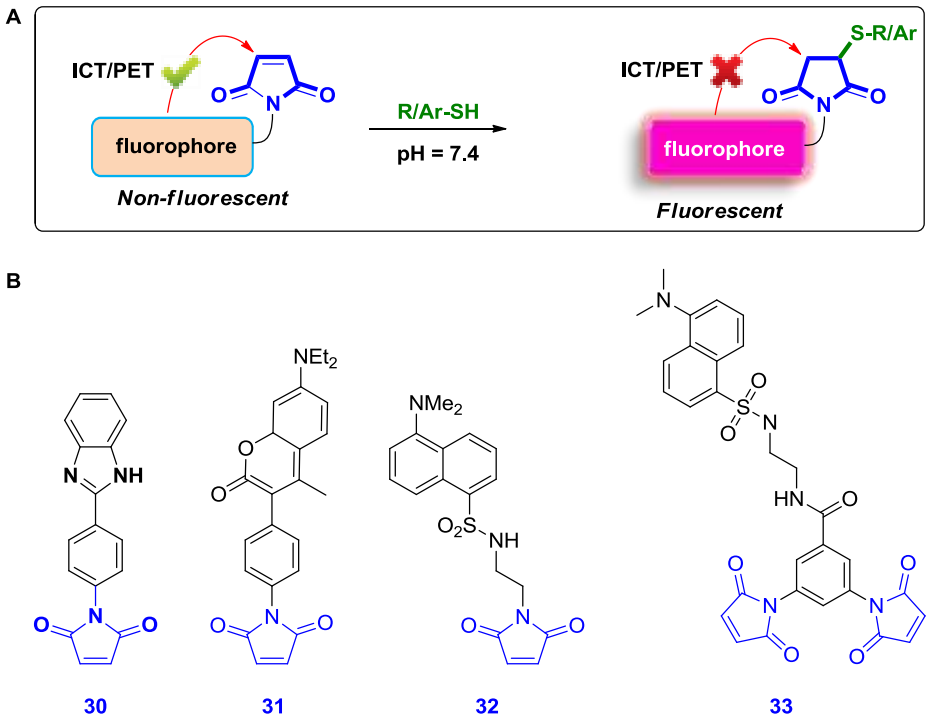

Figure 1.16: (**A**) Schematic diagram illustrating fluorescence turn-*On* mechanism of maleimide bearing probes and (**B**) Structures of fluorescent probes **30 – 33** for selective detection of thiols.

1.7.3 Based on Michael addition to α,β-unsaturated compounds

Apart from maleimides, various other derivatives of α,β-unsaturated moieties have been widely used in nucleophilic addition of sulfhydryl groups. When an alkene group is connected to an electron withdrawing group, a Michael addition can take place in the presence of nucleophilic thiols. Using this approach, several alkenes connected to electron-withdrawing groups such as cyano, nitro, and carbonyl group have been reported in thiol sensing probes **34 – 36** for biothiols (Figure 1.17).[58]

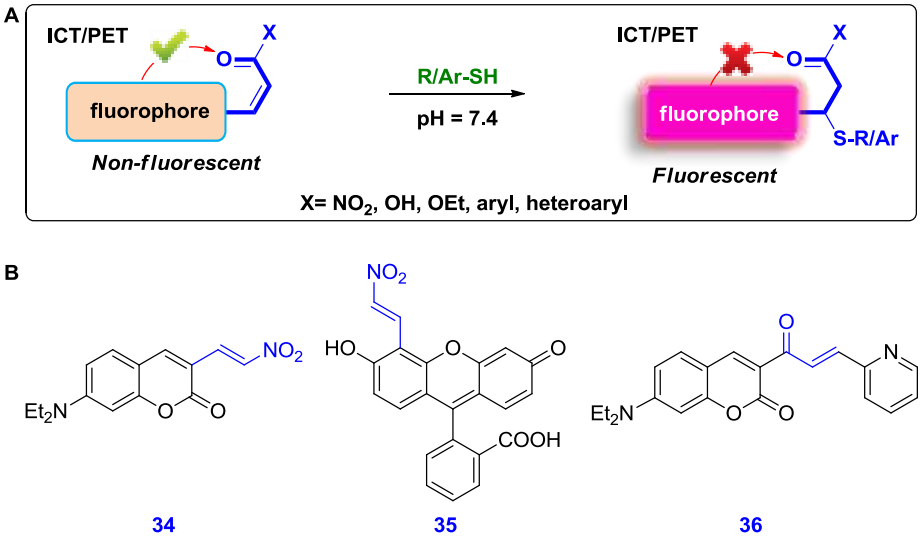

Figure 1.17: (**A**) Schematic diagram illustrating fluorescence turn-*On* mechanism of *α, β*-unsaturated groups bearing probes and (**B**) Structures of fluorescent probes **34 – 36** for selective detection of thiols.

1.7.4 Based on Michael addition/cyclization to α, β-unsaturated carbonyl compounds

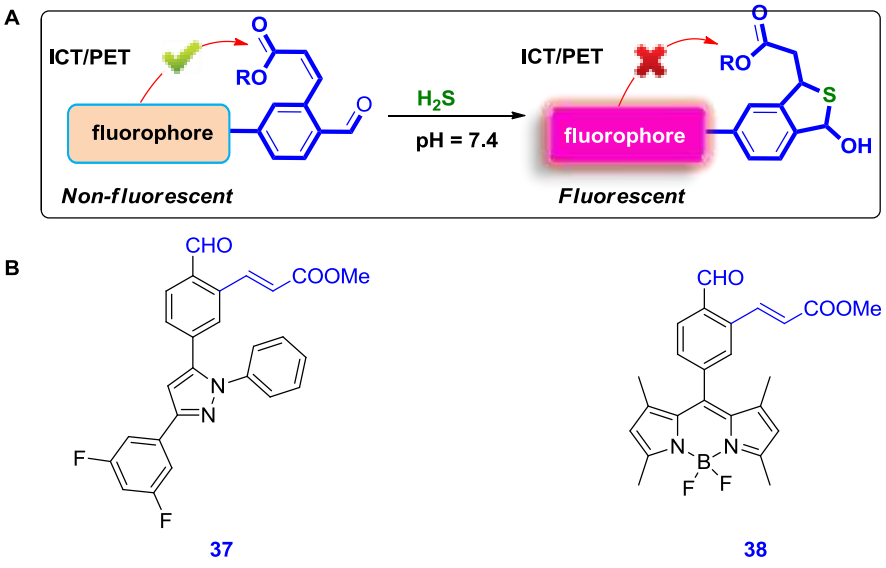

Figure 1.18: (**A**) Schematic diagram illustrating fluorescence turn-*On* mechanism and (**B**) Structures of probes **37** and **38** based on Michael addition/cyclization for selective detection of H_2S.

Reaction of thiols with *α, β*-unsaturated carbonyl compounds involves 1,4-addition to form thioether followed by cyclization with carbonyl group to form a lactams and

release the active fluorophores (Figure 1.18). The differences in ring-formation kinetics allow spectral or kinetic modes to be used to separately identify Cys and Hcy. Using this approach several probes including probes **37** and **38** are reported.[59]

1.7.5 Based on cyclization with aldehydes

Aldehydes can form a rapid 5- or 6-membered ring with Hcy and Cys respectively, while GSH cannot form such thiazinanes/thiazolidine rings (Figure 1.19). Recently, based on this 1, 1-addition reactions of thiols fluorescent probes **39 – 41** for thiol detection are reported.[60]

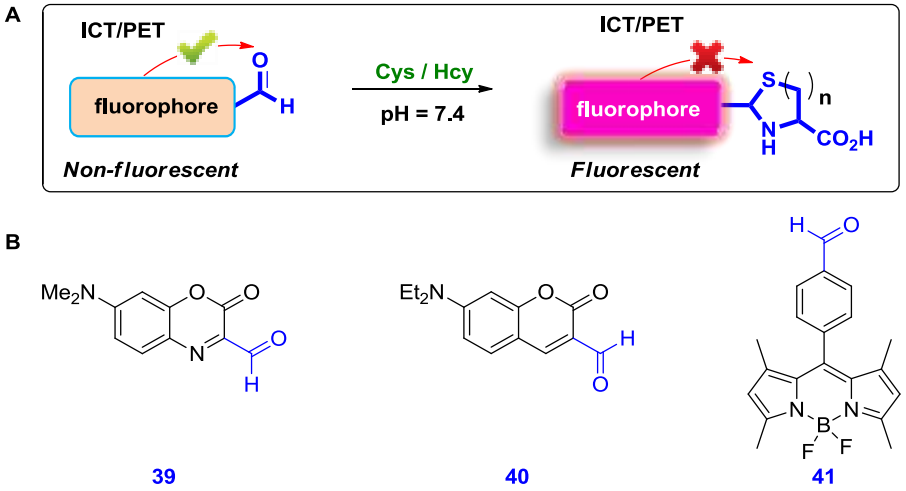

Figure 1.19: (**A**) Schematic diagram illustrating fluorescence turn-*On* mechanism and (**B**) Structures of fluorescent probes **39 – 41** based on cyclization of thiols with aldehydes.

1.7.6 Based on cleavage of disulfide bonds by thiols

Reaction of thiols can trigger the cleavage of disulfide-bonds. Based on this strategy fluorescent probes **42** and **43** were reported for selective detection of GSH (Figure 1.20).[61]

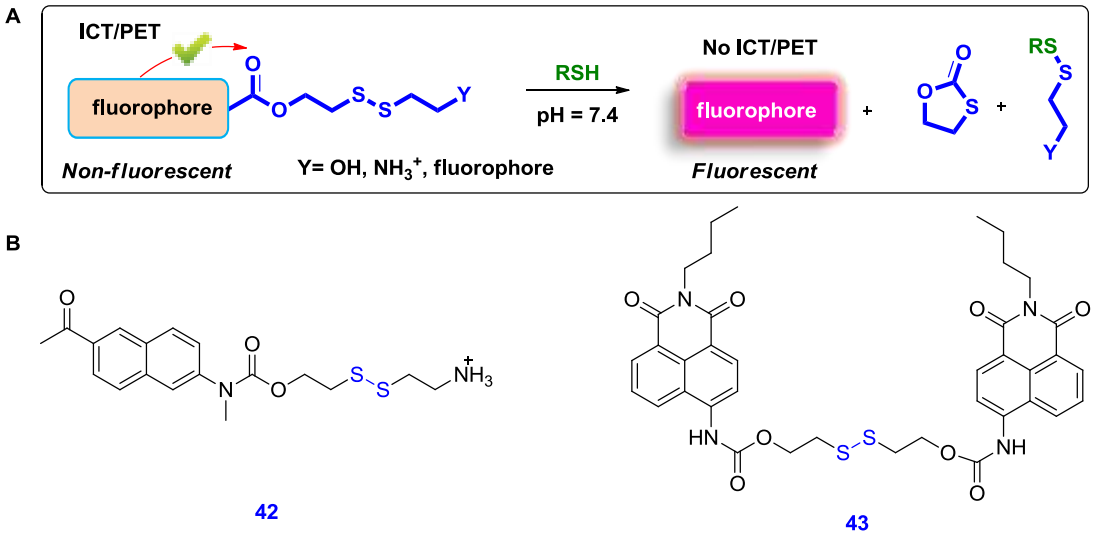

Figure 1.20: (**A**) Schematic diagram illustrating fluorescence turn-*On* mechanism and (**B**) Structures of fluorescent probes **42** and **43** based on cleavage of disulfides by thiols.

1.7.7 Based on aromatic nucleophilic substitution by thiols followed by Smiles rearrangement

Niu *et al*. recently reported two BODIPY-based fluorescence probes **44** and **45**, which could discriminate amongst biothiols *i.e.* Cys, Hcy and GSH (Figure 1.21). In case of probe **44** which is selective for GSH, the chlorine of the monochlorinated BODIPY could be rapidly displaced by the thiolate of biothiols through thiol–halogen nucleophilic substitution. For probe **45** which is selective for Cys/Hcy, 4-Nitro phenoxy group of the BODIPY was displaced by the thiolate of biothiols through thiol–halogen nucleophilic substitution. The amino groups of Cys/Hcy, but not GSH, could further replace the thiolate to form an amino-substituted probe. Based on the differences in absorption and emission properties of amine conjugated BODIPY and thiol conjugated BODIPY the selectivity amongst biological thiols was achieved.[62]

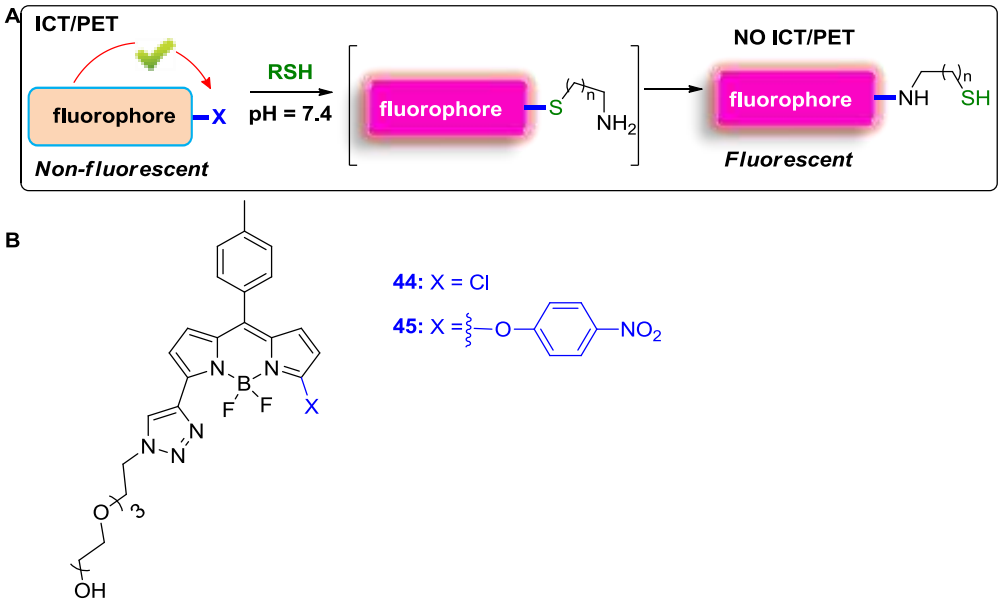

Figure 1.21: (**A**) Schematic diagram illustrating fluorescence turn-*On* mechanism and (**B**) Structures of fluorescent probes **44** and **45** based on nucleophilic substitution of thiols.

1.8 Fluorescent probes for H_2S

Fluorescent probes for selective detection of H_2S are based on different reaction mechanism than those used for biothiols and aromatic thiols. Based on the reaction mechanism involved, reported fluorescent probes for selective H_2S detection can be classified in two types:

1.6.3. Probes based on single step reaction mechanism

1.6.4. 1.8.2 Probes based on cascade reaction mechanism

1.8.1 Probes based on single step reaction mechanism

The pioneering approach involving mediated reduction of azide to amine in fluorescent probe **1** and **2** were reported independently by Chang[63] and Wang[64] respectively, nearly at the same time. Since then, several fluorescent probes including **48** – **51** have been reported based on this concept by changing the fluorophores[39,63-65] (Figure 1.22).

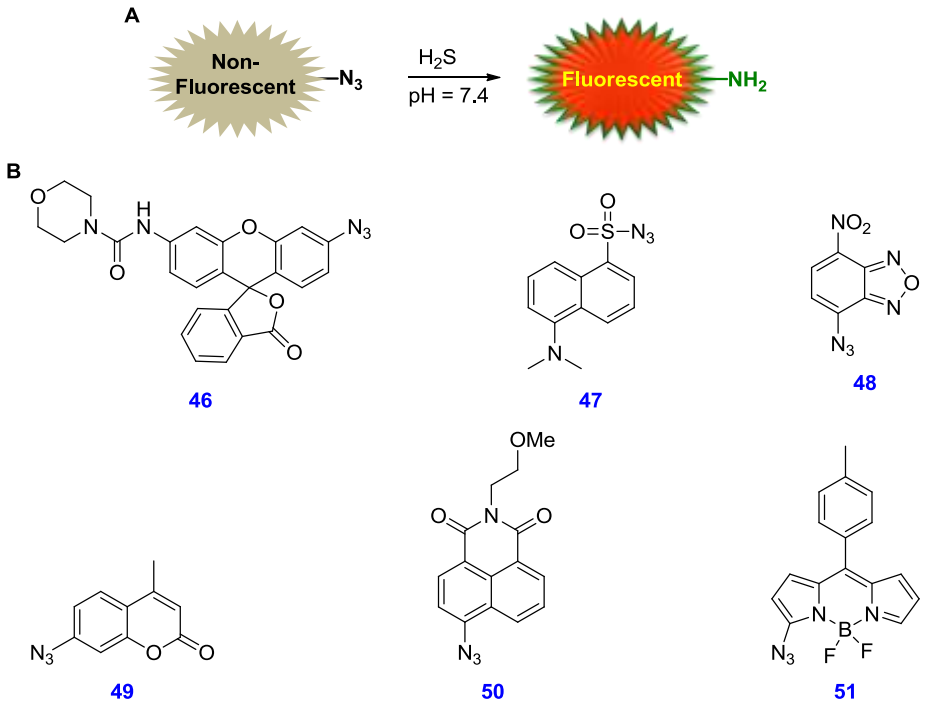

Figure 1.22: (**A**) Schematic diagram for H_2S mediated azide reaction based fluorescence *turn-On* strategies and (**B**) structures of reported probes **46** – **51** for H_2S Sensing.

1.8.2 Probes based on cascade reaction mechanism

Qian and coworkers reported BODIPY based probes in which α,β-unsaturated aldehyde was used as H_2S trapping site.[66] Xian and coworkers developed probes **52**, **55a** and **55b** for sensing of H_2S using nucleophilic substitution and addition strategies, respectively.[5,67] In probe **52**, 2-pyridinyl disulfide and an ester group was employed as two electrophilic sites for reaction of H_2S. Probes **55a** and **55b** were based on Michael addition followed by cyclization to release active fluorophore (Figure 1.23).

Fluorescence *Off-On* probes **52**, **55a** and **55b** exhibited long response times, ranging from 30 to 60 min (Table 4.1) and may not be suitable for monitoring the intracellular level of the species due to high fluctuations in endogenous free H_2S concentration.[68] Qian and coworkers developed probes **57** and **59** in which an aromatic framework substituted by α, β-unsaturated acrylate methyl ester and aldehyde (–CHO) ortho to each other. The aldehyde group reacts readily and reversibly with free sulphide to form a hemithioacetal intermediate which undergoes to a Michael addition to the proximal acrylate to yield a trapped thioacetal. This tandem reaction tunes photoinduced electron transfer of the aromatic system, thus potentially affecting fluorescence of a conjugated

fluorophore. As reversible addition of a thiol to the same aldehyde yields a thioacetal that cannot perform the subsequent Michael addition step, the intermediate simply decomposes to yield the original probe, thus it did not significantly interfere in sulphide detection. The utility of these probes in enzymatic H_2S quantification and cell-based imaging applications was also demonstrated.

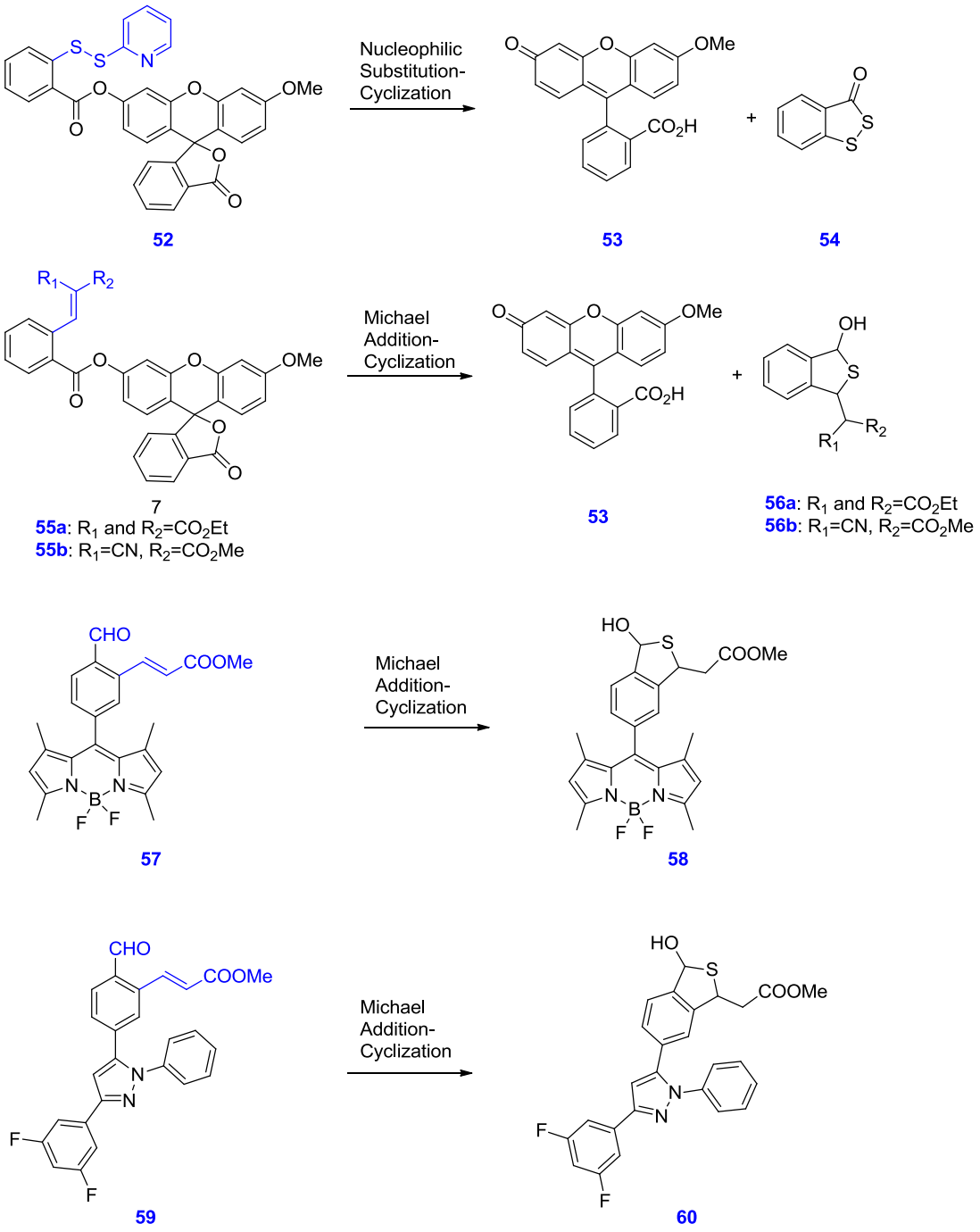

Figure 1.23: Reported cascade reaction based fluorescence *turn-On* probes for H_2S Sensing.

1.9 Research outlook

Although large numbers of fluorescent probes are reported for the detection of thiols, there is wide scope to develop new fluorescent probes with better photophysical properties such as excitation and emission in visible region, good water solubility and improved cell permeability. In this context, we were interested in design and develop new fluorescent probes for selective detection of biothiols, thiophenols and H_2S. With this primary goal in mind, we were also interested in the rational design of fluorescent probes which can discriminate amongst biothiols and fluorescent probes capable of targeting specific cell organelle and selectively detect thiol levels in particular cell component. We aimed to predict fluorescence '*Off*' and '*On'* states of probes using theoretical calculations prior to synthesis of the probes.

For potential application of fluorescent probes for detection of thiols in live cell systems, biological and environmental samples, in the design criteria we tried to address following points:

(a) Excitation and emission wavelengths of probe should be in the visible or Near IR (NIR) region.

(b) Probes should be soluble in aqueous solutions.

(c) Probes should show faster response.

(d) Probes should be highly selective for the target molecule or organelle.

(e) Probes should be resistant enough to photochemical degradation under normal illumination conditions to permit the target cell feature to be visualized conveniently.

(f) After sensing of thiols releasing fluorophore should have a high quantum yield for fluorescence, so that only small amounts of the probes are needed to visualize the cell target of interest.

(g) Stokes shifts should be large to minimize problems from light scattering by the cell.

(h) Probes should be preferably easy to make from readily available, inexpensive starting materials, and chemically stable to permit long-term storage.

1.10 References

(1) (a) Dondoni, A.; Marra, A. *Chem. Soc. Rev.* **2012**, *41*, 573(b) Chatani, S.; Nair, D. P.; Bowman, C. N. *Polym. Chem.* **2013**, *4*, 1048(c) Wasserberg, D.; Nicosia, C.; Tromp, E. E.; Subramaniam, V.; Huskens, J.; Jonkheijm, P. *J. Am. Chem. Soc.* **2013**, *135*, 3104(d) Onbulak, S.; Tempelaar, S.; Pounder, R. J.; Gok, O.; Sanyal, R.; Dove, A. P.; Sanyal, A. *Macromolecules* **2012**, *45*, 1715(e) Zheng, J. S.; Tang, S.; Qi, Y. K.; Wang, Z. P.; Liu, L. *Nat. Protoc.* **2013**, *8*, 2483(f) Cramer, N. B.; Couch, C. L.; Schreck, K. M.; Boulden, J. E.; Wydra, R.; Stansbury, J. W.; Bowman, C. N. *Dent. Mater.* **2010**, *26*, 799(g) Summers, F. A.; Forsman-Quigley, A.; Hawkins, C. L. *Biochem. Biophys. Res. Commun.* **2012**, *425*, 157(h) Kondo, T.; Mitsudo, T. *Chem. Rev.* **2000**, *100*, 3205(i) Massi, A.; Nanni, D. *Org. Biomol. Chem.* **2012**, *10*, 3791(j) Meyer, B. *Chem. Rev.* **1976**, *76*, 367.

(2) (a) Tam, J. P.; Lu, Y. A.; Liu, C. F.; Shao, J. *Proc. Natl. Acad. Sci. U. S. A.* **1995**, *92*, 12485(b) Fang, G. M.; Wang, J. X.; Liu, L. *Angew. Chem., Int. Ed.* **2012**, *51*, 10347(c) Crich, D.; Banerjee, A. *J. Am. Chem. Soc.* **2007**, *129*, 10064(d) Fang, G. M.; Li, Y. M.; Shen, F.; Huang, Y. C.; Li, J. B.; Lin, Y.; Cui, H. K.; Liu, L. *Angew. Chem., Int. Ed.* **2011**, *50*, 7645(e) Markey, L.; Giordani, S.; Scanlan, E. M. *J. Org. Chem.* **2013**, *78*, 4270(f) Pollock, S. B.; Kent, S. B. H. *Chem. Commun.* **2011**, *47*, 2342(g) Ding, H.; Shigenaga, A.; Sato, K.; Morishita, K.; Otaka, A. *Org. Lett.* **2011**, *13*, 5588(h) Dawson, P. E.; Kent, S. B. H. *Annu. Rev. Biochem.* **2000**, *69*, 923(i) Dawson, P. E.; Muir, T. W.; Clark-Lewis, I.; Kent, S. B. H. *Science* **1994**, *266*, 776.

(3) (a) Silveira, C. C.; Mendes, S. R.; Líbero, F. M. *Synlett* **2010**, 790(b) Bichler, P.; Love, J. A. *Top. Organomet. Chem.* **2010**, *31*, 39.

(4) Beletskaya, I. P.; Ananikov, V. P. *Chem. Rev.* **2011**, *111*, 1596.

(5) Liu, C.; Pan, J.; Li, S.; Zhao, Y.; Wu, L. Y.; Berkman, C. E.; Whorton, A. R.; Xian, M. *Angew. Chem., Int. Ed.* **2011**, *50*, 10327.

(6) Dickinson, D. A.; Forman, H. J. *Biochem. Pharmacol.* **2002**, *64*, 1019.

(7) (a) Jung, H. S.; Chen, X.; Kim, J. S.; Yoon, J. *Chem. Soc. Rev.* **2013**, *42*, 6019(b) Hwang, C.; Sinskey, A.; Lodish, H. *Science* **1992**, *257*, 1496.

(8) (a) Yang, Y.; Zhao, Q.; Feng, W.; Li, F. *Chem. Rev.* **2012**, *113*, 192(b) Chen, X.; Zhou, Y.; Peng, X.; Yoon, J. *Chem. Soc. Rev.* **2010**, *39*, 2120.

(9) Prakash M, S. M., Tilak P, Anwar N. *Online J Health Allied Scs* **2009**, *8*, 8.

(10) Wu, G.; Fang, Y.-Z.; Yang, S.; Lupton, J. R.; Turner, N. D. *J. Nutr.* **2004**, *134*, 489.

(11) Meredith, M. J.; Reed, D. J. *J. Biol. Chem.***1982**, *257*, 3747.

(12) C. K. Mathews, K. E. v. H., K. G. Ahern *Biochemistry, Addison-Wesley Publishing Company, San Francisco* **2000**.

(13) Ferna´ndez-Checa J, L. S., Ookhtens M,; DeLeve L, R. M. *The Regulation of Hepatic Glutathione. In:Hepatic Anion Transport and Bile Secretion: Physiology and Pathophysiology, Tavoloni N, Berk PD, eds, Marcel Dekker, New York.* **1992**, 363.

(14) Dalton, T. P.; Shertzer, H. G.; Puga, A. *Annu. Rev. Pharmacol. Toxicol.* **1999**, *39*, 67.

(15) Wang, X. F.; Cynader, M. S. *J. Neurosci.* **2001**, *21*, 3322.

(16) (a) Lipton, S. A.; Choi, Y.-B.; Takahashi, H.; Zhang, D.; Li, W.; Godzik, A.; Bankston, L. A. *Trends Neurosci* **2002**, *25*, 474(b) Peng, H.; Chen, W.; Cheng, Y.; Hakuna, L.; Strongin, R.; Wang, B. *Sensors* **2012**, *12*, 15907.

(17) (a) Mansoor, M. A.; Svardal, A. M.; Ueland, P. M. *Anal. Biochem.* **1992**, *200*, 218(b) Giustarini, D.; Dalle-Donne, I.; Lorenzini, S.; Milzani, A.; Rossi, R. *J. Gerontol. A Biol. Sci. Med. Sci.* **2006**, *61*, 1030(c) Dalle-Donne, I.; Milzani, A.; Gagliano, N.; Colombo, R.; Giustarini, D.; Rossi, R. *Antioxid. Redox Signaling* **2008**, *10*, 445.

(18) Jones, D. P.; Carlson, J. L.; Mody Jr, V. C.; Cai, J.; Lynn, M. J.; Sternberg Jr, P. *Free Radical Biol. Med.* **2000**, *28*, 625.

(19) Shahrokhian, S. *Anal. Chem.* **2001**, *73*, 5972.

(20) Selhub, J. *Annu. Rev. Nutr.* **1999**, *19*, 217.

(21) Seshadri, S.; Beiser, A.; Selhub, J.; Jacques, P. F.; Rosenberg, I. H.; D'Agostino, R. B.; Wilson, P. W. F.; Wolf, P. A. *N. Engl. J. Med.* **2002**, *346*, 476.

(22) Refsum, H.; Ueland, P. M.; Nygard, O.; Vollset, S. E. *Annu. Rev. Med.* **1998**, *49*, 31.

(23) (a) Savage, D. G.; Lindenbaum, J.; Stabler, S. P.; Allen, R. H. *Am. J. Med.* **1994**, *96*, 239(b) Klee, G. G. *Clin. Chem.* **2000**, *46*, 1277.

(24) Cashman Kevin, D. *Nut. Rev.* **2005**, *63*, 29.

(25) Townsend, D. M.; Tew, K. D.; Tapiero, H. *Biomed. Pharmacother.* **2003**, *57*, 145.

(26) (a) Shimada, K.; Mitamura, K. *J. Chromatogr., B: Biomed. Sci. Appl.* **1994**, *659*, 227(b) Love, J. C.; Estroff, L. A.; Kriebel, J. K.; Nuzzo, R. G.; Whitesides, G. M. *Chem. Rev.* **2005**, *105*, 1103.

(27) Shirokov, Y. G. *Kauchuk i Rezina* **1959**, *18*, 43.

(28) Schwarzbauer, J.; Heim, S.; Brinker, S.; Littke, R. *Water Research* **2002**, *36*, 2275.

(29) Verma, R. P.; Kapur, S.; Barberena, O.; Shusterman, A.; Hansch, C. H.; Selassie, C. D. *Chem. Res. Toxicol.* **2003**, *16*, 276.

(30) Heil, T. P.; Lindsay, R. C. *J. Environ. Sci. Health. Part. B* **1989**, *24*, 349.

(31) (a) Jiang, W.; Fu, Q.; Fan, H.; Ho, J.; Wang, W. *Angew. Chem., Int. Ed.* **2007**, *46*, 8445(b) *Material safety data sheet of thiophenol from Sigma–Aldrich:http://www.castleviewuk.com/Frameless/Safe/msds/ex/MSDS_thiophenol.htm;* (c) Anon *USA, DangerousProperties of Industrial Materials Report 14, 92.* **1994**.

(32) Guidotti, T. L. *Int. J. Toxicol.* **2010**, *29*, 569.

(33) (a) Boehning, D.; Snyder, S. H. *Annual Review of Neuroscience* **2003**, *26*, 105(b) WANG, R. *The FASEB Journal* **2002**, *16*, 1792.

(34) Koshland, D. *Science* **1992**, *258*, 1861.

(35) Morita, T.; Perrella, M. A.; Lee, M. E.; Kourembanas, S. *Proc. Natl. Acad. Sci. U. S. A.***1995**, *92*, 1475.

(36) Chen, X.; Jhee, K.-H.; Kruger, W. D. *J. Biol. Chem.***2004**, *279*, 52082.

(37) Ishii, I.; Akahoshi, N.; Yu, X.-N.; Kobayashi, Y.; Namekata, K.; Komaki, G.; Kimura, H. *Biochem. J.* **2004**, *381*, 113.

(38) (a) Shibuya, N.; Mikami, Y.; Kimura, Y.; Nagahara, N.; Kimura, H. *J. Biochem.* **2009**, *146*, 623(b) Tanizawa, K. *J. Biochem.* **2011**, *149*, 357.

(39) Montoya, L. A.; Pluth, M. D. *Chem. Commun.* **2012**, *48*, 4767.

(40) Reiffenstein, R. J.; Hulbert, W. C.; Roth, S. H. *Annu. Rev. Pharmacol. Toxicol.* **1992**, *32*, 109.

(41) (a) Ellman, G. L. *Arch. Biochem. Biophys.* **1959**, *82*, 70(b) Komuro, C.; Ono, K.; Shibamoto, Y.; Nishidai, T.; Takahashi, M.; Abe, M. *J. Chromatogr. B: Biomed.*

Sci. Appl. **1985**, *338*, 209(c) Chen, W.; Zhao, Y.; Seefeldt, T.; Guan, X. *J. Pharm. Biomed. Anal.* **2008**, *48*, 1375(d) Ahmed, M. J.; Banoo, S. *Talanta* **1999**, *48*, 1085(e) Amarnath, K.; Amarnath, V.; Amarnath, K.; Valentine, H. L.; Valentine, W. M. *Talanta* **2003**, *60*, 1229.

(42) (a) Elwaer, A. R.; McLeod, C. W.; Thompson, K. C. *Anal. Chem.* **2000**, *72*, 5725(b) Zinellu, A.; Sotgia, S.; Scanu, B.; Usai, M.; Fois, A.; Spada, V.; Deledda, A.; Deiana, L.; Pirina, P.; Carru, C. *Amino Acids* **2009**, *37*, 395.

(43) (a) Burford, N.; Eelman, M. D.; Mahony, D. E.; Morash, M. *Chem. Commun.* **2003**, 146(b) Rafii, M.; Elango, R.; Courtney-Martin, G.; House, J. D.; Fisher, L.; Pencharz, P. B. *Anal. Biochem.* **2007**, *371*, 71.

(44) Wen, M.; Liu, H.; Zhang, F.; Zhu, Y.; Liu, D.; Tian, Y.; Wu, Q. *Chem. Commun.* **2009**, 4530.

(45) Yin, C.; Huo, F.; Zhang, J.; Martinez-Manez, R.; Yang, Y.; Lv, H.; Li, S. *Chem. Soc. Rev.* **2013**, *42*, 6032.

(46) (a) Chen, X.; Zhou, Y.; Peng, X.; Yoon, J. *Chem. Soc. Rev.* **2010**, *39*, 2120(b) Peng, H.; Chen, W.; Burroughs, S.; Wang, B. *Curr. Org. Chem.* **2013**, *17*, 641.

(47) Sreejith, S.; Divya, K. P.; Ajayaghosh, A. *Angew. Chem., Int. Ed.* **2008**, *47*, 7883.

(48) Wu, Q.-Q.; Xiao, Z.-F.; Du, X.-J.; Song, Q.-H. *Chem. – Asian J.* **2013**, *8*, 2564.

(49) Loudet, A.; Burgess, K. *Chem. Rev.* **2007**, *107*, 4891.

(50) Long, L.; Lin, W.; Chen, B.; Gao, W.; Yuan, L. *Chem. Commun.* **2011**, *47*, 893.

(51) Das, P.; Mandal, A. K.; Reddy G, U.; Baidya, M.; Ghosh, S. K.; Das, A. *Org. Biomol. Chem.* **2013**, *11*, 6604.

(52) Matsumoto, T.; Urano, Y.; Shoda, T.; Kojima, H.; Nagano, T. *Org. Lett.* **2007**, *9*, 3375.

(53) Boens, N.; Leen, V.; Dehaen, W. *Chem. Soc. Rev.* **2012**, *41*, 1130.

(54) Maeda, H.; Matsuno, H.; Ushida, M.; Katayama, K.; Saeki, K.; Itoh, N. *Angew. Chem., Int. Ed.* **2005**, *44*, 2922.

(55) (a) Jiang, W.; Cao, Y.; Liu, Y.; Wang, W. *Chem. Commun.* **2010**, *46*, 1944(b) Zhao, C.; Zhou, Y.; Lin, Q.; Zhu, L.; Feng, P.; Zhang, Y.; Cao, J. *J. Physi. Chem. B* **2010**, *115*, 642.

(56) Y. Kanaoka, M. M., K. Ando T. Sekine *Biochim. Biophys. Acta* **1970**, *207*.

(57) (a) Corrie, J. E. T. *J. Chem. Soc., Perkin Trans. 1* **1994**, 2975(b) Guy, J.; Caron, K.; Dufresne, S.; Michnick, S. W.; Skene; Keillor, J. W. *J. Am. Chem. Soc.* **2007**, *129*, 11969.

(58) (a) Sun, Y.-Q.; Chen, M.; Liu, J.; Lv, X.; Li, J.-f.; Guo, W. *Chem. Commun.* **2011**, *47*, 11029(b) Lin, W.; Yuan, L.; Cao, Z.; Feng, Y.; Long, L. *Chem.- Eur. J.* **2009**, *15*, 5096(c) Wang, H.; Zhou, G.; Mao, C.; Chen, X. *Dyes Pigments* **2013**, *96*, 232.

(59) (a) Qian, Y.; Karpus, J.; Kabil, O.; Zhang, S.-Y.; Zhu, H.-L.; Banerjee, R.; Zhao, J.; He, C. *Nat Commun* **2011**, *2*, 495(b) Yang, X.; Guo, Y.; Strongin, R. M. *Angew. Chem., Int. Ed.* **2011**, *50*, 10690.

(60) (a) Kim, T.-K.; Lee, D.-N.; Kim, H.-J. *Tetrahedron Lett.* **2008**, *49*, 4879(b) Yue, Y.; Guo, Y.; Xu, J.; Shao, S. *New J. Chem.* **2011**, *35*, 61(c) Hu, M.; Fan, J.; Li, H.; Song, K.; Wang, S.; Cheng, G.; Peng, X. *Org. Biomol. Chem.* **2011**, *9*, 980.

(61) (a) Lee, J. H.; Lim, C. S.; Tian, Y. S.; Han, J. H.; Cho, B. R. *J. Am. Chem. Soc.* **2010**, *132*, 1216(b) Zhu, B.; Zhang, X.; Li, Y.; Wang, P.; Zhang, H.; Zhuang, X. *Chem. Commun.* **2010**, *46*, 5710.

(62) (a) Niu, L.-Y.; Guan, Y.-S.; Chen, Y.-Z.; Wu, L.-Z.; Tung, C.-H.; Yang, Q.-Z. *J. Am. Chem. Soc.* **2012**, *134*, 18928(b) Niu, L.-Y.; Guan, Y.-S.; Chen, Y.-Z.; Wu, L.-Z.; Tung, C.-H.; Yang, Q.-Z. *Chem. Commun.* **2013**, *49*, 1294.

(63) Lippert, A. R.; New, E. J.; Chang, C. J. *J. Am. Chem. Soc.* **2011**, *133*, 10078.

(64) Peng, H.; Cheng, Y.; Dai, C.; King, A. L.; Predmore, B. L.; Lefer, D. J.; Wang, B. *Angew. Chem., Int. Ed.* **2011**, *50*, 9672.

(65) (a) Das, S. K.; Lim, C. S.; Yang, S. Y.; Han, J. H.; Cho, B. R. *Chem. Commun.* **2012**, *48*, 8395(b) Wan, Q.; Song, Y.; Li, Z.; Gao, X.; Ma, H. *Chem. Commun.* **2013**, *49*, 502(c) Zhou, G.; Wang, H.; Ma, Y.; Chen, X. *Tetrahedron* **2013**, *69*, 867(d) Chen, B.; Li, W.; Lv, C.; Zhao, M.; Jin, H.; Jin, H.; Du, J.; Zhang, L.; Tang, X. *Analyst* **2013**, *138*, 946(e) Yu, C.; Li, X.; Zeng, F.; Zheng, F.; Wu, S. *Chem. Commun.* **2013**, *49*, 403(f) Saha, T.; Kand, D.; Talukdar, P. *Org. Biomol. Chem.* **2013**, *11*, 8166.

(66) Qian, Y.; Karpus, J.; Kabil, O.; Zhang, S.-Y.; Zhu, H.-L.; Banerjee, R.; Zhao, J.; He, C. *Nat. Commun.* **2011**, *2*, 1506/1.

(67) Liu, C. R.; Peng, B.; Li, S.; Park, C. M.; Whorton, A. R.; Xian, M. *Org. Lett.* **2012**, *14*, 2184.

(68) (a) Furne, J.; Saeed, A.; Levitt, M. D. *Am. J. Physiol. Regul. Integr. Comp. Physiol.* **2008**, *295*, R1479(b) Whitfield, N. L.; Kreimier, E. L.; Verdial, F. C.; Skovgaard, N.; Olson, K. R. *Am. J. Physiol. Regul. Integr. Comp. Physiol.* **2008**, *294*, R1930.

Chapter 2

Design and Synthesis of Fluorescence *Off-On* Probes for Biological Thiols

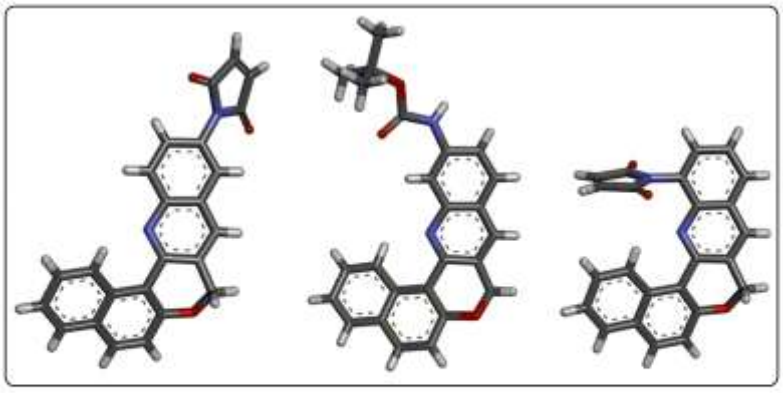

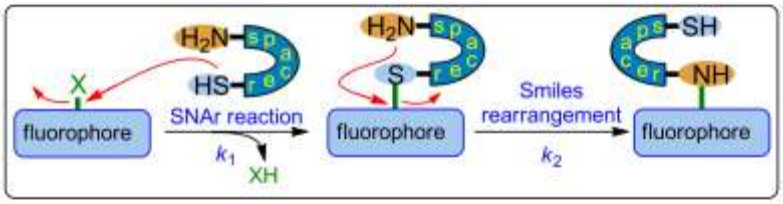

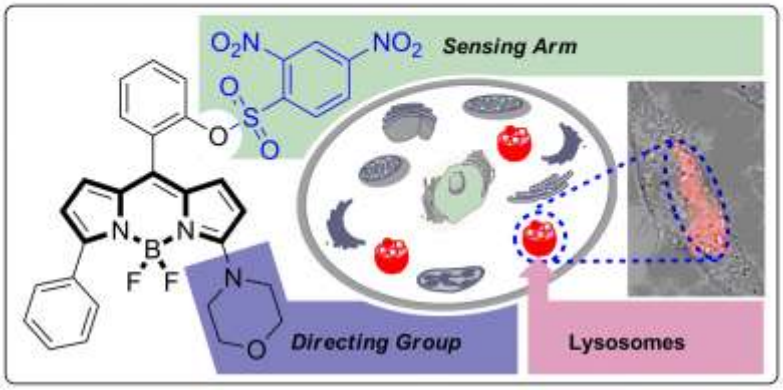

Chapter 2

Section A

Chromenoquinoline Based Fluorescence *Off-On* Probes for Biological Thiols

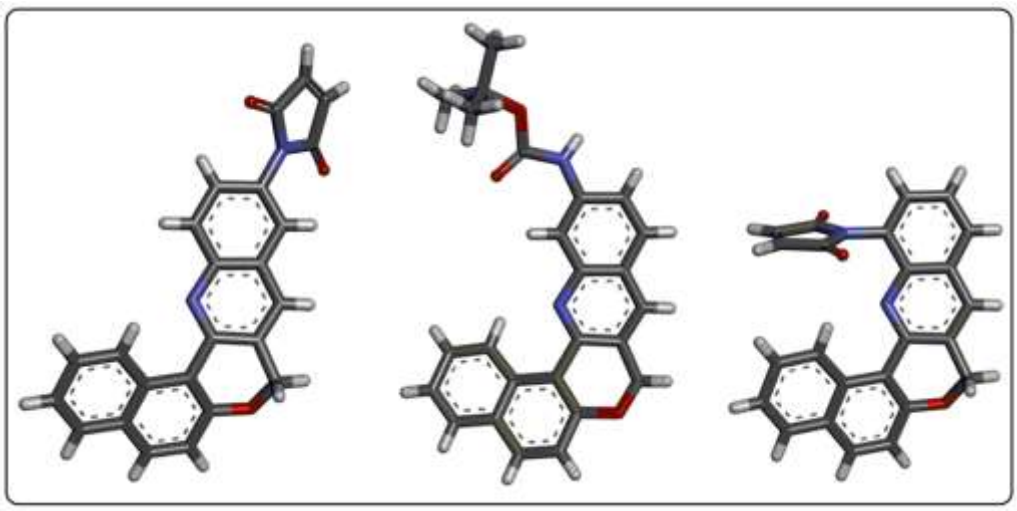

2A.1 Introduction

Our aim was to develop the fluorescent probes for the selective detection of biothiols. We hypothesized that the discrimination amongst the biothiols can be achieved by varying the position of the quencher on the fluorophore. Steric crowding at the groove of fluorophore is expected to contribute to either selectivity by reducing the rate of Michael addition reaction or enhancing the sensitivity, especially with sterically hindered thiols. Chromenoquinolines are known for their biological activity as an estrogenic agent[1] and work on chromenoquinolines is limited mainly towards synthetic methodologies.[2] However, the photophysical properties of the chromenoquinolines were not explored. Owing to easy scalable synthesis, good yields and unexplored fluorescence properties of chromenoquinolines, we selected chromenoquinolines as fluorophore. Maleimide is well explored thiol recognizing unit widely used in the synthesis of thiol selective fluorescent probes.[3] Therefore, maleimide was selected as a quencher.

We designed three chromenoquinoline-based probes **61**, **62** and **63** in which the position of the maleimide moiety is varied at position C-2, C-3 and C-4, respectively (Figure 2A.1). Probes **61** and **63** were predictable to provide better quenching compared to **62** due to the higher electron density at C-2 and C-4 positions and therefore, expected to exhibit better *Off-On* response upon thiol sensing. The probe **63** on the other hand could be crucial as the steric crowding at the groove of the chromenoquinoline is expected to react faster with sterically less hindered biothiols such as Cys and Hcy compared to GSH which is sterically more hindered biothiols. This chapter describes the design, theoretical calculations, synthesis, photophysical properties and thiol sensing abilities of these probes in living cell.

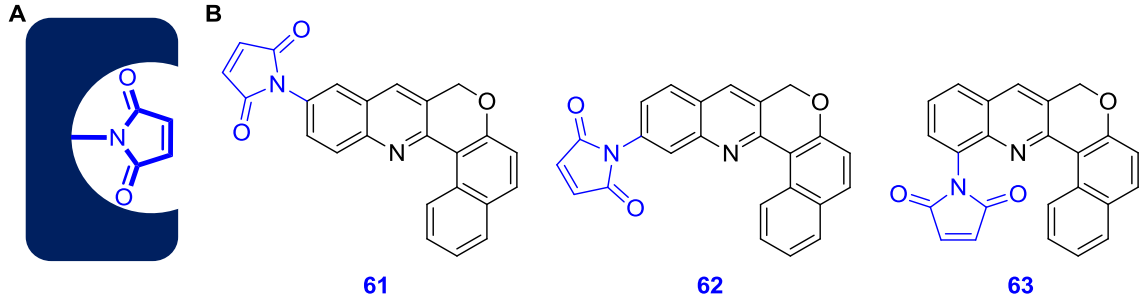

Figure 2A.1: (**A**) Schematic diagram and (**B**) proposed structures of fluorescent turn-*On* probes **61**, **62** and **63** for for discriminating among biothiols.

2A.2 Results and discussion

2A.2.1 Theoretical calculations

The TDDFT calculation at the B3LYP/ 6-311(d,p) level for probe **61** confirmed the S_1 state as a dark state due to the forbidden HOMO→LUMO transition (*i.e.* $S_0 \rightarrow S_1$) with oscillator strength, *f*=0.0005. HOMO→LUMO+1 (*i.e.* $S_0 \rightarrow S_4$) with *f* = 0.3614 is identified as first allowed transition of the chromenoquinoline moiety (Table 2A.1). Therefore, the presence of the S_1 dark state induced by maleimide confirmed a non-radiative $S_1 \rightarrow S_0$ transition responsible for quenching of the fluorescence. In contrast, the allowed $S_0 \rightarrow S_1$ transition (*f* = 0.3858) in the case of the corresponding Cys added product (**61**+Cys), is identified as the HOMO→LUMO transition of the chromenoquinoline moiety. The presence of an emissive S_1 state indicates that the species could be fluorescent.

Similarly, for the probe **62**, the presence of S_1 as dark state was confirmed as the HOMO→LUMO transition (*i.e.* $S_0 \rightarrow S_1$) provided *f* = 0.0001. The first emissive state was S_4 due to HOMO→LUMO+1 transition (*i.e.* $S_0 \rightarrow S_4$) with *f* = 0.2856. On the other hand, the thiol reaction product **62**+Cys confirmed the S_1 state as the emissive state because the HOMO→LUMO transition (*i.e.* $S_0 \rightarrow S_4$) was associated with *f* = 0.2785. Theoretical calculation on probe **63** indicated S_1 as the dark state for HOMO→LUMO transition (*i.e.* $S_0 \rightarrow S_1$) with *f* = 0.0012. The first allowed transition obtained from this calculation was HOMO→LUMO+1 (*i.e.* $S_0 \rightarrow S_2$) with *f* = 0.2247 confirming S_2 as the emissive state. The emission of electron from LUMO+1 level (*i.e.* S_2 state) to HOMO level would proceed via the intermediate LUMO (*i.e.* S_1 state) indicated by a non-radiative pathway from the chromenoquinoline moiety to the maleimide moiety. For corresponding Cys addition product **63**+Cys the HOMO→LUMO transition was allowed because of *f* = 0.2319. Therefore, the emission process which is the LUMO→HOMO transition was confirmed as the turn-*On* state of fluorescence.

Table 2A.1: Electronic excitation energies (eV) and oscillator strengths (*f*), configurations of the low-lying excited states of probes **61**, **62**, **63** and respective Cys adducts, calculated by TDDFT method at the B3LYP/6-311G(d,p) level after obtaining the optimized ground state geometries of each one.

Comp.	Electronic transition	E^a (eV)	λ (nm)	f^b	Main configurations[c]	CI coefficients[d]
61	$S_0 \rightarrow S_1$	2.29	540	0.0005	HOMO→LUMO	0.6937
	$S_0 \rightarrow S_2$	2.95	421	0.0008	HOMO-2→LUMO	0.6260
					HOMO-1→LUMO	0.2853
					HOMO→LUMO	0.1070
	$S_0 \rightarrow S_3$	3.19	389	0.0001	HOMO-1→LUMO	0.6447
	$S_0 \rightarrow S_4$	3.22	385	0.3614	HOMO→LUMO+1	0.6553
61+Cys	$S_0 \rightarrow S_1$	3.32	386	0.3858	HOMO→LUMO	0.6566
62	$S_0 \rightarrow S_1$	2.36	525	0.0001	HOMO→LUMO	0.7043
	$S_0 \rightarrow S_2$	2.89	429	0.0017	HOMO-2→LUMO	0.6301
	$S_0 \rightarrow S_3$	3.19	389	0.0000	HOMO-2→LUMO	0.2877
	$S_0 \rightarrow S_4$	3.24	383	0.2856	HOMO→LUMO+1	0.6560
62+Cys	$S_0 \rightarrow S_1$	3.21	386	0.2785	HOMO→LUMO	0.6576
63	$S_0 \rightarrow S_1$	2.61	476	0.0012	HOMO→LUMO	0.7032
	$S_0 \rightarrow S_2$	3.17	392	0.2247	HOMO→LUMO+1	0.6593
63+Cys	$S_0 \rightarrow S_1$	3.18	389	0.2319	HOMO→LUMO	0.6603

[a] Only the selected low-lying excited states are presented. [b] Oscillator strength. [c] Only the main configurations are presented. [d] The CI coefficients are in absolute values.

2A.2.2 Synthesis

Probes **61**, **62** and **63** were synthesized via the imino-Diels-Alder strategy for one pot construction of chromenoquinolines starting from 2, 3 or 4-substituted anilines. Imino-Diels-Alder reaction of 2-(prop-2-yn-1-yloxy)-1-naphthaldehyde **64** with 4-nitroaniline **65** at 110 ^oC in the presence of CuCl catalyst led to the chromenoquinoline **66** in 21% yield (Scheme 2A.1). Subsequent reduction of nitro group of **66** under the H_2, Pd/C conditions provided the amine **67** in 68% yield. The reaction of **67** with maleic anhydride followed by treatment with acetic anhydride in the presence of catalytic sodium acetate provided the chromenoquinoline probe **61** in 36% yield.

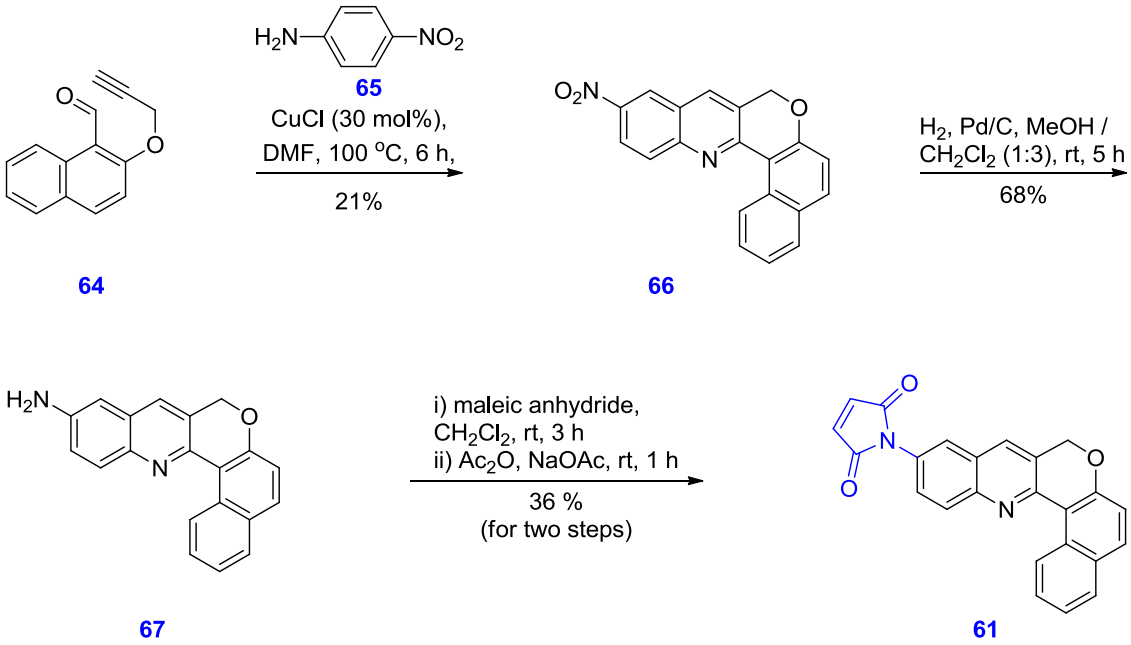

Scheme 2A.1: Synthesis of probe **61**.

A similar strategy starting from *meta* and *ortho*-nitroanilines were not successful in forming the corresponding chromenoquinoline derivatives. Therefore, an alternate strategy was used. The imino-Diels-Alder reaction of mono-Boc-protected *m*-phenylenediamine **68** with **64** in the presence of CuCl catalyst provided single regioselective chromenoquinoline **69** in 50% yield (Scheme 2A.2). Formation of other regioisomer was not observed during the imino-Diels-Alder reaction and the regioselectivity of the formed product was confirmed by the single crystal structure of the product (Figure 2A.2B). The deprotection of Boc group of **69** in presence HCl in MeOH to give amine **70** in 84% yield. The amine **70** was then treated with maleic anhydride at room temperature followed by treatment with acetic anhydride in presence of catalytic sodium acetate to afford the probe **62** in 37% yield.

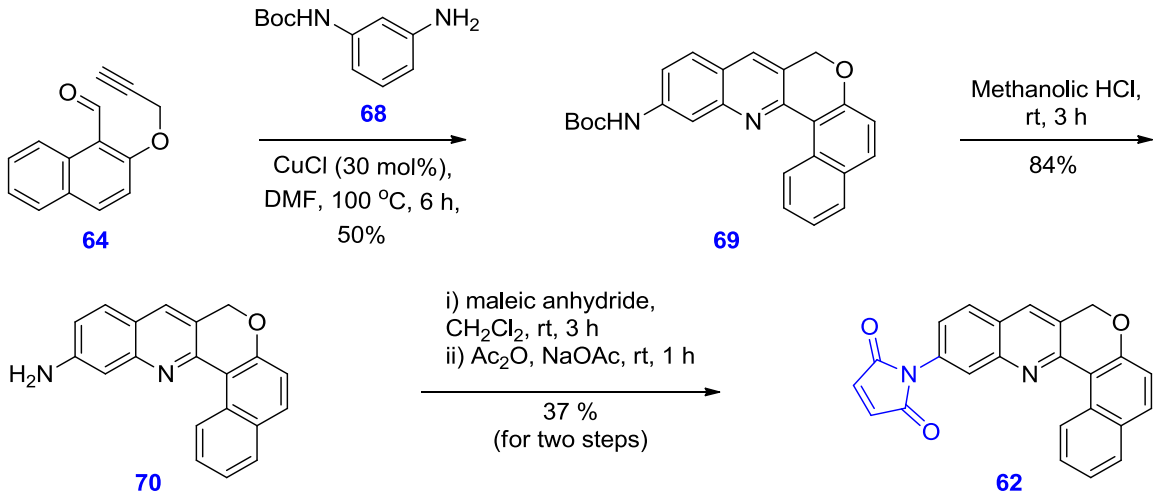

Scheme 2A.2: Synthesis of probe **62**.

To synthesize the probe **63**, mono-Boc-protected *ortho*-phenylenediamine **71** was reacted with **64** under the imino-Diels-Alder reaction conditions to provide **72** in 21% yield (Scheme 2A.3). Deprotection of Boc group of **72** was carried out in presence of HCl in MeOH to give amine **73** in 90% yield. Amine **73** was reacted with maleic anhydride followed by treatment with acetic anhydride in the presence of catalytic sodium acetate to furnish the probe **63** in 32% yield for two steps.

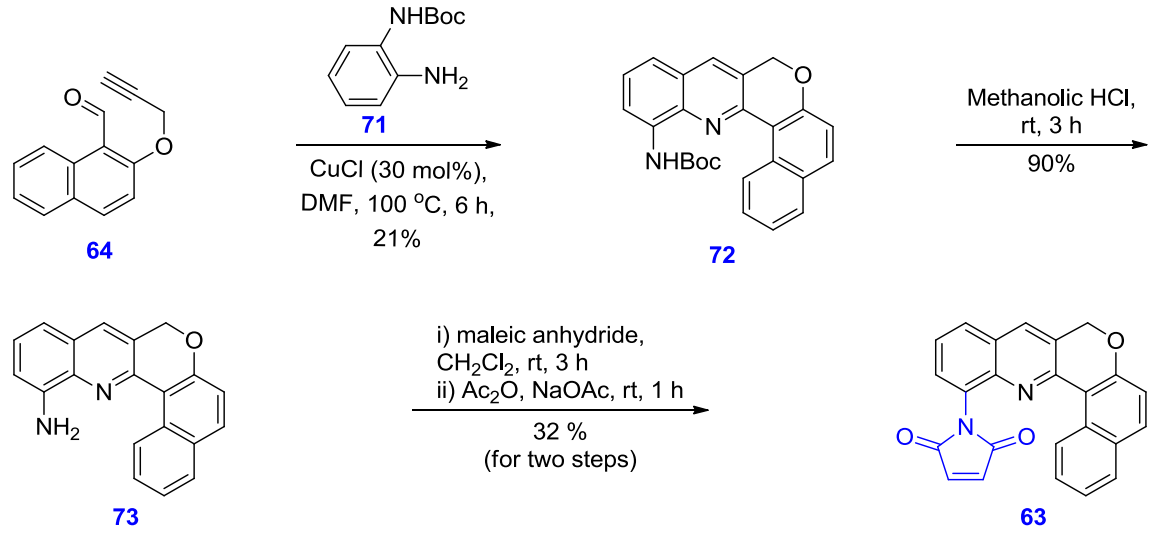

Scheme 2A.3: Synthesis of probe **63**.

Structure of derivatives **61**, **62** and intermediate **69** was confirmed by spectroscopic and single crystal X-Ray Diffraction analysis (Figure 2A.4). The significant difference in the crystal structure of **61** compared to **63** was the dihedral angle between the chromenoquinoline and the maleimide moiety. A dihedral angle to ~ 41° in **61** compared ~

70^{o} in **63** is due to the steric hindrance between the maleimide and the naphthalene units in the molecule.

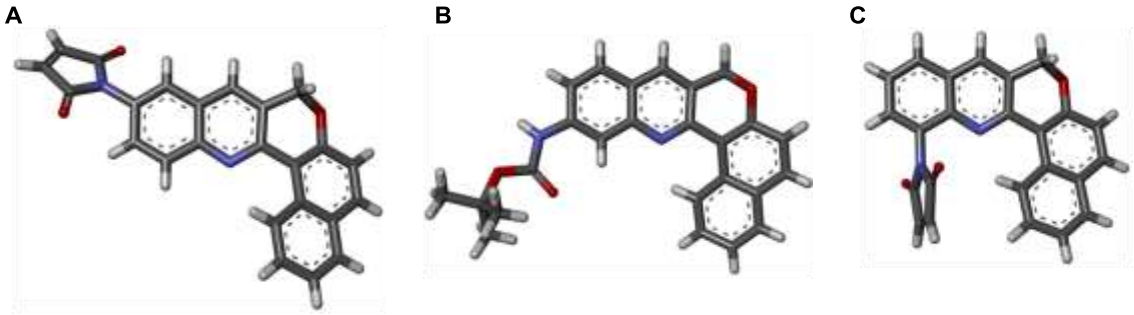

Figure 2A.2: Crystal structures of the probe **61** (**A**), the chromenoquinoline derivative **69** (**B**) and probe **63** (**C**).

2A.2.3 Photophysical studies

Absorption spectra of probes **61**, **62** and **63** (10 μM) recorded in $CHCl_3$, MeOH, DMSO and HEPES buffer (Fig. 2A.3).

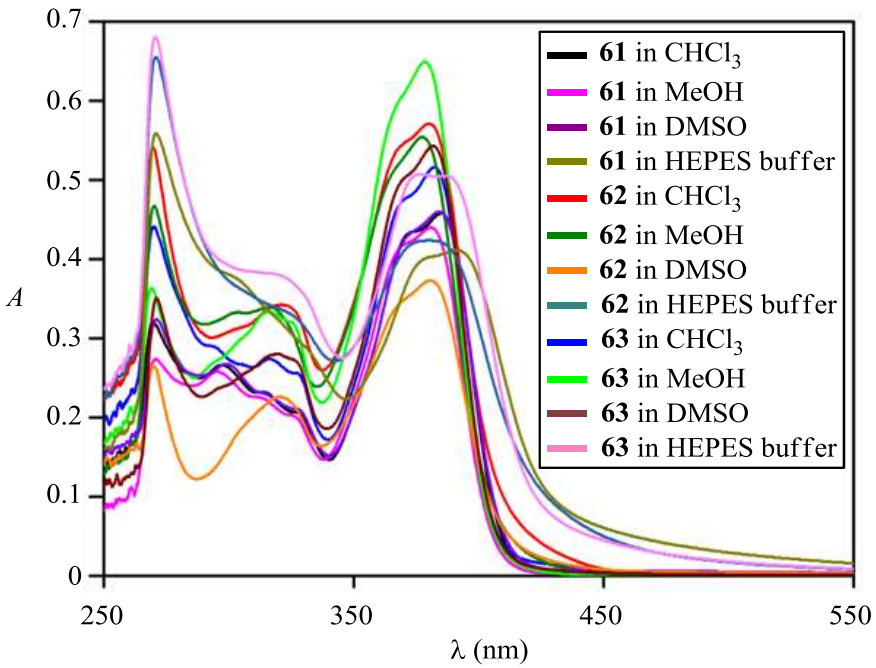

Figure 2A.3: Absorption spectra of probes **61**, **62** and **63** (10 μM) recorded in $CHCl_3$, MeOH, DMSO and HEPES buffer.

Complete solubility of probes **61**, **62** and **63** in various solvents ($CHCl_3$, 70:30 CH_3CN–10 mM HEPES buffer and 10 mM HEPES buffer) was confirmed by dynamic light scattering (DLS) studies in which no measurable aggregation was observed up to 25

μM concentration of probes **61**, **62** and **63**. These results were encouraging to analyze the optical properties of probes **61**, **62** and **63** in 10 mM HEPES buffer (pH = 7.4).

Absorption spectra of the probe **61** displayed a strong absorption band centred at λ_{max} = 384 nm with molar extinction coefficient ε = 14789 L mol^{-1} cm^{-1} (Figure 2A.2). The probe **61** displayed very weak fluorescence at λ_{em} = 457 nm (λ_{ex} = 383 nm). Absorption spectra of the probe **62** displayed a strong absorption band centred at λ_{max} = 374 nm with molar extinction coefficient (ε) up to 11905 L mol^{-1} cm^{-1}. A corresponding λ_{em} = 455 nm was also observed for **62** when excited at λ_{ex} = 383 nm. The probe **63** exhibited strong absorption band centred at λ_{max} = 382 nm with molar extinction coefficient ε = 12089 L mol^{-1} cm^{-1} and very weak fluorescence at λ_{em} = 457 nm (λ_{ex} = 383 nm).

Table 2A.2: Photophysical properties of probes **61**, **62** and **63**.

Probe	λ_{ex} (nm)	ε (L mol^{-1} cm^{-1})	λ_{em} (nm)	Quantum yield
61	383	14789	457	0.0035
62	374	11905	455	0.009
63	382	12089	457	0.0052

When relative fluorescence intensities of probes **61**, **62** and **63** were compared at same concentration (10 μM) in HEPES buffer (10 mM, pH 7.4 containing 1% DMSO), fluorescence intensities at 460 nm were in the order $I_2 >> I_1 > I_3$ (Figure 2A.4). This data indicated that the probe **62** exhibit higher background fluorescence compared to **61** and **63** indicating maleimide substitution at either C-2 or C-4 position is more efficient in providing the quenched state of the probe. Similarly, quantum yield Φ values calculated for all three probes suggested that when the maleimide moiety is connected at either C-2 or C-4 position, greater quenching in fluorescence (Φ_F = 0.0035 and 0.0052 for probe **61** and **63**, respectively) was observed compared to that at position C-3 (Φ_F = 0.009 for **62**) in DMSO (standard: coumarin 102 in acetonitrile; Φ_F = 0.91). These data indicate the potential of molecules **61** and **63** to act as better probes compared to the molecule **62** during their Michael addition reactions with thiols.

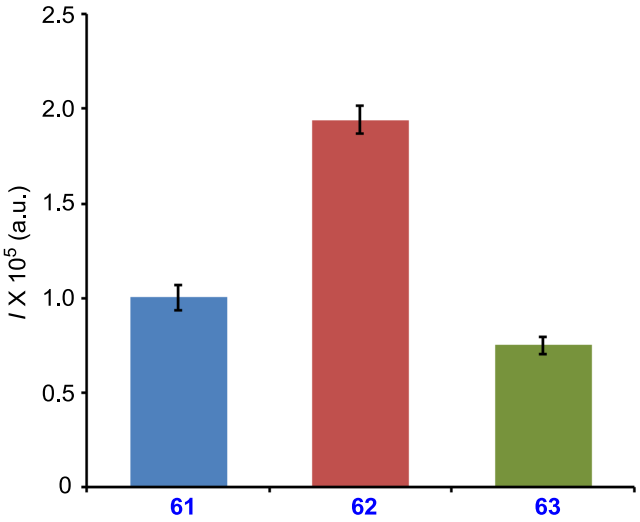

Figure 2A.4: Comparison of the fluorescence intensities recorded at 460 nm for probes **61**, **62** and **63** (10 μM) in HEPES buffer (10 mM, pH 7.4, 1% DMSO) solutions.

The observed difference in fluorescence of molecules **61**, **62** and **63** encouraged us to further investigate into the quenching mechanism working into these two molecules. Figure 2A.5 represents the fluorescence decay profile of chromenoquinoline probes **61**, **62** and **63** recorded in HEPES buffer (10 mM, pH 7.4, 1.0% DMSO) with excitation at 375 nm. Emission at 460 nm for the probe **61** showed tri-exponential decay profile with τ_1 = 0.059 ns (77.33%), τ_2 = 0.840 ns (21.78%) and τ_3 = 3.269 ns (0.89%). The τ_a calculated from these data was 0.256 ns (Table 2A.3). On the other hand, the probe **62** exhibited a bi-exponential decay profile with τ_1 = 0.148 ns (93.84%), τ_2 = 0.986 ns (6.16%) and τ_a = 0.198 ns. The probe **63** decayed tri-exponentially with τ_a = 0.120 ns [τ_1 = 0.799 ns (6.20%), τ_2 = 3.295 ns (0.45%) and τ_3 = 0.053 ns (93.35%)]. From these data, radiative decay rate constant (k_r) and nonradiative decay rate constant (k_{nr}) for probes **61**, **62** and **63** were determined using following equations[4]

$$k_r = \Phi/\tau \qquad (1)$$

$$k_{nr} = (1/\tau) - k_r \qquad (2)$$

The probe **61** displayed k_r value of 0.014 × 10^9 and a corresponding k_{nr} = 3.889 × 10^9 s^{-1}. For the probe **62**, calculated k_r and k_{nr} values were 0.046 × 10^9 and k_{nr} = 5.015 × 10^9 s^{-1}, respectively. Similarly, for the probe **63**, calculated k_r and k_{nr} values were 0.043 × 10^9 and 8.315 × 10^9 s^{-1}, respectively. From these data k_r / k_{nr} values for each probe were

calculated. For probe **61** the k_r / k_{nr} = 0.0035 compared to that of 0.009 calculated for the probe **62** indicated a non-radiative pathway which is responsible for fluorescence quenching is more favorable in the case of **61**. Similarly, for the probe **63**, k_r / k_{nr} = 0.005 also indicated less background fluorescence compared to **62** as a consequence of the ICT process compared from the chromenoquinoline to the maleimide moiety.

Table 2A.3: Time resolved fluorescence data for probes **61**, **62** and **63**.

Probe	τ^a (ns)	k_r (10^9 s^{-1})	k_{nr} (10^9 s^{-1})	k_r / k_{nr}
61	0.256	0.014	3.889	0.0035
62	0.198	0.046	5.015	0.009
63	0.120	0.043	8.315	0.005

[a] Standard deviations of τ are ≤ 0.008 ns for probes **61**, **62** and **63**.

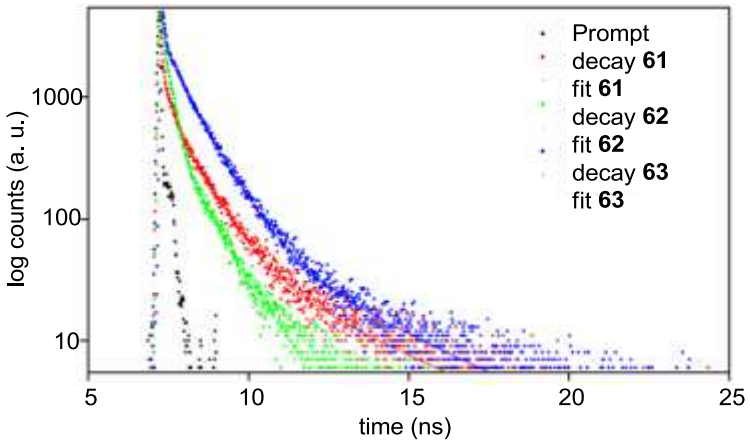

Figure 2A.5: Fluorescence lifetime decay profiles (λ_{ex} = 375 nm) of **61**, **62** and **63** in HEPES buffer (10 mM, pH 7.4, 1.0% DMSO) monitored at 460 nm. Laser profile is shown in ● (prompt). Probe **61** (10 μM) is represented in ●, **62** (10 μM) is represented in ● and **63** (10 μM) is represented in ●. Curve fits are shown in solid lines.

2A.2.4 Thiols sensing

Sensing of biological thiols by the chromenoquinoline-based probes:

Selectivity studies: In order to prove the importance of probes **61**, **62** and **63** in selective thiol detection, reaction of each probe to various Michael donors were studied. In these experiments 10 μM of each probe was seperately reacted with 100 μM solutions of various amino acids (Gly, Ala, Phe, Lys, Arg, His, Met, Tyr, Ser, GSH, Cys and Hcy) in HEPES buffer (10 mM, pH 7.4, 1.0% DMSO) for 20 min and fluorescence spectra were recorded. The fluorescence enhancements in each case was ploted as the ratio of fluorescence

intensity measured at λ_{em} = 457 nm (with λ_{ex} = 384 nm) after addition of analyte to that recorded only for the probe *i.e.* (I/I_0) value versus various analytes. No significant fluorescence enhancement was observed for Gly, Ala, Phe, Lys, Arg, His, Met and Tyr. However, when thiol-containing analytes (Hcy, Cys and GSH) were introduced, large enhancements in fluorescence intensity were observed. The fluorescence intensity enhancements upon addition of Cys, GSH and Hcy to the probe **61** were 185-, 223- and 156-fold, respectively (Figure 2A.6). When similar experiments were carried out with the

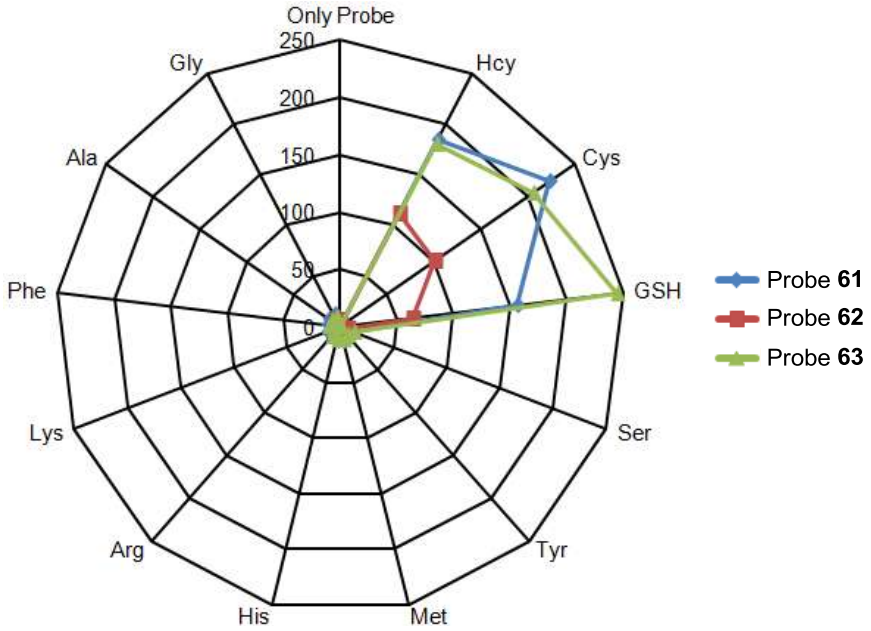

Figure 2A.6: Relative fluorescence intensity enhancements of probe **61 – 63** (10 μM) with or without various amino acids (100 μM) in HEPES buffer (10 mM, pH 7.4, 1.0% DMSO).

probe **62**, enhancement in fluorescence intensities were only 112-, 101- and 64-fold for Hcy, Cys and GSH respectively . The response of the probe **62** to non-thiol analytes were insignificant. Reaction of the probe **63** with Hcy, Cys and GSH resulted in the enhancement of fluorescence intensity by 180-, 205-, 245-fold, respectively. These data suggest that fluorescene *Off-On* characteristic for the probe **61** is comparable when assayed for Cys, GSH and Hcy. On the other hand, the probe **63** displayed significantly higher jump in response to GSH compared to Cys and Hcy. As the reactivity of all thiols towards all probes were similar, the higher jump in the case of **63** in response to GSH can be attributed to the steric crowding between the chromenoquinoline and the succinimide moiety and a contribution from the bulky GSH forcing the succinimide moiety to be in a nearly orthogonal orientation with respect to the chromenoquinoline moiety. The bond

angles values 73.4°, 74.9° and 87.9° for **63**+Hcy, **63**+Cys and **63**+GSH, respectively obtained from theoretical calculations also support our assumption (Figure 2A.7). As a result, increasing order of fluorescence enhancement for **63** upon sensing of thiols were in the order Hcy < Cys < GSH which is in the same order of their relative steric contribution. This explanation can further be supported by the comparable fluorescence enhancement during the sensing of less bulkier thiols by either the probe **61** or **63**.

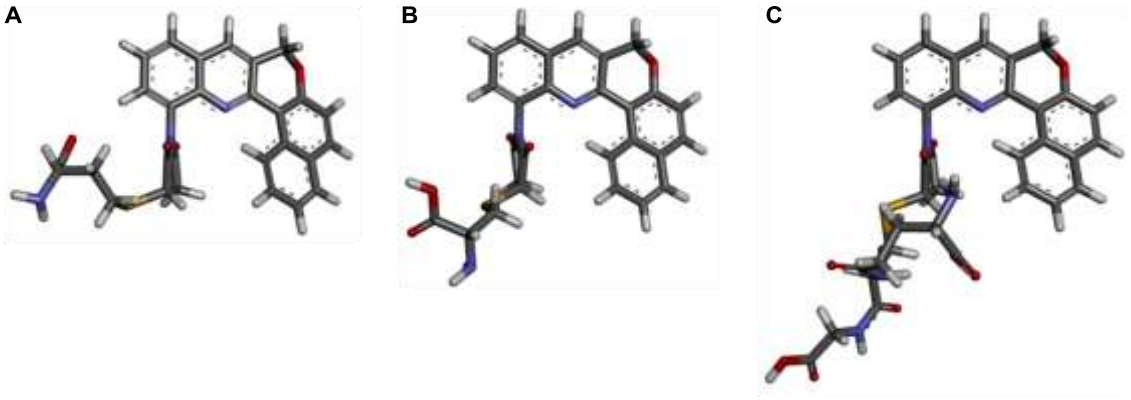

Figure 2A.7: Energy minimised structures of Hcy (**A**), Cys (**B**) and GSH (**C**) adducts with probe **63**.

Formation of stable thioether for each probe **61**, **62** and **63** with GSH were confirmed by the mass spectrometric analysis of reaction mixture after 18 h of mixing (Figure 2A.8 and 2A.9). No significant decomposition- / bi-products were detected from these analyses. These data confirmed that only Michael addition products were responsible for the observed enhancement in fluorescence during thiol sensing process.

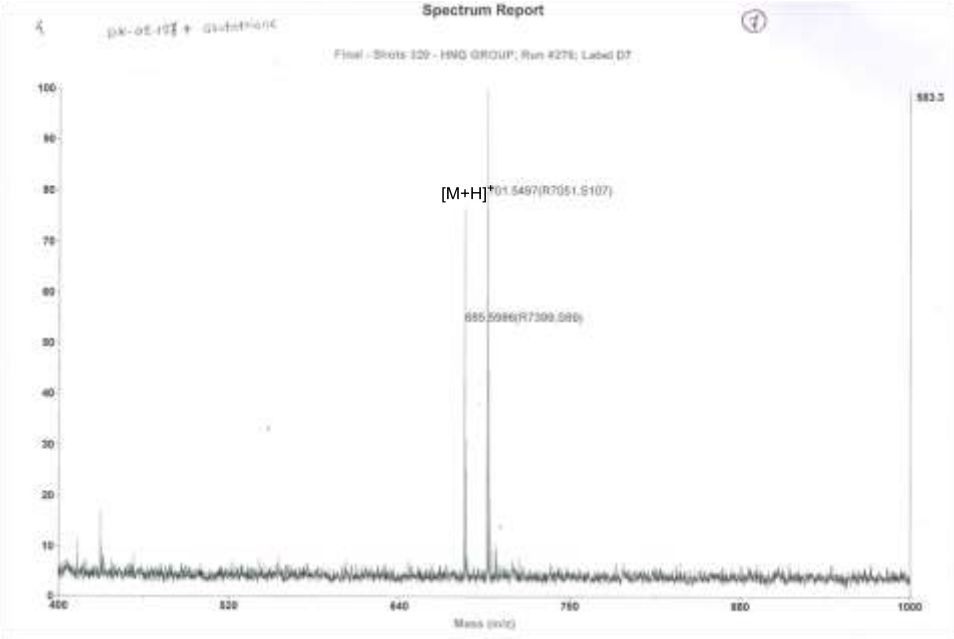

Figure 2A.8: ESI-MS of the probe **63** (10 μM) titrated with GSH (100 μM) in HEPES buffer (10 mM, pH 7.4, 1% DMSO).

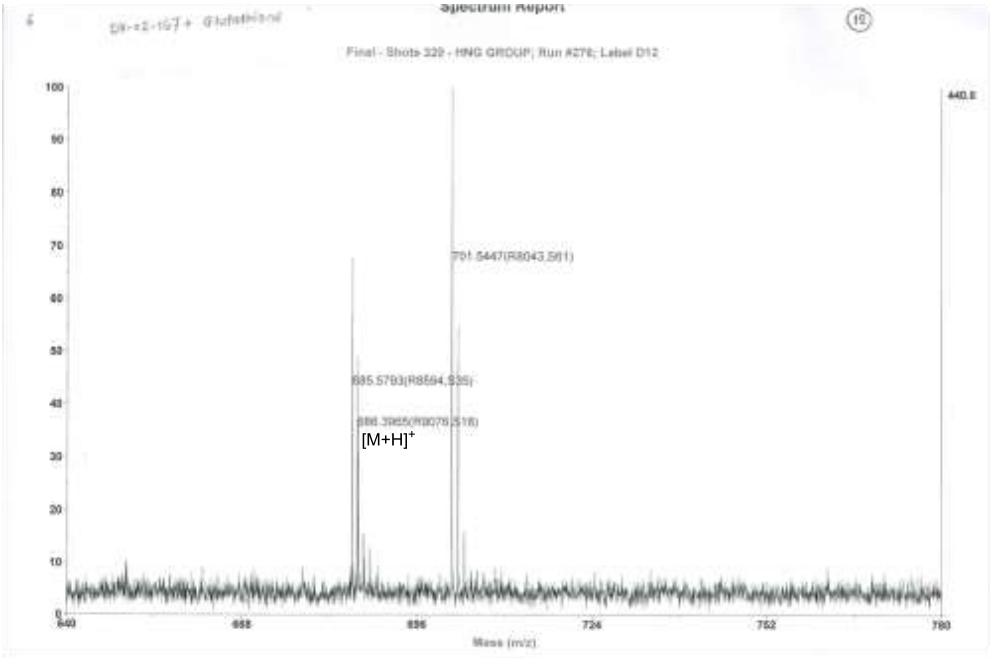

Figure 2A.9: ESI-MS of the probe **63** (10 μM) titrated with GSH (100 μM) in HEPES buffer (10 mM, pH 7.4, 1% DMSO).

We also conducted the naked eye detection experiment of thiol sensing reactions by probes **61**, **62** and **63** (Figure 2A.10). Briefly, first 48-wells of a 96-well plate were used in which each well represented a unique combination of chromenoquinoline probe

and amino acid. The first row and the column represented the blank with respect to probe and amino acid, respectively. In remaining wells 10 µM of each probe and 100 µM of each amino acid were used. The total volume for each reaction was 1000 µL containing HEPES buffer (10 mM, pH 7.4, 1.0% DMSO). All reactions were monitored for 20 min. When images were taken by placing the 96-well plate under a hand-held UV lamp (λ_{ex} = 365 nm), strong fluorescence were observed in wells B4, B5 and B8 for probe **61**, C4, C5 and C8 for probe **2**, and D4, D5 and D8 for probe **63**. These data also confirmed that probes **61**, **62** and **63** show *Off-On* response only in the presence of thiol containing amino acids (Cys, GSH and HCy).

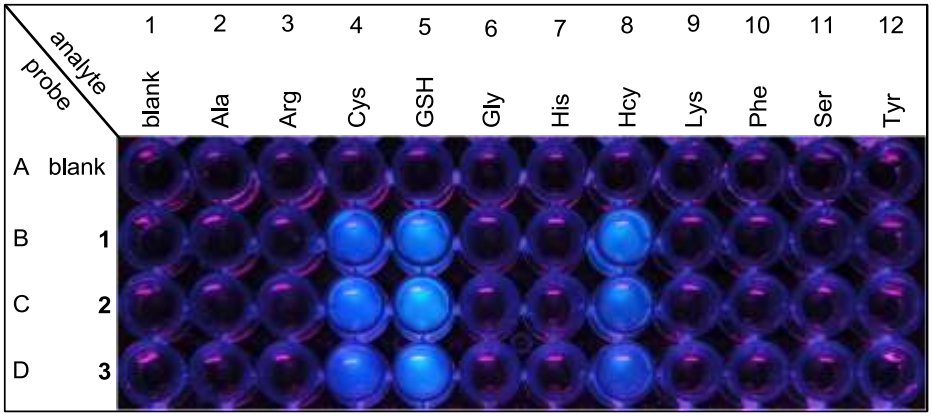

Figure 2A.10: Fluorescence photographs of the compounds, taken under UV light (hand-held UV lamp, 365 nm).

Next, we examined the quantitative *Off–On* responses of probes **61**, **62** and **63** to different biological thiols. In these experiments, each probe (10 µM) was separately treated with varied concentrations (0 – 100 µM) of Cys, GSH and Hcy, respectively. Fluorescence spectra were recorded after 10 min of addition with λ_{ex} = 384 nm. In each case increase in fluorescence intensity was observed (Figure 2A.11). When fluorescence intensities at 457 nm were plotted against concentrations of each amino acids, linear increase were observed only up to 1 equivalent of thiol and further increase of thiol concentration led to saturation of the intensity. We further determined the detection limits for analyzing thiols using each of the probes by plotting fluorescence intensity values at 2 – 10 µM against concentration.

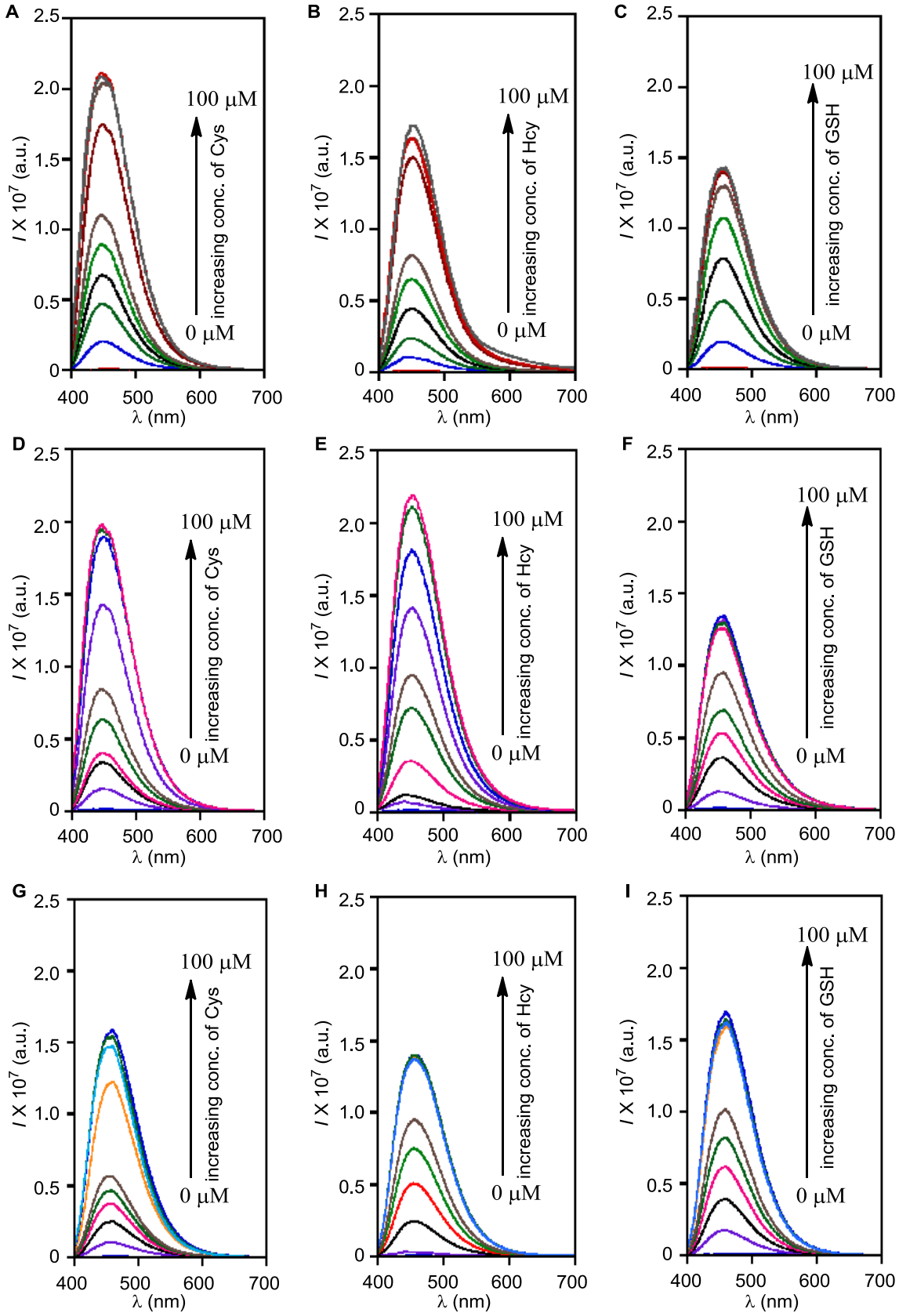

Figure 2A.11: Fluorometric titrations of probes **61**, **62** and **63** in response to biological thiols (0 – 100 μM) of Cys, Hcy and GSH respectively.

Detection limit:

The detection limits were determined based on the fluorescence titrations. To determine the *S/N* ratio, the emission intensity of each probe without thiol was measured by 3 – 4 times and the standard deviation of blank measurements was determined. Under the present conditions, a good linear relationship between the fluorescence intensity and the thiol concentration could be obtained in the 2 – 10 μM (Figure 2A.12). The detection limits were then calculated with the equation: detection limit = $3\sigma_{bl}/m$, where σ_{bl} is the standard deviation of blank measurements, m is the slope between intensity versus sample concentration (Table 2A.4).

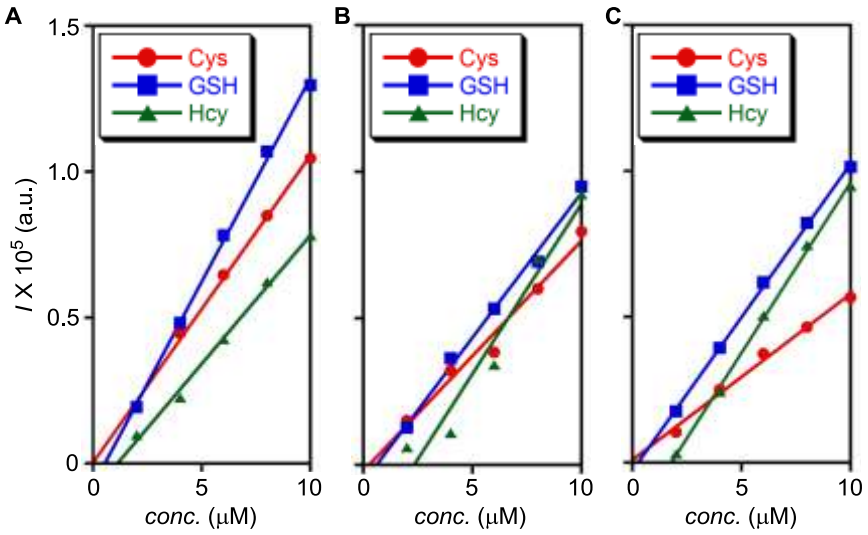

Figure 2A.12: Linearity of fluorometric titrations of probes **61**, **62** and **63** in response to biological thiols (Cys, GSH and Hcy). (**A**) Fluorescence responses of **61** (10 μM) toward various concentrations (0, 2, 4, 6, 8 and 10 μM) of each thiol in HEPES buffer (10 mM, pH 7.4, 1% DMSO). Same experiments were carried out for **62** (**B**) and **63** (**C**).

The detection limits of **61** towards Cys, GSH and Hcy were calculated to be 1.94×10^{-8} M, 1.46×10^{-8} M and 2.31×10^{-8} M, respectively based on the *S/N* = 3. Similarly, the detection limits of **62** towards Cys, GSH and Hcy were calculated to be 2.91×10^{-8} M, 2.31×10^{-8} M and 1.97×10^{-8} M, respectively. Under the comparable conditions the probe **63** detection limits for Cys, GSH and Hcy were 2.40×10^{-8} M, 1.30×10^{-8} M and 1.17×10^{-8} M, respectively. These data indicated that both of the probes **61** and **63** can be potentially employed to quantitatively detect these thiols. Under comparable conditions, the probe **2** was found to be less efficient compared to **61** and **63**.

Table 2A.4: Calculation of detection limit of Cys, GSH and Hcy with probes **61**, **62** and **63**.

Probe	σ_{bl}	*S/N*	Slope From linear plots, *m*			Detection limit		
			Cys (10^5)	GSH (10^5)	Hcy (10^5)	Cys (10^{-8})	GSH (10^{-8})	Hcy (10^{-8})
61	6797	3.0	12	14	8.8	1.9	1.5	2.3
62	34410	3.0	7.9	9.9	12	13.1	10.5	8.9
63	10108	3.0	5.7	11	12	5.3	2.9	2.6

The quantitative responses of the probe **61** to biothiols is also associated with 137-fold (from 0.0035 to 0.48), 71-fold (from 0.0035 to 0.25) and 121-fold (from 0.0035 to 0.42) enhancements in Φ upon addition of Cys, GSH and Hcy, respectively. On the other hand, the probe **62**, exhibited only 39-fold (from 0.009 to 0.22), 49-fold (from 0.009 to 0.28) and 36-fold (from 0.009 to 0.21) enhancements in Φ upon addition of Cys, GSH and Hcy. Enhancements in quantum yield values calculated for the probe **63** were 73-fold (from 0.0052 to 0.38), 64-fold (from 0.0052 to 0.33) and 91-fold (from 0.0052 to 0.48) expressed in the same order of thiol containing amino acids indicated that enhancements in Φ, upon addition of Cys, GSH and Hcy, respectively.

Table 2A.5: Quantum yields of probes **61**, **62** and **63** before and after sensing of biothiols in different solvents.

Compound	Solvent			
	HEPES Buffer	Acetonitile/HEPES buffer	DMSO	$CHCl_3$
61	0.0035	ND	0.0031	ND
61+Cys	0.48	ND	ND	ND
61+GSH	0.25	ND	ND	ND
61+Hcy	0.42	ND	ND	ND
62	0.009	0.009	0.0083	0.0075
62+Cys	0.22	0.24	ND	ND
62+GSH	0.28	0.27	ND	ND
62+Hcy	0.21	ND	ND	ND
63	0.0052	0.004	0.0045	0.0033
63+Cys	0.38	0.32	ND	ND
63+GSH	0.33	0.30	ND	ND
63+Hcy	0.48	ND	ND	ND

ND = Not determined.

In order to prove that these probes didn't aggregate in aqueous buffer solution we measured the quantum yields in chloroform, DMSO and in Acetonitrile/HEPES buffer (70:30) mixture. In all solvents quantum yields were approximately similar to that of HEPES buffer (Table 2A.5).

2A.2.5 Cell imaging

We further investigated the permeability of probes **61**, **62** and **63** through the cell membranes and their ability to detect intracellular thiols by the fluorescence imaging of living cells using confocal microscopy. In these experiments, the human metastatic breast cancer cells, MDA-MB 231 cells, were incubated with a solution of either the probe **61**, **62** and **63** (25 μM in 1:1000 DMSO-PBS v/v, pH 7.4) for 30 min at 37 ^{o}C followed by the detection with fluorescence microscopic technique. Under these conditions, all three probes were found to be cell-permeable and their reactions with intracellular thiols, resulted in fluorescence emission with varied intensity as observed by the fluorescence microscopy. Intensity of fluorescent enhancement were higher for probe **61** (Figure 2A.13A and 2A.13B) and **63** Figure 2A.13I and 2A.13J) compared to that of probe **62** (Figure 2A.13E and 2A.13F). In control experiments, cells were pre-treated for 30 min with the *N*-phenylmaleimide (5 mM) followed by incubation with either the probe **61**, **62** and **63** (25 μM in 1:1000 DMSO-PBS v/v, pH 7.4). In these cases, the confocal microscopic studies did not show any significant fluorescence signal (Figure 2A.13C and 2A.13D for the probe **61**, Figure 2A.13G and 2A.13H for the probe **62** and Figure 2A.13K and 2A.13L for the probe **63**). These data confirm the specificity of probes **61**, **62** and **63** for thiols over other analytes in living cells. Intensities of fluorescence images also suggested the chromenoquinolines **61** and **63** are better in sensing intracellular thiols when compared to the probe **62**.

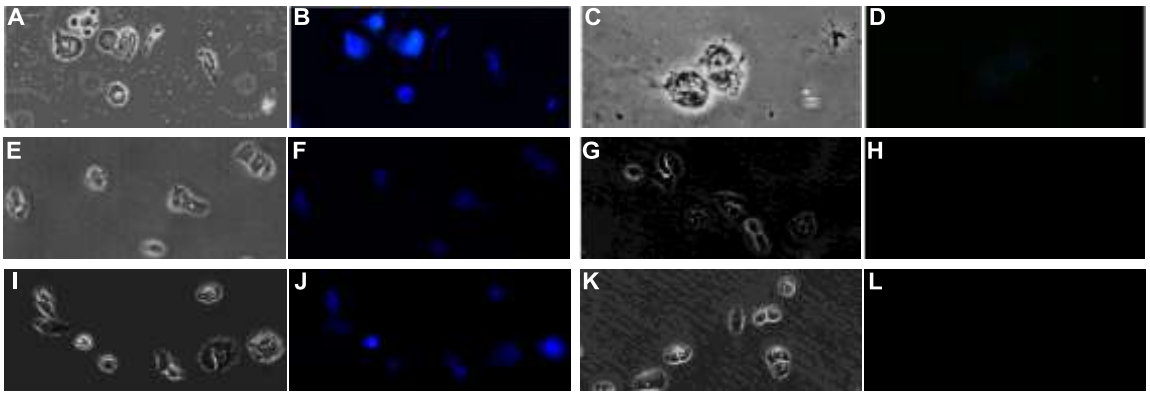

Figure 2A.13: Live-cell imaging with probes **61** – **63** in MDA-MB 231 cells. Transmission image (**A**) and fluorescence images (**B**) of cells treated with 25 μM probe **61**. Transmission (**C**) and fluorescence image (**D**) of cells pre-incubated with *N*-phenylmaleimide (5 mM) for 30 min and then treated with 25 μM of probe **61**. (**E**) and (**F**) are transmission and fluorescence images after incubation with **62**. (**G**) and (**H**) are transmission and fluorescence images of control experiments for the probe **62**. (**I**) and (**J**) are transmission and fluorescence images after incubation with **63**. (**K**) and (**L**) are transmission and fluorescence images of control experiments for the probe **63**.

2A.3 Summary and conclusions

In conclusion we have synthesised and characterised chromenoquinoline-based fluorescent probes **61**, **62** and **63** for sensing of biothiols via the Michael addition of thiol to maleimide. The Cu(I)-catalyzed imino-Diels-Alder reaction was employed to construct the chromenoquinoline moiety followed by conversion of amine to maleimide. All probes showed fast and selective *Off-On* response to only thiol-containing amino acids however, with varied level of fluorescence enhancement. Although we anticipated that GSH will react slower with ortho probe than Cys and Hcy, experimental results showed that the reactivity of all biothiols is similar towards ortho probe. In fact GSH sensing process by **63** was significantly better compared to **61**. These data confirmed that in the reaction product of **63** with GSH, the fluorescence quenching by the succinimide unit is less pronounced due to the orthogonal orientation of succinimide and chromenoquinoline units. All probes showed quantitative response to biothiols only up to 1:1 probe/thiol concentration indicating their usefulness as quantitative thiol probe. The detection limits calculated during the sensing of thiol containing amino acids including GSH (1.46×10^{-8} M for **61**, 10.45×10^{-8} M for **62** and 2.89×10^{-8} M for **63**) confirmed that probes **61** and

63 are more efficient than **62** in detecting low concentration of GSH. Applicability of these probes was successfully demonstrated by live cell imaging of intracellular thiols.

2A.4 References

(1) Vu, A. T.; Campbell, A. N.; Harris, H. A.; Unwalla, R. J.; Manas, E. S.; Mewshaw, R. E. *Bioorg. Med. Chem. Lett.* **2007**, *17*, 4053.

(2) (a) Tomashevskaya, M. M.; Tomashenko, O. A.; Tomashevskii, A. A.; Sokolov, V. V.; Potekhin, A. A. *Russ. J. Org. Chem.* **2007**, *43*, 77(b) Ramesh, S.; Gaddam, V.; Nagarajan, R. *Synlett* **2010**, 757.

(3) (a) Girouard, S.; Houle, M.-H.; Grandbois, A.; Keillor, J. W.; Michnick, S. W. *J. Am. Chem. Soc.* **2005**, *127*, 559(b) Matsumoto, T.; Urano, Y.; Shoda, T.; Kojima, H.; Nagano, T. *Org. Lett.* **2007**, *9*, 3375(c) Guy, J.; Caron, K.; Dufresne, S.; Michnick, S. W.; Skene, W. G.; Keillor, J. W. *J. Am. Chem. Soc.* **2007**, *129*, 11969(d) Langmuir, M. E.; Yang, J.-R.; Moussa, A. M.; Laura, R.; LeCompte, K. A. *Tetrahedron Lett.* **1995**, *36*, 3989(e) De Silva, A. P.; Gunaratne, H. Q. N.; Gunnlaugsson, T. *Tetrahedron Lett.* **1998**, *39*, 5077(f) Corrie, J. E. T. *J. Chem. Soc., Perkin Trans. 1* **1994**, 2975(g) Mare, S.; Penugonda, S.; Ercal, N. *Biomed. Chromatogr.* **2005**, *19*, 80.

(4) Lakowicz, J. R. *Principles of fluorescence spectroscopy*, 3rd Edition; 1999.

Chapter 2

Section B

NBD Chloride as Fluorescence *Off-On* Probe for Selective Detection of Cysteine and Homocysteine over Glutathione

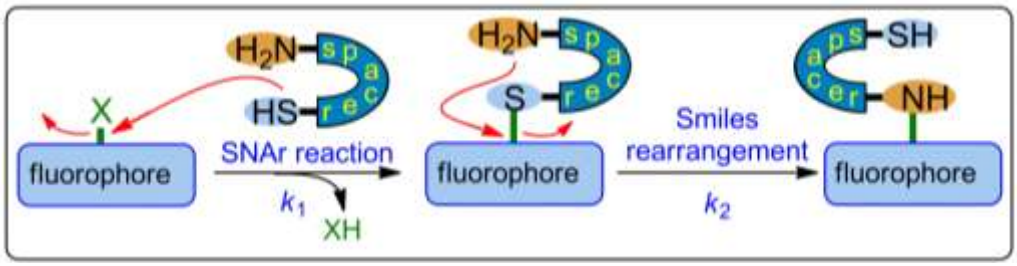

2B.1 Introduction

Chromenoquinoline based probes did not offered significant differences in terms of response time, fluorescence enhancements and detection limits. Therefore developing fluorescent probes for discriminating among biothiols based on their steric differences is challenging task. As each biothiols is associated with specific cellular function, selective detection of plasma and intracellular concentrations of the same is of great importance.[1] Significant efforts have been made for the selective and sensitive detection of biothiols using fluorescent probes.[2] However, limited Cys specific probes which are capable of discriminating other sulfhydryls (Hcy and GSH) are known.

Among diverse fluorescence-based approaches, thiol mediated Michael addition on maleimide, aromatic nucleophilic substitution reactions (SNAr) on 2,4-dinitrophenylsulfonyl (DNs) have been used for developing thiol probes.[3] However, the selectivity of these probes could not be predicted prior to experimental evaluation. More predictive approach for selective Cys sensing involves the formation of thiazolidine from aldehyde.[4] Involvement of both –SH and $–NH_2$ groups contribute to better selectivity although, Hcy is reported to compete in the sensing process by forming thiazinane product. Recently, an alternate two-step strategy has been reported by Yang and co-workers which involves the addition (rate = k_1) of thiol on the nonfluorescent species **74** leading to thiol-conjugate **74(*S*)** as a kinetically controlled product (Figure 2B.1A). [5]Subsequent conversion of **74(*S*)** to thermodynamically controlled amine-conjugate **74(*N*)** is characterized as S-N Smiles rearrangement. The rate k_2 of the rearrangement is determined by the covalent-length of the spacer between the sulfur and the nitrogen atoms (Figure 2B.1A). The rearrangement is more feasible for Cys because, it involves cyclic five-membered transition state. For Hcy, the rearrangement would proceed at slower rate due to formation of a cyclic six-membered transition state. Corresponding rearrangement involving GSH would not be feasible due to the formation of a cyclic ten-membered transition state. According to this two-step strategy, the *Off-On* response of probe **74** to either of Cys, Hcy and GSH can be dictated by rate, k_2 of each rearrangement reaction and fluorescent properties of **74(*S*)** and **74(*N*)** species formed. The BODIPY-based probe **44** was reported for its better sensitivity toward GSH because, corresponding BODIPY-thiol conjugate exhibited better emission property compared to BODIPY-amine conjugates formed during reactions of **44** with Cys and Hcy (Figure 2B.1B). Probe **45** on the other

hand, displayed ~1200-fold sensitivity toward Cys because, corresponding BODIPY-amine conjugate exhibited better emission property compared to the BODIPY-amine conjugate of Hcy addition and the BODIPY-thiol conjugate of GSH addition.

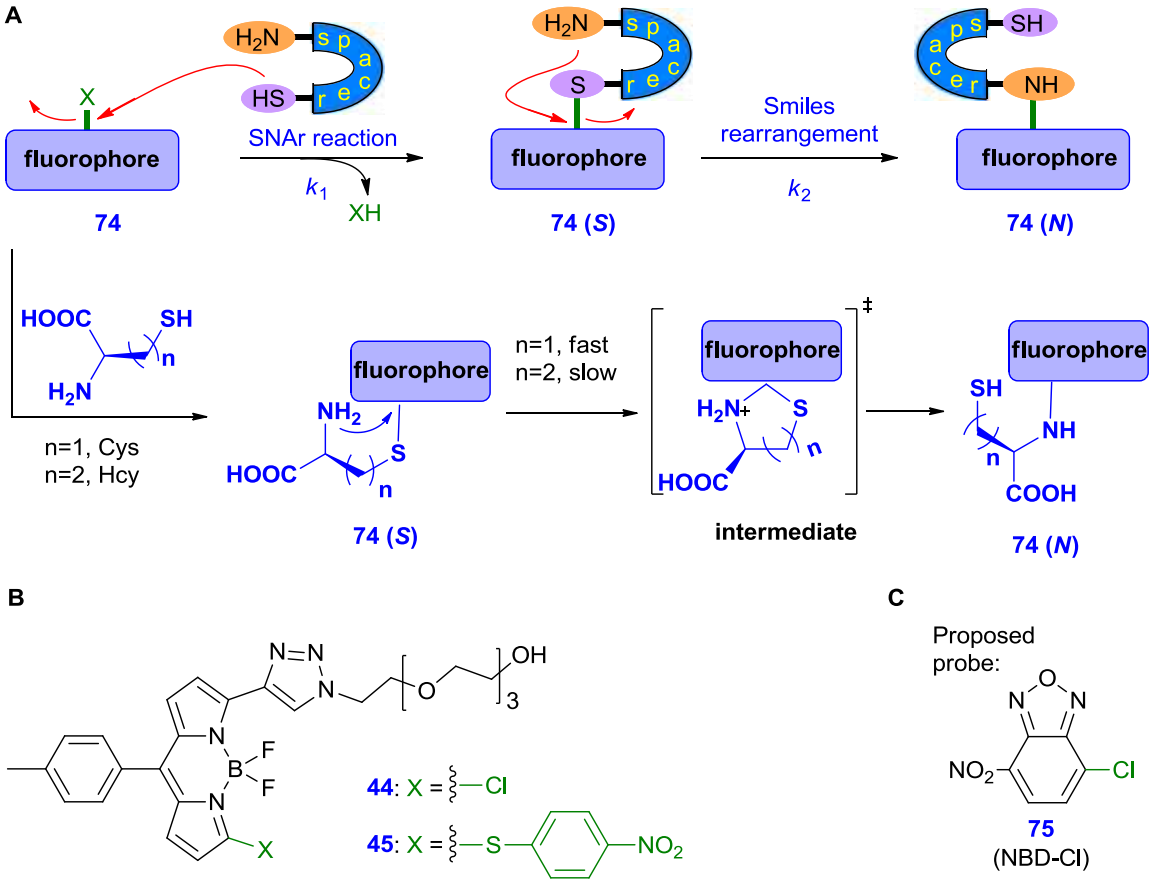

Figure 2B.1: Schematic diagram for illustrating the two-step thiol sensing process by **74** (**A**). Structures of BODIPY-based *Off-On* thiol probes **44** and **45** (**B**). Structure of NBD-based *Off-On* Cys sensing probe **75** (**C**).

We realized that NBD-chloride **75** could be used for selective and sensitive detection of Cys relying on the two-step SNAr reaction and *S-N* Smiles rearrangement. Probe **75** is commonly used as an efficient probe for selective labeling of thiols, such as free thiols and sulfhydryl groups in proteins because of the feasibility of thiol-conjugation under physiological conditions compared to more basic and elevated temperature conditions for amine-conjugation.[6] In 1983, Houk *et. al.* during the labeling native actin protein, observed a very slow conversion of NBD-thiol conjugate of cysteine-residue into a NBD-amine conjugate triggered by a neighbouring lysine-residue.[7] In 2012, Botta and coworkers also reported a similar *S-N* rearrangement during the acylation of 4-(2-aminoethylthio)-7-nitrobenzofuran under basic conditions.[8] A plausible mechanism of the

process was provided by them based on the S-N Smiles rearrangement. We realized the importance of the rearrangement in establishing **75** as more specific fluorescent probe for either Cys or *N*-terminal Cys containing peptides/proteins compared to other biothiols (Hcy, GSH and proteins) under physiological conditions. Formation of NBD-amine conjugates with expected longer absorption wavelength and stronger emission would contribute to better sensitivity during labelling.

2B.2 Results and discussion

2B.2.1 Theoretical calculations

We believed that theoretical calculations would provide crucial insights of the fluorescence *Off-On* process during the reaction of **75** with Cys, forming the intermediate NBD-thiol conjugate **75(*S*)$_{Cys}$** as nonfluorescent species which would rearrange to the NBD-amine conjugate **75(*N*)$_{Cys}$** as highly fluorescent species. Therefore, gas phase geometry optimized structures of **75**, **75(*S*)$_{Cys}$** and **75(*N*)$_{Cys}$** were obtained by using density functional theory (DFT) at the B3LYP/6-311G(d,p) level (Figure 2B.2-2B.4). Optimized geometries were then subjected to time-dependent DFT (TDDFT) calculations to predict the emission properties of these species. For probe **75**, the $S_0 \rightarrow S_1$ transition (*i.e.* HOMO-1→LUMO or HOMO-1→LUMO+1 electronic excitation) provided an oscillator strength, f = 0.0000 indicating a forbidden transition process and S_1 as the dark state (Table 2B.1). The first allowed transition obtained from this calculation was $S_0 \rightarrow S_2$ (*i.e.* HOMO→LUMO electronic excitation) with f = 0.2173 confirming S_2 as the emissive state. This data indicate that an emission of electron from S_2 to S_0 would proceed via the intermediate S_1 state and this can be corroborated to a non-radiative pathway from the NBD-moiety to the Cl-moiety. For corresponding thiol addition product **75(*S*)$_{Cys}$**, the $S_0 \rightarrow S_1$ transition was associated with f = 0.0004 confirming the presence of a dark S_1 state. The next $S_0 \rightarrow S_2$ transition was determined as allowed (f = 0.2269). This data confirm **75(*S*)$_{Cys}$** as a nonfluorescent species because $S_2 \rightarrow S_0$ emission would involve the intermediate S_1 state, characteristic of a non-radiative pathway. On the other hand, TDDFT calculation for **75(*N*)$_{Cys}$** confirms an allowed $S_0 \rightarrow S_1$ transition (f = 0.281) and S_1 as the emissive state. Therefore, the corresponding emission process $S_1 \rightarrow S_0$ (*i.e.* LUMO→HOMO electronic transition) corroborates with the strong fluorescence of **75(*N*)$_{Cys}$**.

Table 2B.1: Electronic excitation energies (eV) and oscillator strengths (*f*), configurations of the low-lying excited states of **75**, **75(*S*)$_{Cys}$** and **75(*N*)$_{Cys}$**, calculated by TDDFT method at the B3LYP/6-311G(d,p) level after obtaining the optimized ground state geometries of each one using DFT calculations at the same level.

Species	Electronic transition	E [a] (eV)	λ (nm)	f [b]	Main configurations	CI coefficients
75	$S_0 \rightarrow S_1$	3.45	359	0.0000	HOMO-1→LUMO	0.6614
					HOMO-1→LUMO+1	0.2354
	$S_0 \rightarrow S_2$	3.65	340	0.2173	HOMO→LUMO	0.7026
75(*S*)$_{Cys}$	$S_0 \rightarrow S_1$	2.96	419	0.0004	HOMO-1→LUMO	-0.1225
					HOMO→LUMO	0.6949
	$S_0 \rightarrow S_2$	3.1	400	0.2269	HOMO-1→LUMO	0.6827
					HOMO→LUMO	0.1260
75(*N*)$_{Cys}$	$S_0 \rightarrow S_1$	3.37	368	0.2810	HOMO→LUMO	0.6987

[a] Only the selected low-lying excited states are presented. [b] Oscillator strength.

The molecular geometries of **75** were fully optimized at a level of density functional theory employing the hybrid functional B3LYP with Pople's basis set 6-311G (d, p) where polarization functions were added to all the atoms and diffuse functions to the heavy atoms. All the calculations were performed with the development version of Gaussian 09.

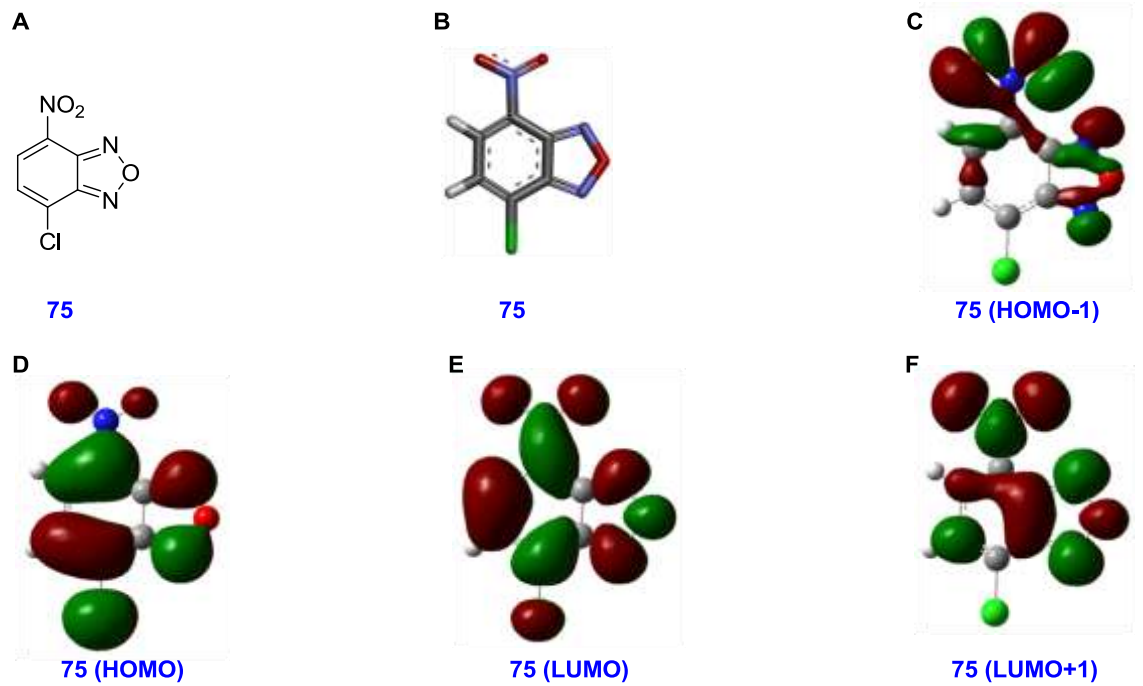

Figure 2B.2: Geometry optimized structures and molecular orbitals (MOs) of different electronic states for **75**.

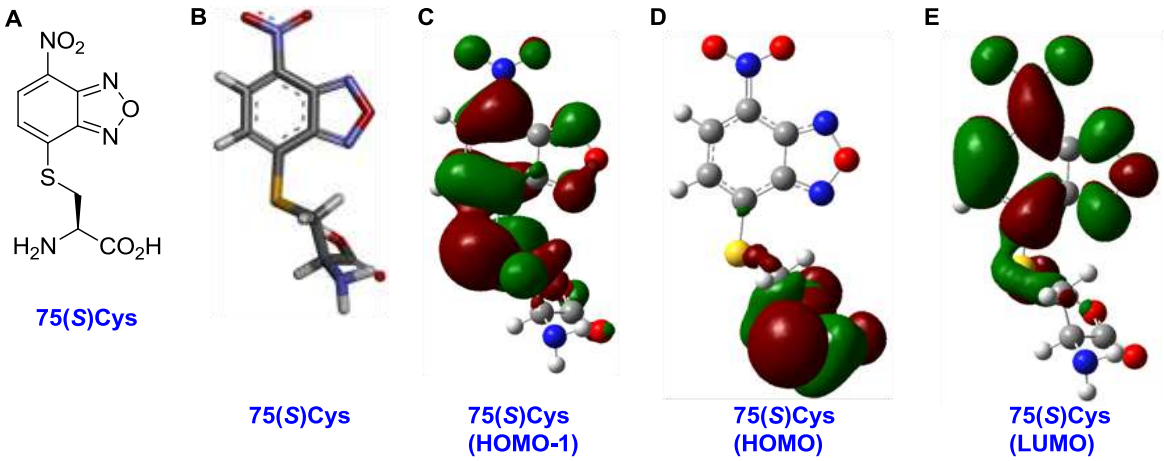

Figure 2B.3: Geometry optimized structures and molecular orbitals (MOs) of different electronic states for **75(*S*)$_{Cys}$**.

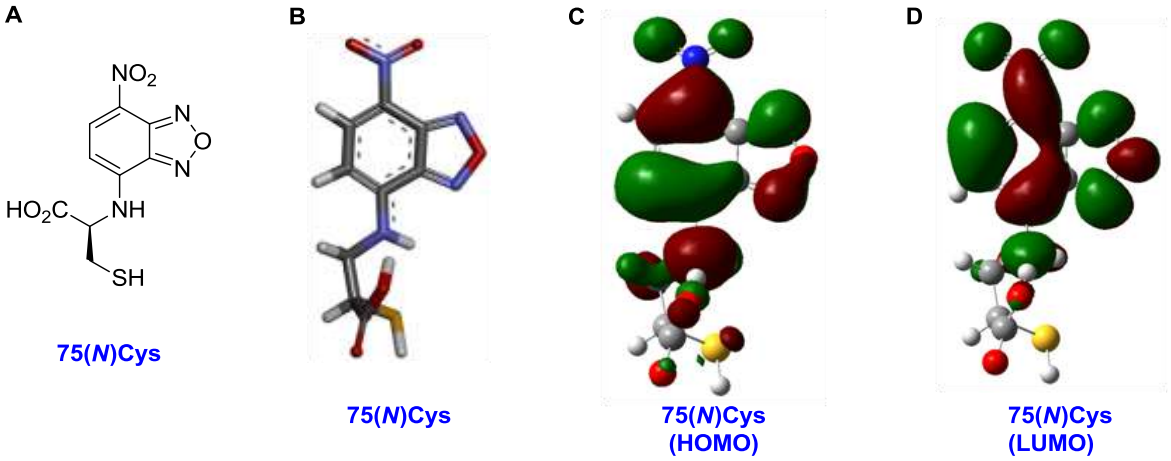

Figure 2B.4: Geometry optimized structures and molecular orbitals (MOs) of different electronic states for **75(*N*)$_{Cys}$**.

2B.2.2 Synthesis

Probe **75** is commercially available. However, reference molecules **76** and **77** were synthesized in order to experimentally verify the fluorescence properties. Compound **76** as representative molecule for NBD-thiol conjugate was synthesized in 80% yield by reacting **75** with *N*-(tert-Butoxycarbonyl)-L-cysteine methyl ester in CH_3CN and using K_2CO_3 base at room temperature (Scheme 2B.1). Similarly, NBD-amine conjugate NBD-NHBu **77** was also synthesized following a reported procedure.[9] Structures of few other analytes *N*-acetyl cysteine **78**, *S*-methyl cysteine **79** and cysteamine **80** are also presented in Scheme 2B.1.

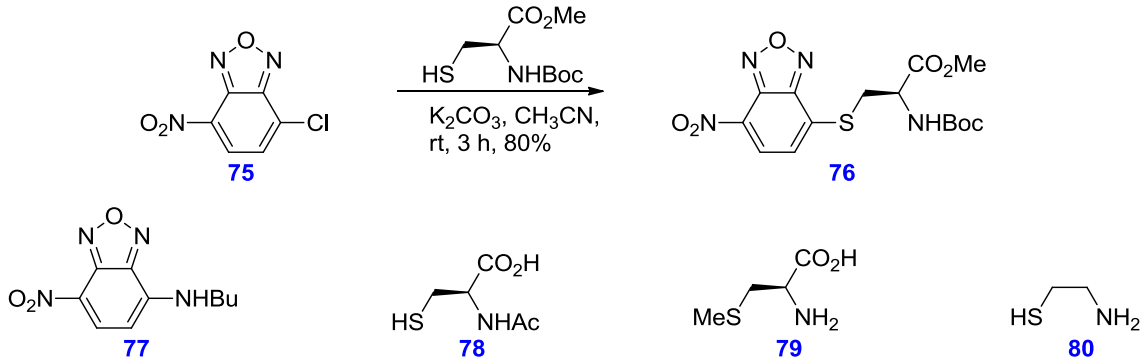

Scheme 2B.1: Synthesis of compound **76** and structures of compounds **77**, **78**, **79** and **80**.

2B.2.3 Thiol sensing

To establish the two-step process involving SNAr substitution followed by Smiles rearrangement, UV-visible studies on **75** (10 μM) in presence of various analytes *e.g.* Cys, **78**, **79**, **80**, Gly Ala, Ser, $BuNH_2$, Hcy, and GSH (100 μM each) were carried out in parallel under the comparable conditions. As shown in Figure 2B.5A, the UV-vis spectrum of the probe **75** (10 μM, HEPES buffer 10 mM, pH = 7.4, 1.0% DMSO) displayed a strong absorption **76** and **77** (10 μM each) were also recorded under comparable conditions. Treatment of *N*-acetyl cysteine **78** to **75** in HEPES buffer (10 mM, pH 7.4, 1.0% DMSO) for 15 min resulted in the appearance of a second absorption band at maxima at λ = 425 nm. A similar band with λ_{max} = 420 nm was also displayed by the compound **76**. On the other hand, addition of *S*-methyl cysteine **79** to **75** did not generate any new band when it was compared to **75**. The response of the probe **75** to $BuNH_2$ was also similar to its response to **79**. In order to analyze these observations, the UV-vis spectrum of the isolated NBD-NHBu **77** was recorded. The spectrum exhibited a strong absorption band centered at λ_{max} = 485 nm. This data clearly confirm that the free $-NH_2$ group of either **79** or $BuNH_2$ did not participate in the SNAr reaction under physiological conditions.

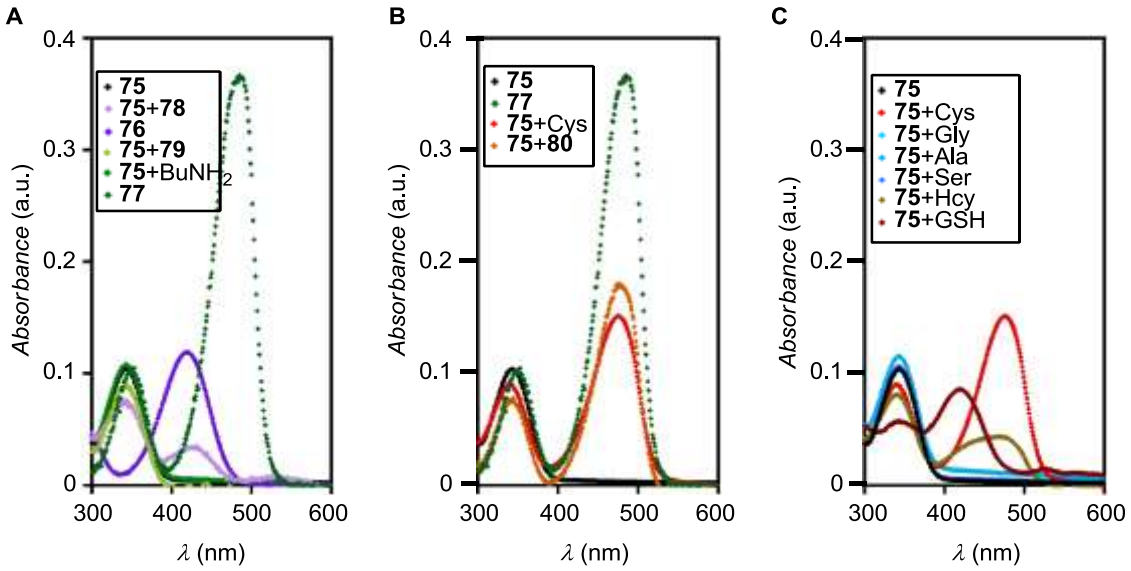

Figure 2B.5: Comparison of UV-vis spectra of free **75** (10 μM), **76** (10 μM), **77** (10 μM) and **75** in the presence of **78**, **79** and $BuNH_2$ (100 μM each) recorded in HEPES (10 mM, pH = 7.4, 1.0% DMSO) buffer (**A**). Comparison of UV-vis spectra of free **75** (10 μM), **77** (10 μM) and **75** in the presence of Cys and **80** (**B**). Comparison of UV-vis spectra of free **75** (10 μM) and **75** in the presence of analytes Cys, Gly, Ala, Ser, Hcy and GSH (**C**).

When Cys was added to **75**, a new intense absorption band at λ_{max} = 478 nm was observed (Figure 2B.5B). This new band which resembles the UV-visible band of **77**, confirms the formation of a NBD-amine conjugate as final product during the reaction of Cys with **75**. Similarly, when cysteamine **80** was treated with **75**, a similar absorption band at λ_{max} = 478 nm was observed. Formation of NBD-amine conjugates in these cases can be rationalized by the fast S-N Smiles rearrangement of intermediate NBD-thiol conjugates. When non-thiol containing amino acids Gly, Ala and Ser were separately added to **75** UV-visible diagrams did not provide any new signal clearly confirming the inertness of probe **75** toward the $-NH_2$ group under the physiological conditions (Figure 2B.5C). According to Figure 2C, addition of Hcy to **75** displayed a broad absorption band from 400 nm to 520 nm. The appearance of this broad band can be attributed to overlap of two absorptions, one around 425 nm (due to NBD-thiol conjugate) and other at 478 nm (due to NBD-amine conjugate) indicating the presence of both NBD-thiol and NBD-amine species. This data confirms the slower rate of Smiles rearrangement involving Hcy compared to Cys. Addition of GSH on the other hand, displayed a single band λ_{max} = 425 nm that corresponding to NBD-thiol species. Absence of any UV-visible absorption around λ = 478 nm in this case, confirms the non-feasibility of the S-N Smiles rearrangement.

Response times of Cys, **80**, Hcy and GSH toward **75** were determined by fluorescence emission kinetics in HEPES buffer (10 mM, pH = 7.4, 1.0% DMSO). In each experiment, reactions of **75** (10 μM) with these analytes were monitored in parallel by recoding emission intensity at λ = 548 nm (λ_{ex} = 470 nm) with respect to time. To the solution, either of Cys, **80**, Hcy and GSH (10 μM each) was added at *t* = 50 seconds. During the addition of Cys, the fluorescence enhancement reached the maximum level after 11 min of addition (Figure 2B.6). A similar response was also observed in upon addition of **80** to **75**. Addition of Hcy to **75** displayed a response time > 30 min. When GSH was added with **75**, only a small enhancement of emission intensity was observed up to 30 min of addition and this can be attributed to the weak fluorescence of NBD-thiol species.

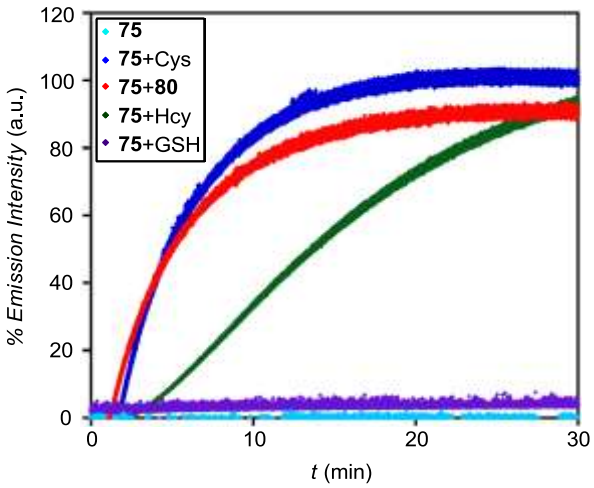

Figure 2B.6: Emission kinetics profiles of free **75** (10 μM) and reactions of **75** with Cys, Hcy, GSH and **80** (100 μM each) in HEPES buffer (10 mM, pH = 7.4, 1.0% DMSO). All analytes were added at *t* = 50 s and emission intensities were monitored at λ = 548 nm (λ_{ex} = 470 nm).

In the next stage, selectivity and sensitivity of the probe **75** towards various analytes were determined. In these experiments, a solutions of Gly, Ala, Ser, $BuNH_2$, Hcy, **78**, **79**, Cys and **80** (100 μM each) were separately added to **75** (10 μM) in HEPES buffer (10 mM, pH 7.4, 1.0% DMSO) and emission spectra were recorded after 15 min of stirring at room temperature. Emission spectra of probe **75**, NBD-thiol conjugate **76** and NBD-amine conjugate **77** were also recorded. Probe **75** in presence of non-thiol containing amino acids, displayed negligible enhancements in emission intensity confirming the non-feasibility of NBD-amine conjugate formation (Figure 2B.7). Similar observations were recorded when probe **75** was treated with either $BuNH_2$ or *S*-methyl cysteine **79**. These results indicate that the direct SNAr substitution of –Cl by $–NH_2$ is not feasible under physiological conditions. The strong fluorescence of NBD-NHBu **77** further confirms the inertness of either $BuNH_2$ or *S*-methyl cysteine **79** toward **75**.

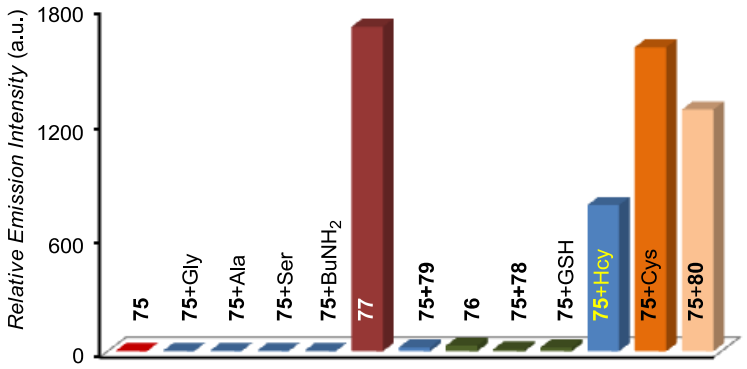

Figure 2B.7: Relative emission intensity at λ_{em} = 548 nm (λ_{ex} = 470 nm) of **75** (10 μM) before and after addition of various analytes Gly, Ala, Ser, $BuNH_2$, **78**, **79**, GSH, Hcy, Cys and **80** (100 μM each) recorded in HEPES buffer (10 mM, pH = 7.4, 1.0% DMSO). The diagram also represents comparison of the data with conjugates **76** and **77**.

Enhancement of emission intensity after the addition of *N*-acetyl cysteine **78** to **75** was also very small. This data along with UV-visible studies suggests the formation of NBD-thiol conjugate. Only 20-fold emission intensity for **76** compared to **75** confirms the weak fluorescence of the NBD-thiol conjugate. Addition of GSH to **75** did not provide any considerable jump in fluorescence suggesting the NBD-thiol conjugate of GSH addition is nonfluorescent. Probe **75** in response of Cys displayed 1592-fold enhancement in emission intensity. A comparison of this data with the fluorescence of **77** indicates the formation of NBD-amine conjugate as active species. A similar enhancement (1265-fold) was also observed when cysteamine **80** was added to **75**. Therefore, the two-step process involving SNAr reaction followed by a fast Smiles rearrangement occurs fast for either Cys or **80** due to formation of a cyclic five-membered transition state. To the best of our knowledge, this is the highest fold enhancement in emission intensity observed during detection of Cys under physiological conditions. When Hcy was treated with **75**, a 765-fold enhancement in emission intensity was observed. Based on UV-visible data, supported by fluorescence emission data the incomplete Smiles rearrangement can be confirmed even after 30-min of addition.

In order to evaluate the quantitative fluorescent *Off-On* response of **75** for Cys, both UV-visible and fluorometric titrations were carried out. In these experiments, the probe **75** (10 μM) was separately treated with increasing concentrations of Cys (0-100 μM) in HEPES buffer (10 mM, pH = 7.4, 1.0% DMSO) at room temperature for 15 min and UV-visible followed by fluorescence spectra were recorded. During the titration, a

gradual decrease of the absorption band at 343 nm and appearance of a new band at 478 nm were observed (Figure 2B.8A). From this diagram an isosbestic point at 382 nm was also obtained. Upon plotting the ratio of absorbance at 478 and 344 nm (A_{478}/A_{343}) against the concentration of Cys, a linear correlation was obtained (Figure 2B.8B) suggesting the importance of the probe **75** for quantitative determination of Cys concentrations.

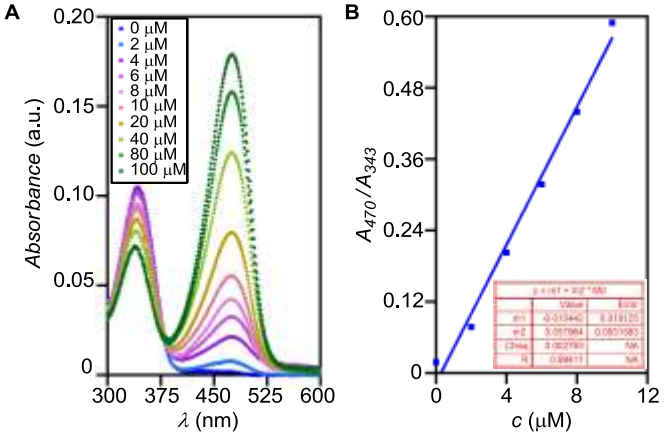

Figure 2B.8: Changes on absorbance of **75** (10 μM) upon addition of Cys (0, 2, 4, 6, 8, 10, 20, 40, 80 and 100 μM) measured by UV-visible spectroscopy (**A**). Ratiometric calibration curve of the absorbance at 470 nm and 343 nm as a function of the Cys concentration (**B**). Each spectrum was recorded 15 min after addition in HEPES buffer (10 mM, pH = 7.4, 1.0% DMSO).

Fluorometric titrations were carried out by treating **75** (10 μM) with Cys (0 – 100 μM) in HEPES buffer (10 mM, pH = 7.4, 1.0% DMSO) for 15 min and recording fluorescence spectra (λ_{ex} = 470 nm). As shown in Figure 2B.9, sensing of Cys by **75** resulted in a significant increase in emission intensity with emission maxima λ_{em} = 548 nm. When fluorescence intensities at 548 nm were plotted against concentrations of Cys linear increase was observed up to 1.0 equivalent of Cys added. Using this data, a detection limit of 2.0×10^{-8} M (*S/N* = 3) was calculated during the sensing of Cys (Table 2B.2).

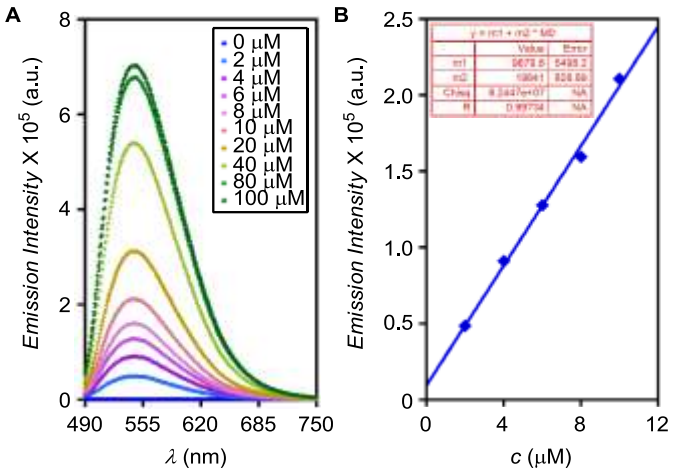

Figure 2B.9: Changes on emission intensity of **75** (10 µM) upon addition of Cys (0, 2, 4, 6, 8, 10, 20, 40, 80 and 100 µM) measured by fluorescence spectroscopy (**A**). The linear relationship (at 548 nm) between the fluorescence emission intensity of **75** and concentration (2, 4, 6, 8 and 10 µM) of Cys (**B**). Each spectrum was recorded 15 min after addition (λ_{ex} = 470 nm) in HEPES buffer (10 mM, pH = 7.4, 1.0% DMSO).

Table 2B.2: Calculation of detection limits of Cys sensing by probes **75**.

Probe	σ	m	S/N	detection limit
75	192.76	2.805×10^4	3	2.0×10^{-8} M

2B.2.4 ^{1}H NMR titration

^{1}H NMR titrations were carried out to identify the product formed and confirm the slow rate of Smiles rearrangement for Hcy compare to that of Cys (Figure 2B.10). Addition of Hcy (2.0 equivalents) to **75** in 3:1 DMSO-d_6/HEPES buffer (in D_2O pH = 7.4) resulted in the formation of new peak at 7.53 δ corresponding to $\mathbf{75(}\boldsymbol{S}\mathbf{)_{Hcy}}$ adduct (Figure 2B.10D). After addition of 4.0 equivalents of Hcy, intensity of peak at 7.53 δ was increased but the peak at 6.38 δ corresponding to $\mathbf{75(}\boldsymbol{N}\mathbf{)_{Hcy}}$ was not observed (Figure 2B.10E). Addition of Cys (2.0 equivalents) to **75** in DMSO-d_6: HEPES buffer in D_2O (3:1) resulted in the formation of new peak at 7.53 δ corresponding to $\mathbf{75(}\boldsymbol{S}\mathbf{)_{Cys}}$ adduct. In this case, a smaller peak at 6.38 δ corresponding to $\mathbf{75(}\boldsymbol{N}\mathbf{)_{Cys}}$ was also observed (Figure 2B.10F). After addition of 4.0 equivalents of Cys, intensity of both peaks (at 7.53 δ and 6.38 δ) increased remarkably (Figure 2B.10G).

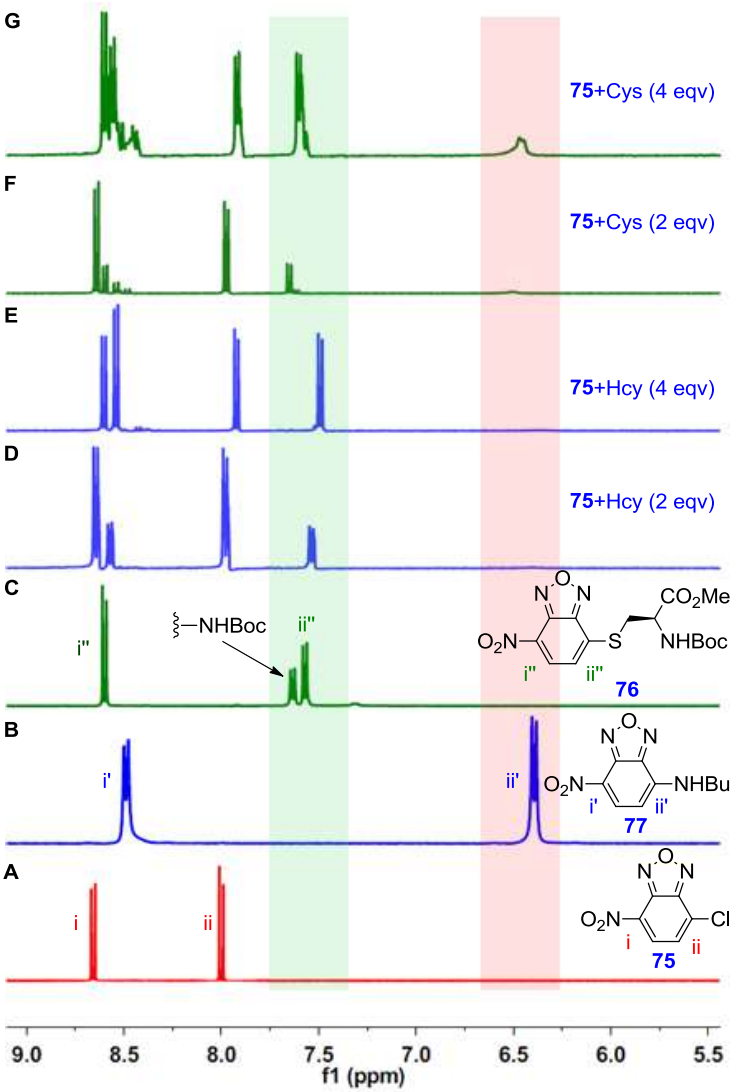

Figure 2B.10: Partial ^{1}H NMR spectra of **75**.in DMSO-d_6(**A**) **77** (**B**) and **76**, (**C**). ^{1}H NMR of **75** with 2.0 eq of Hcy, (**D**) 4.0 eq of Hcy, (**E**) ^{1}H NMR of **75** with 2.0 eq of Cys and (**F**) 4.0 eq of Cys (**G**). Each spectrum **D-G** was recorded after 5 min of addition.

2B.2.5 Cell imaging

IC_{50} for probe 75 was 6.91 μM.[10] Imaging of intracellular Cys of HeLa cells with probe **75** was carried out. When cells were incubated with **75** (10 μM) for 30 min, weak fluorescence was observed (Figure 2B.11A, 2B.11B and 2B.11C). Considering UV-vis, fluorescence based results on selectivity of **75** toward Cys and reported low intracellular free Cys concentration, the imaging data can be corroborated to fluorescent Cys-addition product. When the cells were pre-treated with Cys (500 μM) for 30 min and then incubated again with **75** (10 μM) for another 30 min, strong fluorescence was observed

inside HeLa cells (Figure 2B.11D, 2B.11E and 2B.11F) indicating the imaging of Cys inside the cells. In control experiment, cells were pre-treated with an excess (5 mM) of the thiol-reactive *N*-phenylmaleimide and then incubated with the probe **75**. The confocal microscopic studies did not show fluorescence signal (Figure 2B.11G, 2B.11H and 2B.11I). This confirms the specificity of probe **75** for thiols over other analytes in living cells.

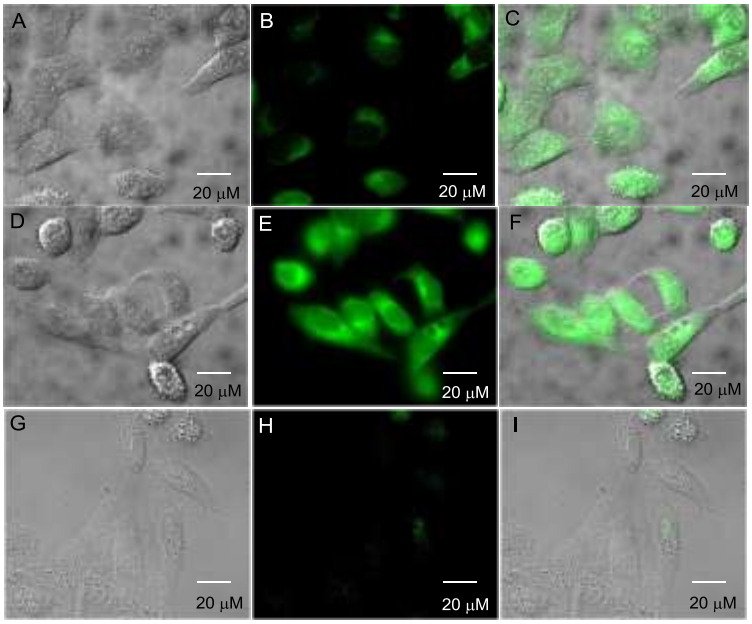

Figure 2B.11: Brightfield (**A**), fluorescence (**B**) and overlay (**C**) images of living HeLa cells incubated with (10 μM) of **75** for 30 min. Brightfield (**D**), fluorescence (**E**) and overlay (**F**) images of living HeLa cells pre-treated with Cys (500 μM) for 30 min and then incubated with **75** (10 μM) for 30 min (**G**) Brightfield, (**H**) fluorescence and (**I**) overlay images of cells pre-incubated with *N*-phenylmaleimide (5 mM) for 30 min followed by incubation with **75** (10 μM) for 30 min.

In order to quantify the fluorescence increment, cells pre-treated with probe **75**, intensities at selected regions of interest (ROIs) were recorded before incubation and at 30

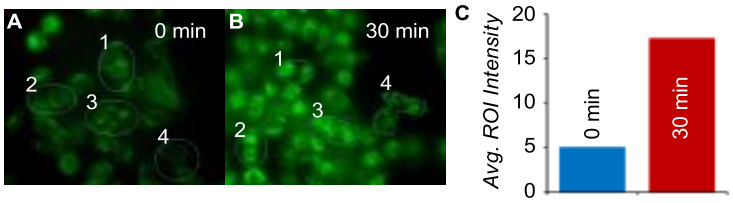

Figure 2B.12: (A) Fluorescence images of HeLa cells incubated with only probe **75**; (B) followed by incubation with Cys for 30 min; and (C) Bar diagram presenting average fluorescence intensity of *ROI* before and after incubation with Cys.

min after incubation with 500 μM of Cys (Figure 2B.12A and 2B.12B). The difference in average pixel intensity obtained from the selected ROIs can be corroborated to the gradual increase in the concentration of fluorescent species **75(*N*)$_{Cys}$** with time (Figure 2B.12C).

2B.3 Summary and conclusions

In summary, we have demonstrated that NBD-chloride **75** which is commonly used for labeling of sulfhydryl groups in proteins can be used more specifically for rapid, selective, and sensitive sensing of Cys. UV-visible and fluorescence spectroscopic methods were used to establish the two-step sensing mechanism via SNAr substitution followed by S-N Smiles rearrangement which ensures selectivity of **75** toward Cys. The rearrangement of NBD-thiol conjugate of Cys occurs at faster rate through a cyclic five-membered transition state and formation of fluorescent NBD-amine conjugate contribute to the ~ 1592-fold *Off-On* sensitivity. Relatively slower rearrangement was observed for NBD-thiol conjugate of Hcy as the process involves cyclic six-membered transition state and 765-fold enhancement was recorded. Sensing of GSH by probe **75** stopped at the corresponding nonfluorescent NBD-thiol conjugate establishing the specificity of the probe. A detection limit of 2.0×10^{-8} M was calculated during the sensing of Cys. The sensing of Cys by probe **75** was also demonstrated by live HeLa cell imaging.

2B.4 References

(1) (a) Mego, J. L. *Biochem. J.* **1984**, *218*, 775(b) Staal, F. J. T.; Ela, S. W.; Roederer, M.; Anderson, M. T.; Herzenberg, L. A.; Herzenberg, L. A. *Lancet* **1992**, *339*, 909(c) White, A. C.; Thannickal, V. J.; Fanburg, B. L. *J. Nutr. Biochem.* **1994**, *5*, 218(d) Refsum, H.; Ueland, P. M.; Nygard, O.; Vollset, S. E. *Annu. Rev. Med.* **1998**, *49*, 31(e) Seshadri, S.; Beiser, A.; Selhub, J.; Jacques, P. F.; Rosenberg, I. H.; D'Agostino, R. B.; Wilson, P. W. F.; Wolf, P. A. *N. Eng. J. Med.* **2002**, *346*, 476(f) Townsend, D. M.; Tew, K. D.; Tapiero, H. *Biomed. Pharmacother.* **2003**, *57*, 145(g) Wang, W.; Rusin, O.; Xu, X.; Kim, K. K.; Escobedo, J. O.; Fakayode, S. O.; Fletcher, K. A.; Lowry, M.; Schowalter, C. M.; Lawrence, C. M.; Fronczek, F. R.; Warner, I. M.; Strongin, R. M. *J. Am. Chem. Soc.* **2005**, *127*, 15949(h) Zou, C.-G.; Banerjee, R. *Antioxid. Redox Signal.* **2005**, *7*, 547.

(2) (a) Yin, C.; Huo, F.; Zhang, J.; Martinez-Manez, R.; Yang, Y.; Lv, H.; Li, S. *Chem. Soc.Rev.* **2013**, *42*, 6032(b) Jung, H. S.; Chen, X.; Kim, J. S.; Yoon, J. *Chem. Soc. Rev.* **2013**, *42*, 6019(c) Chen, X.; Zhou, Y.; Peng, X.; Yoon, J. *Chem. Soc. Rev.* **2010**, *39*, 2120(d) Yin, L.-L.; Chen, Z.-Z.; Tong, L.-L.; Xu, K.-H.; Tang, B. *Fenxi Huaxue* **2009**, *37*, 1073.

(3) (a) Jiang, W.; Cao, Y.; Liu, Y.; Wang, W. *Chem. Commun.* **2010**, *46*, 1944(b) Jiang, W.; Fu, Q.; Fan, H.; Ho, J.; Wang, W. *Angew. Chem., Int. Ed.* **2007**, *46*, 8445(c) Bouffard, J.; Kim, Y.; Swager, T. M.; Weissleder, R.; Hilderbrand, S. A. *Org. Lett.* **2008**, *10*, 37.

(4) (a) Kim, T.-K.; Lee, D.-N.; Kim, H.-J. *Tetrahedron Lett.* **2008**, *49*, 4879(b) Yue, Y.; Guo, Y.; Xu, J.; Shao, S. *N. J. Chem.* **2011**, *35*, 61(c) Hu, M.; Fan, J.; Li, H.; Song, K.; Wang, S.; Cheng, G.; Peng, X. *Org. Biomol. Chem.* **2011**, *9*, 980.

(5) (a) Niu, L.-Y.; Guan, Y.-S.; Chen, Y.-Z.; Wu, L.-Z.; Tung, C.-H.; Yang, Q.-Z. *J. Am. Chem. Soc.* **2012**, *134*, 18928(b) Niu, L.-Y.; Guan, Y.-S.; Chen, Y.-Z.; Wu, L.-Z.; Tung, C.-H.; Yang, Q.-Z. *Chem. Commun.* **2013**, *49*, 1294.

(6) (a) Ghosh, P. B.; Whitehouse, M. W. *Biochem. J.* **1968**, *108*, 155(b) Yang, C.; Jiang, X.; Guo, L.; Zhang, H.; Liu, M. *J. Sep. Sci.* **2007**, *30*, 3154(c) Elbashir, A. A.; Suliman, F. E. O.; Aboul-Enein, H. Y. *Appl. Spectrosc. Rev.* **2011**, *46*, 220.

(7) Houk, T. W.; Ovnic, M.; Karipides, S. *J. Biol. Chem.* **1983**, *258*, 5419.

(8) Castagnolo, D.; Pagano, M.; Bernardini, M.; Botta, M. *Tetrahedron Lett.* **2012**, *53*, 5008.

(9) Saha, S.; Samanta, A. *J. Phys. Chem. A* **1998**, *102*, 7903.

(10) Cummins, I.; Wortley, D. J.; Sabbadin, F.; He, Z.; Coxon, C. R.; Straker, H. E.; Sellars, J. D.; Knight, K.; Edwards, L.; Hughes, D.; Kaundun, S. S.; Hutchings, S.-J.; Steel, P. G.; Edwards, R., *PNAS* **2013,** *110*, 5812.

Chapter 2

Section C

BODIPY based Fluorescence *Off-On* probes for Detection of Biological Thiols in Lysosomes

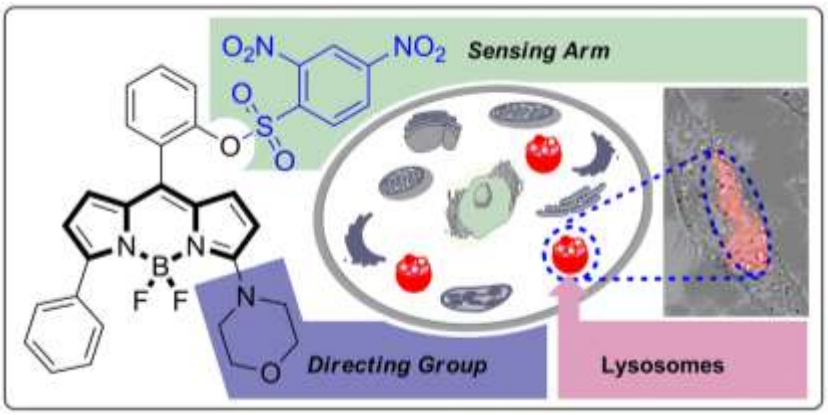

2C.1 Introduction

In the past few decades, the development of fluorescent probes for detection of thiols has attracted great attention because fluorescent probes offer high selectivity, sensitivity and have an excellent potential as useful tools for real time imaging in biological samples and living systems. Many fluorescent probes are reported for the selective detection of biothiols in biological samples and living cells but without location specificity, in particular sub cellular localization.[1]

Eukaryotic cells contain various compartments and cell organelles such as nucleus, mitochondria, endoplasmic reticulum, lysosomes, *etc*. Each cell organelle is associated with specific function/s essential for life. For example, lysosomes have intracompartmental pHs of 4.0–6.0 and it contain approximately 50 different degradative enzymes that are active at acidic pH.[2] The lysosome membrane constitutes a physiological barrier between the lysosome matrix and the surrounding cytoplasm. The membrane's impermeability ensures the retention of both the lysosomal enzymes and their substrates within lysosomes.[3] It is believed that GSH may be involved in stabilizing lysosome membranes.[4] Thiols facilitate intralysosomal proteolysis by reducing disulphide bonds.[5] For example, Cys is an effective stimulator of albumin degradation in liver lysosomes.[4] For better understanding of the role of lysosomal thiols it is important to develop fluoresent probes capable of targeting lysosomes. Mitochondria targeting fluorescent probes for selective detection of biothiols are known. To the best of our knowledge, till date, lysosome targetting fluorescent probe for selective detection of biothiols is not known.

Our objective was to develop of lysosome targeting fluorescence turn-*on* probe for biothiols To obtain a photostable water soluble fluorescent thiol probe, excitable in the visible region and applicable for live-cell imaing, boron-dipyrromethene (BODIPY) was selected as the fluorophore.[6] The necessary molecular decorations for thiol recognition and lysosome targeting were incorporated via 2,4-dinitrobenzenesulfonyl (DNs) group and morpholine ring,[7] respectively. As BODIPY-based chemosensors operate by perturbing the reduction potential of the *meso*-substituent, the DNs group was attached to aryl group at *meso*-position. Moreover, a phenyl ring at 5-position was considered for extended conjugation and thereby, exciting at longer wavelengths while maintaining high quantum yield. Based on these fragments we designed probe **81** (Figure 2C.1).

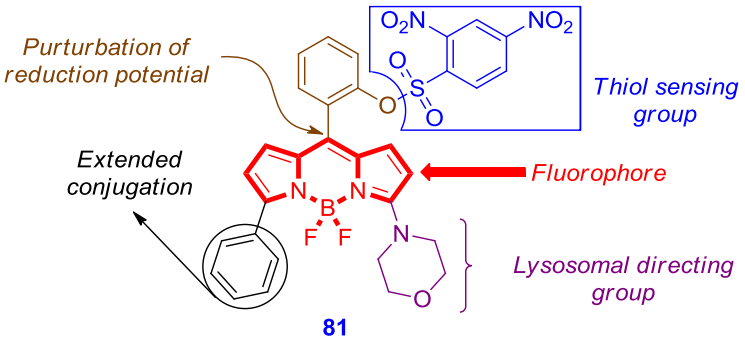

Figure 2C.1: Structure of the lysosome targeting probe **81**.

2C.2 Results and discussion

2C.2.1 Synthesis

Synthesis of the probe was carried out in five steps (Scheme 2C.1). Dipyrromethane **83** was synthesized from salicylaldehyde **82** and pyrrole in presence of catalytic CF_3COOH in 64% yield. Dipyrromethane **83** was dibrominated with two equivalent of *N*-bromosuccinimide in tetrahydrofuran at -78 °C and oxidized with DDQ in dichloromethane followed by the addition of $BF_3{\cdot}OEt_2$ and Et_3N afforded the BODIPY core **84** in 60% yield. Reaction of dibromo BODIPY **84** with morpholine resulted in monobromo BODIPY **85** in 80% yield which on Suzuki coupling reaction with phenyl boronic acid resulted in the formation of compound **86** in 79% yield. Probe **81** was synthesized in high yield by sulfonating the hydroxyl group of **86** with 2,4-dinitrobenzene-1-sulfonyl chloride. Single crystal X-ray diffraction structures for compound **85** and probe **81** were recorded.

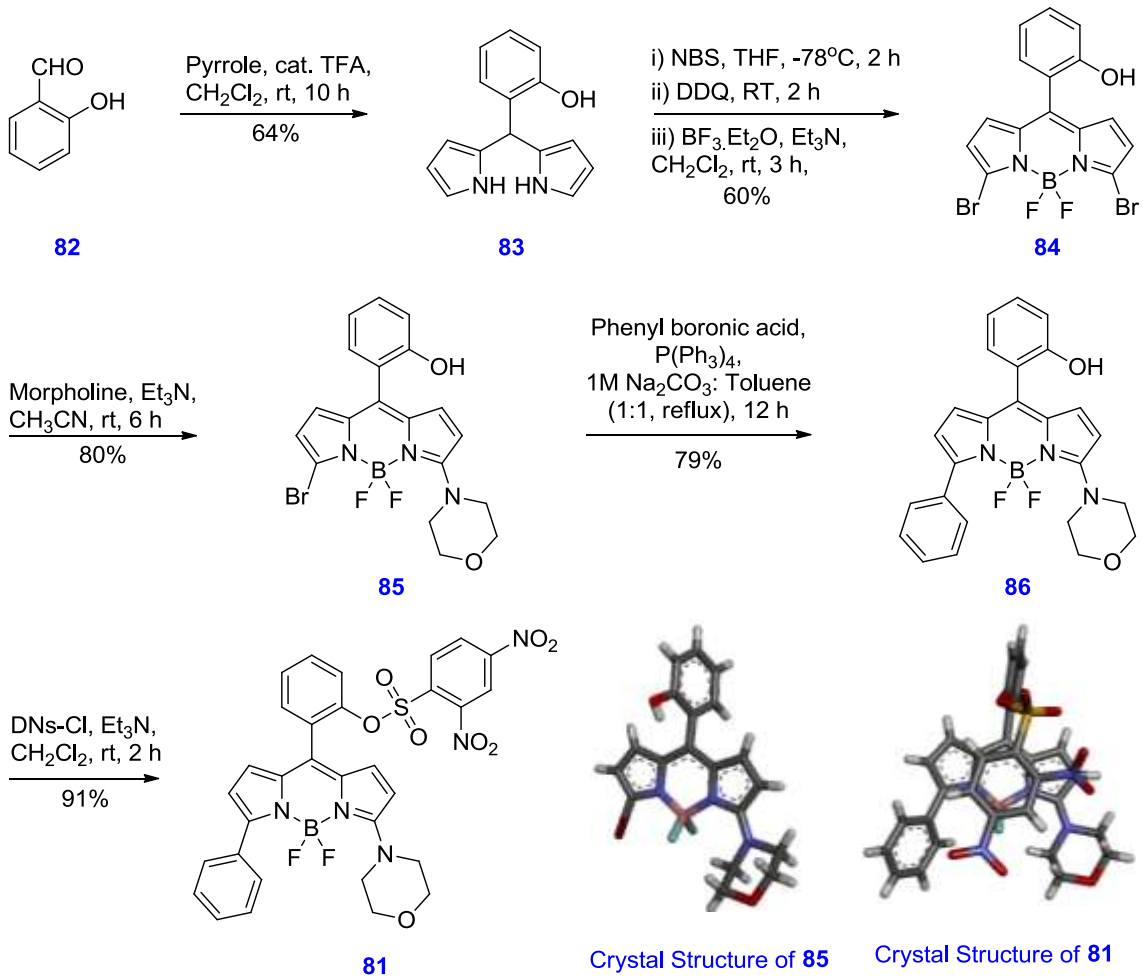

Scheme 2C.1: Synthesis of probe **81**.

2C.2.2 Photophysical studies

To validate the *Off–On* nature of sensing, the photophysical properties of probe **81** and compound **81** were investigated in aqueous HEPES buffer (10 mM, pH 7.4, 1 mM CTAB) solution. The absorption spectrum of probe **81** exhibited λ_{max} = 510 nm with a molar extinction coefficient ε = 18600 L mol^{-1} cm^{-1} (Figure 2C.2 and 2C.3) and is weakly fluorescent (λ_{ex} = 510 nm, ϕ = 0.003, standard fluorescein, Φ = 0.85 in 0.1 N NaOH). Compound **86** exhibited an absorption band centred at λ_{max} = 515 nm in with a molar extinction coefficient ε = 23966 L mol^{-1} cm^{-1}. The fluorescence spectra acquired for **86** indicate a strong fluorescence emission (λ_{ex} = 510 nm, ϕ = 0.003, standard fluorescein, Φ = 0.85 in 0.1 N NaOH) centred at λ_{em} = 584 nm. These photophysical data satisfy the criteria of probe **81** to act as an efficient fluorescent turn-*On* probe.

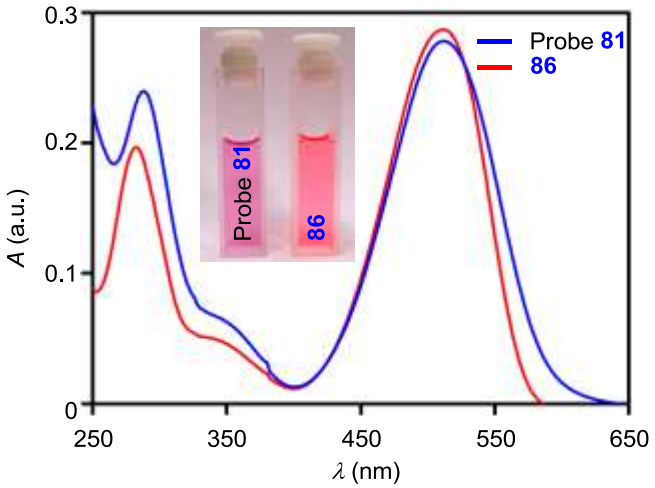

Figure 2C.2: Absorbance spectra of probe **81** (10 μM) and compound **86** (10 μM) in HEPES buffer (10 mM, 1 mM CTAB, pH 7.4).

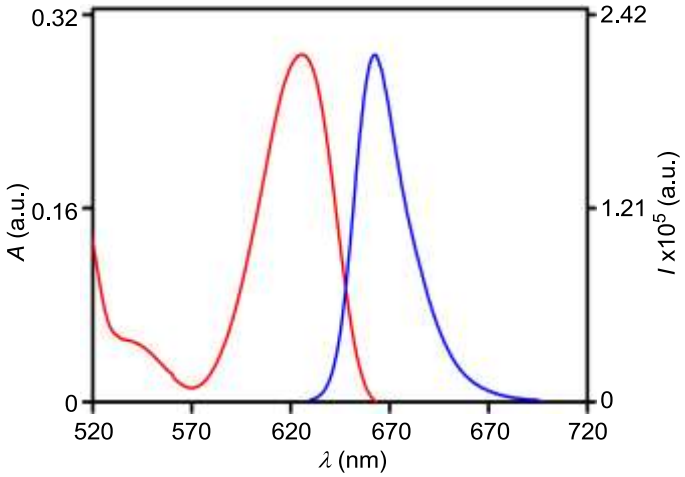

Figure 2C.3: Normalised absorbance and fluorescence spectra of probe **81** (10 μM) in HEPES buffer (10 mM, 1 mM CTAB, pH 7.4).

2C.2.3 Thiol sensing

Reactivity of the probe **81** (10 μM) towards *n*-$BuNH_2$, Cys, GSH and Hcy (100 μM) were determined by fluorescence emission kinetics in HEPES buffer (10 mM, 1 mM CTAB, pH = 7.4). In each experiment, emission intensity at λ = 585 nm (λ_{ex} = 510 nm) was recorded with time. Addition of *n*-$BuNH_2$ to probe **81** did not indicate formation of fluorescent species during the reaction (Figure 2C.4A). A pronounced fluorescent intensity increase up to ~64-fold was obtained even 1 min after the addition of Cys ($t_{1/2}$ = 0.64 s and pseudo first order rate constant, k = 1.08 s^{-1}), Hcy ($t_{1/2}$ = 14.49 s and k = 0.0478 s^{-1}) and GSH ($t_{1/2}$ = 7.47 s and k = 0.0928 s^{-1}). No significant fluorescent enhancement was

observed upon treatment of the probe with *n*-$BuNH_2$. Fluorescence *turn-On* response by **81** during sensing of Cys was also confirmed by appearance of orange fluorescence (Figure 2C.4C) when cuvette images were taken under hand held UV-lamp (λ_{ex} = 365 nm).

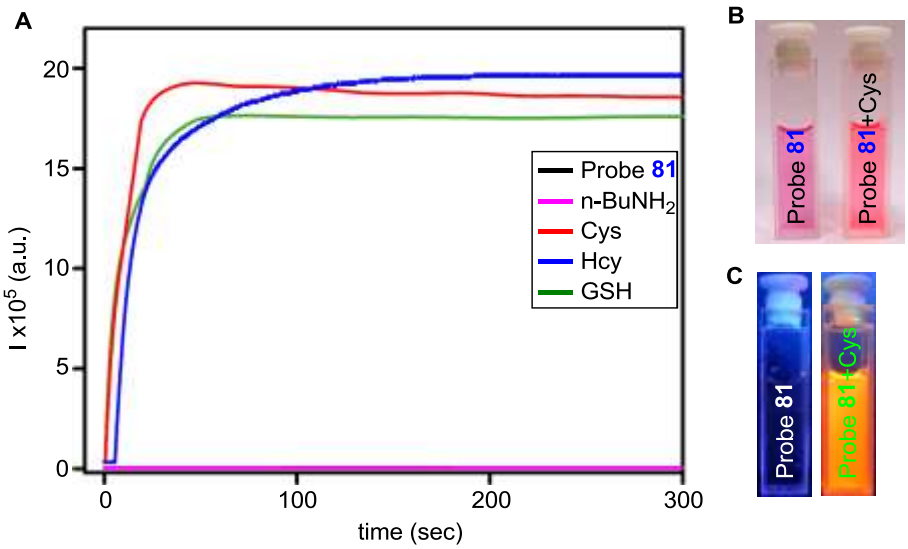

Figure 2C.4: Fluorescence kinetics of probe **81** (10 μM in 10 mM HEPES buffer, 1 mM CTAB, pH = 7.4) with various analytes (100 μM). All data were recorded at λ_{em} = 585 nm (λ_{ex} = 510 nm) (**A**) and changes in visible and emission color in the presence of various analytes (**B** and **C**).

In next stage, the selectivity of probe **81** towards biological thiols was examined. In each case, probe **81** (10 μM) was treated separately with 100 μM of each analyte (either of Ala, Arg, His, NaCl, Na_2SO_4, NaSCN, $NaNO_3$, $BuNH_2$, Ser, GSH, Cys and Hcy) in HEPES buffer (10 mM, pH = 7.4, 1 mM CTAB) and fluorescence spectra were recorded after 5 min at room temperature. However no significant fluorescence enhancement (λ_{ex} = 510 nm) was observed for analytes other than GSH, Cys and Hcy (Figure 2C.5). Treatment of probe **81** with GSH, Cys and Hcy under identical conditions provided strong fluorescence (λ_{em} = 585 nm). When fluorescence intensities at 585 nm were compared, ~ 64-fold enhancement was observed in the case of GSH, Cys and Hcy and the sensing process is also associated with 64-fold enhancement in Φ (from Φ = 0.003 to 0.62).

Figure 2C.5: Relative fluorescence intensity enhancements (I/I_0) at 585 nm for probe **81** (10 μM) towards Cys (100 μM) in HEPES buffer. Front row: changes in intensities in the presence of various analytes (100 μM); back row: Cys was added in the presence of the respective analyte.

In the next stage, we examined the quantitative response of **81** towards Cys by fluorometric titrations. Sharp enhancements in fluorescence (λ_{em} = 585 nm) were observed (Figure 2C.6) when titrations were carried out by addition of increasing concentrations of Cys (0 to 40 μM) in the probe **81** (10 μM) in HEPES buffer (10 mM, pH = 7.4, 1 mM CTAB).

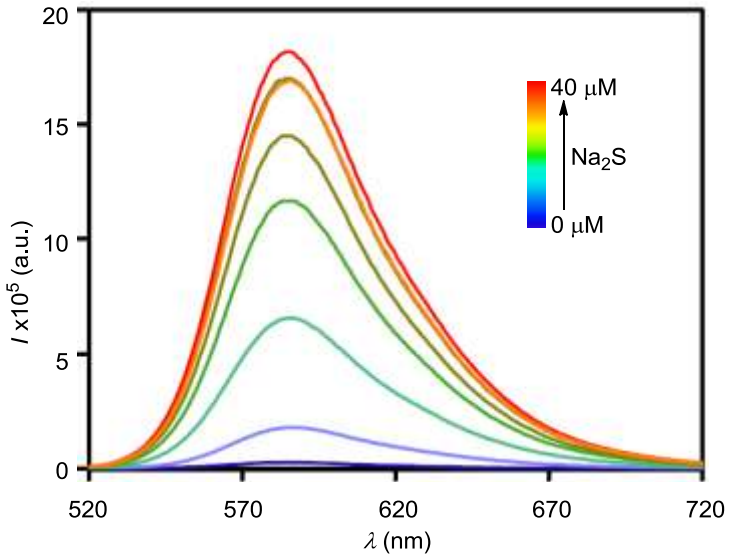

Figure 2C.6: Fluorescence spectra of **81** (10 μM) in presence of Cys (0, 2, 4, 6, 8, 10, 20 and 40 μM) with λ_{ex} = 510 nm.

Determination of detection limits of probe 81 towards Cysteine sensing:

When fluorescence intensities at 585 nm were plotted against concentrations of Cys, good linear correlation (Regression factor, R = 0.9686) was observed up to one equivalent of the Cys added (Figure 2C.7). The detection limit was then calculated with the equation: detection limit = $3\sigma/m$, where σ is the standard deviation of 7 blank measurements, m is the slope between intensity versus Cys concentration. The detection limits of **81** towards Cys was calculated to be 8.2×10^{-9} M at S/N = 3 (signal-to-noise ratio of 3:1).

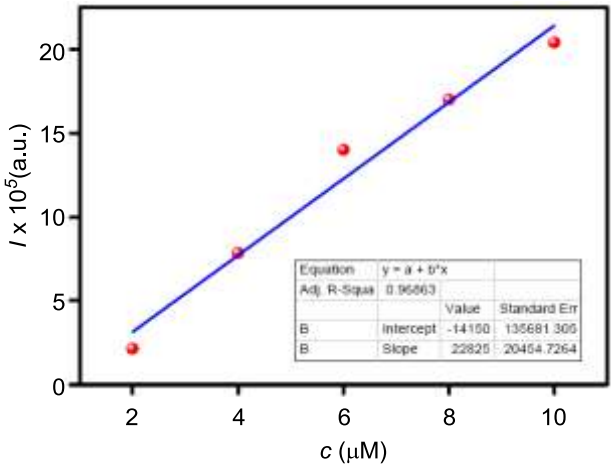

Figure 2C.7: The linearity of the Cys titration assay of probe **81** (10 μM) in the presence of a Cys (2, 4, 6, 8 and 10 μM) recorded in HEPES buffer (10 mM, 1 mM CTAB, pH = 7.4).

2C.2.4 ^{1}H NMR titration

The proposed mechanism of thiol sensing by probe **81** was confirmed by ^{1}H-NMR titration studies (Fig. 2C.8). Upon addition of Cys (0 – 4 equivalent) to **81** (4.3 mg in 0.7 mL DMSO-d 6), peaks at δ = 5.93 and 6.21 ppm corresponding to probe **81** were disappeared gradually. A simultaneous gradual increase of new peaks at δ = 6.05 and 6.35 ppm corresponding to **86** was observed.

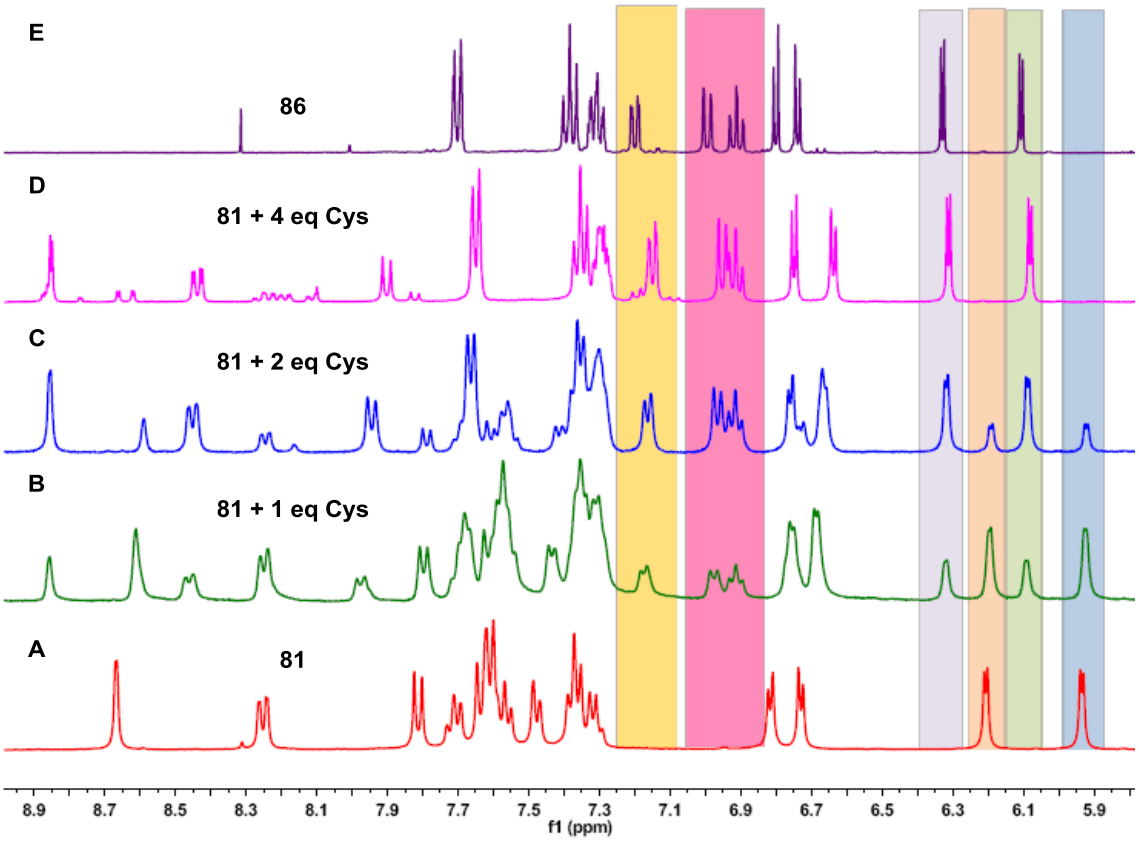

Figure 2C.8: ^{1}H NMR spectrum of **81** (**A**);.**81** + 1.0 eq of Cys (**B**); **81** + 2.0 eq of Cys (**C**); **81** + 4.0 eq of Cys (**D**) and **86** (**E**).

HPLC chromatograms recorded in the gradient method using acetonitrile and H_2O eluent show that the reaction of probe **81** (t_R = 17.56 min) with Cys resulted in the cleavage of DNs to form compound **86** (Figure 2C.9). UV active peak appearing at t_R = 16.34 min when collected and analyzed by MALDI-*TOF* which showed peak at *m/z* = 445.13 corresponding to compound **86** (Figure 2C.10).

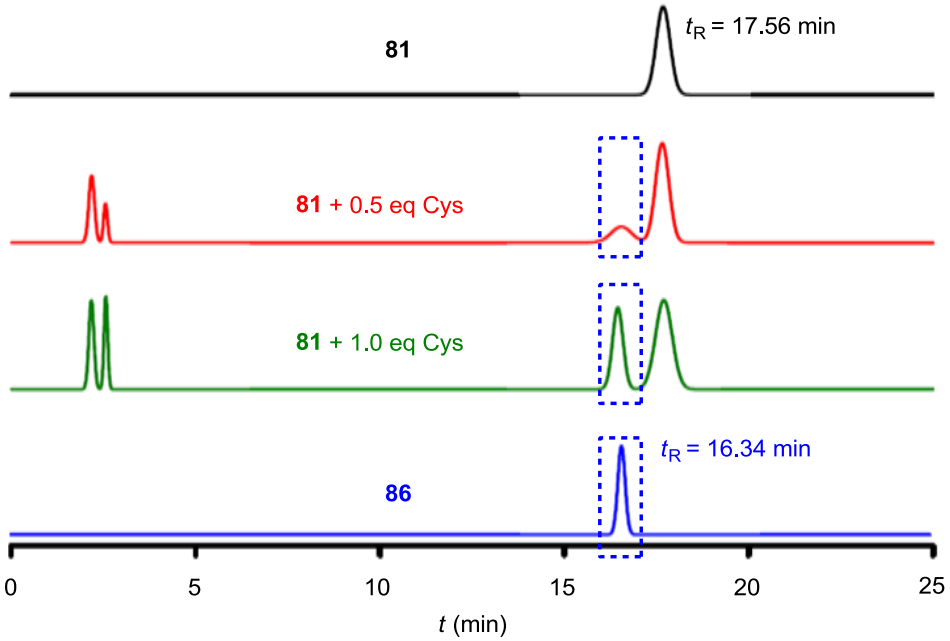

Figure 2C.9: HPLC chromatograms of probe **81** (10 μM) upon reaction with Cys (0.5 and 1.0 equivalent) recorded in a gradient solvent system of acetonitrile and H_2O.

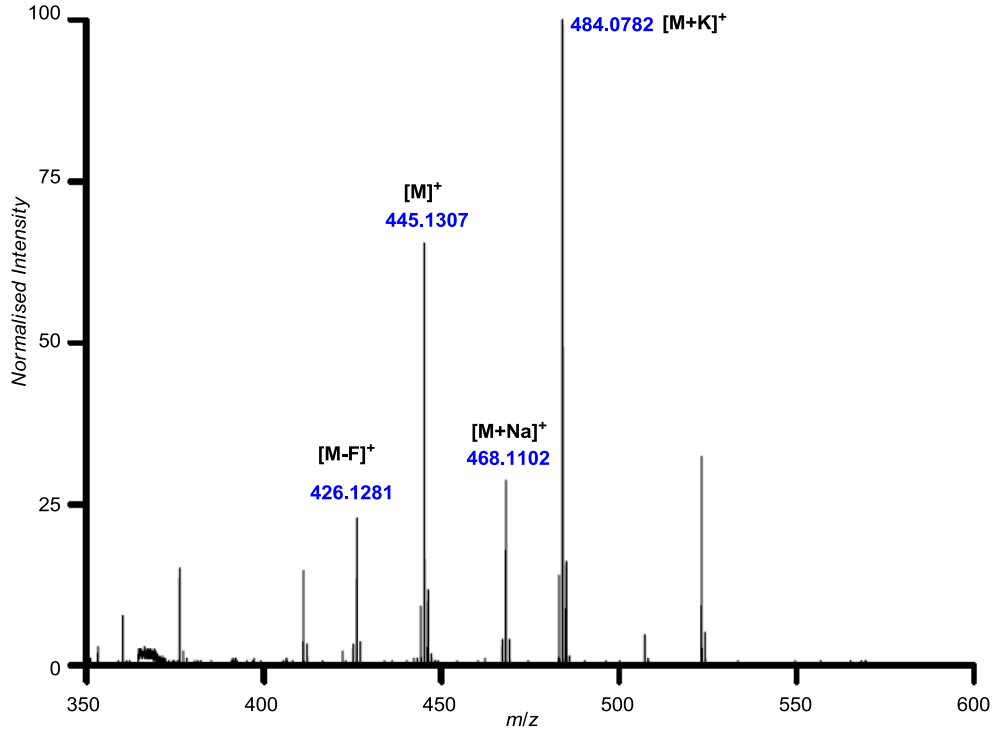

Figure 2C.10: MALDI-*TOF* spectrum probe **81** (10 μM) in the presence of a Cys (100 μM) recorded in HEPES buffer (10 mM, 1 mM CTAB, pH = 7.4).

2C.2.5 Cell imaging

We then sought to examine whether probe **81** can localize to the lysosome and sense biological thiols in living cells. First the cell permeability of probe **81** was evaluated. Live-cell imaging studies were carried out by using Human cervical cancer cell line (HeLa). Strong fluorescence was observed when HeLa cells were incubated with probe **81** (10 μM in 1:100 DMSO-DNEM v/v, pH = 7.4) at 37 ^{o}C for 10 min (Figure 2C.11A and B). In a control experiment, cells were pre-treated with an excess (5 mM) of the thiol-reactive *N*-phenylmaleimide, which consumes all of the free thiols within the cell, and then incubated with the probe **81**. The confocal microscopic studies did not show a significant fluorescence signal (Figure 2C.11C and D). This confirms the specificity of probe **81** for thiols over other analytes in living cells.

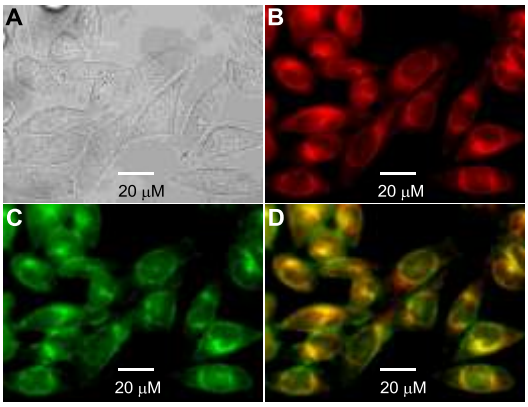

Figure 2C.11: Image of HeLa cells: brightfield (**A**), fluorescence (**B-E**). Images were accuired at each 5 min time interval (0, 5, 10, 15 min) after the incubation with Cys (100 μM). Bar diagram (**F**) of relative pixel intensities obtained from selected ROIs at different time interval images.

In the next stage, we performed the quantitative colocalization experiments by co-staining HeLa cells with Lysosensor Green and probe.

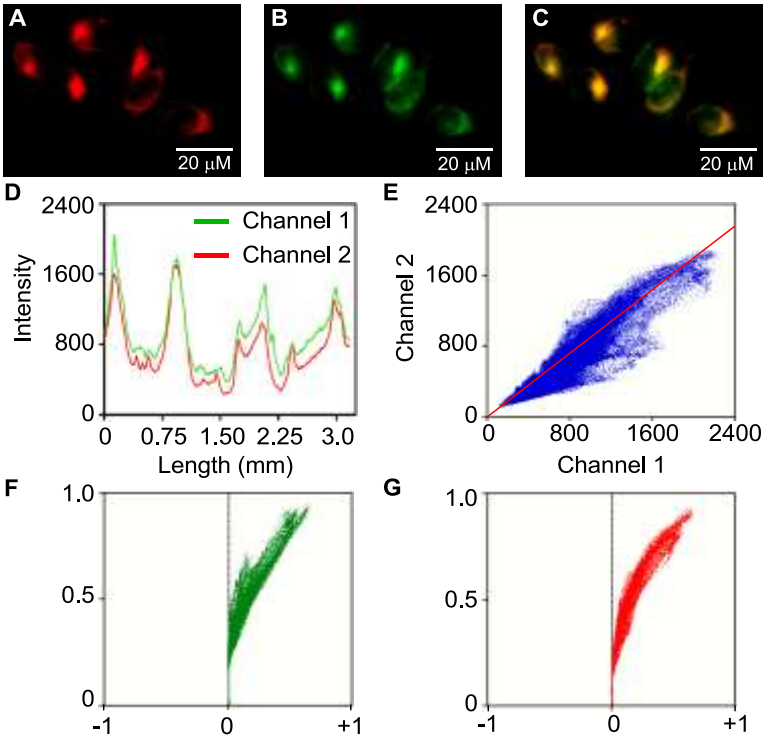

Figure 2C.12: Colocalization experiments using probe **81** to lysosomes in HeLa cells. HeLa cells were stained with (**A**) probe **81** (5.0 μM) for 5 min at 37 °C and (**B**) LysoSensor Green (1.0 μM) (**C**) Overlay of (**A**) and (**B**). (**D**) Intensity profile of regions of interest (*ROI*) across HeLa cells. (**E**) Intensity correlation plot of stain probe **81** and LysoSensor Green. ICA plots of (**F**) stain LysoSensor Green and (**G**) probe **81**.

When Hela cells were incubated with probe **81** (5 μM in 1:100 DMSO-DNEM v/v, pH = 7.4) at 37 ^{o}C for 10 min, strong red fluorescence was observed (Figure 2C.12A). These cells were then incubated with LysoSensor Green (1 μM in 1:100 DMSO- DNEM v/v, pH = 7.4) at 37 ^{o}C for 10 min showed green fluorescence (Figure 2C.12B). As shown in Figure 2C.12C the fluorescence image of probe **81** was mainly overlapped with that of LysoSensor Green indicates ability of probe **81** to target lysosomes. The intensity profiles of the linear regions of interest (*ROI*) across HeLa cells stained with probe **81** and LysoSensor Green vary in close synchrony (Figure 2C.12D). Pearson's coefficient and overlap coefficient are 0.963 and 0.984, respectively, evaluated using the conventional dye overlay method. Overlap coefficients k_1 and k_2 found to be 0.9 and 1.1 respectively. Colocalization coefficients (Manders' Coefficients) M_1=0.77 (fraction of LysoSensor Green overlapping probe) and M_2=0.818 (fraction of probe overlapping LysoSensor Green) also confirms an excellent overlap (Table 2C.1). An intensity correlation analysis (ICA) is employed to assess the intensity distribution of the two co- existing dyes. The

intensity of stain LysoSensor Green against that of probe was plotted for each pixel. The dependent staining results in a highly correlated plot (Figure 2C.12E), and the ICA plots for the two stains generate an unsymmetrical hourglass-shaped scatter plot that are markedly skewed toward positive values (Figure 2C.12F, G). Li's intensity correlation quotient (ICQ) for the two dyes is 0.459, very close to 0.5, suggesting that the staining intensities are dependent on each other.

Table 2C.1: Various coefficients determined from colocalization studies.

Sr. No.	Description	Values
1	Pearson's coefficient	0.963
2	Overlap coefficient	0.984
3	Overlap coefficients	k_1 = 0.9; k_2 = 1.1
4	Colocalization coefficients	M_1=0.77; M_2=0.818

2C.2.6 MTT cell viability assay

The cytotoxicity of probe **81** was determined by MTT assay. Various concentrations of probe **81** (2, 10, 20 and 50 μM) were used to determine toxicity level of probe towards HeLa cell. The result revealed that cells were not affected by incubation with probe **81** (up to 10 μM) for 16 h as about 95% cell viability was determined at 10 μM concentration of probe **81** .

2C.3 Summary and conclusions

In conclusion, lysosome targeting BODIPY-DNs based fluorescence *turn-On* probe for rapid, selective and sensitive detection of biological thiols was developed. The probe provided ~64-fold fluorescence enhancement with response time = 5 min during the detection of biothiols. Cell imaging studies confirmed the cell permeability, lysosome speccifity and intracellular biothiol detection ability of the probe.

To summary, we have developed three different types of probes for selective detection of biothiols. Chromenoquinoline based probes **61**, **62** and **63** are capable of discriminating biothiols (Cys, Hcy and GSH) from other amino acids. NBD chloride **75** was used as fluorescent probe for discriminating Cys and Hcy from GSH. Selectivity of NBD chloride for Cys and Hcy over GSH was explained on the basis of Smiles rearrangement. BODIPY based probe **81** was designed and synthesized for the selective

detection of biothiols in lysosomes inside cells. All the probes described in chapter 2 were found to be cell permeable and capable of detection of intracellular biothiols.

2C.4 References

(1) (a) Chen, X.; Ko, S.-K.; Kim, M. J.; Shin, I.; Yoon, J. *Chem. Commun.* **2010**, *46*, 2751(b) Lin, W.; Long, L.; Tan, W. *Chem. Commun.* **2010**, *46*, 1503(c) Sun, Y.-Q.; Chen, M.; Liu, J.; Lv, X.; Li, J.-f.; Guo, W. *Chem. Commun.* **2011**, *47*, 11029(d) Tang, B.; Yin, L.; Wang, X.; Chen, Z.; Tong, L.; Xu, K. *Chem. Commun.* **2009**, 5293(e) Zhang, M.; Yu, M.; Li, F.; Zhu, M.; Li, M.; Gao, Y.; Li, L.; Liu, Z.; Zhang, J.; Zhang, D.; Yi, T.; Huang, C. *J. Am. Chem. Soc.* **2007**, *129*, 10322(f) Bouffard, J.; Kim, Y.; Swager, T. M.; Weissleder, R.; Hilderbrand, S. A. *Org. Lett.* **2008**, *10*, 37(g) Sun, W.; Li, W.; Li, J.; Zhang, J.; Du, L.; Li, M. *Tetrahedron Lett.* **2012**, *53*, 2332(h) Zhu, B.; Zhang, X.; Li, Y.; Wang, P.; Zhang, H.; Zhuang, X. *Chem. Commun.* **2010**, *46*, 5710(i) Guo, Z.; Nam, S.; Park, S.; Yoon, J. *Chem. Sci.* **2012**, *3*, 2760(j) Shao, J.; Sun, H.; Guo, H.; Ji, S.; Zhao, J.; Wu, W.; Yuan, X.; Zhang, C.; James, T. D. *Chem. Sci.* **2012**, *3*, 1049.

(2) Zhu, H.; Fan, J.; Xu, Q.; Li, H.; Wang, J.; Gao, P.; Peng, X. *Chem. Commun.* **2012**, *48*, 11766.

(3) Andrew, C. L.; Klemm, A. R.; Lloyd, J. B. *Biochim. Biophys. Acta* **1997**, *1330*, 71.

(4) Mego, J. L. *Biochem. J.* **1984**, *218*, 775.

(5) Arunachalam, B.; Phan, U. T.; Geuze, H. J.; Cresswell, P. *Proc. Natl. Acad. Sci.USA* **2000**, *97*, 745.

(6) Boens, N.; Leen, V.; Dehaen, W. *Chem. Soc. Rev.* **2012**, *41*, 1130.

(7) Liu, T.; Xu, Z.; Spring, D. R.; Cui, J. *Org. Lett.* **2013**, *15*, 2310.

Chapter 3

Design and Synthesis of Fluorescence *Off-On* Probes for Rapid Detection of Aromatic Thiols

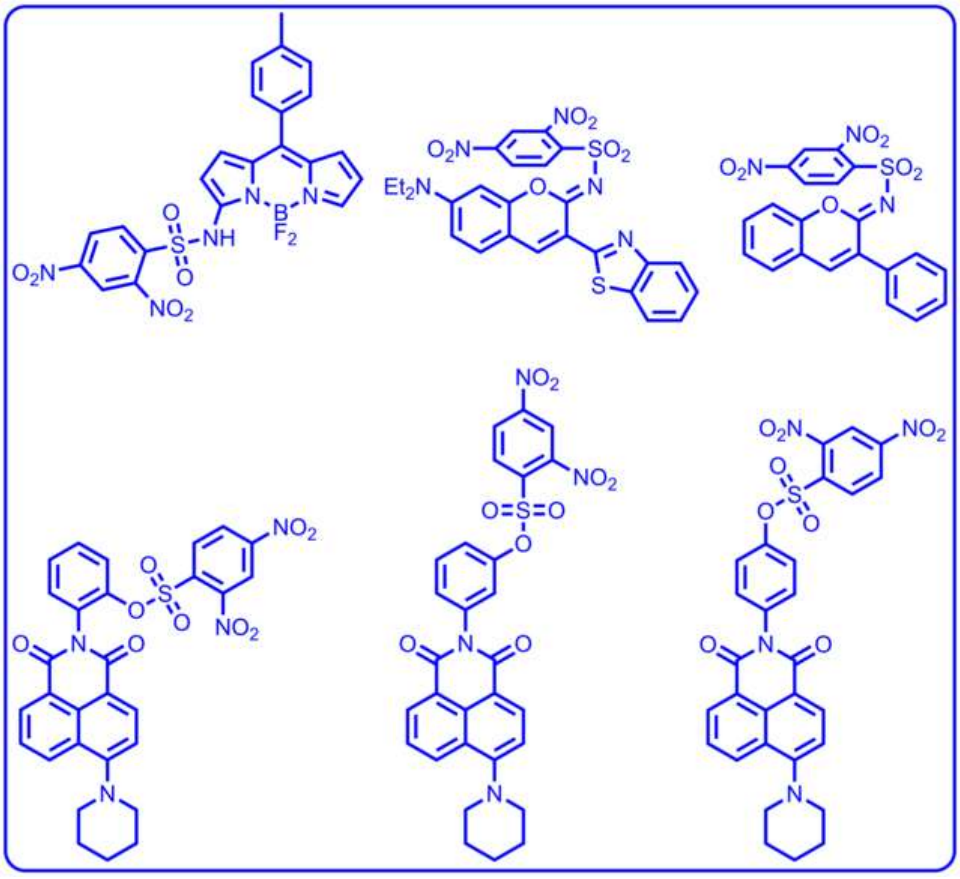

3.1 Introduction

A large number of *off-on* fluorescent probes are reported for biological thiol detection.[1] However, limited numbers of fluorescent probes are known for selective and rapid discrimination of aromatic thiols over aliphatic ones.[2] Reported probes used DNs group as recognising unit for thiophenol detection. These probes undergo thiolate mediated SNAr reaction on the DNs-ring to cleave free amine or alcohol as fluorophore (Figure 3.1A). Either an intramolecular charge transfer (ICT) or photoinduced electron transfer (PET) pathway from the fluorophore to the DNs moiety is responsible for the *Off*-fluorescence state of these probes. Since, the first report of 2,4-dinitrophenylsulfonyl (DNs) based fluorescent thiophenol probe **26** (Figure 3.1B) by Jiang *et. al.*,[2c] few DNs-based and other thiophenol probes have been developed.[2a,b] Selectivity of these probes toward aromatic thiols by discriminating aliphatic ones, has paved their significance in sensing applications *e.g.* detection of thiophenol in water, living cells, etc. However, slow reactivity of these probes with PhSH has resulted in relatively long response times (t_Rs). For example, with a 1:10 molar ratio of probe versus PhSH, probe **26** displayed a t_R = 17 min. For probe **29**, an increased t_R = 20 min was determined, when studied under comparable conditions. Till date the best t_R = 2 min was reported by Lin *et. al.* for a probe **87** in which a coumarin fluorophore was linked to the 2,4-dinitrophenol quencher.[2a] However, a molar ratio of 1:20 was used during the sensing experiment and a decrease in molar ratio to 1:5 resulted in an increase in t_R value to 7 min. Hence, it is essential to develop fast responsive *Off-On* thiophenol probes because of the high reactivity of the analyte, particularly in the presence of various Michael acceptors present in the biological and natural systems can lead to the fluctuations in the concentrations with time.

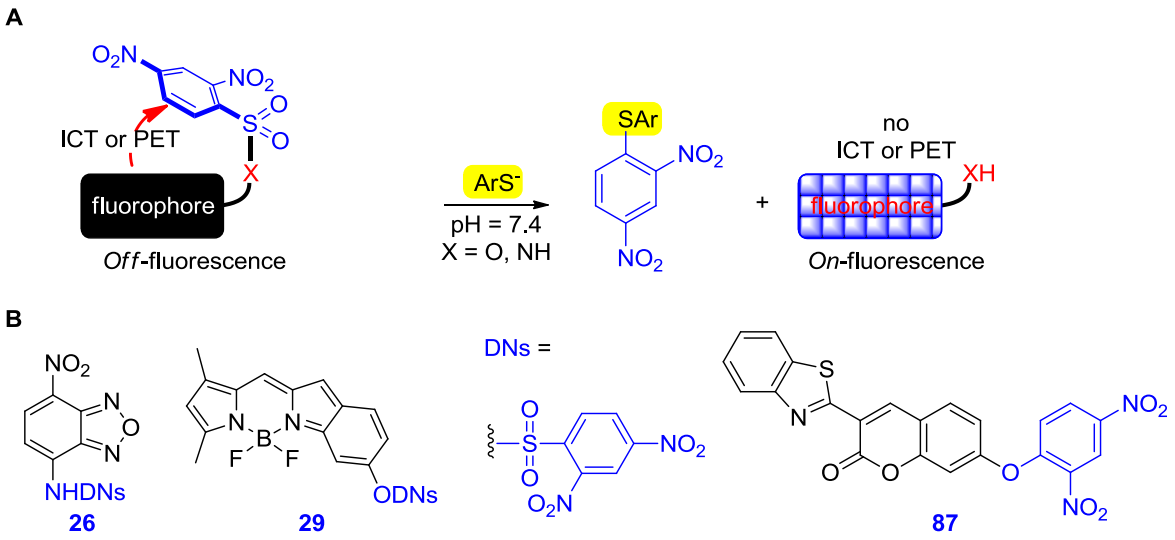

Figure 3.1: (**A**)The *Off-On* mechanism for DNs appended fluorescent thiophenol probes; (**B**) Structures of reported DNs-based thiophenol probes **26**, **29** and **87**.

Our objective was to develop new fluorescent probes for rapid and selective detection of thiophenols. A rational approach for controlling the rates of decomposition of DNs-amides was reported recently by Malwal *et. al.*[3] A structure activity relationship (SAR) study provided crucial insight into the reaction mechanism of cysteine-activated SO_2 (a gaseous antimycobacterial agent) release from these pro-drugs. During the thiol mediated decomposition of DNs-linked anilines **88** – **90** to free anilines **88a – 90a**, a reactivity order **90a** > **89a** > **88a** was observed based on half-lives ($t_{1/2}$) of these DNs-derivatives (Table 3.1). Based on these results, a correlation of pK_{aH} values of **90a**, **89a** and **88a** with determined $t_{1/2}$ values confirmed a linear relation between these parameters.

Table 3.1: Correlation of calculated half lives ($t_{1/2}$) of prodrugs **88-90** with and pK_{aH} values of released amines **88a-90a**.

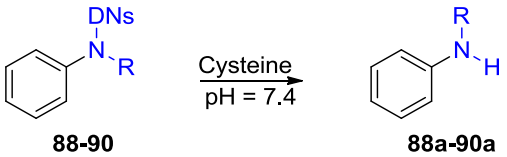

88-90 **88a-90a**

Compound	R	$t_{1/2}$ (min)	pK_{aH}
88	H	2.0	9.34
89	Me	4.0	9.58
90	^{n}Pr	4.6	9.68

This structure activity relationship (SAR) study suggests that the protonation of aniline *N*-center is the rate determining step (*rds*) and this step occurs after a thiol mediated ipso attack (for –SH group of Cys, pK_a = 8.0) on the DNs ring (Scheme 3.1). This study has provided a simple and effective methodology to alter onset times of SO_2 releasing prodrugs by adjusting the basicity (pK_{aH}) of the released amine.[3] We realized the importance of this work in the design of new thiophenol probes to ensure faster response times compared to reported probes.

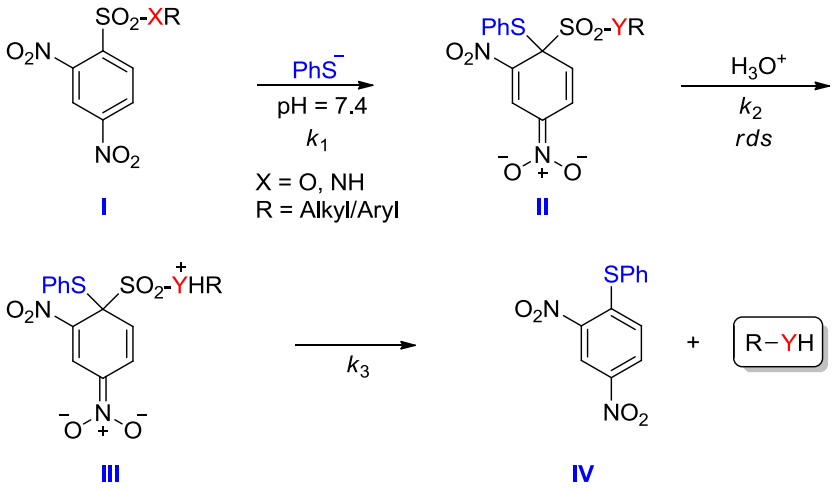

Scheme 3.1: Mechanism of thiophenol sensing by DNS-based probe.

3.2 Results and discussion

Boron-dipyrromethene (BODIPY), iminocoumarin and naphthalimide were selected as fluorophores owing to their extraordinary photophysical properties such as intense absorptions in visible light, relatively high molar extinction coefficients (ε) and stability against light and chemicals. 2,4-Dinitrobenzenesulfoyl (DNs) group which is an established quencher in the design of the thiol sensitive probes was selected in our design. Thiol-mediated cleavage of the resulting sulfonyl group through S_NAr process will release the fluorophore resulting in the turn-*on* of fluorescence. The arenesulphonamide was selected over arenesulfonate in the probe design due to better reactivity towards thiols compared to oxygen and nitrogen nucleophiles. Based on these considerations we designed probes **91** – **96** (Figure 3.2).

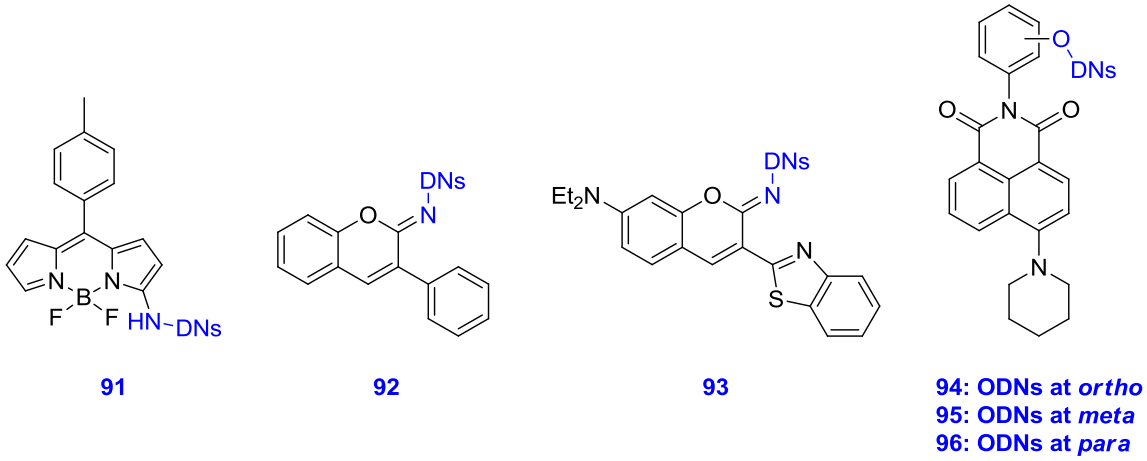

Figure 3.2: Structures of proposed probes **91 – 96** for selective detection of thiophenols.

Marvin software from ChemAxon[4] was used for predicting pK_{aH} values of reported fluorophores **26a** (pK_{aH} = -1.62), **29a** (pK_{aH} = -5.71) and proposed new fluorophores **91a** (pK_{aH} = 2.84), **92a** (pK_{aH} = 5.75), **93a** (pK_{aH} = 5.22), **94a** (pK_{aH} = 8.25), **95a** (pK_{aH} = 9.05) and **96a** (pK_{aH} = 8.98). For reported fluorescent probes a decrease in t_R values of probes toward PhSH was observed upon increase in pK_{aH} of released fluorophore. Similar to the report of Malwal *et. al.*, protonation of the heteroatom, (X = O or NH) of a fluorophore can be considered as the *rds* in each case. However, a thiolate mediated ipso attack on the DNs-ring is more feasible (for –SH group of PhSH, pK_a = 6.62) according to the mechanism under the physiological conditions. Based on these, a correlation between experimentally determined t_R values of DNs-based PhSH probes *versus* pK_{aH} values of respective free fluorophores can be established (Figure 3.3).

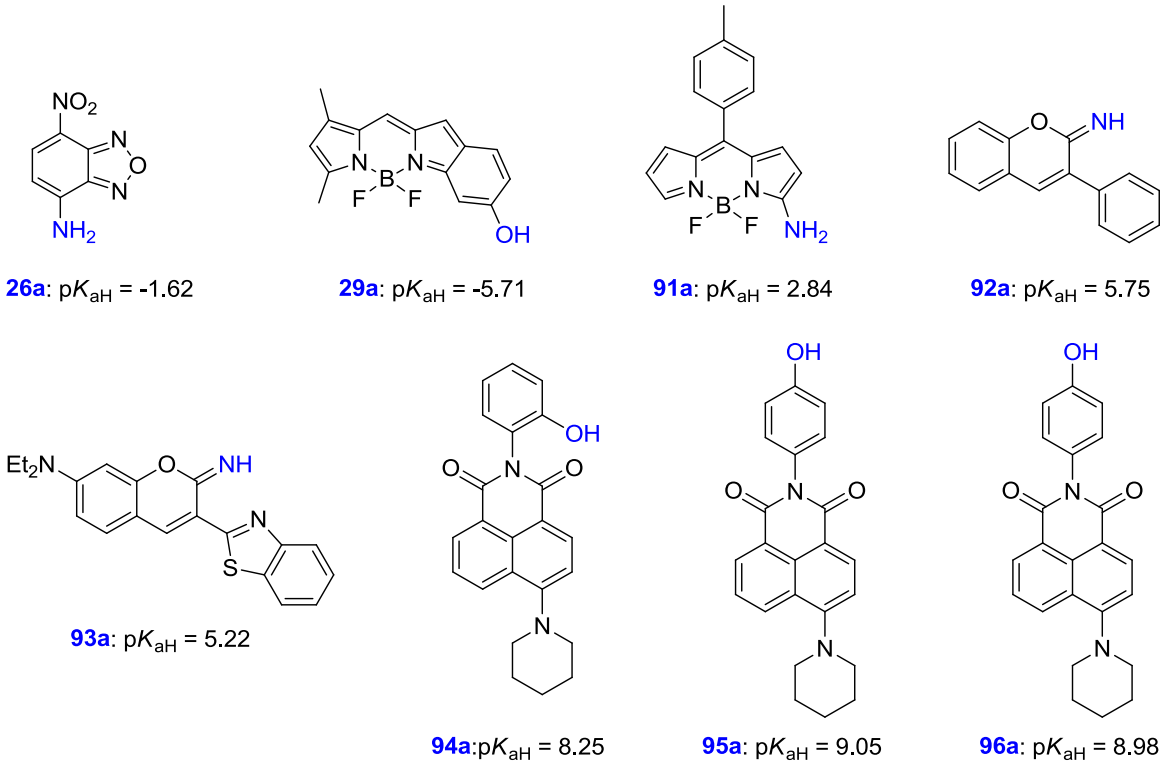

Figure 3.3: Structures of fluorophores **26a**, **29a** and **91a – 96a** released from probes **26**, **29** and **91 – 96**, respectively.

3.2.1 Theoretical Calculations

The design of new probes was also verified first with theoretical calculations using density functional theory (DFT) and time-dependent density functional theory (TDDFT). The TDDFT calculation for probe **91** at B3LYP/6-311(d,p) level indicated a forbidden $S_0 \rightarrow S_1$ transition (oscillator strength, f = 0.0561) indicating the presence of dark S_1 state (Table 3.2). The first allowed $S_0 \rightarrow S_3$ electronic transition (f = 0.4016) is characterized as the HOMO→LUMO+1 transition of the BODIPY moiety. Therefore, the presence of the S_1 dark state induced by the DNs moiety confirmed that a non-radiative $S_1 \rightarrow S_0$ emission process responsible for quenching of the fluorescence. The probe **91** upon reaction with thiols would generate the amine **91a** in which the allowed $S_0 \rightarrow S_1$ transition (f = 0.4693) is characterized as the HOMO→LUMO transition. This calculation confirmed the S_1 state as an emissive state indicating amine **91a** as a fluorescent species. Geometry optimized structure and frontier molecular orbitals (MOs) for probe **91** as well as corresponding amine **91a** were shown in Figure 3.4 and Figure 3.5, respectively.

Table 3.2: Selected electronic excitation energies (eV) and oscillator strengths (*f*), configurations of the low-lying excited states of the probe **91** and Amine **99**.

Species	Electronic transition	TDDFT/B3LYP/6-311(d,p)			
		Energy [a] (eV)	Oscillator strength (*f*)	Main configurations	CI coefficients
91	$S_0 \rightarrow S_1$	2.26	0.0561	HOMO→LUMO	0.67671
				HOMO→LUMO+1	-0.16337
	$S_0 \rightarrow S_2$	2.78	0.0192	HOMO→LUMO+1	-0.12733
				HOMO→LUMO+2	0.68664
	$S_0 \rightarrow S_3$	2.93	0.4016	HOMO-2→LUMO+1	-0.12250
				HOMO→LUMO+1	0.56209
				HOMO→LUMO+2	0.15205
	$S_0 \rightarrow S_4$	3.31	0.1218	HOMO-1→LUMO	0.62194
				HOMO-1→LUMO+1	0.28074
91a	$S_0 \rightarrow S_1$	3.00	0.4693	HOMO→LUMO	0.57663
	$S_0 \rightarrow S_2$	3.64	0.0896	HOMO-2→LUMO	-0.44157
				HOMO-1→LUMO	0.49678

[a] λ values were calculated from respective energies of transition using formula $\lambda = hc/E$.

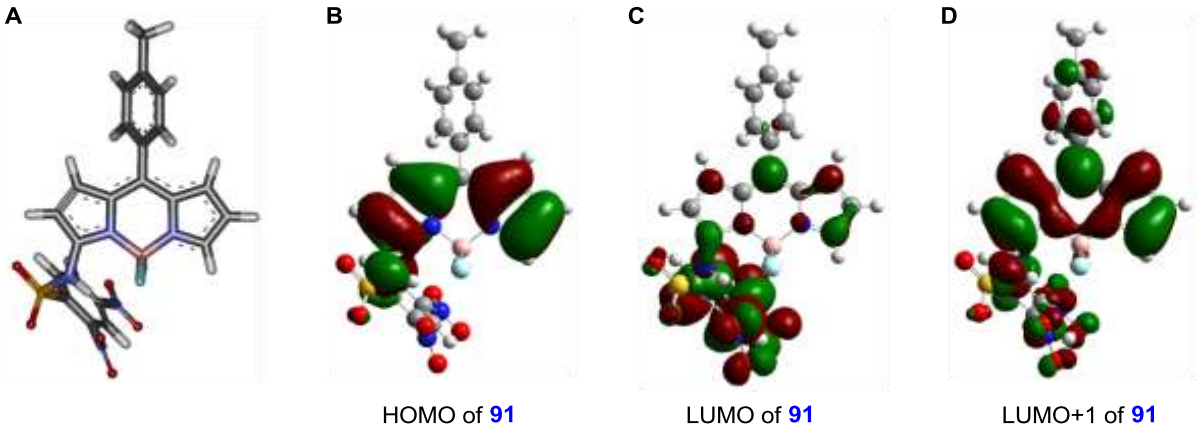

Figure 3.4: View of the DFT B3LYP/6-311G(d,p) geometry optimized structure (**A**), frontier molecular orbitals (MOs), HOMO (**B**), LUMO (**C**) and LUMO+1 (**D**) of the probe **91.**

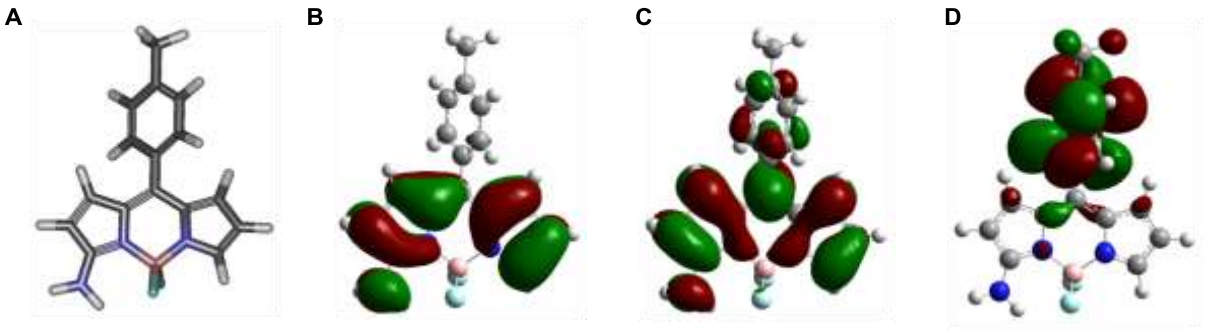

Figure 3.5: View of the DFT B3LYP/6-311G(d,p) geometry optimized structure (**A**), frontier molecular orbitals (MOs), HOMO (**B**), LUMO (**C**) and LUMO+1 (**D**) of **91a.**

For probe **92**, gas phase geometry optimization using density functional theory (DFT) at the B3LYP/6-311G (d,p) level followed by time-dependent DFT (TDDFT) calculation at the same level, provided a $S_0 \rightarrow S_1$ transition with oscillator strength, f = 0.0020 (Table 3.3). Next higher energy $S_0 \rightarrow S_2$ and $S_0 \rightarrow S_3$ transitions are associated with f = 0.0298 and 0.0018, respectively. These data indicate the presence of three dark states S_1, S_2 and S_3. The first allowed $S_0 \rightarrow S_4$ transition (f = 0.2072) suggests S_4 as the first emissive state. According to these calculations, the $S_4 \rightarrow S_0$ emission process is expected to proceed via intermediate S_3, S_2 and S_1 states, suggesting a non-radiative pathway from the iminocoumarin to the DNs moiety. On the other hand, presence of an emissive S_1 state (f = 0.3927 for $S_0 \rightarrow S_1$ transition) in **92a** corroborate with its proposed fluorescent behaviour. Similar theoretical calculations on **93** provided $S_0 \rightarrow S_1$ (f = 0.0004) and $S_0 \rightarrow S_2$ (f = 0.0610) and $S_0 \rightarrow S_3$ (f = 0.1257) suggesting S_1, S_2 as dark states and S_3 as the first emissive state. Therefore, $S_3 \rightarrow S_0$ emission process can be considered as non-radiative due to the involvement of S_3 and S_2 dark states. However, for free iminocoumarin **93a** the $S_0 \rightarrow S_1$ transition with f = 0.4239, indicates a radiative pathway present in the species. Therefore, theoretical calculations using TDDFT methods predicted an *Off-On* change in fluorescence in each probe during cleavage of the DNs group. Frontier molecular orbitals (MOs) for **92**, **92a**, **93** and **93a** were shown in Figure 3.6.

Table 3.3: Wavelengths (λ), oscillator strengths (f) and CI coefficients (CIC) of low-lying excited state transitions of **92**, **92a**, **93** and **93a**, calculated by TDDFT method at the B3LYP/6-311G(d,p) level.

Species	Electronic transition	λ (nm)[a]	Oscillator strength (f)	Main Configurations	CI coefficient
92	$S_0 \rightarrow S_1$	424	0.0020	HOMO→LUMO	0.69508
	$S_0 \rightarrow S_2$	377	0.0298	HOMO→LUMO	-0.1069
				HOMO→LUMO+1	0.6641
				HOMO→LUMO+2	0.2000
	$S_0 \rightarrow S_3$	360	0.0018	HOMO-1→LUMO	0.6941
				HOMO-1→LUMO+2	0.1098
	$S_0 \rightarrow S_4$	353	0.2072	HOMO→LUMO+1	-0.1892
				HOMO→LUMO+2	0.6520
92a	$S_0 \rightarrow S_1$	335	0.3927	HOMO→LUMO	0.6911
93	$S_0 \rightarrow S_1$	407	0.0004	HOMO-1→LUMO	0.6952
				HOMO→LUMO	-0.1048
	$S_0 \rightarrow S_2$	382	0.0610	HOMO-1→LUMO+1	-0.4673
				HOMO-1→LUMO+2	-0.1880
				HOMO→LUMO+1	0.4870
	$S_0 \rightarrow S_3$	378	0.1257	HOMO-1→LUMO+1	0.4595
				HOMO-1→LUMO+2	0.1111
				HOMO→LUMO+1	0.4842
				HOMO→LUMO+2	-0.1618
93a	$S_0 \rightarrow S_1$	358	0.4239	HOMO→LUMO	0.6918

[a] λ values were calculated from respective energies of transition using formula $\lambda = hc/E$.

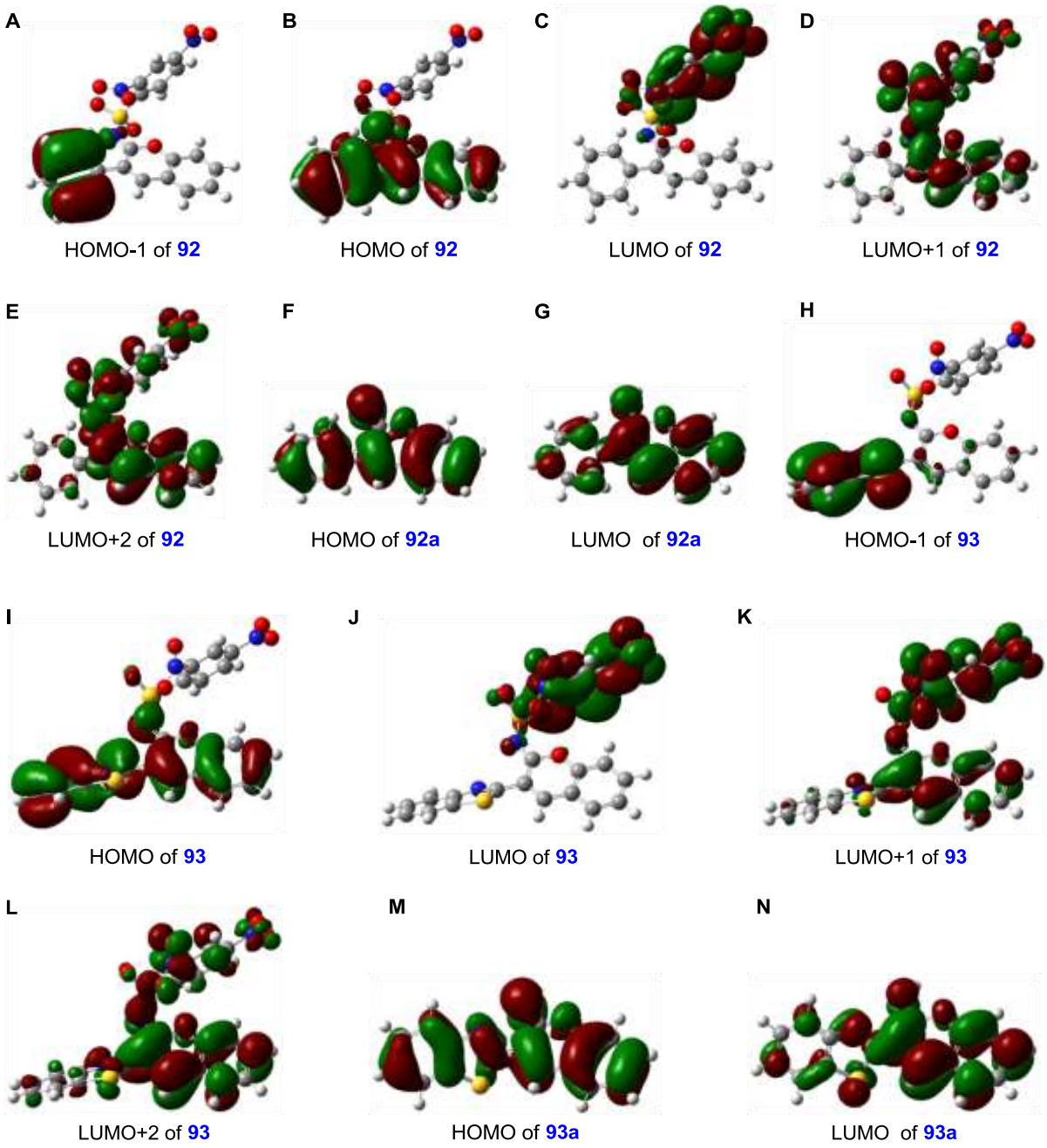

Figure 3.6: Frontier molecular orbitals (MOs), (**A**) HOMO-1, (**B**) HOMO, (**C**) LUMO, (**D**) LUMO+1 and (**E**) LUMO+2 of the probe **92**; (**F**) HOMO and (**G**) LUMO of **92a**. Frontier molecular orbitals (MOs), (**H**) HOMO-1, (**I**) HOMO, (**J**) LUMO, (**K**) LUMO+1 and (**L**) LUMO+2 of the probe **93**; (**M**) HOMO and (**N**) LUMO of **93a**.

The reaction of **94**, **95** and **96** with PhSH will result in the formation of **94a**, **95a** and **96c** respectively. Therefore, gas phase geometry optimized structures of **94a**, **95a**, **96a**, **94**, **95** and **96** were obtained by using density functional theory (DFT) at the B3LYP/6-311G(d,p) level. Optimized geometries were then subjected to time-dependent

DFT (TDDFT) calculations to predict the emission properties of these species. For probe **94**, the $S_0 \rightarrow S_1$

Table 3.4: Wavelengths (λ), oscillator strengths (f) and CI coefficients (CIC) of low-lying excited state transitions of **94 – 96** and **94a – 96a**.

Species	Electronic transition	E^a (eV)	λ (nm)	Oscillator strength (f)	Main configurations	CI coefficients
94	$S_0 \rightarrow S_1$	2.2133	560	0.0003	HOMO→LUMO	0.70374
	$S_0 \rightarrow S_2$	2.8024	442	0.0010	HOMO→LUMO+1	0.70271
	$S_0 \rightarrow S_3$	3.0668	404	0.2362	HOMO→LUMO+2	0.69263
94a	$S_0 \rightarrow S_1$	3.1947	388	0.2537	HOMO-3→LUMO	0.10196
					HOMO→LUMO	0.69199
95	$S_0 \rightarrow S_1$	2.3752	522	0.0003	HOMO→LUMO	0.70584
	$S_0 \rightarrow S_2$	3.0919	401	0.2733	HOMO→LUMO+1	0.69214
95a	$S_0 \rightarrow S_1$	2.3126	536	0.0001	HOMO→LUMO	0.70681
96	$S_0 \rightarrow S_2$	2.9899	415	0.0000	HOMO→LUMO+1	0.70677
	$S_0 \rightarrow S_3$	3.1219	397	0.0305	HOMO-4→LUMO	-11715
					HOMO-2→LUMO	0.12158
					HOMO-1→LUMO	0.65436
					HOMO→LUMO+2	0.19142
	$S_0 \rightarrow S_4$	3.1320	396	0.2464	HOMO-1→LUMO	0.18829
					HOMO→LUMO+2	0.66621
96a	$S_0 \rightarrow S_1$	3.1797	390	0.2567	HOMO→LUMO	0.69196

[a] λ values were calculated from respective energies of transition using formula $\lambda = hc/E$.

transition (*i.e.* HOMO→LUMO electronic excitation) provided an oscillator strength, f = 0.0003 indicating a forbidden transition process and S_1 as the dark state (Table 3.4). The first allowed transition obtained from this calculation was $S_0 \rightarrow S_3$ (*i.e.* HOMO→LUMO+2 electronic excitation) with f = 0.2362 confirming S_3 as the emissive state. This data indicate that an emission of electron from S_3 to S_0 would proceed via the intermediate S_2 and S_1 states and this can be corroborated to a non-radiative pathway from the aminonaphthalimide-moiety to the DNs-moiety. For corresponding product **94a** after thiophenol detection, the $S_0 \rightarrow S_1$ transition was associated with f = 0.2537 confirming the presence of S_1 as the emissive state. Therefore, the corresponding emission process $S_1 \rightarrow S_0$

(*i.e.* LUMO→HOMO electronic transition) corroborates with the strong fluorescence of **94 – 96** and **94a – 96a** were shown in Figure 3.7 –3.12.

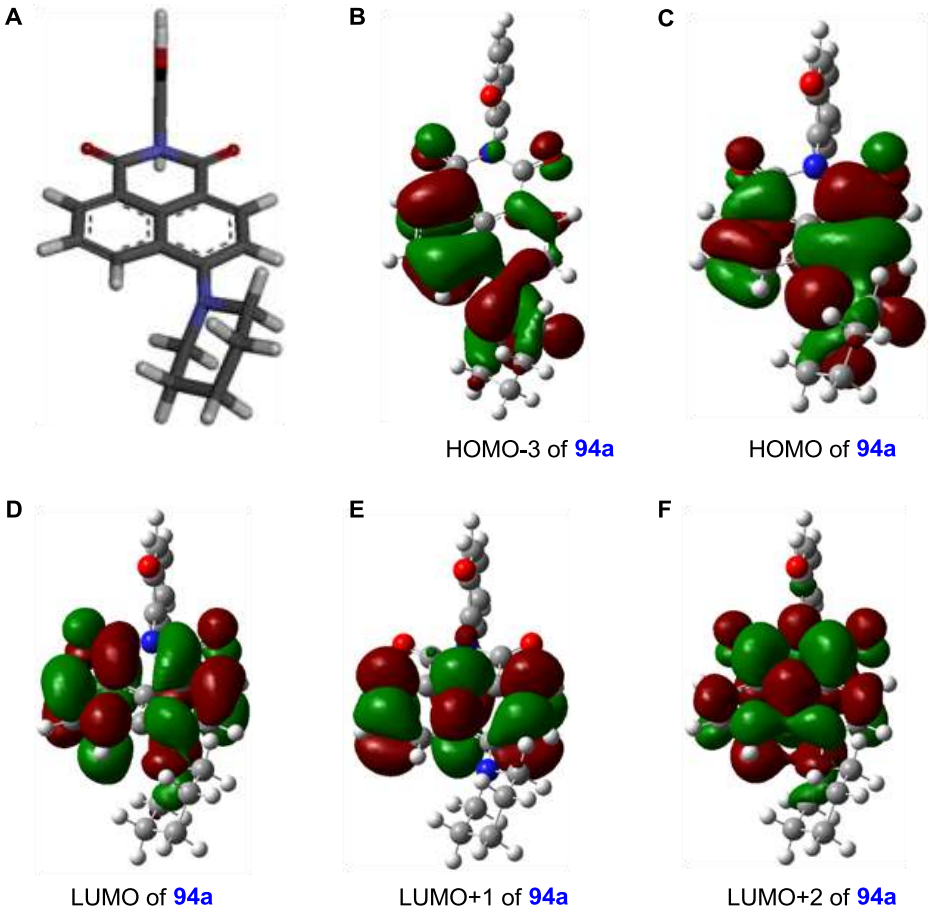

.

Figure 3.7: View of the DFT B3LYP/6-311G(d,p) geometry optimized structure of **94a** (**A**) and the frontier molecular orbitals (MOs), HOMO-3 (**B**), HOMO (**C**), LUMO (**D**), LUMO+1 (**E**) and LUMO+2 (**F**) of **94a**.

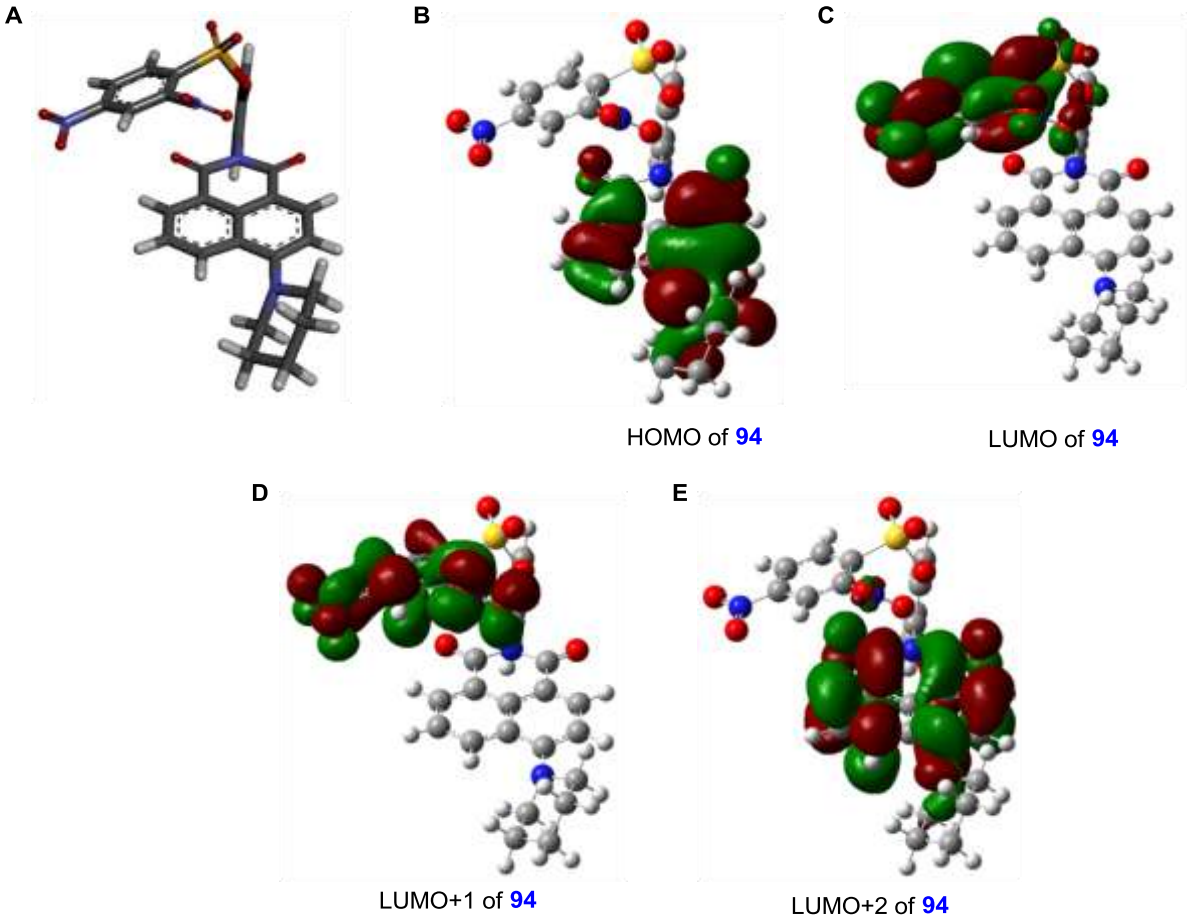

Figure 3.8: View of the DFT B3LYP/6-311G(d,p) geometry optimized structure of **94** (**A**) and the frontier molecular orbitals (MOs), HOMO (**B**), LUMO (**C**), LUMO+1 (**D**) and LUMO+2 (**E**) of **94.**

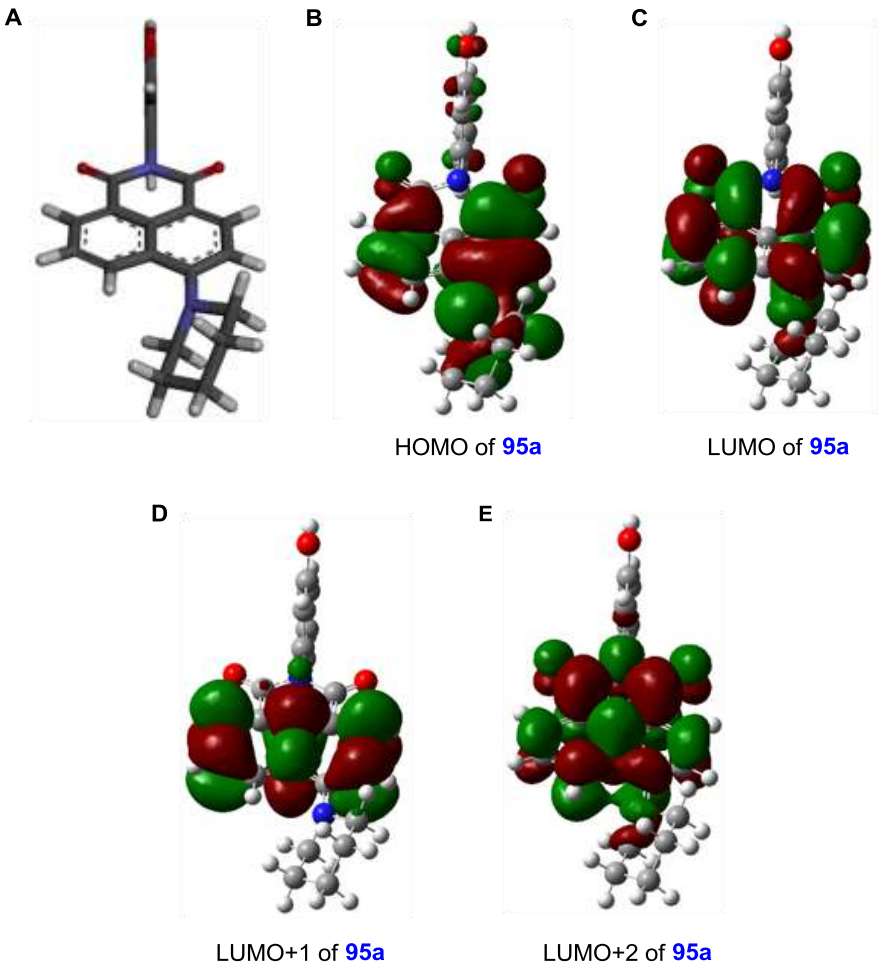

Figure 3.9: View of the DFT B3LYP/6-311G(d,p) geometry optimized structure of **95a** (**A**) and the frontier molecular orbitals (MOs), HOMO (**B**), LUMO, (**C**) LUMO+1 (**D**) and LUMO+2 (**E**) of **95a.**

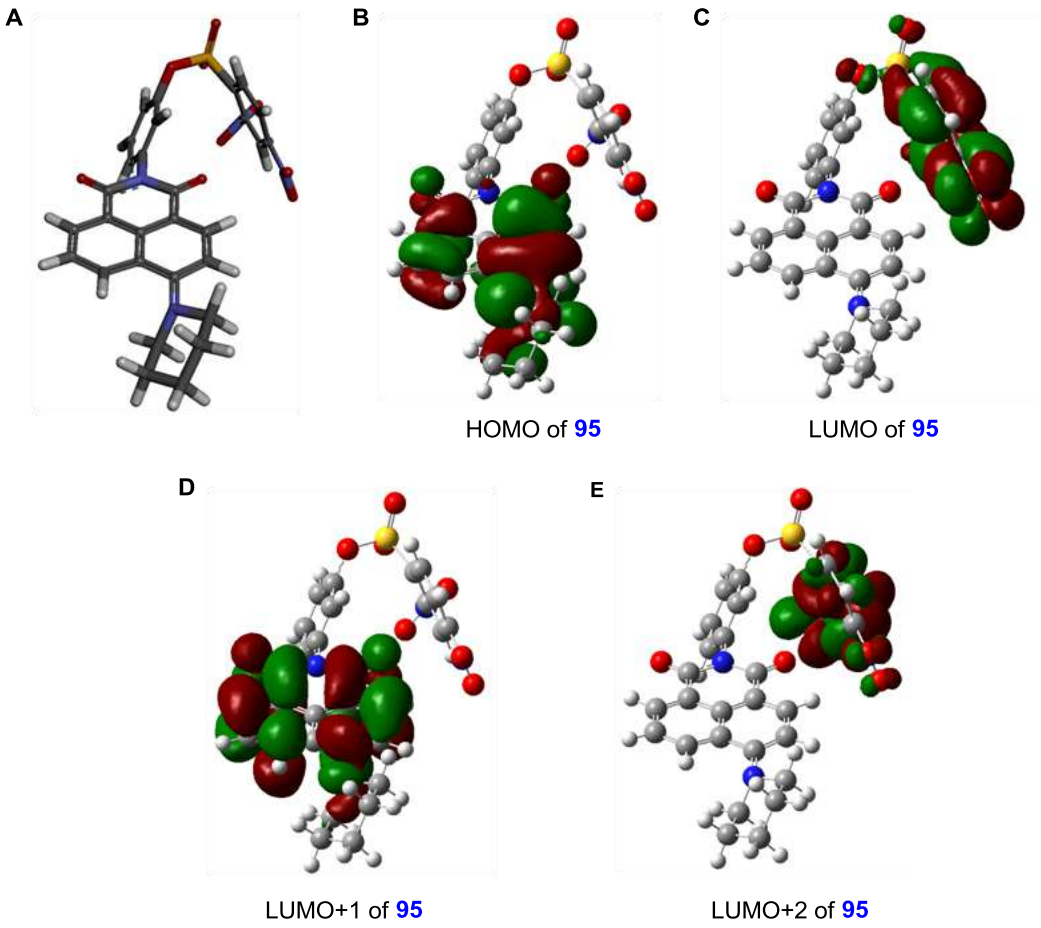

Figure 3.10: View of the DFT B3LYP/6-311G(d,p) geometry optimized structure of **95** (**A**) and the frontier molecular orbitals (MOs), HOMO, (**B**) LUMO (**C**), LUMO+1 (**D**) and LUMO+2 (**E**) of **95.**

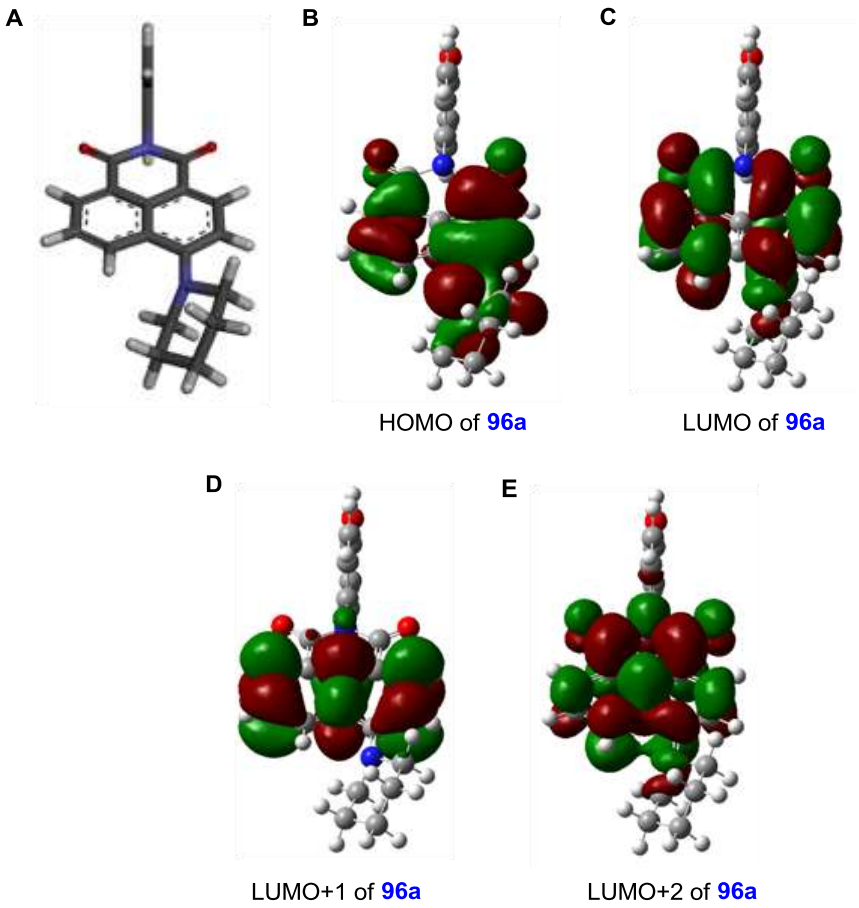

Figure 3.11: View of the DFT B3LYP/6-311G(d,p) geometry optimized structure of **96a** (**A**) and the frontier molecular orbitals (MOs), HOMO, (**B**) LUMO (**C**), LUMO+1 (**D**) and LUMO+2 (**E**) of **96a.**

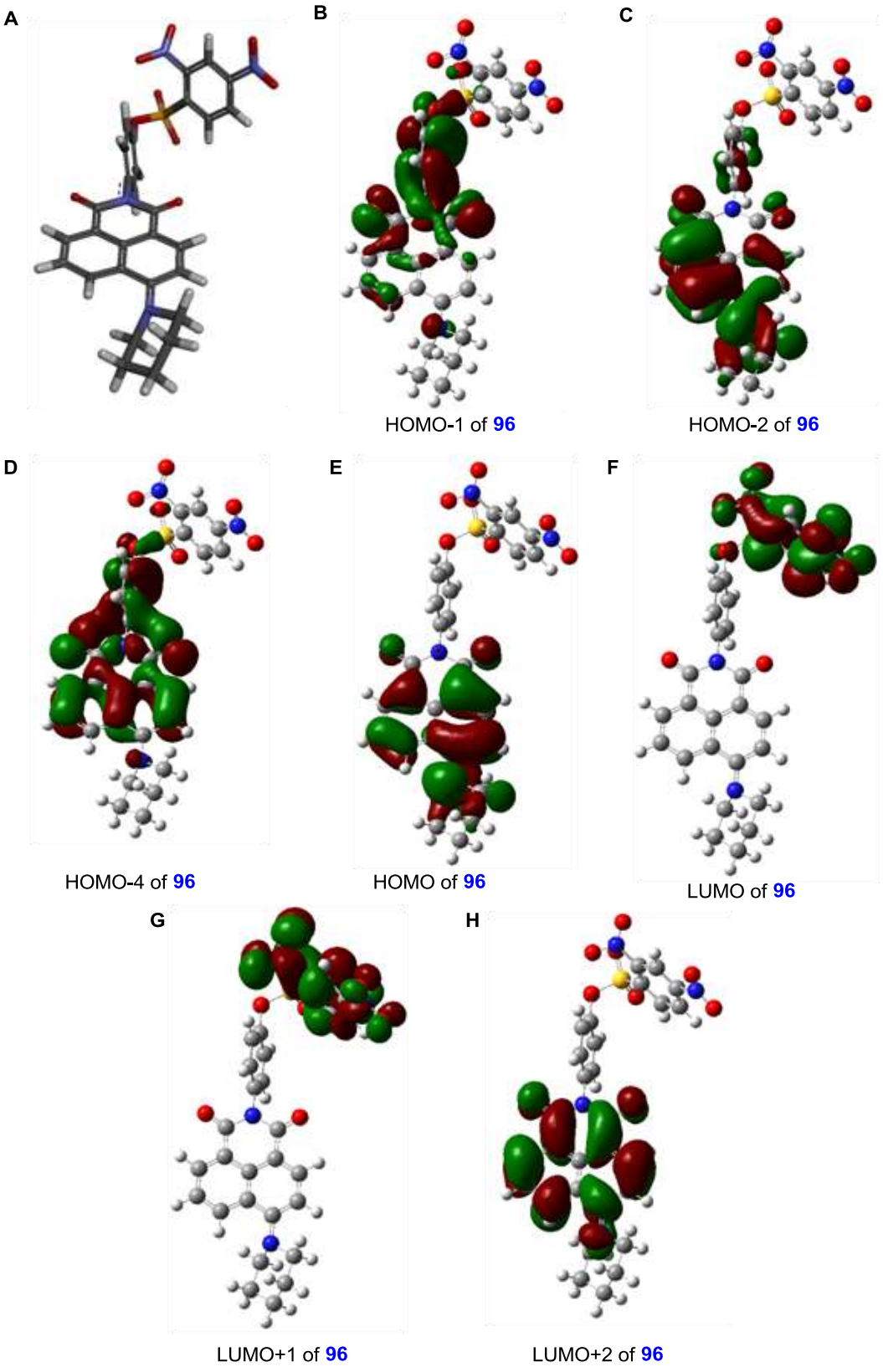

Figure 3.12: View of the DFT B3LYP/6-311G(d,p) geometry optimized structure of **96** (**A**) and the frontier molecular orbitals (MOs), HOMO-1 (**B**), HOMO-2 (**C**), HOMO-4 (**D**), HOMO (**E**), LUMO (**F**), LUMO+1 (**G**) and LUMO+2(**H**) of **96.**

3.2.2 Synthesis

Encouraged by theoretical pK_{aH} values and theoretical fluorescence *Off-On* predictions, synthesis of probes **91** – **96** was carried out. Probe **91** was synthesized in three steps with moderate yields. The 3-Bromo BODIPY derivative **98** was synthesized starting from reported *meso*-(*p*-tolyl)dipyrromethane **97** via conventional route (Scheme 3.2). Compound **98** was then treated with a 15% solution of ammonia in H_2O/CH_3CN (1:1) to afford BODIPY amine **91a** in 96% yield. In the final step, the amine **91a** was treated with DNs chloride in presence of NaH to afford probe **91** in 56% yield.

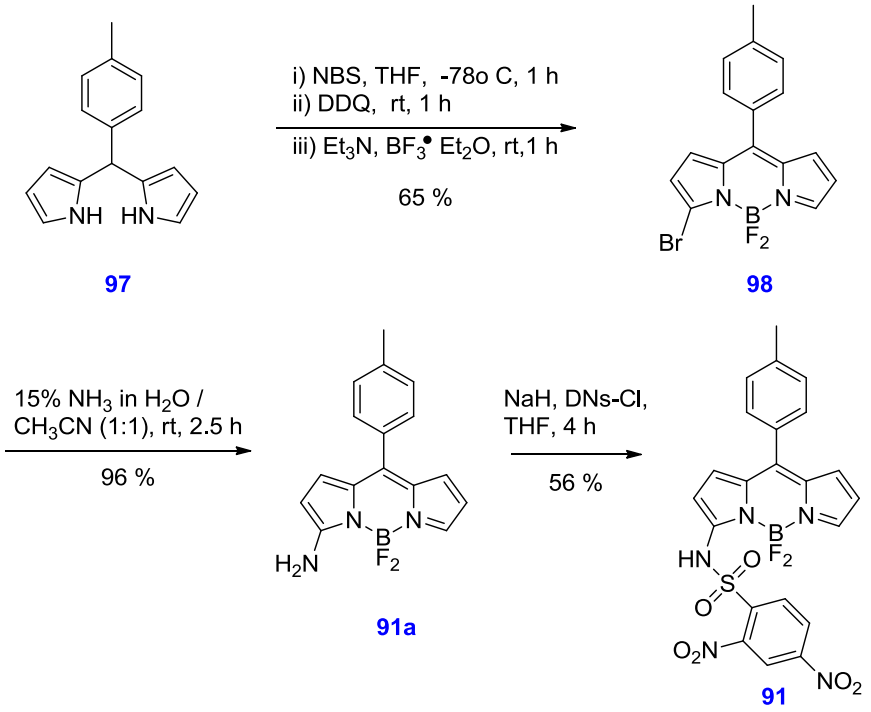

Scheme 3.2: Synthesis of Fluorescent thiophenol probe **91**.

Synthesis of probes **92** and **93** were carried out from **92a** and **93a**, respectively. Free iminocoumarins **92a** and **93a** were synthesized following reported methodologies.[5] Treatment of **92a** with 2,4-dinitrophenylsulfonyl chloride (DNs-Cl) in the presence of pyridine at room temperature provided **92** in 35% yield (Scheme 3.3A). Similarly, probe **93** was synthesized from **93a** under comparable conditions in 72% yield (Scheme 3.3D). Single crystal X-ray diffraction structures of **92a** and **92** was also carried out (Scheme 3.3B, C).

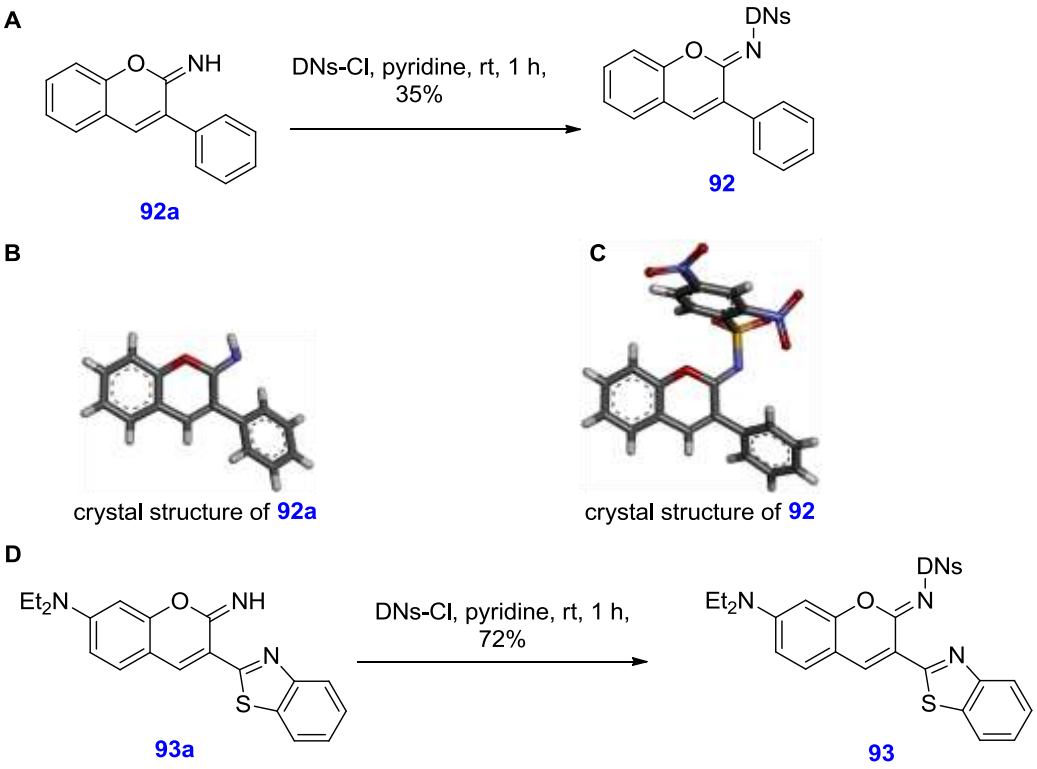

Scheme 3.3: (**A**) Synthesis of probes **92**; (**B**) Crystal structures of **92a**; (**C**) Crystal structures of **92** and (**D**) Synthesis of probes **93**.

Synthesis of probes **94**, **95** and **96** were carried from commercially available 4-Bromo-1,8-naphthalic anhydride **99** (Scheme 3.4). Anhydride **99** when refluxed with 2-aminophenol **100a** in pyridine the imide **101a** was formed in 51% yield. Subsequently, **101a** was converted to the fluorophore **94a** upon refluxing with piperidine in 2-methoxyethanol with 60% isolated yield. Compound **94a** when treated with 2,4-dinitrophenylsulfonyl chloride (DNs-Cl) in CH_2Cl_2 using Et_3N as base the probe **94** was obtained in 83% yield. Similarly, **99** was reacted with 3-aminophenol **100b** in pyridine under the refluxed conditions to obtain imide **101b** in 79% yield which was then converted to the fluorophore **95a** by refluxing with piperidine in 2-methoxyethanol with 95% yield. Finally, **95a** was converted to **95** (yield = 51%) by treating with DNs-Cl in CH_2Cl_2 using Et_3N base. In order to synthesize the probe **96**, the anhydride **99** was first converted to **101c** (yield = 53%) by reacting with 4-aminophenol. Subsequently, **101c** was converted first to **96a** (yield = 97%) which was then transformed to **96** (yield = 86%) following similar strategies used for synthesizing **94**.

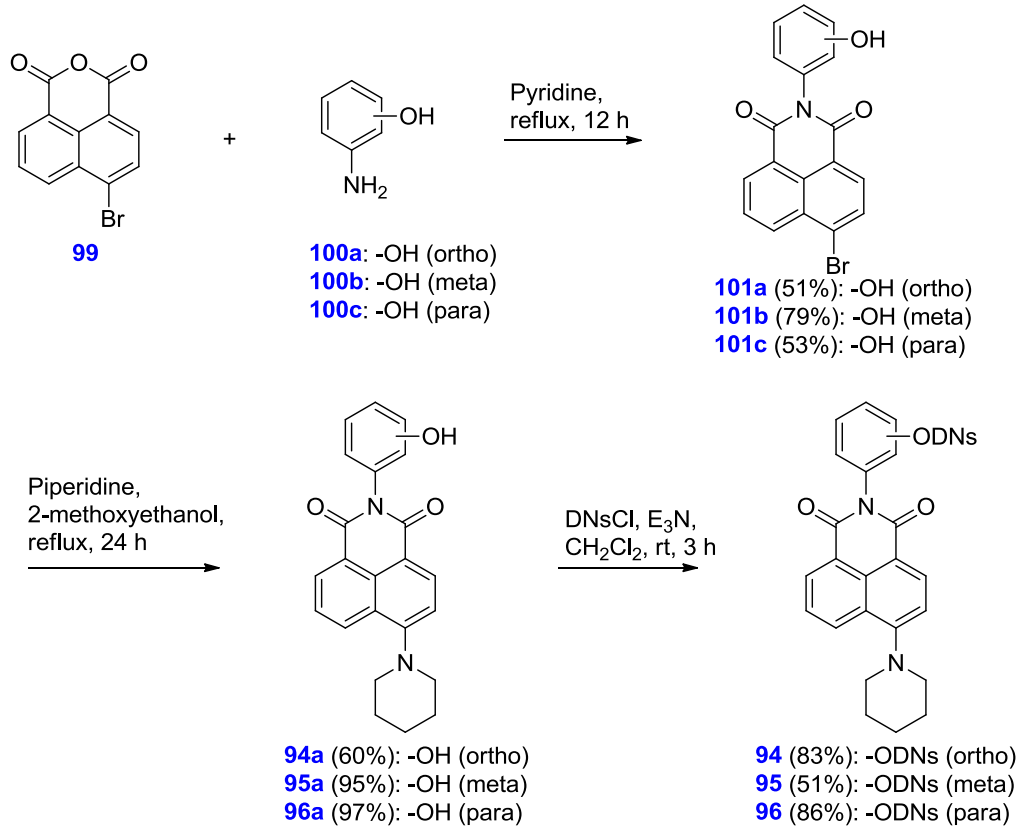

Scheme 3.4 Synthesis of naphthaleneimide based probes **94 – 96**.

The structures of the probe **94** and **95** were confirmed by spectroscopic and single crystal X-ray diffraction analysis (Figure 3.13).

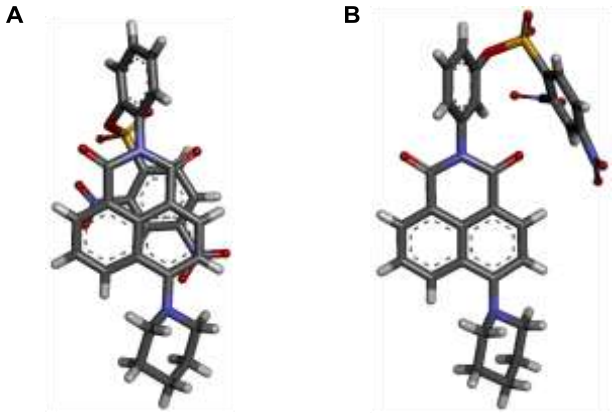

Figure 3.13 Crystal structures of probe **94** and **95**.

3.2.3 Photophysical studies and thiol sensing

Reaction of PhSH with probes **91 – 96** would result in the formation of compounds **91a – 96a**. When fluorescence intensities for these probes with their expected respective products were compared, higher fold in the fluorescence increment was expected for

probes **91 – 94** (Figure 3.14). In case of probes **95** and **96** fluorescence increments were not significant. Therefore, probes **95** and **96** were not selected for further studies.

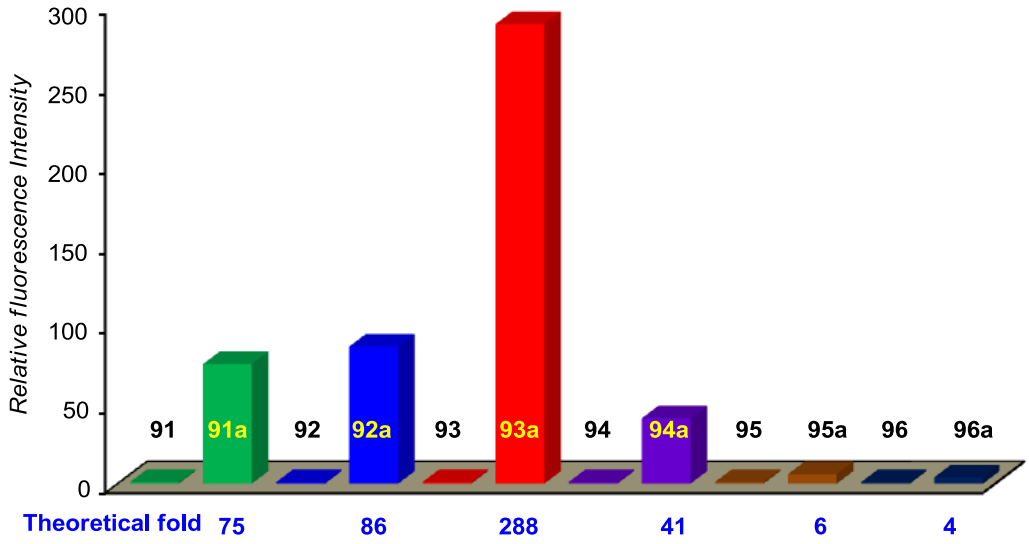

Figure 3.14 Comparison of the fluorescence intensities for probes **91 – 96** (10 μM) with their expected resultant products **91a – 96a** respectively (each 10 μM) in buffer (10 mM, pH 7.4) solutions.

To determine the response time for thiophenol detection, reaction of each probe (10 μM) and thiophenol (100 μM) in buffer (10 mM, pH = 7.4) was monitored by fluorescence kinetics experiments. Fluorescence intensity at λ = 529 nm (λ_{ex} = 444 nm) was separately monitored upon addition of various thiols (PhSH, $HS(CH_2)_2OH$, Cys and GSH, 100 μM each) to probe **91** (10 μM) Sensing process of PhSH by probe **91** was completed within 12 min (Figure 3.15A). No reaction was observed for any aliphatic thiol even at the end of 30 min after addition. When fluorescence intensity at λ = 435 nm (λ_{ex} = 333 nm) was monitored upon addition of PhSH (100 μM) to probe **92** (10 μM), a pseudo first order kinetics was observed with rate constant, k = 0.0069 s^{-1} and half-life, $t_{1/2}$ = 100.4 s. From this plot, a t_R = 5.5 min was determined for probe **92** (Figure 3.15B). Similarly, when probe **93** (10 μM) was subjected PhSH (100 μM) addition and fluorescence intensity was monitored at λ = 524 nm (λ_{ex} = 487 nm), a pseudo first order rate constant, k = 0.0290 s^{-1} and $t_{1/2}$ = 23.9 s were obtained. The fluorescence kinetics plot of the probe provided an excellent t_R = 1.5 min (Figure 3.15C). Reaction monitoring at λ = 548 nm (λ_{ex} = 425 nm) of PhSH (100 μM) with **94** (10 μM) provided a pseudo first order kinetics with rate constant, k = 0.063 s^{-1} and $t_{1/2}$ = 11 s (Figure 3.15D). The fluorescence kinetics plot of the probe provided an excellent t_R < 1 min Under the applied assay conditions, the reaction of

either probe **92**, **93** or **94** was limited to only PhSH and other aliphatic thiols (*e.g.* Cys and GSH) did not show any significant reactivity These data confirm faster response of the probes **91**, **92**, **93** and **94** toward PhSH compared to DNs-based thiophenol probes **26** and **29**.

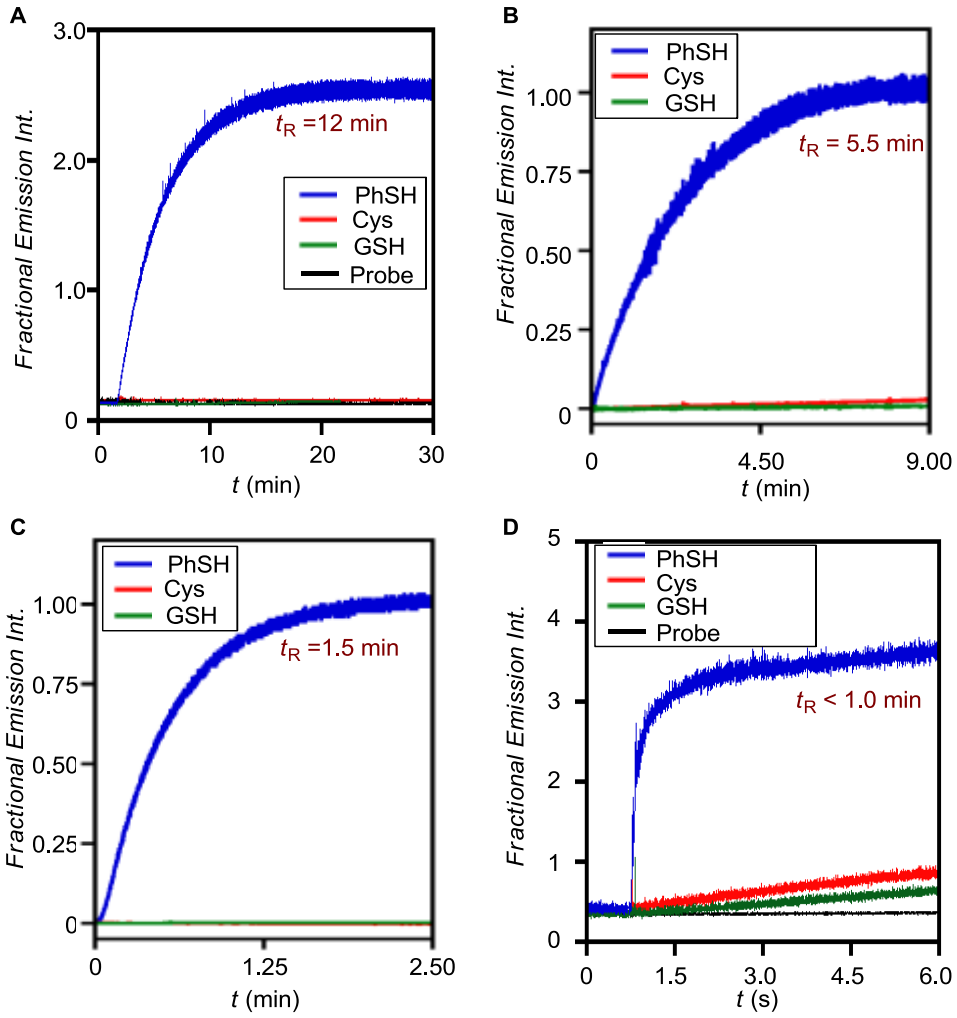

Figure 3.15: Determination of t_R values for probes **91** (**A**), **92** (**B**), **93** (**C**) and **94** (**D**) each (10 μM) in buffer (10 mM, pH = 7.4) toward various sulfhydryls (100 μM of PhSH, Cys and GSH).

The correlation diagram demonstrates a decrease in t_R value of probe toward PhSH upon increase in pK_{aH} of released fluorophore (Figure 3.16). Among probes **94** – **96**, probe **91** with pK_{aH} of 2.84 shows slower response towards PhSH with response time (t_R) 12 min. For probe **92** with pK_{aH} of 5.22 response time t_R was found to be 5.5 min. Probe **93** with pK_{aH} of 5.75 shows rapid response towards PhSH with t_R = 1.5 min. Probe **94** with pK_{aH} of 8.25 shows fastest response towards PhSH with t_R < 1 min.

A

Fluorophore	t_R (min)	pK_{aH}	Fluorophore	t_R (min)	pK_{aH}
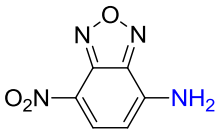 **26a**	17	-1.62	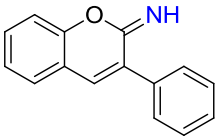 **92a**	5.5	5.22
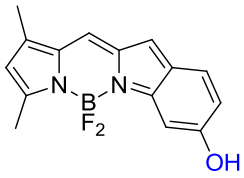 **29a**	20	-5.71	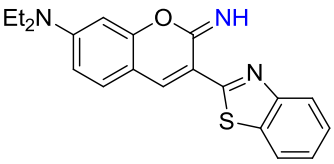 **93a**	1.5	5.75
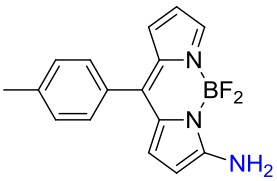 91a	12	2.84	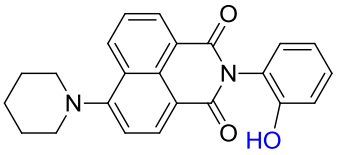 **94a**	<1.0	8.25

B

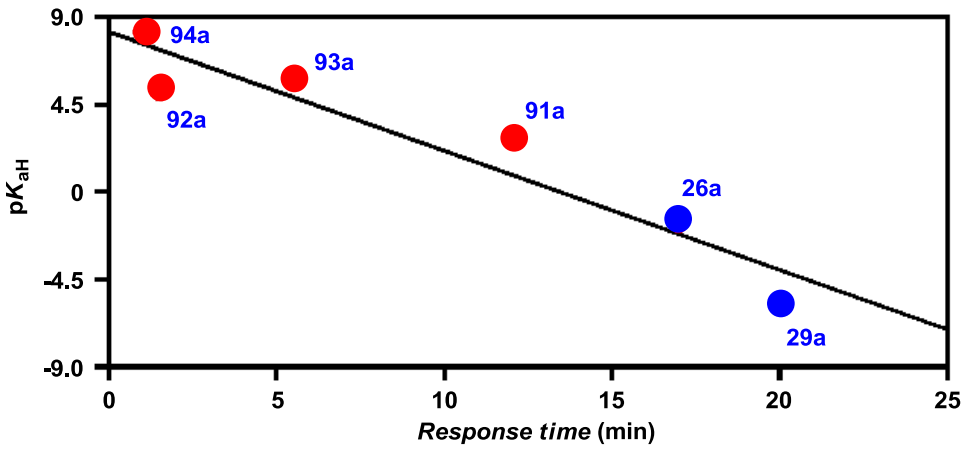

Figure 3.16: (**A**) t_R, pK_{aH} values and (**B**) correlation diagram of t_R values of probes **26**, **29** and **91** – **94** with pK_{aH} of **26a**, **29a** and **91a** – **94a**.

Each probe was further examined to test competitive sensing ability, calculate detection limits and demonstrate their applications in either detection of PhSH in natural water systems or living cells.

Probe **91** and amine **91a** displayed appreciable water solubility to perform further investigations in an aqueous phosphate buffer (10 mM, pH = 7.3, 1.0% DMSO).

Absorption spectrum of **91** displayed an excitation maxima, λ_{ex} = 483 nm with molar extinction coefficient, ε = 28744 L mol^{-1} cm^{-1} (Figure 3.17). When excited at λ = 483 nm, the probe exhibited low fluorescence with emission maxima, λ_{em} = 530 nm and quantum yield, Φ = 0.0018 (standard: Rhodamin G in water; Φ = 0.76). On the other hand, the amine **91a** displayed absorption band with λ_{ex} = 444 nm (ε = 21192 L mol^{-1} cm^{-1}) and strong fluorescence at λ_{em} = 521 nm with Φ = 0.153 (Figure 3.18). These data ensured that an enhancement in quantum yield upto 85-fold can be achieved during thiol sensing process by using probe **91**.

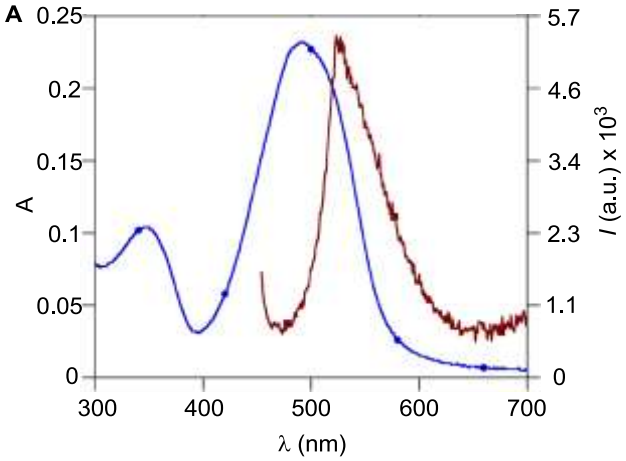

B

compound	λ_{ex} (nm)	ε (L mol^{-1} cm^{-1})	λ_{em} (nm)	Φ
91	483	28744	530	0.0018

Figure 3.17: (**A**) Normalised UV-vis and fluorescence spectra and (**B**) photophysical properties of the probe **91** recorded in phosphate buffer.

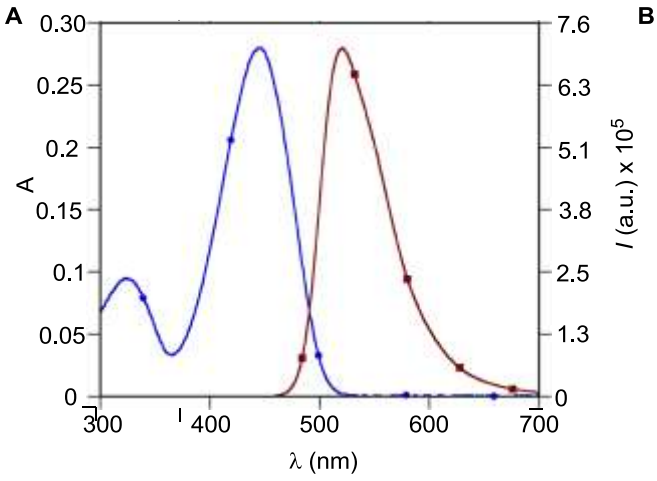

B

compound	λ_{ex} (nm)	ε (L mol^{-1} cm-1)	λ_{em} (nm)	Φ
91a	444	21192	521	0.153

Figure 3.18: (**A**) Normalised UV-vis and fluorescence spectra and (**B**) photophysical properties of amine **91a** recorded in phosphate buffer.

In the next stage, reactivity of the probe **91** with presence of various analytes was examined. In each case, 10 μM of the probe **91** was treated with 100 μM of analyte (either of PhSH, $PhNH_2$, PhOH, NaN_3, $ZnCl_2$, $FeCl_3$, $HS(CH_2)_2OH$, Ala, Cys and GSH) in PBS

buffer (10 mM, pH = 7.3, 1.0% DMSO) and fluorescence was recorded after 15 min stirring at room temperature. In the case of PhSH addition, more than 63-fold enhancement of fluorescence was observed (Figure 3.19). However, for other analytes no significant enhancement of fluorescence was observed. We also tested the specificity of the probe towards PhSH in presence of all other analytes as competing reagents. Probe **91** remains essentially unaffected in the presence of various analytes and the fluorescent enhancements were observed only after the addition of thiophenol. These observations confirmed the usefulness of **91** as selective thiophenol probe.

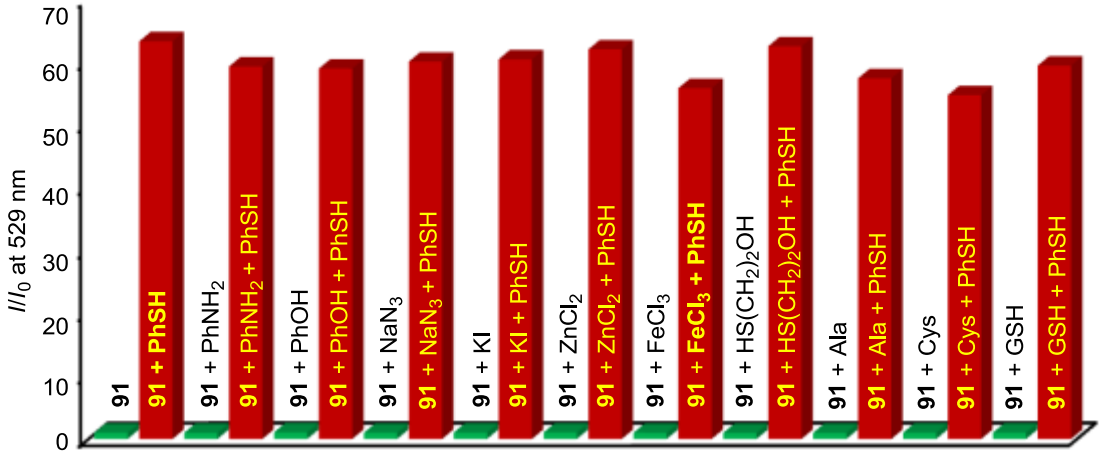

Figure 3.19: Relative fluorescence intensity of probe **91** (10 μM in 10 mM PBS buffer containing 1% DMSO, pH 7.3) toward PhSH (100 μM) in the presence and absence of different analytes (100 μM). All data (λ_{ex} = 444 nm) were recorded at 15 min after addition of analyte(s) at room temperature with λ_{em} = 529 nm.

When a solution containing the probe **91** and PhSH was further analyzed by mass spectrometry, only signals corresponding to BODIPY-amine **91a** (*m/z* = 261, 283 for $[M-2F+H]^+$ and $[M-2F+Na]^+$, respectively) and the by-product 2,4-dinitro-1-(phenylthio)benzene (*m/z* = 277 for $[M+H]^+$ and *m/z* = 289 for $[M+Na]^+$) were detected (Figure 3.20).

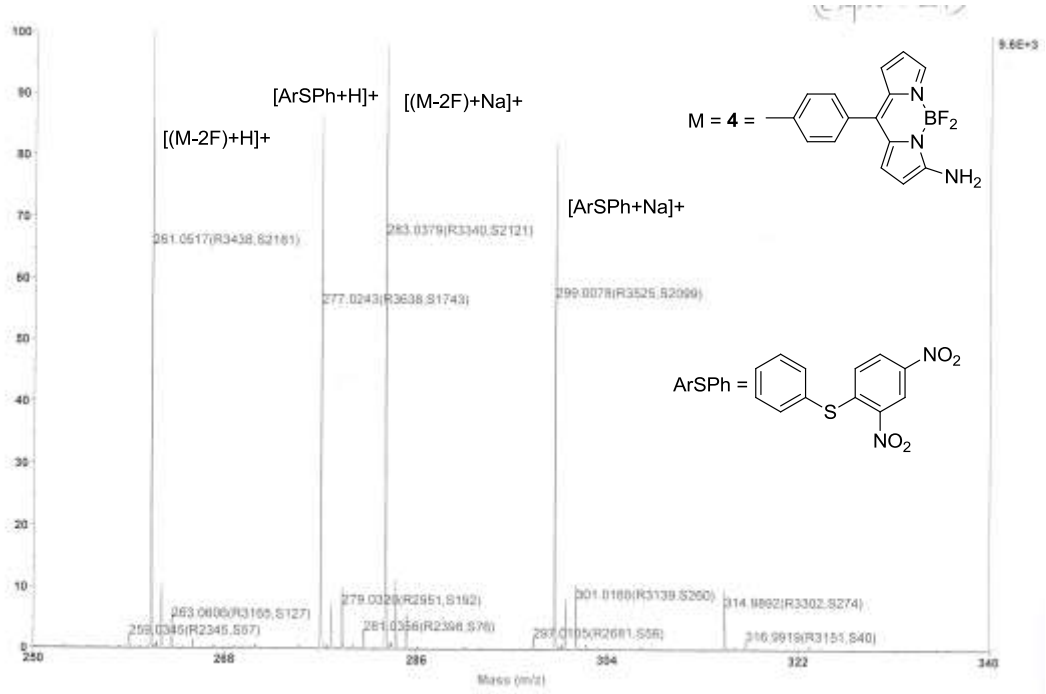

Figure 3.20: ESI-MS of the probe **91** (10 μM in 10 mM PBS buffer containing 1% DMSO, pH 7.3) titrated with PhSH (100 μM).

The response of the probe **91** (10 μM) to thiophenol (100 μM) was investigated by UV-visible spectroscopy (Figure 3.21A). Upon addition of thiophenol, the absorption band displayed a blue shift of 39 nm (from λ_{max} = 483 nm to λ_{max} = 444 nm) as expected from our initial studies. A corresponding change in visible color from red to yellow was also observed in this case (Figure 3.21B).

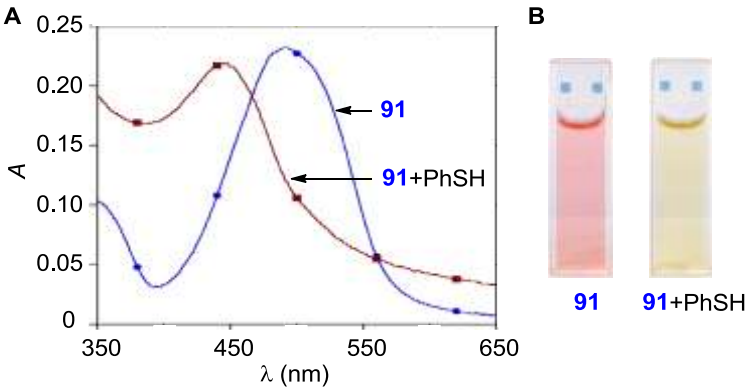

Figure 3.21: (A) UV-vis absorption of probe **91** (10 μM in 10 mM PBS buffer containing 1% DMSO, pH 7.3) before and after addition of PhSH (100 μM); **(B)** Photographs taken under ambient light.

Quantitative *Off-On* response of the probe **91** to thiophenol was assayed by fluorometric titrations. Titration of the probe **91** (10 μM) with increased concentration of PhSH (0 – 100 μM) in phosphate buffer (10 mM, pH = 7.3, 1.0% DMSO) resulted in enhancement of fluorescence in a concentration dependent manner (Figure 3.22A). When the fluorescence emission intensity values at 529 nm were plotted against concentrations of PhSH, a linear enhancement on fluorescence intensity was observed only upto one equivalent of thiol concentration (Figure 3.22A, inset). This linear increase (regression factor, R = 0.99516) for PhSH (0.2 - 1.0 equivalent) proved the usefulness of the probe **91** for the quantitative detection of thiophenol (Figure 3.23). The detection limit for PhSH addition under this condition was determined as 3.44×10^{-8} M based on *S/N* = 3. This data demonstrates the importance of the probe **91** for the quantitative determination of low PhSH concentrations. PhSH sensing process by probe **91** was also associated with 61-fold enhancement (0.0018 to 0.1108) in quantum yield (Φ_F). The fluorescence *Off-On* characteristic of the probe **91** was also ascertained by the appearance of strong green fluorescence (Figure 3.22B). In these experiments, observed *off*-fluorescence for the probe **91** can be rationalized by an intramolecular charge transfer (ICT) pathway working from the BODIPY to the DNs group. During the thiophenol mediated cleavage of the DNs group the ICT pathway is destroyed resulting in the *On*-fluorescence.

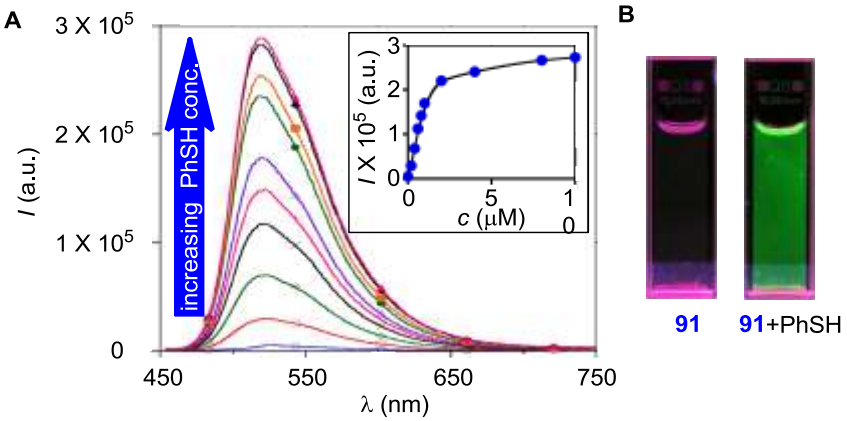

Figure 3.22: (**A**) Fluorescence spectra of **91** (10 μM in 10 mM PBS buffer, 1% DMSO, pH 7.3) in the presence of a PhSH (0, 2, 4, 6, 8, 10, 20, 40, 80, 100 μM) with λ_{ex} = 444 nm. Inset: fluorescence intensity *I* of **91** at 529 nm *vs* PhSH concentration; (**B**) Photographs taken under hand-held UV lamp (λ_{ex} = 365 nm).

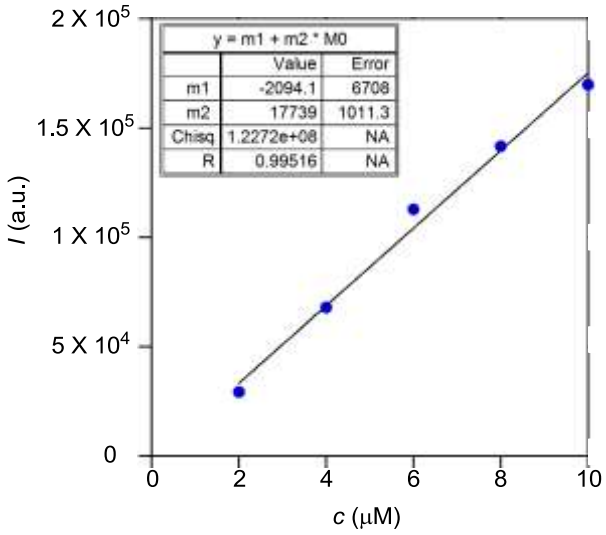

Figure 3.23: The linear relationship (at 529 nm) between the fluorescence intensity and PhSH concentration (2, 4, 6, 8 and 10 μM) for the probe **91** (10 μM in 10 mM PBS buffer containing 1% DMSO, pH 7.3).

Photophysical studies of probe **92** (10 μM) in HEPES buffer (10 mM, pH = 7.4) displayed a strong UV-absorption band centered at λ_{max} = 368 nm (Figure 3.24) with molar extinction coefficient, $\varepsilon = 1.7 \times 10^4$ L mol^{-1} cm^{-1} (Table 3.5). When excited at λ_{ex} = 368 nm, the probe **92** displayed negligible fluorescence. On the other hand, **92a** (10 μM) exhibited an intense UV-absorption band with λ_{max} = 333 nm ($\varepsilon = 1.4 \times 10^4$ L mol^{-1} cm^{-1}) and a strong fluorescence with λ_{em} = 435 nm (λ_{ex} = 333 nm). The UV-visible spectrum of probe **93** provided a red-shifted λ_{max} = 498 nm ($\varepsilon = 2.5 \times 10^4$ L mol^{-1} cm^{-1}), when compared to probe **92**. Upon excitation at λ_{ex} = 498 nm, **93** exhibited negligible fluorescence. The free iminocoumarin **93a** displayed strong UV-absorption band at λ_{max} = 487 nm ($\varepsilon = 2.8 \times 10^4$ L mol^{-1} cm^{-1}) and a strong fluorescence emission band centered at λ_{em} = 524 nm (λ_{ex} = 478 nm).

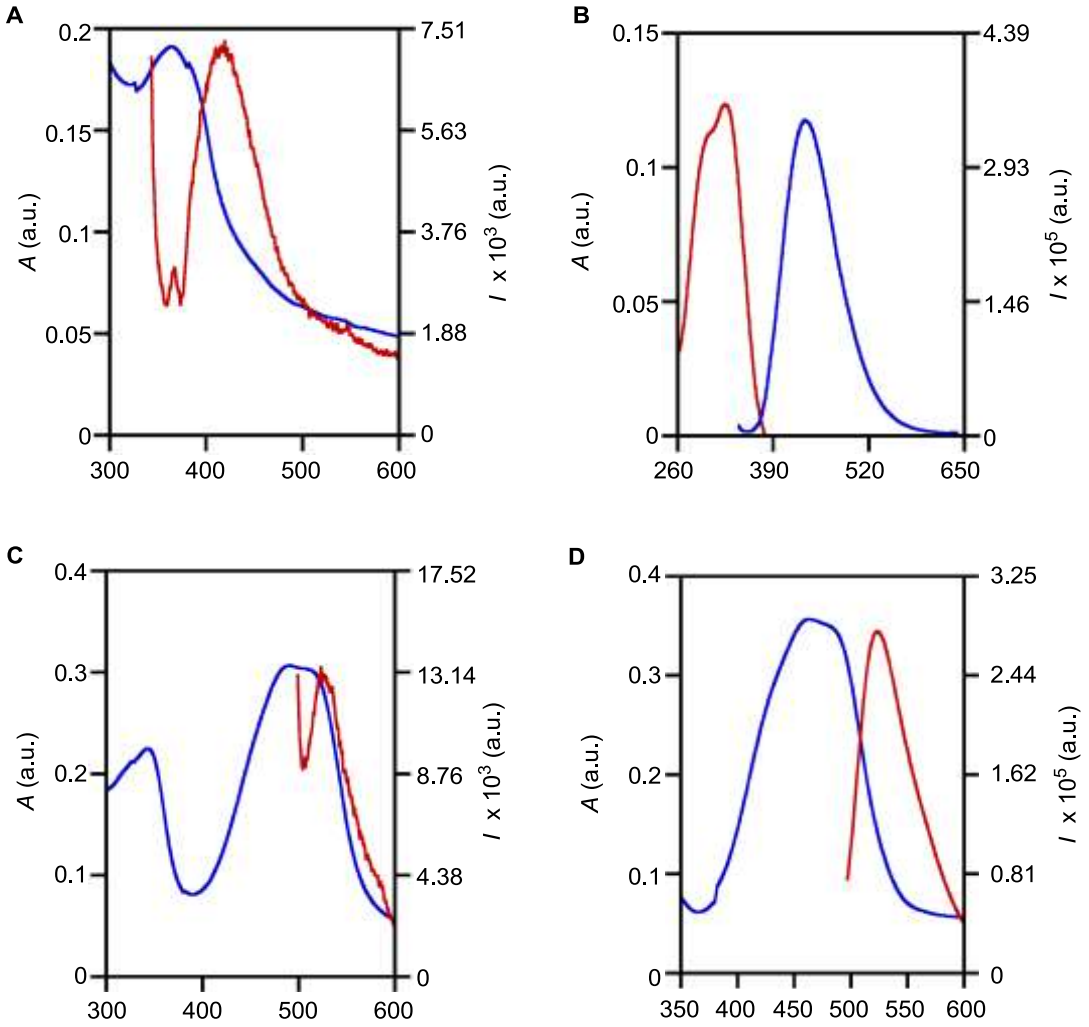

Figure 3.24: Normalized UV-vis absorption and fluorescent spectra of probe (**A**) **92**, (**B**) **92a**, (**C**) **93** and (**D**) **93a**.

Table 3.5: Phtophysical properties of **92**, **92a**, **93** and **93a**.

Entry	Probe	λ_{max} (nm)	ε (L mol^{-1} cm^{-1})	λ_{em} (nm)[a]
1	**92**	368	1.7×10^4	-
2	**92a**	333	1.4×10^4	435
3	**93**	498	2.5×10^4	-
4	**93a**	478	2.8×10^4	524

[a] Fluorescence spectra were recorded by exciting at λ_{max} values of respective compounds.

Selectivity of thiol detection determined

To evaluate the selectivity and sensitivity of **92** and **93** toward PhSH, various analytes were examined in parallel under the comparable conditions. As shown in Figure 3.25A, reaction of **93** with PhSH and substituted thiophenols resulted in a 260-fold

increase of the fluorescence intensity (back row, red bar), whereas Ala, Lys, Arg, His, Tyr, Ser, GSH, Cys, MeCOSH, $PhNH_2$, PhOH, NaN_3 and KI had negligible influence (front row, green bars). Fluorescence spectra profiles also confirm the sensitivity of the probe **93** toward PhSH in the presence of other analytes (back row, blue bars). A 220-fold enhancement in quantum yield, Φ (from 0.003 to 0.66; standard: fluorescein in 0.1 N NaOH, Φ = 0.85) was also calculated during the sensing. Similar selectivity for probe **92** toward PhSH was also observed however, with significantly lower sensitivity of 65-fold (Figure 3.25B).

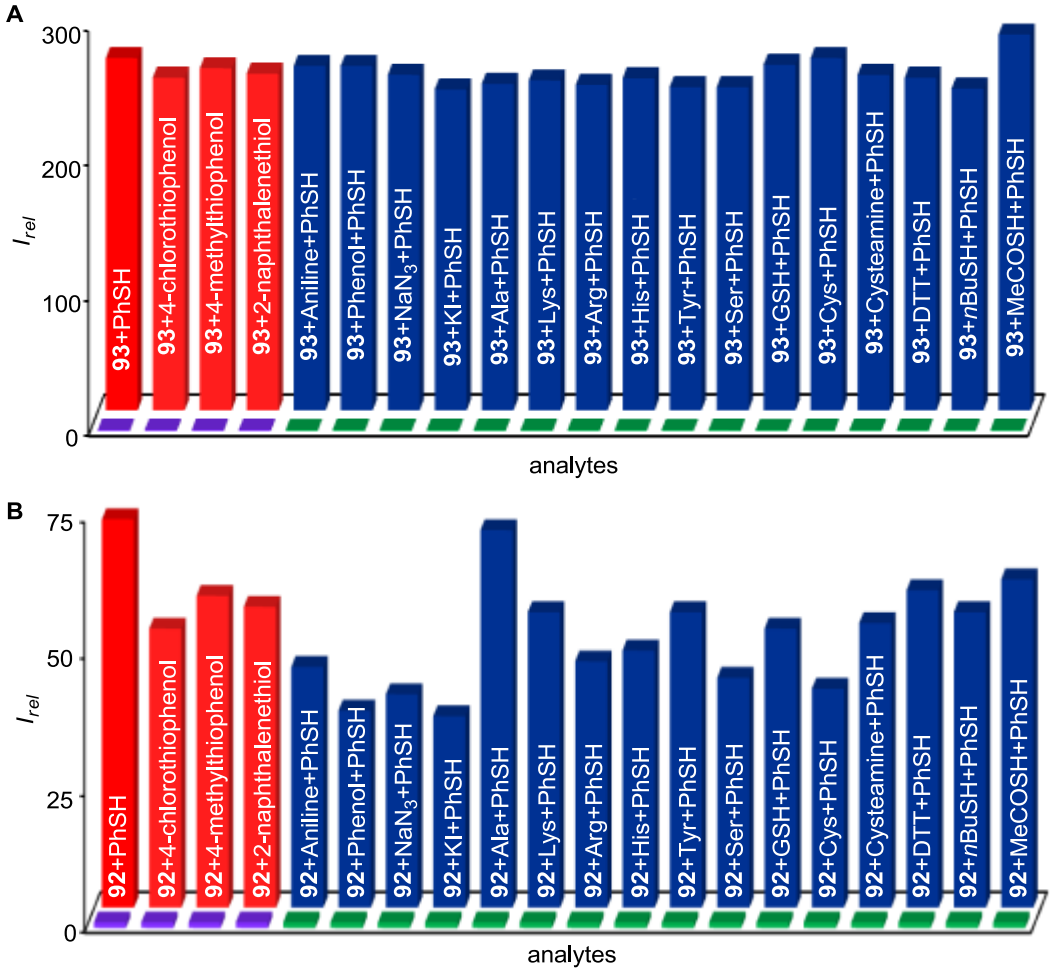

Figure 3.25: Relative fluorescence intensity (at λ_{em} = 524 nm upon λ_{ex} = 487 nm) of (**A**) **93** and (**B**) **92** each (10 μM) in HEPES (10 mM, pH = 7.4) with various analytes after 5 min of mixing. Front row represents the addition of the analytes (100 μM): free compound, Ala, Lys, Arg, His, Tyr, Ser, GSH, Cys, MeCOSH, $PhNH_2$, PhOH, NaN_3 and KI (from left to right); back row represents the subsequent addition of substituted thiophenols (red bar) and thiophenol (blue bar) to the solution.

We further examined the quantitative response of probes **92** and **93** toward PhSH. Fluorometric titrations of **7** (10 μM) with varied concentrations (0–100 μM) of PhSH displayed sharp increase in fluorescence intensity (Figure 3.26A). Based on these results a linear correlation for fluorescence intensity and PhSH concentration was observed only up to one equivalent of the analyte (Figure 3.26B). A detection limit of 1.9×10^{-8} M for **92** toward PhSH was calculated based on a signal-noise ratio, *S/N* = 3.

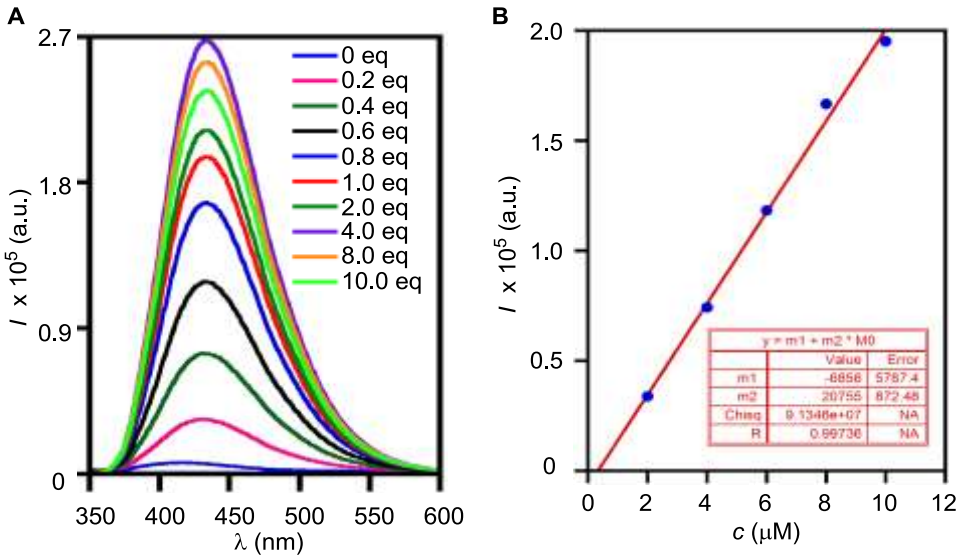

Figure 3.26: (**A**) Fluorescence spectral profile of probe **92** (10 μM) upon titration with 0 – 100 μM of PhSH and (**B**) the linearity of PhSH titration assay of probe **92** in HEPES buffer (10 mM, pH = 7.4).

PhSH sensing by probe **93** was also characterized by a visible color change from red to yellow within 1.5 min confirming a fast and naked eye detection of the process (Figure 3.27A). When placed under the hand-held UV lamp (λ_{ex} = 365 nm), probe **93** exhibited no fluorescence while a strong green fluorescence was observed for cuvette containing **93** and PhSH (Figure 3.27B). We further examined the quantitative response of the probe **93** toward PhSH. Fluorometric titrations of **93** (10 μM) with varied concentrations (0–100 μM) of PhSH displayed sharp increase in fluorescence intensity (Figure 3.27C).

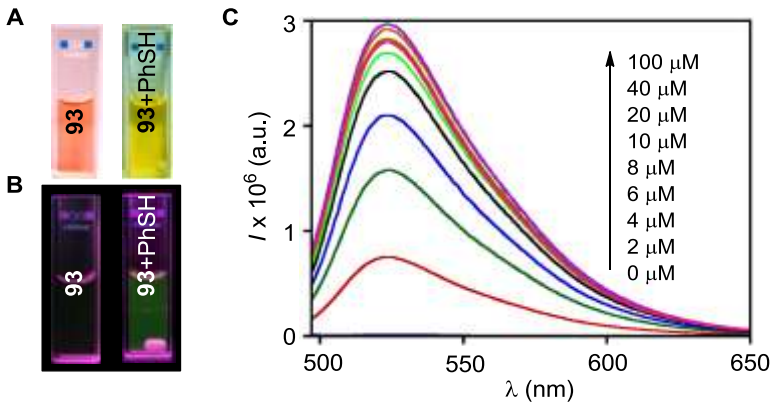

Figure 3.27: (**A**) Change in color for probe **93** during addition of sensing of PhSH. Photographs were taken under ambient light. (**B**) *Off-On* fluorescence for probe **93** during addition of sensing of PhSH. Photographs were taken under handheld UV-lamp (λ_{ex} = 365 nm). (**C**) Fluorescence spectral profile of probe **93** (10 μM) upon titration with 0 – 100 μM of PhSH.

Based on these results a linear correlation for fluorescence intensity and PhSH concentration was observed only up to one equivalent of the analyte (Figure 3.28). A detection limit of 6.9×10^{-9} M for **93** toward PhSH was calculated based on a signal-noise ratio, *S/N* = 3. These data established the usefulness of **93** as selective thiophenol sensing probe.

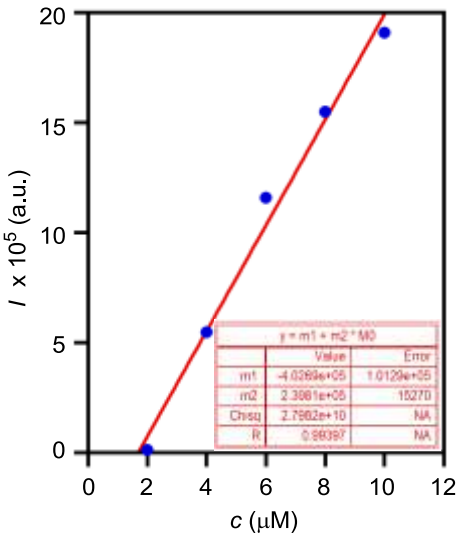

Figure 3.28: The linearity of the PhSH titration assay of probe **93** in HEPES buffer (10 mM, pH = 7.4).

Estimation of PhSH in natural water samples by probe 93:

Probe **93** due its high selectivity and sensitivity was further applied for estimation of PhSH in water samples collected from Mula-Mutha River in Pune (Table 3.6). In these assays, a linear calibration curve was generated by plotting fluorescence intensities at λ_{ex} = 524 nm against 0–10 μM PhSH concentrations (Figure 3.29). An internal standard method[6] was also employed for validating the experimental data. The crude water samples from Mula-Mutha River were adjusted to pH 7.4 HEPES buffer, and different concentrations of thiophenol (0.3, 1, 5, 10, 30, 100 μM) were obtained by diluting the stock solution into HEPES buffer. The resulting samples were further treated with probe **8** (10 μM). The resulting solution was shaken well. After 3 min, the fluorescence was recorded. The fluorescence response (λ_{em} = 524 nm) was plotted against different concentrations of thiophenol, a calibration curve revealing a good linear relationship was obtained, with *R*-value = 0.99899. Then the unknown concentration of thiophenols in the Mula-Mutha river sample was determined by the calibration curve. From these measurements, no PhSH in the collected river water sample was detected. When the river water samples were spiked with marked concentrations of PhSH, an excellent coherence between concentrations determined experimentally using probe **93** and from internal standard method were observed. These data illustrate the significance of probe **93** for quantitative detection of PhSH in natural water samples.

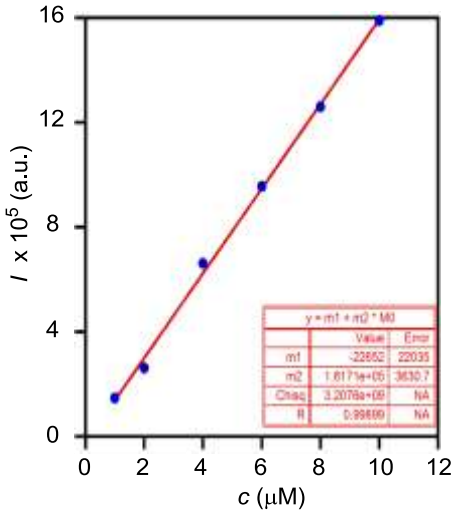

Figure 3.29: Calibration curve for titration of probe **93** with PhSH. This curve was used as calibration curve for Internal Standard Method.

Table 3.6: Estimation of PhSH in Mula-Mutha River water by probe **93**.

Entry	Conc. of PhSH added (μM)	Conc. determined by probe **93** (μM)
1	0	Not detected
2	1.53	1.29
3	3.62	3.29
4	6.38	6.18

The photophysical studies for compounds **94a** and **94** were carried out in HEPES buffer (10 mM, pH 7.4, 1% DMSO) solutions. Absorption spectra of probe **94** displayed a strong absorption band centred at λ_{max} = 438 nm with a molar extinction coefficient of ε = 7340 L mol^{-1} cm^{-1} (Table 3.7). Probe **94** displayed very weak fluorescence when excited at 383 nm (Figure 3.30). Absorption spectra of **94a** displayed a strong absorption band centred at λ_{max} = 425 nm with molar extinction coefficient (ε) 8189 L mol^{-1} cm^{-1}. For compound **94a** strong fluorescence at λ_{em} = 548 nm was a observed when excited at λ_{ex} = 425 nm.

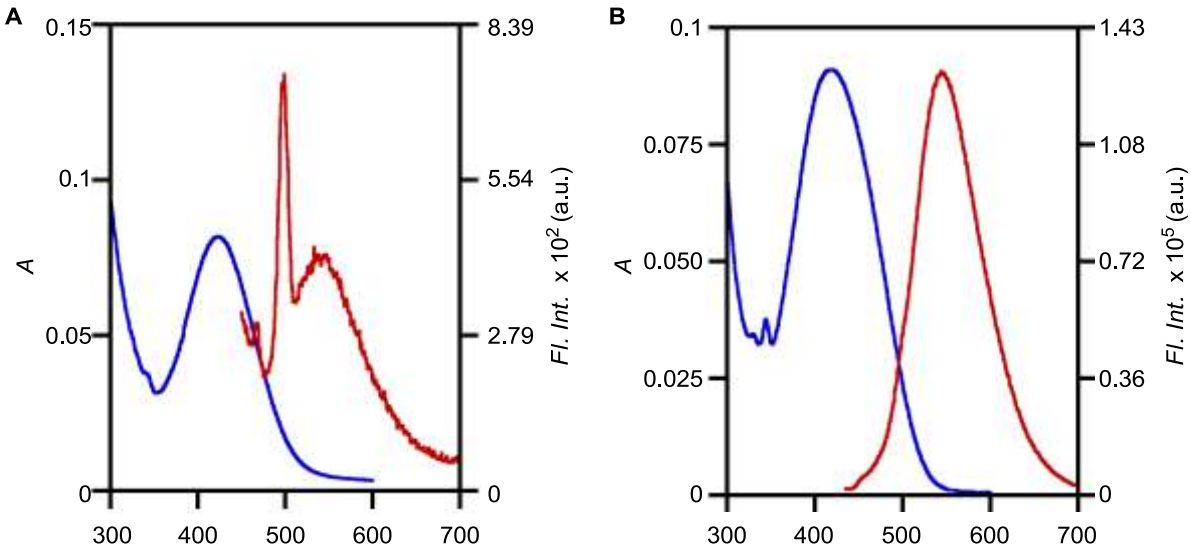

Figure 3.30: Normalized UV-vis absorption and fluorescent spectra of probe (**A**) **94** and (**B**) **94a**.

Table 3.7. Photophysical properties of compounds **94** and **94a**.

Compound	λ_{max}(nm)	ε (L mol^{-1} cm^{-1})	λ_{max}(nm)
94	438	7340	-
94a	425	8189	548

When background fluorescence for compounds **94 – 96** were compared, the fluorescence intensities at λ_{em} = 425 nm were in the order $I_{94} < I_{95} < I_{96}$ (Figure 3.31). As expected, the compound **94** shows lower fluorescence intensity than that of **95** and **96**

which confirms that DNs group at *ortho* position is quenching the fluorescence much effectively than at *meta* and *para* positions. Reaction of PhSH with **94** would result in the formation of compound **94a**. Similarly probes **95** and **96** will result in the formation of compounds **95a** and **96a** respectively. When fluorescence intensities for these probes with their expected respective products were compared at 548 nm, higher fold in the fluorescence increment was expected for probe **94**. Therefore, probe **94** was selected and used for further studies.

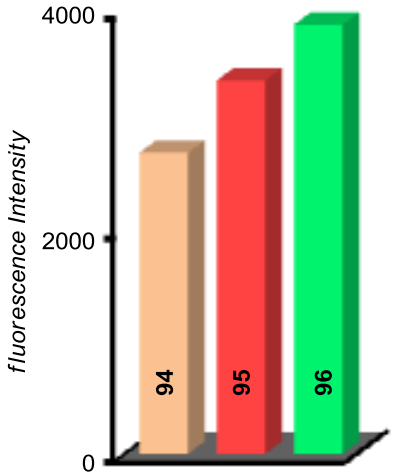

Figure 3.31: Comparison of the fluorescence intensities recorded at 460 nm for probes **94 – 96** (10 μM) in HEPES buffer (10 mM, pH 7.4, 1% DMSO) solutions

The selectivity of probe **94** towards PhSH was examined. In each case, probe **94** (10 μM) was treated separately with 100 μM of each analyte (either of Ala, Lys, Arg, Tyr, Ser, GSH, Cys, Aniline, Phenol, NaN_3 and KI) in HEPES buffer (10 mM, pH = 7.4) and fluorescence spectra were recorded after 2 min at room temperature. However no significant fluorescence enhancement (λ_{ex} = 425 nm) was observed for these analytes (Figure 3.32). Treatment of probe **94** with PhSH under identical conditions provided strong fluorescence (λ_{em} = 548 nm). When fluorescence intensities at 548 nm were compared, 20-fold enhancement was observed in the case of PhSH.

Figure 3.32: Relative emission intensity at λ_{em} = 548 nm (λ_{ex} = 425 nm) of **94** (10 μM) towards PhSH in the presence and absence of various analytes (Ala, Lys, Arg, Tyr, Ser, GSH, Cys, Aniline, Phenol, NaN_3 and KI, 100 μM each) recorded in HEPES buffer (10 mM, pH = 7.4, 1.0% DMSO).

In the next stage, we examined the quantitative response of **94** towards PhSH by fluorometric titrations. Sharp enhancements in fluorescence (λ_{em} = 548 nm) were observed (Figure 3.33A) when titrations were carried out by addition of increasing concentrations of PhSH (0 to 100 μM) in the probe **94** (10 μM) in HEPES buffer (10 mM, pH = 7.4). When fluorescence intensities at 548 nm were plotted against concentrations of PhSH, excellent linear correlation (Regression factor, R = 0.99335) was observed up to one equivalent of the PhSH added (Figure 3.33B). A detection limit of 22.4×10^{-8} M was calculated for the probe **94**, based on signal to noise ratio, S/N = 3. Sensing process is also associated with 5.3-fold enhancement in quantum yield (from Φ = 0.009 to 0.048).

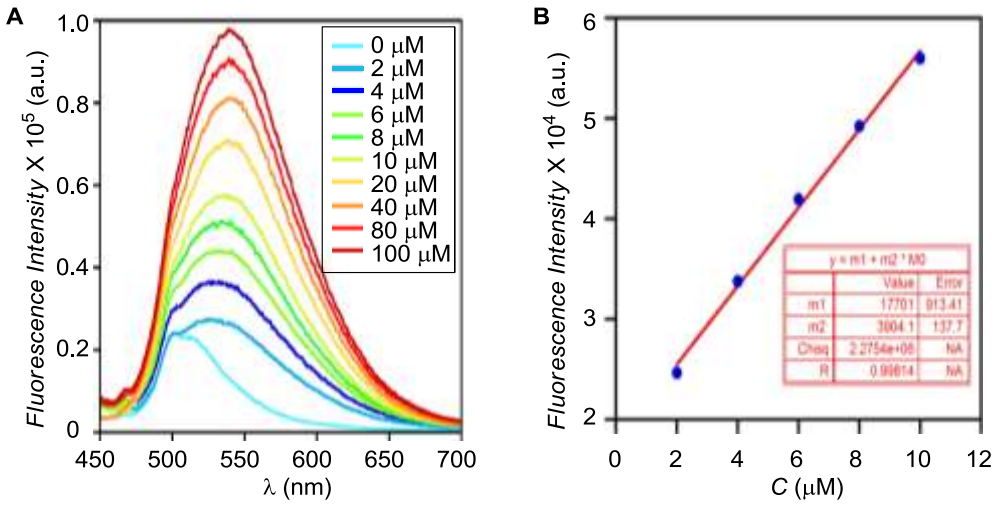

Figure 3.33: (**A**) Fluorescence spectral profile of probe **93** (10 μM) upon titration with 0–100 μM of PhSH and (**B**) linearity of the PhSH titration assay of probe **94** in HEPES buffer (10 mM, pH = 7.4).

3.2.4 Cell imaging

Application of probe **91** was demonstrated by the live cell fluorescence microscopic technique using HeLa cells. When cells were incubated with only probe **91** (10 mM in 1:200 DMSO–DMEM v/v, pH = 7.4) at 37 ^{o}C for 30 min, no significant fluorescence was observed (Figure 3.34A–C). These data indicate that the probe does not react with the intracellular aliphatic thiols. On the other hand, cells pretreated with thiophenol (1 mM in 1:1000 DMSO–DMEM v/v, pH = 7.4) for 30 min and then incubated with probe **91** (10 mM in 1:200 DMSO–DMEM v/v, pH = 7.4) for 30 min showed strong fluorescence inside these cells (Figure 3.34D–F). A control experiment was also carried out by treating the cultured cells, first with thiophenol (1 mM in 1:1000 DMSO–DMEM v/v, pH = 7.4) for 30 min, then incubated with N-phenylmaleimide (1 mM 1:100 DMSO–DMEM v/v, pH = 7.4) for 30 min. These pre-treated cells when incubated with probe **91** (10 mM in 1:200DMSO–DMEM v/v, pH = 7.4) for 30 min no fluorescence was observed (Figure 3.34G–I). These data demonstrated the usefulness of probe **91** in the selective detection of thiophenol in the intracellular environment by discriminating thiol containing amino acids and proteins.

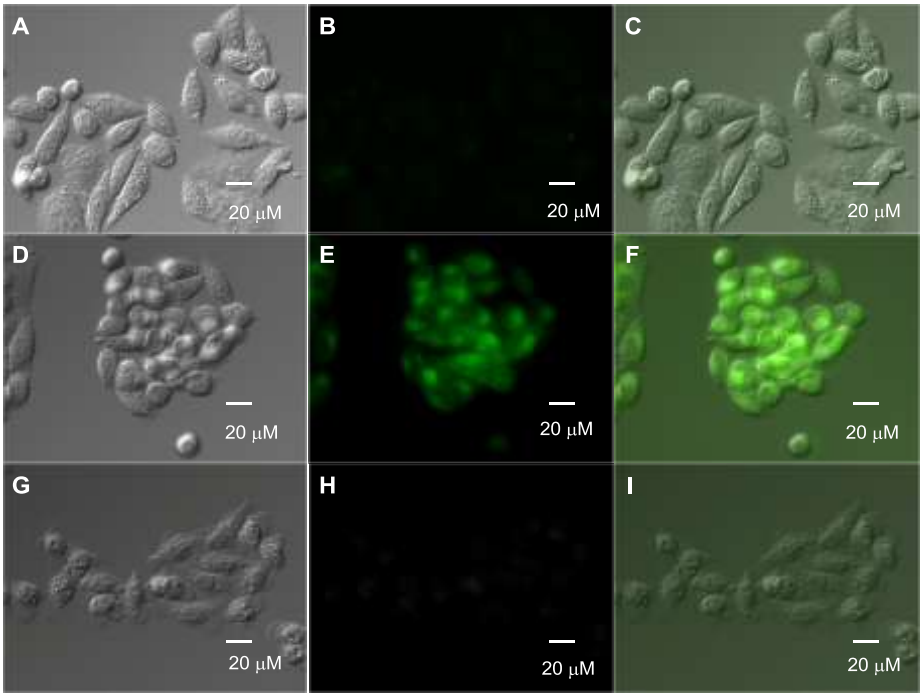

Figure 3.34: Imaging of thiophenol in living cells: (**A**) brightfield, (**B**) fluorescence and (**C**) overlay images of HeLa cells incubated with only probe **91** (10 mM). Microscopy of HeLa cells treated first with PhSH (1 mM) and then with probe **91** (10 mM), represented by (**D**) brightfield, (**E**) fluorescence and (**F**) overlay images. Control experiment by successively treating with PhSH (1 mM), N phenylmaleimide (1 mM) and **91** (10 mM) represented by (**G**) brightfield, (**H**) fluorescence and (**I**) overlay images.

Further the cell permeability and thiophenol sensing ability of probe **94** in inside cells was evaluated. Live-cell imaging studies were carried out by using Human cervical cancer cell line (HeLa). No significant fluorescence intensity was observed when HeLa cells were incubated with probe **94** (10 μM in 1:100 DMSO-DNEM v/v, pH = 7.4) at 37 ^{o}C for 30 min (Figure 3.35A-C). These HeLa cells when incubated with PhSH (100 μM in 1:100 H_2O-DMEM, pH = 7.4) at 37 ^{o}C for 30 min, strong fluorescence inside the cells were observed (Figure 3.35D-F).

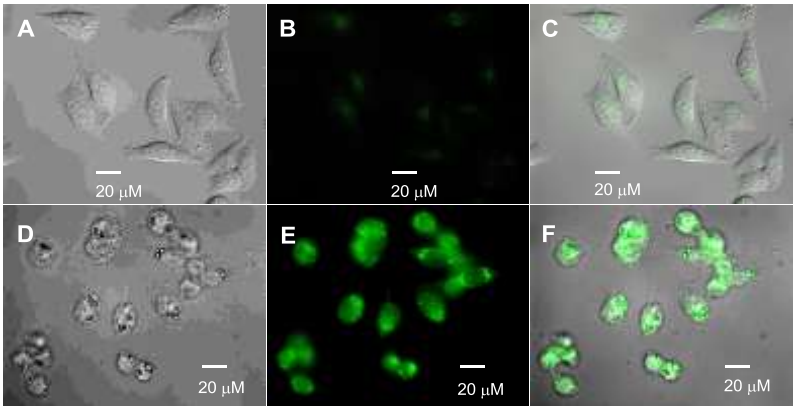

Figure 3.35: Imaging of thiophenol in living cells: Brightfield (**A**), fluorescence (**B**) and overlay (**C**) images of HeLa cells incubated with only the probe **94** (10 μM). Images of HeLa cells treated first with PhSH (1 μM) and then with the probe **94** (10 μM), represented by brightfield (**D**), fluorescence (**E**) and overlay (**F**) images.

3.3 Summary and conclusions

In summary, we have successfully developed four 2,4-dinitrophenylsulfonyl-derivatized probes **91** – **94** for rapid, selective and sensitive detection of thiophenol. These probes were designed based on the understanding of the reaction mechanism to improve response time (t_R) of thiophenol sensing. This design was based on a correlation of pK_{aH} values with experimentally determined t_R *Off-On* response of these probes were predicted by theoretical calculations. Probe **91** exhibited a t_R = 12 min. A pseudo first order kinetics observed during the reaction of the probe **92** with thiophenol with k = 0.0069 s^{-1} and $t_{1/2}$ = 100.4 s. The kinetics also afforded a t_R = 5.5 min. A similar pseudo first order kinetics with k = 0.0290 s^{-1} was determined for probe **93**. Probe **93** exhibited a faster $t_{1/2}$ = 23.9 s and t_R = 1.5 min. An improved pseudo first order kinetics was observed for the probe **94** during the reaction of with thiophenol with k = 0.063 s^{-1}, $t_{1/2}$ = 11 s and t_R <1 min. Although probe **94** showed an excellent response time, the sensitivity of the same towards thiophenol is compromised as only 20-fold *Off-On* fluorescence enhancement was observed upon sensing of thiophenol. Probes **91** and **94** were cell permeable and application of these probes was demonstrated by live cell imaging.

3.4 References.

(1) (a) Chen, X.; Ko, S.-K.; Kim, M. J.; Shin, I.; Yoon, J. *Chem. Commun.* **2010**, *46*, 2751(b) Sun, Y.-Q.; Chen, M.; Liu, J.; Lv, X.; Li, J.-f.; Guo, W. *Chem. Commun.* **2011**, *47*, 11029(c) Tang, B.; Yin, L.; Wang, X.; Chen, Z.; Tong, L.; Xu, K. *Chem. Commun.* **2009**, 5293(d) Zhang, M.; Yu, M.; Li, F.; Zhu, M.; Li, M.; Gao, Y.; Li, L.; Liu, Z.; Zhang, J.; Zhang, D.; Yi, T.; Huang, C. *J. Am. Chem. Soc.* **2007**, *129*, 10322(e) Bouffard, J.; Kim, Y.; Swager, T. M.; Weissleder, R.; Hilderbrand, S. A. *Org. Lett.* **2008**, *10*, 37(f) Sun, W.; Li, W.; Li, J.; Zhang, J.; Du, L.; Li, M. *Tetrahedron Lett.* **2012**, *53*, 2332(g) Zhu, B.; Zhang, X.; Li, Y.; Wang, P.; Zhang, H.; Zhuang, X. *Chem. Commun.* **2010**, *46*, 5710(h) Guo, Z.; Nam, S.; Park, S.; Yoon, J. *Chem. Sci.* **2012**, *3*, 2760(i) Shao, J.; Sun, H.; Guo, H.; Ji, S.; Zhao, J.; Wu, W.; Yuan, X.; Zhang, C.; James, T. D. *Chem. Sci.* **2012**, *3*, 1049.

(2) (a) Lin, W.; Long, L.; Tan, W. *Chem. Commun.* **2010**, *46*, 1503(b) Jiang, W.; Cao, Y.; Liu, Y.; Wang, W. *Chem. Commun.* **2010**, *46*, 1944(c) Jiang, W.; Fu, Q.; Fan, H.; Ho, J.; Wang, W. *Angew. Chem., Int. Ed.* **2007**, *46*, 8445.

(3) Malwal, S. R.; Sriram, D.; Yogeeswari, P.; Konkimalla, V. B.; Chakrapani, H. *J. Med. Chem.* **2012**, *55*, 553.

(4) Marvin 5.8.0, 2012, ChemAxon (http://www.chemaxon.com).

(5) (a) Ammar, H.; Abid, S.; Le Bigot, Y.; El Gharbi, R. *Synthetic Commun.* **2012**, *42*, 799(b) Ammar, H.; Fakhfakh, M.; Le Bigot, Y.; El Gharbi, R. *Synthetic Commun.* **2003**, *33*, 1821(c) Komatsu, K.; Urano, Y.; Kojima, H.; Nagano, T. *J. Am. Chem. Soc.* **2007**, *129*, 13447.

(6) Wang, X.; Cao, J.; Zhao, C. *Org. Biomol. Chem.* **2012**, *10*, 4689.

Chapter 4

Cascade Reaction Based Fluorescence turn-*On* Probe for Selective Detection of Hydrogen Sulfide

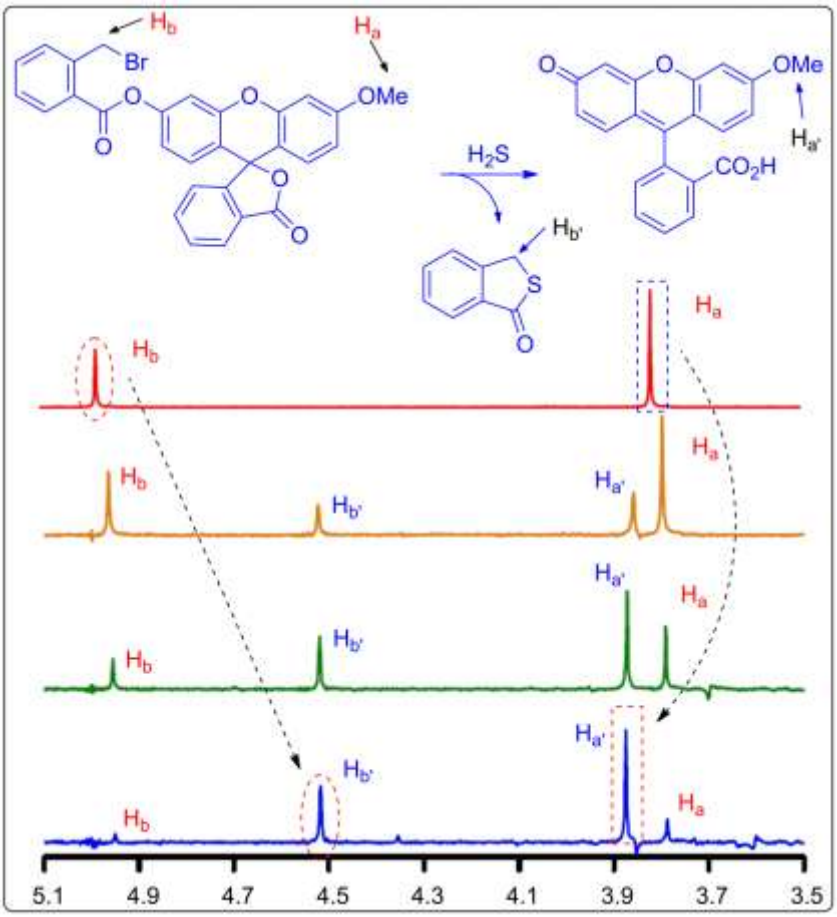

4.1 Introduction

Hydrogen sulfide (H_2S) has traditionally been known as a toxic chemical species in biological systems. However, emerging studies have challenged this view and recognized the importance of H_2S as one of the three essential gasotransmitters (NO and CO being other two). Considering the complex biological roles of H_2S along with its volatile and reactive nature, the accurate detection of H_2S is necessary in order to monitor its production and consumption in biological systems. The methods for selective detection and quantification of the H_2S are important in the areas of diagnostics and therapeutics. Monitoring of H_2S levels using traditional methods such as, gas chromatography,[1] electrochemical methods[2] and polarographic methods[3] require multistep sample preparation, which limits their use in live systems for real time analysis. Owing to high sensitivity and the ability to conduct analysis in live systems, fluorescent probes offer promising approach for the detection of H_2S.

4.2 Review of literature

The pioneering approach involving H_2S mediated reduction of azide to amine in fluorescent probe **46** and **47** were reported independently by Chang[4] and Wang[5] respectively, nearly at the same time. Since then, several fluorescent probes including **48** – **51** have been reported based on this concept by changing the fluorophores[4-6]. Alternatively, dual nucleophilic reactivity of H_2S can be employed to discriminate it from other biothiols. Qian and coworkers reported BODIPY based probes **57** and **59** in which α, β- unsaturated aldehyde was used as H_2S trapping site.[7] Xian and coworkers developed probes **52** and **55** for sensing of H_2S using nucleophilic substitution and addition strategies, respectively.[8] In probe **52**, 2-pyridinyl disulfide and an ester group was employed as two electrophilic sites for reaction of H_2S. Probe **55** was based on Michael addition followed by cyclization to release active fluorophore.

Table 4.1: Properties of reported fluorescence probes **52**, **55a** and **55b**.

Probe	Response time	Detection limit	Fold enhancement
52	60 min	2.5 μM	55-77
55a	30 min	~ 1 μM	11
55b	30 min	~ 1 μM	160

Fluorescence *Off-On* probes **52** and **55** exhibited long response times, ranging from 30 to 60 min (Table 4.1) and may not be suitable for monitoring the intracellular level of the species due to high fluctuations in endogenous free H_2S concentration.[1b,9]

We aimed to develop nucleophilic substitution-cyclization reaction based probe **102** for fast, highly selective and sensitive detection H_2S. We anticipated that probe having halide as good leaving group at benzylic position will undergo fast SN^2 reaction by nucleophilic attack of H_2S (Scheme 4.1). This should result in the decrease in response time. Other nucleophiles including biological thiols such as Cysteine (Cys), Homocysteine (Hcy) and Glutathione (GSH) could also undergo nucleophilic substitution at benzylic position to substitute bromide. However, absence of the reactive intermediate limits the possibility of second nucleophilic attack to release fluorophore.

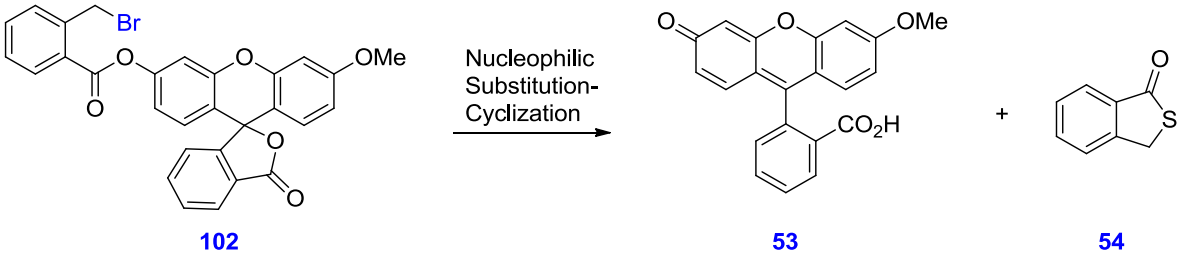

Scheme 4.1: Proposed cascade reaction based fluorescence *turn-On* probe for H_2S Sensing.

4.3 Results and discussion

4.3.1 Synthesis

Synthesis of the probe **102** was carried out in four steps (Scheme 4.2). Fluorescein derivative **102c** was prepared using literature procedure.[10] Fluorescein derivative **102c** was subjected to esterification with ortho-toluic acid using EDC·HCl and DIPEA in presence of catalytic DMAP in CH_2Cl_2 to afford ester **103** in 50% yield. The ester **103** was refluxed with N-bromosuccinimide in the presence of AIBN in CCl_4 to afford probe **102** in 68% yield.

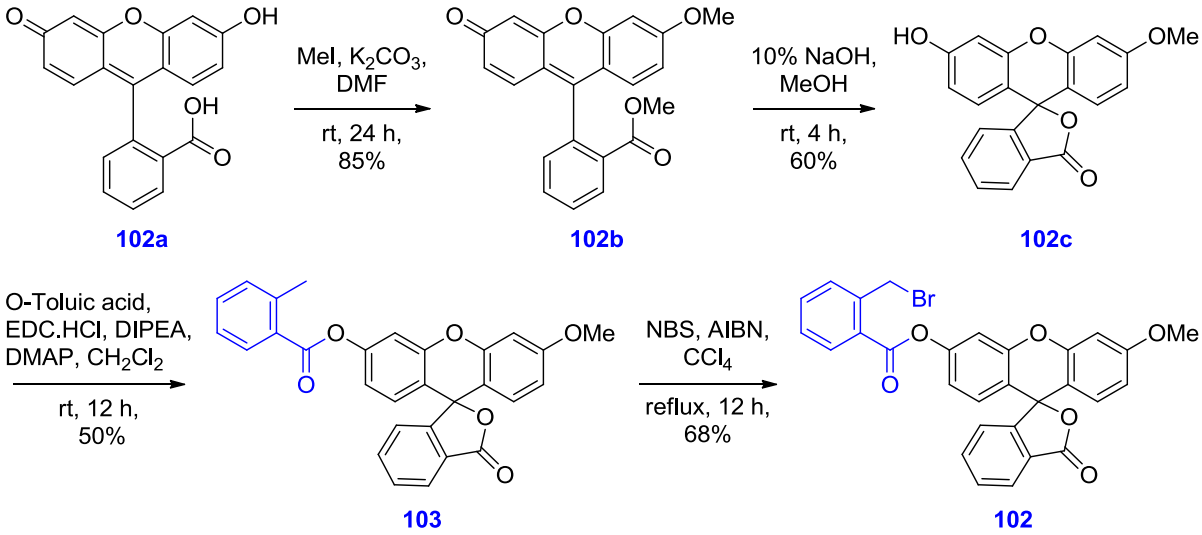

Scheme 4.2: Synthesis of probe **102**.

Compound **105** was prepared in 90% yield from methyl 2-methylbenzoate **104** (Scheme 4.3). Then compound **105** was treated with NaSH in MeOH for 1 h at room temperature to afford the thiophthalide **54** in 88% yield.

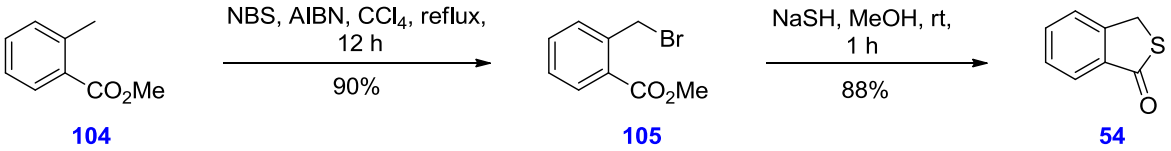

Scheme 4.3: Synthesis of thiophthalide **54**.

4.3.2 Photophysical studies and Hydrogen sulfide sensing

Probe **102** did not show any significant absorbance in the UV-visible absorption spectrum and was nonfluorescent (Φ = 0.003, standard: fluorescein, Φ = 0.85 in 0.1 N NaOH). The selectivity of probe **102** towards H_2S was examined. In each case, probe **102** (10 μM) was treated separately with 100 μM of each analyte (either of NaCl, NaBr, NaI, NaF, Na_2SO_3, Na_2SO_4, $Na_2S_2O_3$, NaSCN, Cys, Hcy, GSH, $BuNH_2$, $NaNO_2$, $NaNO_3$) in HEPES buffer (10 mM, pH = 7.4, 1 mM CTAB) and fluorescence spectra were recorded after 5 min at room temperature. No significant fluorescence enhancement (λ_{ex} = 465 nm) was observed for these analytes (Figure 4.1). Treatment of probe **102** with Na_2S under identical conditions provided strong fluorescence (λ_{em} = 515 nm).

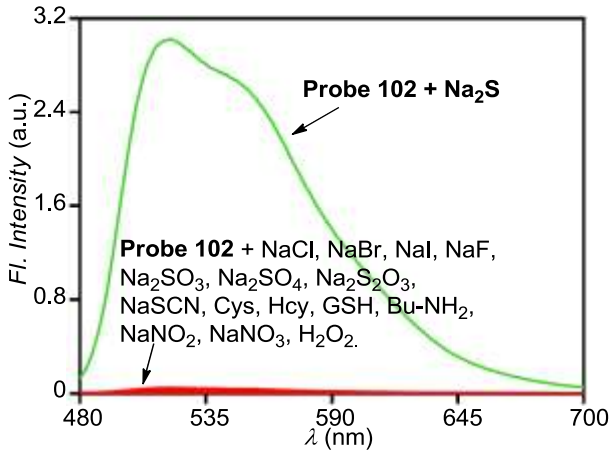

Figure 4.1: Fluorescence spectra recorded by reaction of probe **102** (10μM in 10 mM HEPES buffer, 1 mM CTAB, pH 7.4) with various analytes (100 μM).

When fluorescence intensities at 515 nm were compared, 375-fold enhancement was observed in the case of Na_2S (Figure 4.2A) and the sensing process is also associated with 198-fold enhancement in Φ (from Φ = 0.003 to 0.62). The colorless solution of probe **102**, up on reacting with Na_2S, was changed to a yellow solution which can be confirmed by naked eye detection (Figure 4.2B). For other analytes, no change in color was observed. Fluorescence *turn-On* response by **102** during sensing of H_2S was also confirmed by appearance of green fluorescence (Figure 4.2C) when cuvette images were taken under hand held UV-lamp (λ_{ex} = 365 nm).

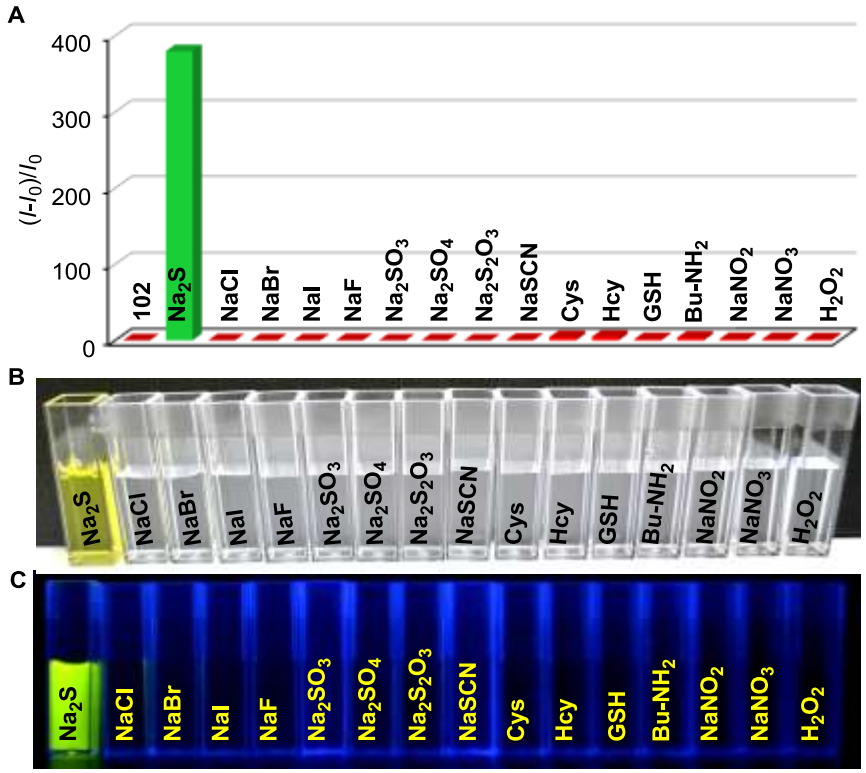

Figure 4.2: Relative fluorescence intensity of probe **102** (10μM in 10 mM HEPES buffer, 1 mM CTAB, pH 7.4) in the presence of various analytes (100 μM). All data (λ_{ex} = 465 nm) were recorded at 5 min after addition of analyte(s) at room temperature with λ_{em} = 515 nm (**A**) and changes in visible and emission color in the presence of various analytes (**B** and **C**).

Reactivity of the probe **102** (10 μM) towards H_2S (100 μM) and other analytes ($BuNH_2$, Cys, GSH and Hcy) were determined by fluorescence emission kinetics in HEPES buffer (10 mM, 1 mM CTAB, pH = 7.4). In each experiment, emission intensity at λ = 515 nm (λ_{ex} = 465 nm) was recorded with time. Addition of $BuNH_2$, Cys, GSH and Hcy to **102** did not indicate formation of fluorescent species during the reaction. Reaction of H_2S with **102** provided a pseudo first order kinetics with rate constant, k = 0.0062 s^{-1} and $t_{1/2}$ = 111 s. (Figure 4.3A).

In order to study the reactivity of probe **102** towards various biologically abundant thiol containing analytes, probe **102** (10 μM) was reacted with 2 mM of each of GSH, Cys and Dithiothreitol (DTT), separately in HEPES buffer (10 mM, 1 mM CTAB, pH 7.4) for 30 min at room temperature. As shown in Figure 4.3B, no significant increment in fluorescence intensity was observed even after 30 min.

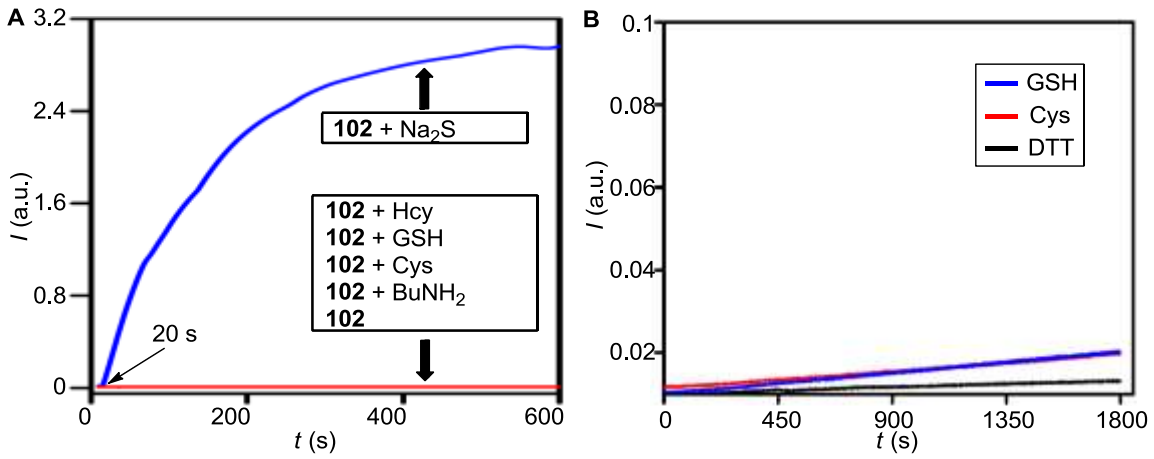

Figure 4.3: (**A**) Fluorescence kinetics plot of **102** (10 μM) in HEPES buffer (10 mM, 1 mM CTAB, pH = 7.4) recorded with time in absence and presence of various analytes (100 μM) (**B**) Fluorescence kinetics plot of **102** (10 μM) in recorded with time in presence of GSH, Cys or DTT (2 mM each) at λ = 515 nm (λ_{ex} = 465 nm).

In the next stage, we examined the quantitative response of **102** towards H_2S by fluorometric titrations. Sharp enhancements in fluorescence (λ_{em} = 515 nm) were observed (Figure 4.4) when titrations were carried out by addition of increasing concentrations of Na_2S (0 to 100 μM) in the probe **102** (10 μM) in HEPES buffer (10 mM, pH = 7.4, 1 mM CTAB).

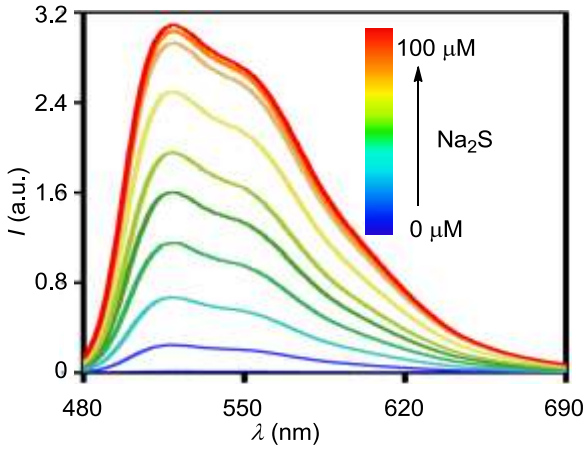

Figure 4.4: Fluorescence spectra of **102** (10 μM) in presence of Na_2S (0, 2, 4, 6, 8, 10, 20, 40, 80 and 100 μM) with λ_{ex} = 465 nm.

When fluorescence intensities at 515 nm were plotted against concentrations of H_2S, excellent linear correlation (Regression factor, R = 0.99666) was observed up to one

equivalent of the H_2S added (Figure 4.5B). A detection limit of 6.4 nM was calculated for the probe **102**, based on signal to noise ratio, *S/N* = 3.

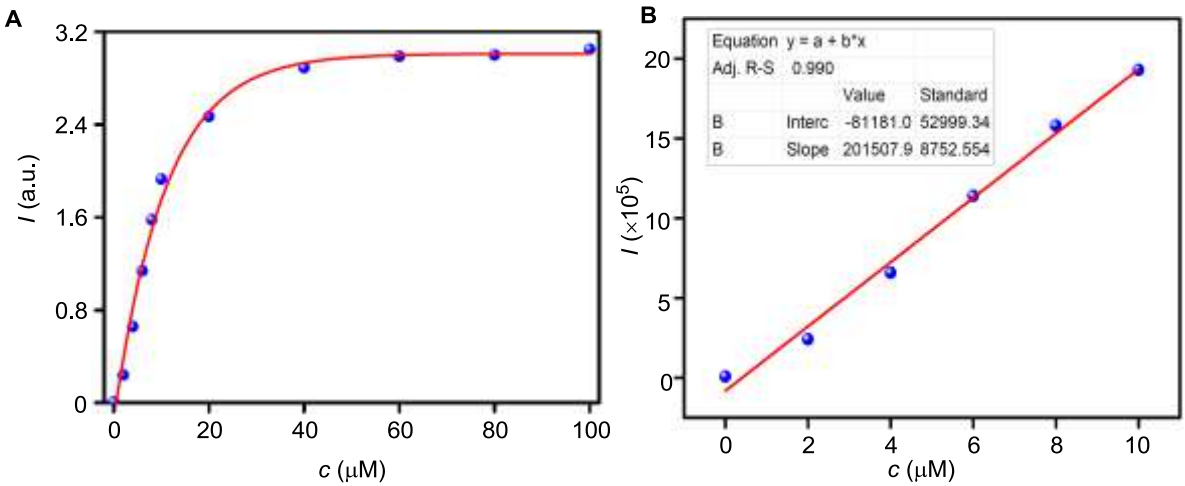

Figure 4.5: (**A**) Fluorescence intensity of **102** (10 μM) at 515 nm (λ_{ex} = 465 nm) in the presence of a Na_2S (0, 2, 4, 6, 8, 10, 20, 40, 80 and 100 μM) recorded in HEPES buffer (10 mM, 1 mM CTAB, pH = 7.4). (**B**) The linearity of the H_2S titration assay of probe **102** (10 μM) in the presence of a Na_2S (2, 4, 6, 8 and 10 μM).

4.3.3 ^{1}H NMR Titration

The nucleophilic substitution-cyclization mechanism was further studied by ^{1}H NMR titration (Figure 4.6) and mass analysis. To a solution of the probe with increasing equivalents of Na_2S, singlet at δ = 3.82 ppm (H_a protons) for probe was disappeared and new singlet at δ = 3.88 ppm ($H_{a'}$ protons), corresponding to fluorescein **10a** was emerged. Similarly, singlet at δ = 4.98 ppm (H_b) for probe **102** decreased and new singlet at δ = 4.52 ppm ($H_{b'}$) corresponding to thiophthalide **54** was appeared.

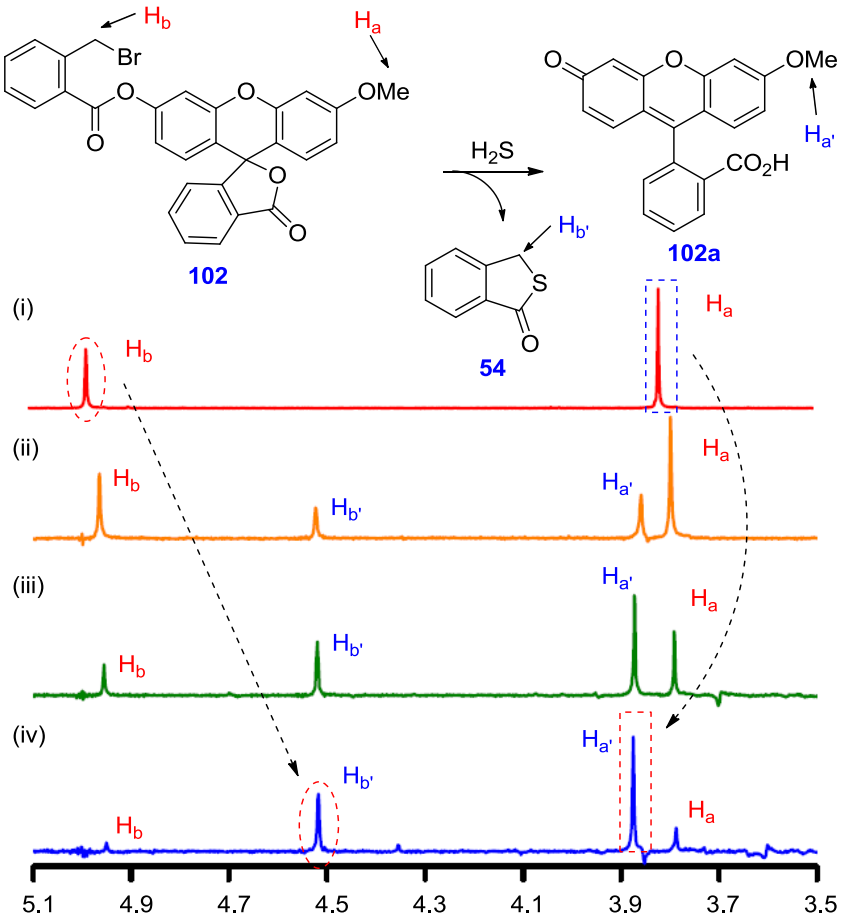

Figure 4.6: ^{1}H NMR spectral change of **102** upon addition of Na_2S. (**i**) **102** only, (**ii**) **102** and 0.4 equiv. Na_2S, (**iii**) **102** and 0.8 equiv. Na_2S and (**iv**) **102** and 2.0 equiv. Na_2S. in CD_3CN at 25 ^{o}C.

Mass (MALDI-TOF) analysis

Probe **102** was reacted with Na_2S in acetonitrile at room temperature for 5 min and mass analysis of reaction mixture was carried out (Figure 4.7). In mass spectrum peaks corresponding to $[M+H]^+$, $[M+Na]^+$, $[M+K]^+$ were observed which confirms the formation of fluorescent compound **102a**.

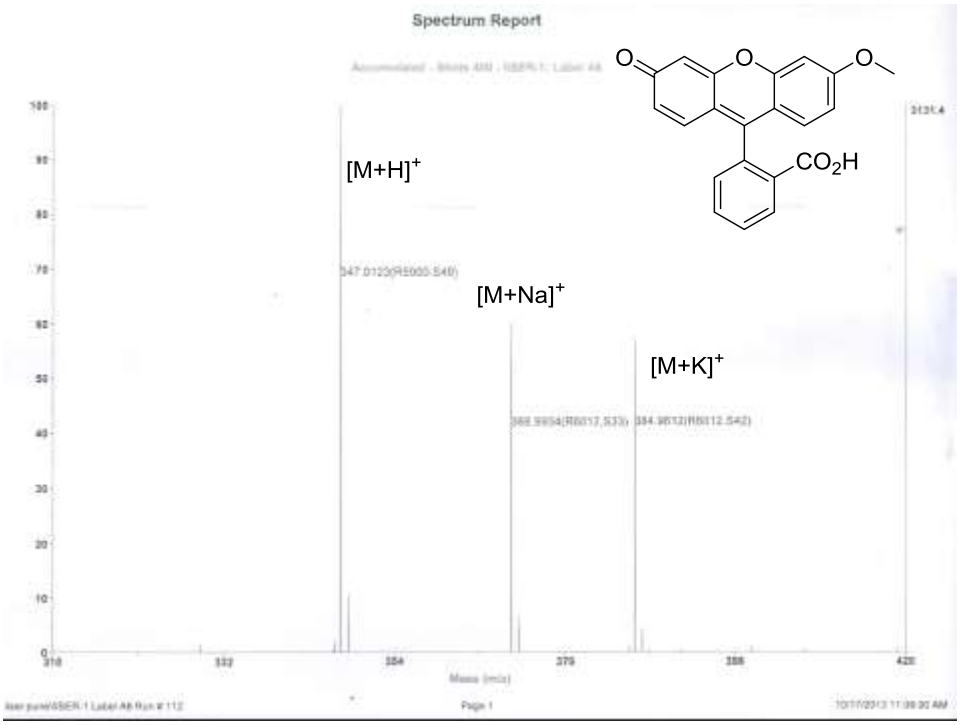

Figure 4.7: MALDI-TOF spectrum of the probe **102** titrated with Na_2S in acetonitrile.

4.3.4 Cell Imaging

No significant fluorescence intensity was observed when HeLa cells were incubated with only probe **102** (10 μM in 1:100 DMSO-DNEM v/v, pH = 7.4) at 37 ^oC for 30 min (Figure 4.8B). Same HeLa cells when incubated with Na_2S (100 μM in 1:100 H_2O-DMEM, 1 mM CTAB pH = 7.4) at 37 ^oC for 30 min, strong fluorescence inside the cells were observed (Figure 4.8E). Images at GFP channel were acquired in each 5 min time interval after the addition of Na_2S (Figure 4.8C-E). Quantitative estimation of fluorescence intensity was done (obtained from cell images taken at different time intervals) by recording the pixel intensity at the selected regions of interest (*ROI*), which shows the gradual increment in fluorescence intensity with time (Figure 4.8F). This data confirms that probe **102** was not consumed by biological thiols *i.e.* GSH and Cys. This observation can be attributed to the difference in pK_a of H_2S (pK_a = 7.0),[11] Cys (pK_a = 8.3) and GSH (pK_a = 9.2).[12] Because of low pK_a, reactivity of H_2S toward probe **102** was higher compared to that of GSH and Cys.

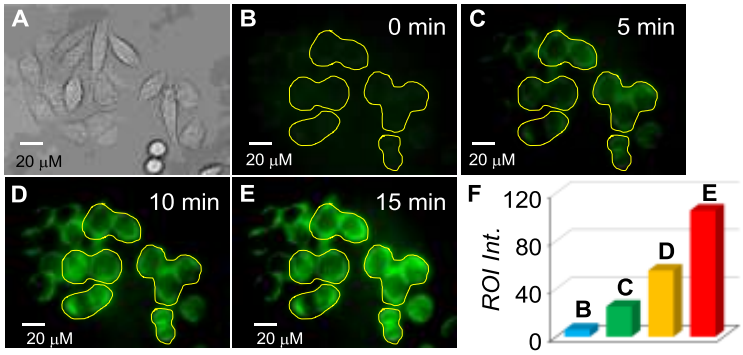

Figure 4.8: Image of HeLa cells: brightfield (**A**), fluorescence (**B-E**). Images were acquired at each 5 min time interval (0, 5, 10, 15 min) after the incubation with Na_2S (100 μM). Bar diagram (**F**) of relative pixel intensities obtained from selected *ROI*s at different time interval images.

4.4 Summary and conclusions

In summary, a cascade reactions based fluorescence *turn-On* probe for rapid, selective and sensitive detection of H_2S was developed. The probe provided 375-fold fluorescence enhancement with response time = 5 min during the detection of H_2S. A detection limit of 6.4 nM was calculated for the probe. The nucleophilic substitution-cyclization based sensing mechanism was monitored by ^1H NMR titrations. An application of the probe in live cell imaging was also demonstrated.

4.5 References

(1) (a) Hannestad, U.; Margheri, S.; Sörbo, B. *Anal. Biochem.* **1989**, *178*, 394; (b) Furne, J.; Saeed, A.; Levitt, M. D. *Am. J. Physiol - Reg. I.* **2008**, *295*, R1479.

(2) (a) Searcy, D. G.; Peterson, M. A. *Anal. Biochem.* **2004**, *324*, 269; (b) Menon, S. K.; Sathyapalan, A.; Agrawal, Y. K. *Rev. Anal. Chem.* **1997**, *16*, 333; (c) Schiavon, G.; Zotti, G.; Toniolo, R.; Bontempelli, G. *Anal. Chem.* **1995**, *67*, 318; (d) Hseu, T.-M.; Rechnitz, G. A. *Anal. Chem.* **1968**, *40*, 1054.

(3) (a) Canterford, D. R. *Anal. Chem.* **1973**, *45*, 2414; (b) Doeller, J. E.; Isbell, T. S.; Benavides, G.; Koenitzer, J.; Patel, H.; Patel, R. P.; Lancaster Jr, J. R.; Darley-Usmar, V. M.; Kraus, D. W. *Anal Biochem.* **2005**, *341*, 40.

(4) Lippert, A. R.; New, E. J.; Chang, C. J. *J. Am. Chem. Soc.* **2011**, *133*, 10078.

(5) Peng, H.; Cheng, Y.; Dai, C.; King, A. L.; Predmore, B. L.; Lefer, D. J.; Wang, B. *Angew. Chem. Int. Ed.* **2011**, *50*, 9672.

(6) (a) Montoya, L. A.; Pluth, M. D. *Chem. Commun.* **2012**, *48*, 4767(b) Das, S. K.; Lim, C. S.; Yang, S. Y.; Han, J. H.; Cho, B. R. *Chem. Commun.* **2012**, *48*, 8395(c) Wan, Q.; Song, Y.; Li, Z.; Gao, X.; Ma, H. *Chem. Commun.* **2013**, *49*, 502(d) Zhou, G.; Wang, H.; Ma, Y.; Chen, X. *Tetrahedron* **2013**, *69*, 867(e) Chen, B.; Li, W.; Lv, C.; Zhao, M.; Jin, H.; Jin, H.; Du, J.; Zhang, L.; Tang, X. *Analyst* **2013**, *138*, 946(f) Yu, C.; Li, X.; Zeng, F.; Zheng, F.; Wu, S. *Chem. Commun.* **2013**, *49*, 403(g) Saha, T.; Kand, D.; Talukdar, P. *Org. Biomol. Chem.* **2013**, *11*, 8166.

(7) Qian, Y.; Karpus, J.; Kabil, O.; Zhang, S.-Y.; Zhu, H.-L.; Banerjee, R.; Zhao, J.; He, C. *Nature Commun.* **2011**, *2*, 1506/1.

(8) (a) Liu, C.; Pan, J.; Li, S.; Zhao, Y.; Wu, L. Y.; Berkman, C. E.; Whorton, A. R.; Xian, M. *Angew. Chem. Int. Ed.* **2011**, *50*, 10327; (b) Liu, C. R.; Peng, B.; Li, S.; Park, C. M.; Whorton, A. R.; Xian, M., *Org. Lett.* **2012**, *14*, 2184.

(9) Whitfield, N. L.; Kreimier, E. L.; Verdial, F. C.; Skovgaard, N.; Olson, K. R. *Am. J. Physiol - Reg. I.* **2008**, *294*, R1930.

(10) Mugherli, L.; Burchak, O. N.; Chatelain, F.; Balakirev, M. Y. *Bioorg. Med. Chem. Lett.* **2006**, *16*, 4488.

(11) Ferguson, S. J.; Lloyd, W. J.; Radda, G. K. *Eur. J. Biochem.* **1975**, *54*, 127.

(12) Iciek, M.; Chwatko, G.; Lorenc-Koci, E.; Bald, E.; Wlodek, L. *Acta Biochim. Pol.* **2004**, *51*, 815.

Chapter 5

Experimental Procedures

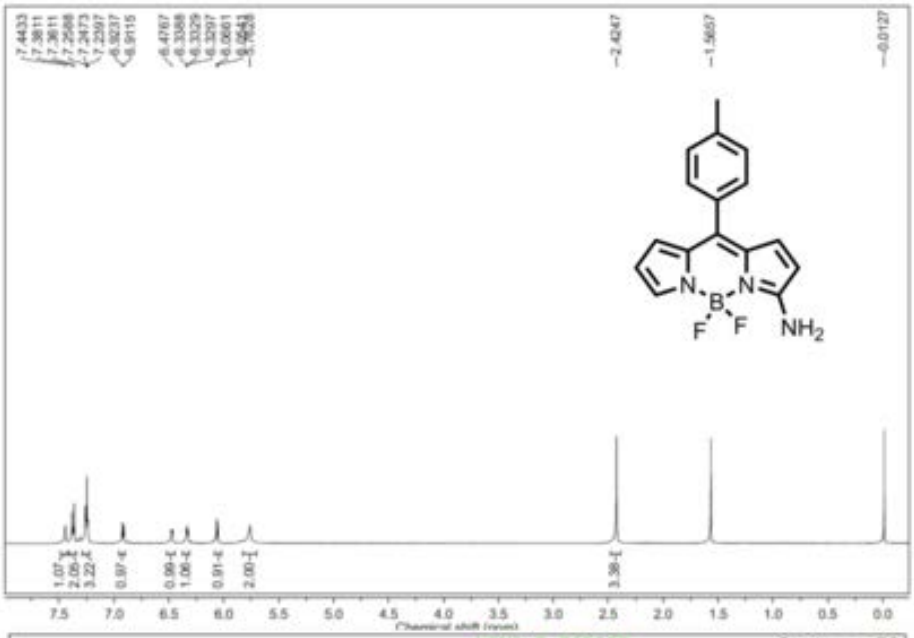

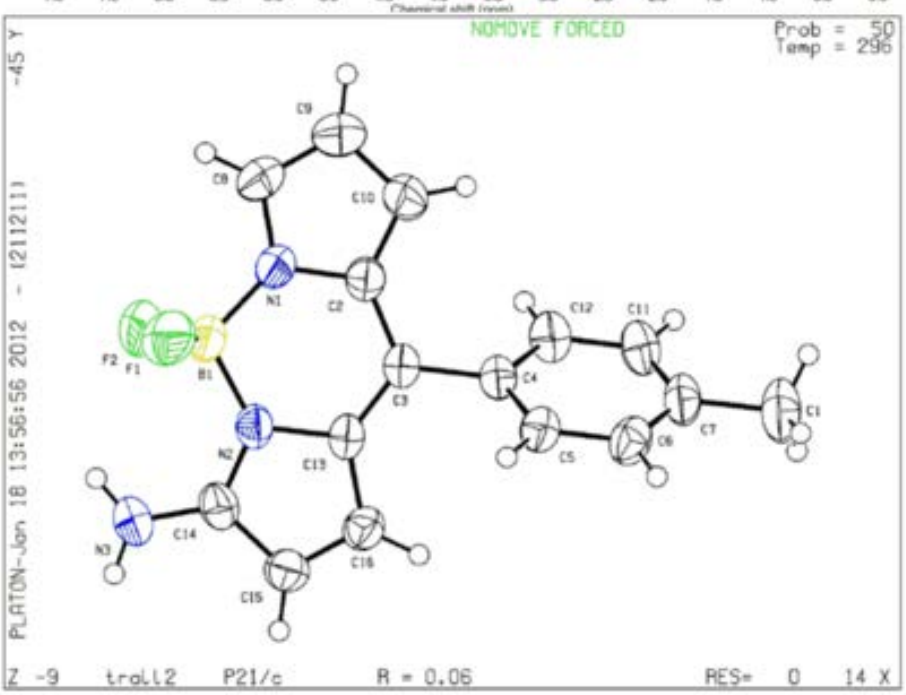

5.1 Methods and materials

5.1.1 General methods

All reactions were conducted under the nitrogen atmosphere. All the chemicals were purchased from commercial sources and used as received unless stated otherwise. Solvents: petroleum ether, chloroform, dichloromethane (CH_2Cl_2), methanol and ethyl acetate (EtOAc) were distilled prior to thin layer and column chromatography. *N*, *N*-Dimethylformamide (DMF), Carbon tetrachloride and dichloromethane (CH_2Cl_2) were pre-dried over calcium hydride and then distilled under vacuum. THF was pre-dried and refluxed over Na (1% w/v) and benzophenone (0.2% w/v) under an inert atmosphere until the blue colour of the benzophenone ketyl radical anion persists and then distilled. Column chromatography was performed on Merck silica gel (100–200 mesh). TLC was carried out with E. Merck silica gel 60-F-$_{254}$ plates.

5.1.2 Physical measurements

^{1}H and ^{13}C spectra were recorded on 400 MHz Jeol ECS-400 (or 100 MHz for ^{13}C) spectrometers using either residual solvent signals as an internal reference or from internal tetramethylsilane on the δ scale ($CDCl_3$ δ H, 7.24 ppm, δ C 77.0 ppm and for DMSO-d_6 δ H, 2.52 ppm, δ C 41.23 ppm). The chemical shifts (δ) are reported in ppm and coupling constants (*J*) in Hz. The following abbreviations are used: m (multiplet), s (singlet), br s (broad singlet), d (doublet), t (triplet) dd (doublet of doublet). Low-resolution mass spectra were recorded on an Applied Biosystems 4800 Plus MALDI TOF/TOF analyzer. High-resolution mass spectra were obtained from MicroMass ESI-TOF MS spectrometer. Absorption spectra were recorded on PerkinElmer, Lambda 45 or Thermo Scientific, Evolution 300 UV-Vis spectrophotometer. Steady State fluorescence experiments were carried out in a micro fluorescence cuvette (Hellma, path length 1.0 cm) on a TCSPC instrument (Horiba Jobin Yvon, Fluorolog-3) or FluoroMax-4 (Horiba JobinYvon) instrument. (FT-IR) spectra were obtained using NICOLET 6700 FT-IR spectrophotometer as KBr disc and reported in cm^{-1}. Melting points were measured using a VEEGO Melting point apparatus. All melting points were measured in open glass capillary and values are uncorrected. Crystal structures were recorded on a Bruker single crystal X-Ray diffractometer. All theoretical calculations (DFT and TDDFT) were carried

out using Gaussian 03 software.[1] Cell images were taken in 35 mm (diameter) dishes. The media (DMEM) and PBS buffer were purchased from commercial sources. Fluorescence images were taken using Olympus Inverted IX81 equipped with Hamamatsu Orca R2 microscope. ChemBio Draw Ultra and Image *J* software were used for drawing structure and for processing cell image respectively.

5.1.3 Live cell imaging

Live-cell imaging studies were carried out by using the human metastatic breast cancer cells, MDA-MB 231 cells (for probes **61**, **62** and **63**), and Human cervical cancer cell line (HeLa) for all other probes. HeLa cells were purchased from National Centre for Cell Science, Pune (India). HeLa cells were grown in DMEM supplemented with 10% heat inactivated fetal bovine serum (FBS), 100 IU/ml penicillin, 100 mg/ml streptomycin and 2 mM L-glutamine. Cultures were maintained in a humidified atmosphere with 5% CO_2 at 37 ^{o}C. The cultured cells were subcultured twice in each week, seeding at a density of about 15×10^3 cells/mL. Typan blue dye exclusion method was used to determine Cell viability. The fluorescence images were taken using Olympus Inverted IX81 equipped with Hamamatsu Orca R2 microscope by exciting at respective wavelengths (by using filters). For measuring the intensity of cell fluorescence quantitatively, images were taken after specified time intervals. Five different region of interest (*ROI*) were selected and the intensity was obtained by using *image j* software. The average intensity of *ROI*s for each image was plotted in bar.

5.1.4 Procedures

Preparation of the medium:

Deionized water was used throughout all experiments. Conjugate addition reactions were carried out either in phosphate saline buffer (PBS) (10 mM, pH 7.4) or in HEPES buffer (10 mM, pH 7.4).

Preparation of the solution of probes:

Stock solutions of probes were prepared in either DMSO or acetonitrile (ACN). The stock solution was then diluted to 3000 µM in respective buffer solution. Final concentration of all probes during each assay was 10 µM with 1% DMSO or ACN (maximum).

Preparation of the solution of amino acids:

Stock solutions of amino acids Gly, Ala, Arg, His, Ser, GSH, Cys and Hcy Stock solutions of NaCl, NaBr, NaI, NaF, Na_2SO_3, Na_2SO_4, $Na_2S_2O_3$, NaSCN, NaOH, $NaNO_2$, $NaNO_3$, H_2O_2 were prepared in deionized water (concentrations 20 mM). Calculated volumes of analytes were added from respective stock solutions to fluorescence each cuvette to provide 100 µM.

UV-visible studies:

UV-visible studies were carried out either in absence or in the presence of different analytes (100 µM) in respective buffer. From UV-visible measurements, ε was calculated using Equation 1:

$$\varepsilon = A/(c \times l) \quad \text{(Eq. 1)}$$

where, A = absorbance, ε = molar extinction coefficient, c = concentration of the solution and l = path length of UV cuvette (l = 1 cm).

Normalization of fluorescence:

Fluorescence studies were carried out either in absence or in the presence of different analytes (100 µM) in respective buffer. Fluorescence emission spectral data were normalized whenever necessary. In fluorescence kinetics experiments emission intensity values at λ_{em} were monitored with respect to time and data was normalized according to the Equation 2:

$$\%\ Emission\ Intensity = [(F^t - F^0)/(F^{30}{}_{Cys} - F^0)] \times 100 \quad \text{(Eq. 2)}$$

where, F^t = Emission intensity at time t, F^0 = Emission intensity of the probe at t = 0, $F^{30}{}_{Cys}$.

Relative emission intensities were calculated according to the Equation 3:

$$Relative\ Emission\ Intensity = F/F_0 \quad \text{(Eq. 3)}$$

where, F = Emission intensity λ_{em} after addition of analyte and F_0 = Emission intensity of the probe at the same wavelength without the addition of any analyte.

Determination of quantum yields:

The quantum yields of probe were determined according to the Equation 4:

$$\Phi_1 \equiv \Phi_B \times \frac{I_1 \times A_B \times \lambda_{exB} \times (\eta_1)^2}{I_B \times A_1 \times \lambda_{ex1} \times (\eta_B)^2} \quad \text{(Eq. 4)}$$

where, Φ is quantum yield; I is integrated area under the corrected emission spectra; A is absorbance at the excitation wavelength; λ_{ex} is the excitation wavelength; η is the refractive index of the solution; the subscripts 1 and B refer to the unknown and the standard, respectively.

Determination of reaction rate (k) and half-life ($t_{1/2}$) for probe:

Reaction rate (k), half-life ($t_{1/2}$) and response time (t_R) for probes were determined by fluorescence kinetics experiments. In fluorescence kinetics experiment, a solution of probe (10 μM) in respective buffer was placed in a fluorescence cuvette and fluorescence intensity at λ_{em} was monitored. At t = 30 s an analyte of interest was added. Rate constant, k for each reaction was calculated according to the Equation 5:

$$Y = a \times [1 - e^{(-kt)}] \quad \text{(Eq. 5)}$$

where, Y = fractional fluorescence intensity, a = arbitrary constant, k = pseudo first order rate constant, t = time.

Half-life of the reaction ($t_{1/2}$) was calculated using Equation 6

$$t_{1/2} = 0.693/k \quad \text{(Eq. 6)}$$

where k = pseudo first order rate constant.

Detection limits

The detection limits were determined based on the fluorescence titrations. In each case probe was employed at 10 μM. The emission intensity of probe was measured without analyte (thiol) by 7-times and the standard deviation of blank measurements was

determined. A linear relationship between the fluorescence intensity and the analyte concentration was obtained. The detection limit (DL) was then calculated with the Equation 7:

$$DL = \frac{3 \times \sigma_{bl}}{m} \qquad \text{(Eq.7)}$$

where, σ_{bl} is the standard deviation of six blank measurements, m is the slope between intensity versus analyte concentration with S/N = 3 (signal-to-noise ratio of 3:1).[2]

5.2 Experimental section

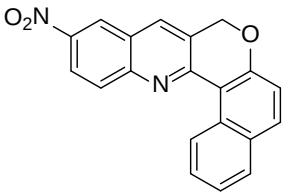

Synthesis of 11-nitro-8H-benzo[5,6]chromeno[4,3-b]quinoline (66): In a 25 ml round bottomed flask placed under nitrogen atmosphere were added 2-(prop-2-ynyloxy)-1-naphthaldehyde **64** (1.0 g, 4.7 mmol), CuCl (139 mg, 1.4 mmol) and dissolved in dry DMF (15 mL). To the mixture was then added *p*-nitroaniline **65** (650 mg, 4.7 mmol) and the reaction mixture was stirred at 100 ^{o}C for 6 h. After completion of the reaction, the reaction mixture was poured on crushed ice and extracted with Ethyl acetate (20 mL x 3). The combined organic layer was washed with water (10 mL x 3), brine (20 mL) and dried over Na_2SO_4. The solvent was removed under reduced pressure to obtain a brown residue which was purified by column chromatography over silica gel (Eluent: 4% EtOAc in petroleum ether) to furnish the pure **61** (328 mg, 21%) as a yellow solid. M.p. = 246 – 247 ^{o}C; IR (KBr): ν_{max}/cm^{-1} 3446, 1619, 1505, 1480, 1331, 1216, 1024; ^{1}H NMR (400 MHz, $CDCl_3$): δ 9.83 (d, *J* = 8.7 Hz, 1H), 8.72 (d, *J* = 2.3 Hz, 1H), 8.44 (dd, *J* = 9.2, 2.8 Hz, 1H), 8.28 (d, *J* = 9.2 Hz, 1H), 8.07 (s, 1H), 7.90 (d, *J* = 9.2 Hz, 1H), 7.84 (d, *J* = 8.2 Hz, 1H), 7.72 – 7.67 (m, 1H), 7.51 – 7.47 (m, 1H), 7.22 (d, *J* =8.6 Hz, 1H), 5.33 (s, 2H); ^{13}C NMR (100 MHz, $CDCl_3$): δ 158.9, 154.2, 150.2, 145.0, 134.7, 132.2, 131.2, 131.0, 130.7, 128.7, 128.4, 126.9, 125.4, 124.9, 124.0, 123.0, 118.3, 115.4, 68.6; HRMS (ESI): Calc. for $C_{20}H_{13}N_2O_3$ $[M+H]^+$: 329.0926; Found: 329.0925.

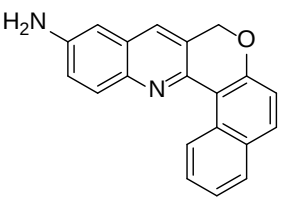

Synthesis of 8H-benzo[5,6]chromeno[4,3-b]quinolin-11-amine (67): In a 50 ml round bottomed flask placed under nitrogen atmosphere were added compound **66** (650 mg, 1.98 mmol) and dissolved in 30 mL methanol/CH_2Cl_2 (1:3). To the solution was

added 10% Pd/C (10% weight of **66**) and the atmosphere was replaced with hydrogen and reaction was carried out at room temperature for 5 h under the ambient hydrogen pressure (balloon). The reaction mixture was filtered using a celite cake and the filtrate was removed under reduced pressure to give a brown residue which was subjected to column chromatography over silica gel (Eluent: 2% Methanol in chloroform) to furnish pure products **67** (400 mg, 68%) as a yellow solid. M.p. = 150 ^{o}C (decomposed); IR (KBr): ν_{max}/cm^{-1} 3421, 2924, 2852, 1560, 1498, 1376, 1225, 1025,1007; ^{1}H NMR (400 MHz, $CDCl_3$): δ 9.95 (d, *J* = 8.68 Hz, 1H); 8.05 (d, *J* = 9.16 Hz, 1H), 7.84 (d, *J* = 7.8 Hz, 1H), 7.83 (d, *J* = 8.72 Hz, 1H), 7.69 – 7.66 (m, 2H), 7.48 – 7.44 (m, 1H), 7.24 (d, *J* = 9.16 Hz, 1H), 7.17 – 7.13 (m, 1H), 6.89 – 6.86 (m, 1H), 5.24 (s, 2H), 4.01 (br s, 2H); ^{13}C NMR (100 MHz, $CDCl_3$); δ 157.03, 147.45, 144.72, 143.15, 132.15, 131.29, 130.90, 130.84, 128.75, 128.44, 128.31, 127.73, 127.24, 127.20, 124.43, 121.39, 118.38, 116.65, 107.47, 68.90; LRMS (MALDI): 337 $[M+K]^+$. HRMS (ESI): Calc. for $C_{20}H_{15}N_2O$ $[M+H]^+$: 299.1184; Found: 299.1171.

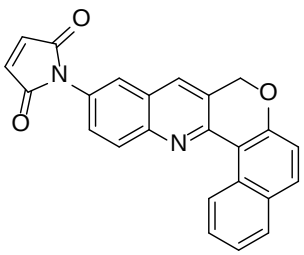

Synthesis of 1-(8H-benzo[5,6]chromeno[4,3-b]quinolin-11-yl)-1H-pyrrole-2,5-dione (61): Amine **67** (50 mg, 0.16 mmol) and maleic anhydride (25 mg, 0.24 mmol) were placed in a dry 50 mL round bottom flask. Dichloromethane (4 mL) was added and the solution was stirred at rt for 3 h. The mixture was then filtered and the recovered solid was rinsed liberally with dichloromethane and then dried under vacuum. To this solid was added acetic anhydride (4 mL) and catalytic sodium acetate (5 mg) and the reaction was stirred vigorously for another 1h. The mixture was then cooled to 4 ^{o}C for 3 h and filtered. The beige solid thus obtained was dried over vacuum to give compound **61** as a yellow solid with 36% yield (25 mg). M.p. = 228 – 229 ^{o}C; IR (KBr): ν_{max}/cm^{-1} 3446, 2924, 1495, 1400, 1370, 1225, 1046; ^{1}H NMR (400 MHz, $CDCl_3$): δ 9.90 (d, *J* = 8.68 Hz, 1H); 8.30 (d, *J* = 9.16 Hz, 1H), 7.95 (s, 1H), 7.87 – 7.81 (m, 3H), 7.73 – 7.66 (m, 2H), 7.48 – 7.44 (m, 1H), 7.22 (d, *J* = 8.72 Hz, 1H), 6.91 (s, 2H), 5.30 (s, 2H); ^{13}C NMR (100 MHz, $CDCl_3$): δ 169.5, 158.1, 151.6, 146.9, 134.4, 133.5, 131.3, 130.9, 130.8, 130.7, 129.1, 128.6, 128.1, 127.5, 127.1, 126.6, 124.7, 123.9, 118.4, 116.0, 68.8; LRMS (MALDI): 379 $[M+H]^+$; HRMS (ESI): Calc. for $C_{24}H_{15}N_2O_3$ $[M+H]^+$: 379.1082; Found: 379.1033.

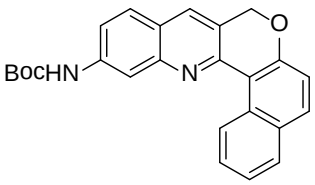

Synthesis of tert-butyl 8H-benzo [5,6]chromeno[4,3-b]quinolin-13-ylcarbamate (69): In a 25 ml round bottomed flask placed under nitrogen atmosphere were added 2-(prop-2-ynyloxy)-1-naphthaldehyde **64** (200 mg, 0.95 mmol), CuCl (38 mg, 0.38 mmol) and dissolved in dry DMF (6 mL). Aryl amine **68** (200 mg, 0.95 mmol) was then added and the reaction mixture was stirred at 110 ^{o}C for 3 h under inert atmosphere. After completion, the reaction mixture was poured on crushed ice and extracted with Ethyl acetate (20 mL x 3). The combined organic layer was washed with water (10 mL x 2), brine (20 mL) and dried over Na_2SO_4. The solvent was removed under reduced pressure to give a brown residue which was subjected to column chromatography over silica gel (Eluent: 7 % EtOAc in petroleum ether to furnish pure **69** (190 mg, 50%) as a yellow solid. M.p. = 184-185^{o}C ; IR (KBr): γ_{max}/cm^{-1} 3464, 1711, 1577, 1511, 1477, 1433, 1421, 1247, 1156, 1010; ^{1}H NMR (400 MHz, $CDCl_3$): δ 9.72 (d, *J* = 8.72 Hz, 1H), 9.10 (s, 1H), 8.38 (d, *J* = 7.6 Hz, 1H), 7.92 (s, 1H), 7.86(d, *J* = 8.4 Hz, 2H), 7.65 – 7.63 (m, 1H), 7.50 – 7.45 (m, 2H), 7.41 – 7.38 (m, 1H), 7.23 (d, *J* = 8.4 Hz, 1H), 5.31 (s, 2H), 1.60 (s, 9H), ^{13}C NMR (100 MHz, $CDCl_3$): δ 157.89, 152.97, 148.50, 137.93, 135.33, 133.22, 131.35, 131.10, 130.74, 128.75, 127.60, 127.25, 126.82, 126.62, 124.69, 119.82, 118.49, 116.04, 114.68, 80.37, 68.73, 28.50; LRMS (MALDI): Calc. for $C_{25}H_{22}KN_2O_3$ $[M+K]^+$: 437.1267; Found: 437.2028; HRMS (ESI): Calc. for $C_{25}H_{23}N_2O_3$ $[M+H]^+$: 399.1709; Found: 399.1693.

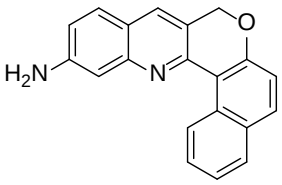

Synthesis of 8H-benzo [5, 6] chromeno [4, 3-b] quinolin-13-amine (70): In a 25 mL round bottomed flask placed under nitrogen atmosphere was added compound **69** (300 mg, 0.75 mmol) and dissolved in methanol (10 mL). To the resulting solution was added conc. HCl (36% solution, 5.0 mL) and stirred at room temperature for 5 h. After completion, methanol was evaporated under reduced pressure and the aqueous solution was quenched with saturated aqueous $NaHCO_3$ solution (pH = 10). The aq. layer was extracted with EtOAc (15 mL x 3). The combined organic layers were dried over Na_2SO_4. The solvent was removed under reduced pressure to afford **70** (189 mg, 84%) as yellow oil. The crude product was pure enough to use for the next reaction without any purification. IR (KBr): γ_{max}/cm^{-1} 3467, 3372, 1578, 1508, 1435, 1375, 1223, 1043, 1009; 3370, 3275, 1610, 1508, 1328, 1211, 1091; ^{1}H NMR (400 MHz, $CDCl_3$): δ 9.84 (d, *J* =

8.72 Hz, 1H), 7.85 – 7.82 (m, 3H), 7.67 – 7.63 (m, 1H), 7.47 – 7.44 (m, 1H), 7.32 – 7.28 (m, 1H), 7.23 (d, *J* = 8.72 Hz, 1H), 7.14 (d, *J* = 8.24 Hz, 1H), 6.95 (d, *J* = 7.76 Hz, 1H), 5.27 (s, 2H), 5.0 (br s, 2H); ^{13}C NMR (100 MHz, $CDCl_3$): δ 157.57, 147.90, 144.28, 138.06, 132.66, 131.09, 130.76, 128.64, 127.71, 127.38, 126.87, 126.85, 124.47, 118.51, 116.62, 115.85, 110.45; LRMS (MALDI): Calc. for $C_{20}H_{15}N_2O$ $[M+H]^+$: 299.1184; Found: 299.2033; HRMS (ESI): Calc. for $C_{20}H_{15}N_2O$ $[M+H]^+$: 299.1184; Found: 299.1171

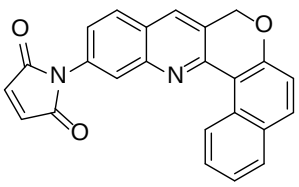

Synthesis of 1-(8H-benzo [5, 6] chromeno [4, 3-b] quinolin-13-yl)-1H-pyrrole-2, 5-dione (62): Amine **70** (200 mg, 0.67 mmol) and maleic anhydride (66 mg, 0.67 mmol) were placed in a dry 50-mL round bottom flask. Dichloromethane (4 mL) was added and the solution was stirred at rt for 3 h. The mixture was then filtered and the recovered solid was rinsed liberally with dichloromethane and then dried under vacuum. To this solid was added acetic anhydride (8 mL) and catalytic sodium acetate (5 mg) and the reaction was stirred vigorously for another 3 h. The mixture was then cooled to 4 ^{o}C for 3 h and filtered. The beige solid thus obtained was dried over vacuum to give compound **62** (94 mg, 37%) as a yellow solid. M.p. = 226 – 227 ^{o}C; IR (KBr): γ_{max}/cm^{-1} 3464, 1711, 1577, 1511, 1477, 1433, 1421, 1247, 1156, 1010; ^{1}H NMR (400 MHz, $CDCl_3$): δ 9.47 – 9.44 (m, 1H), 7.99 (s, 1H), 7.98 – 7.88 (m, 1H), 7.83 (d, *J* = 8.72 Hz, 1H), 7.79-7.76 (m, 1H), 7.68 (dd, *J* = 1.32 Hz, 1.4 Hz, 1H), 7.58 (t, *J* = 7.8 Hz, 1H), 7.42 – 7.39 (m, 2H), 7.18 (d, *J* = 8.72 Hz, 1H), 6.99 (s, *2*H), 5.27 (s, 2H); ^{13}C NMR (100 MHz, $CDCl_3$): δ 170.58, 158.28, 151.40, 144.03, 134.85, 133.58, 131.25, 131.18, 130.64, 129.23, 128.40, 127.51, 127.45, 125.88, 124.46, 118.42, 116.07, 68.68; LRMS (MALDI): Calc. for $C_{24}H_{15}N_2O_3$ $[M+H]^+$: 379.1082; Found: 379.2017; HRMS (ESI): Calc. for $C_{24}H_{15}N_2O_3$ $[M+H]^+$: 379.1082; Found: 379.1033

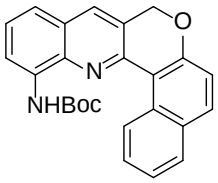

Synthesis of tert-butyl 8H-benzo [5, 6] chromeno [4, 3-b] quinolin-12-ylcarbamate (72): In a 25 ml round bottomed flask placed under nitrogen atmosphere were added 2-(prop-2-ynyloxy)-1-naphthaldehyde **64** (1.0 g, 4.7 mmol), CuCl (23 mg, 2.37 mmol) and dissolved in dry DMF (10 mL). Aryl amine **71** (1.0 g, 4.7 mmol) was then added and the reaction mixture was stirred at 100 ^{o}C for 2 h under inert atmosphere. After completion, the reaction

mixture was poured on crushed ice and extracted with Ethyl acetate (20 mL x 3). The combined organic layer was washed with water (10 mL x 2), brine (20 mL) and dried over Na_2SO_4. The solvent was removed under reduced pressure to give a brown residue which was subjected to column chromatography over silica gel (Eluent: 15% EtOAc in petroleum ether to furnish pure **72** (398 mg, 21%) as a yellow solid. M.p. = 175 – 176 ^oC; IR (KBr): γ_{max}/cm^{-1} 3376, 2969, 2853, 1722, 1616, 1522, 1370, 1230, 1018; ^1H NMR (400 MHz, $CDCl_3$): δ 9.95 (d, *J* = 8.72 Hz, 1H), 8.14 (d, *J* = 1.8 Hz, 1H), 7.92 – 7.79 (m, 3H), 7.76 – 7.59 (m, 3H), 7.52– 7.42 (m, 1H), 7.22 (d, *J* = 8.9 Hz, 1H), 6.79 (br s, 1H), 5.27 (s, 2H), 1.57 (s, 9H); ^{13}C NMR (100 MHz, $CDCl_3$): δ 157.73; 152.57, 151.28, 148.72, 139.40, 132.98, 131.31, 130.65, 130.41, 128.32, 127.93, 127.90, 127.25, 125.23, 124.44, 122.98, 119.25, 118.26, 116.22, 115.88, 80.73, 68.80, 28.34; HRMS (ESI): Calc. for $C_{25}H_{22}N_2O_3$ $[M+H]^+$: 399.1709; Found: 399.1714.

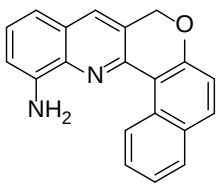

Synthesis of 8H-benzo [5, 6] chromeno [4, 3-b] quinolin-12-amine (73): In a 25 ml round bottomed flask placed under nitrogen atmosphere were added compound **72** (400 mg, 1.0 mmol), CH_2Cl_2 (4 mL) and trifluoroacetic acid (4 mL). The reaction mixture was stirred at rt for 6 h under inert atmosphere. After completion, the reaction mixture was evaporated under reduced pressure and basified with saturated $NaHCO_3$ solution and extracted with Ethyl acetate (20 mL x 3). The combined organic layer was washed with water (10 mL x 2), brine (20 mL) and dried over Na_2SO_4. The solvent was removed under reduced pressure to give **73** (300 mg, 90%) as a brown residue which was used for next reaction without any purification. M.p. = 102 ^oC (decomposed); IR (KBr): γ_{max}/cm^{-1} 3366, 2923, 2852, 2355, 1722, 1617, 1506, 1444,1370, 1223, 1149, 1009; ^1H NMR (400 MHz, $CDCl_3$): δ 9.91 (d, *J* = 8.72 Hz, 1H), 7.83–7.77 (m, 3H), 7.66 – 7.62 (m, 1H), 7.60 (d, *J* = 8.68 Hz, 1H), 7.46 – 7.42 (m, 1H), 7.36 (d, *J* = 2.28 Hz, 1H), 7.21 (d, *J* = 8.72 Hz, 1H), 6.95 (dd, *J* =2.28, 8.68 Hz, 1H), 5.23 (s, 2H), 4.20 (br s, 2H); ^{13}C NMR (100 MHz, $CDCl_3$): δ 157.57, 150.96, 149.70. 147.58, 132.63, 131.34, 130.66, 130.61, 128.34, 128.31, 127.66, 127.19, 124.31, 123.29, 120.58, 118.29, 118.23, 116.52, 109.93, 68.89; HRMS (ESI): Calc. for $C_{20}H_{14}N_2O$ $[M+H]^+$: 299.1184; Found: 299.1184.

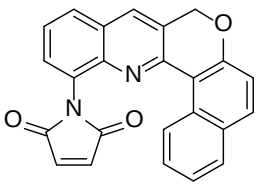

Synthesis of 1-(8H-benzo [5, 6] chromeno [4, 3-b] quinolin-12-yl)-1H-pyrrole-2,5-dione (63): Amine **73** (200 mg, 0.67 mmol) and

maleic anhydride (66 mg, 0.67 mmol) were placed in a dry 50-mL round bottom flask. Dichloromethane (4 mL) was added and the solution was stirred at rt for 14h. The mixture was then filtered and the recovered solid was rinsed liberally with dichloromethane and then dried under vacuum. To this solid was added acetic anhydride (8 mL) and catalytic sodium acetate (5 mg) and the reaction was stirred vigorously for another 12h. The mixture was then cooled to 4 ^{o}C for 3 h and filtered. The beige solid thus obtained was dried over vacuum to give compound **63** in 32% yield (81 mg) as a yellow solid. M.p. = 215 – 216 ^{o}C; IR (KBr): γ_{max}/cm^{-1} 3447, 1716, 1577, 1427, 1139, 1012; ^{1}H NMR (400 MHz, $CDCl_3$): δ 9.92 (d, *J* = 8.68 Hz, 1H); 8.23 (s, 1H), 7.94 (s, 1H), 7.87 (d, *J* = 3.68 Hz, 1H), 7.84 (d, *J* = 3.68 Hz, 1H), 7.82 (d, *J* = 7.8 Hz, 1H), 7.66 (t, *J* = 7.6 Hz, 1H), 7.52 (dd, *J* = 1.84, 8.72 Hz, 1H), 7.45 (t, *J* = 7.6 Hz, 1H), 7.21 (d, *J* = 9.16 Hz, 1H), 6.90 (s, *2*H), 5.29 (s, 2H); ^{13}C NMR (100 MHz, $CDCl_3$): δ 169.44, 158.10, 151.71, 148.02, 134.47, 133.52, 132.06, 131.34, 130.75, 130.58, 128.51, 128.20, 127.21, 126.53, 125.91, 124.70, 118.37, 115.98, 68.80; LRMS (MALDI): Calc. for $C_{25}H_{23}N_2O_3$ $[M+H]^+$: 399.1709; Found: 399.1714; HRMS (ESI): Calc. for $C_{25}H_{23}N_2O_3$ $[M+H]^+$: 399.1709; Found: 399.1693.

Synthesis of (R)-methyl 2-((tert-butoxycarbonyl)amino)-3-((7-nitrobenzo[c][1,2,5]oxadiazol-4-yl)thio)propanoate (76):

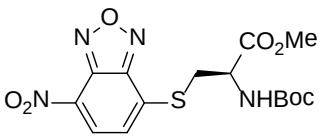

To a 25 mL round bottom flask containing a solution of **75** (100 mg, 0.50 mmol) in acetonitrile (6 mL) were added potassium carbonate (70 mg, 0.50 mmol) and *N*-(tert-butoxycarbonyl)-L-*cysteine methyl ester* (118 mg, 0.7 mL, 5.01 mmol) at room temperature. After stirring at room temperature for 3 h, the reaction mixture was evaporated under reduced pressure. H_2O (5 mL) was added to the residue and aqueous layer was extracted with EtOAc (2 x 10 mL). The combined organic layer was washed with brine, dried over Na_2SO_4 and concentrated to afford a residue, which was chromatographed over silica gel (*Eluent*: 40% EtOAc in petroleum ether) to afford compound **76** (159 mg, 80%) as yellow solid. M.p. = 146 – 147 ^{o}C; IR (KBr): ν_{max}/cm^{-1} 3365, 2925, 1745, 1691, 1528, 1384, 1334, 1165, 1053; ^{1}H NMR (400 MHz, $CDCl_3$): δ 8.39 (d, *J* = 7.9 Hz, 1H), 7.42 (d, *J* = 7.9 Hz, 1H), 5.37 (d, *J* = 6.8 Hz, 1H), 4.72 (d, *J* = 6.3 Hz, 1H), 3.85 (dd, *J* = 14.0, 5.2 Hz, 1H), 3.78 (s, 3H), 3.67 (dd, *J* = 14.0, 5.2 Hz, 2H), 1.41 (s, 9H); ^{13}C NMR (100 MHz, $CDCl_3$): δ 170.2, 155.1, 149.4, 142.5, 139.7, 133.4,

130.7, 122.2, 81.1, 53.3, 52.9, 34.1, 28.3; HRMS (ESI): Calc. for $C_{15}H_{18}N_4NaO_7S$ $[M+Na]^+$: 421.0794; Found: 421.0792.

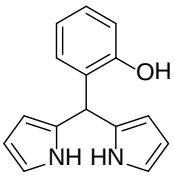

Synthesis of 2-(di(1H-pyrrol-2-yl)methyl)phenol (83): In a 1000 mL round bottom flask Salicylaldehyde **82** (2.0 g, 16.4 mmol) and Pyrrole (5.7 mL, 82 mmol) were dissolved in 500 mL CH_2Cl_2. To this solution, catalytic (2-3 drops) TFA was added and the reaction mixture was stirred at room temperature for 10 h. After completion of the reaction, solvent was removed under reduced pressure to obtain a residue which was purified by column chromatography over silica gel (Eluent: 25 % EtOAc in petroleum ether) to furnish the pure **83** (2.5 g, 64 %) as gray solid. M.p.: 117 – 118 ^oC; IR (KBr): ν/cm^{-1} 3427, 3393, 1635, 1559, 1501, 1454, 1384, 1280, 1257, 1200, 1189, 1171, 1118, 1085; ^1H NMR (400 MHz, $CDCl_3$): δ 8.17 (s, 2H), 7.18 (td, *J* = 7.8, 1.7 Hz, 1H), 7.07 (dd, *J* = 7.6, 1.6 Hz, 1H), 6.90 (td, *J* = 7.4, 0.9 Hz, 1H), 6.88 – 6.84 (m, 1H), 6.71 (dd, *J* = 4.1, 2.5 Hz, 2H), 6.15 (dd, *J* = 5.8, 2.9 Hz, 2H), 6.05 – 5.95 (m, 2H), 5.54 (s, 1H), 5.18 (s, 1H); ^{13}C NMR (100 MHz, $CDCl_3$): δ 153.7, 131.1, 130.2, 128.8, 128.5, 121.6, 118.1, 117.6, 108.6, 107.1, 40.3; HRMS (ESI): Calc. for $C_{15}H_{15}N_2O^+$ $[M+H]^+$: 239.1184; Found: 239.1173.

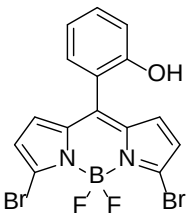

Synthesis of 3,7-dibromo-5,5-difluoro-10-(2-hydroxyphenyl)-5H-dipyrrolo[1,2-c:2',1'-f][1,3,2]diazaborinin-4-ium-5-uide (84): In a 100 mL round bottom flask Dipyrromethane **83** (500 mg, 2.1 mmol) was dissolved in 40 mL dry THF and cooled to -78 ^oC. To this solution N-bromosuccinimide (781 mg, 4.2 mmol) was added and the reaction mixture was stirred at -78 ^oC for 2 h. To this reaction mixture 2,3-Dichloro-5,6-Dicyanobenzoquinone (DDQ) was added at room temperature and stirred at room temperature for 2 h. THF was evaporated under reduced pressure and residue obtained was dissolved in CH_2Cl_2 and filtered through silica column using CH_2Cl_2 Eluent was evaporated to reduce the volume to 100 mL. To this Et_3N (6.13 mL, 44.0 mmol) and $BF_3 \bullet Et_2O$ (5.5 mL, 44.0 mmol) were added at room temperature and stirred for 3 h. After completion of the reaction, the reaction mixture was diluted with H_2O and CH_2Cl_2 layer was separated. The aqueous layer was extracted with CH_2Cl_2 (20 mL × 3). The combined organic layer was washed with water (20 mL × 1), brine (20 mL) and dried over Na_2SO_4. The solvent was removed under reduced pressure to obtain a brown residue which was

purified by column chromatography over silica gel (Eluent: 20 % EtOAc in petroleum ether) to furnish the pure **84** (555 mg, 60 %) as brown solid. M.p.: 190 – 192 ^{o}C; IR (KBr): ν/cm^{-1} 3491, 1610, 1553, 1449, 1409, 1384, 1308, 1255, 1183, 1093; ^{1}H NMR (400 MHz, $CDCl_3$): δ 7.47 – 7.35 (m, 1H), 7.20 (d, *J* = 7.6 Hz, 1H), 7.04 – 6.98 (m, 2H), 6.76 (d, *J* = 4.2 Hz, 2H), 6.49 (d, *J* = 4.2 Hz, 2H), 5.25 (s, 1H); ^{13}C NMR (100 MHz, $CDCl_3$): δ 153.5, 138.6, 135.9, 133.3, 132.2, 131.7, 131.6, 123.1, 120.6, 118.8, 117.0; HRMS (ESI): Calc. for $C_{15}H_9BBr_2FN_2O^+$ $[M-F]^+$: 422.9138; Found: 422.9139.

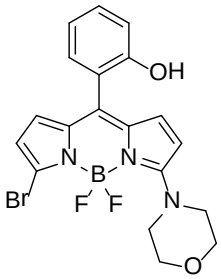

Synthesis of 7-bromo-5,5-difluoro-10-(2-hydroxyphenyl)-3-morpholino-5H-dipyrrolo[1,2-c:2',1'-f][1,3,2]diazaborinin-4-ium-5-uide (85): In a 25 mL round bottomed flask were added compound **84** (100 mg, 0.23 mmol), Et_3N (80 µL, 0.58 mmol) and morpholine (20 µL, 0.23 mmol) dissolved in CH_3CN (8 mL). The reaction mixture was stirred at room temperature for 6 h. After completion of the reaction, the reaction mixture was evaporated under reduced pressure to remove CH_3CN to obtain residue which was purified by column chromatography over silica gel (Eluent: 1 % methanol in chloroform) to furnish the pure **85** (80 mg, 80%) as brown solid. M.p.: 185 – 186 ^{o}C (decomposed); IR (KBr): ν/cm^{-1} 3436, 1654, 1561, 1504, 1449, 1384, 1289, 1103, 1061; ^{1}H NMR (400 MHz, CD_3OD): δ 7.87 (s, 1H), 7.27 (td, *J* = 7.9, 1.7 Hz, 1H), 7.14 (dd, *J* = 7.8, 1.6 Hz, 1H), 6.88 (d, *J* = 7.8 Hz, 2H), 6.79 (d, *J* = 5.3 Hz, 1H), 6.54 (d, *J* = 5.2 Hz, 1H), 6.18 (d, *J* = 3.7 Hz, 1H), 6.04 (d, *J* = 3.7 Hz, 1H), 4.07 – 3.93 (m, 4H), 3.90 – 3.70 (m, 4H); ^{13}C NMR (100 MHz, DMSO-d_6): δ 162.4, 155.9, 136.1, 136.0, 133.1, 132.2, 130.7, 125.7, 120.9, 119.2, 117.3, 117.0, 116.4, 116.4, 111.8, 66.7, 51.1; HRMS (ESI): Calc. for $C_{19}H_{18}BBrF_2N_3O_2^+$ $[M+H]^+$: 447.0565; Found: 447.0592.

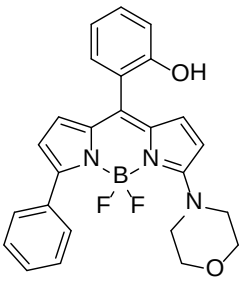

Synthesis of 5,5-difluoro-10-(2-hydroxyphenyl)-3-morpholino-7-phenyl-5H-dipyrrolo[1,2-c:2',1'-f][1,3,2]diazaborinin-4-ium-5-uide (86): In a 100 mL round bottomed flask compound **85** (350 mg, 0.78 mmol) was dissolved in 1:1 mixture of 1M Na_2CO_3/ Toluene (40 mL) and degassed with N_2 gas. To this solution phenylboronic acid (95 mg, 0.78 mmol) and Tetrakis (triphenylphosphine) palladium (91 mg, 0.08 mmol) were added at room temperature. The reaction mixture was refluxed for 12 h. After completion of the reaction, the reaction mixture was partitioned

between ethyl acetate and water. The aqueous layer was extracted with ethyl acetate (20 mL × 3). The combined organic layer was washed with water (20 mL × 1), brine (20 mL) and dried over Na_2SO_4. The solvent was removed under reduced pressure to obtain a brown residue which was purified by column chromatography over silica gel (Eluent: 25 % EtOAc in petroleum ether) to furnish the pure **86** (275 mg, 79%) as dark brown solid. M.p.: 204 – 206 ^oC; IR (KBr): ν/cm^{-1} 3452, 2926, 2851, 1577, 1561, 1451, 1384, 1299, 1267, 1167, 1121, 1049; ^1H NMR (400 MHz, $CDCl_3$): δ 7.83 – 7.67 (m, 2H), 7.45 – 7.29 (m, 4H), 7.26 – 7.22 (m, 1H), 7.00 (td, *J* = 8.4, 4.2 Hz, 2H), 6.82 (d, *J* = 5.1 Hz, 1H), 6.41 (dd, *J* = 12.3, 3.9 Hz, 2H), 6.23 (d, *J* = 5.2 Hz, 1H), 5.27 (s, 1H), 3.94 – 3.85 (m, 4H), 3.84 – 3.70 (m, 4H); ^{13}C NMR (100 MHz, DMSO-d_6): δ 162.0, 155.9, 145.6, 135.4, 135.2, 133.9, 132.2, 130.6, 129.1, 128.4, 127.7, 127.7, 121.7, 119.1, 118.6, 116.4, 115.9, 115.8, 66.7, 50.9; HRMS (ESI): Calc. for $C_{25}H_{23}BF_2N_3O_2^+$ $[M+H]^+$: 446.1851; Found: 446.1843.

Synthesis of 10-(2-(((2,4-dinitrophenyl)sulfonyl)oxy)phenyl)-5,5-difluoro-3-morpholino-7-phenyl-5H-dipyrrolo[1,2-c:2',1'-f][1,3,2]diazaborinin-4-ium-5-uide (81): In a 25 mL round bottomed flask compound **86** (100 mg, 0.22 mmol) was dissolved in CH_2Cl_2 (5 mL) and cooled to -78 ^oC. To this solution Et_3N (35 µL, 0.25 mmol) and 2, 4-dinitrobenzenesulfonyl chloride (67 mg, 0.25 mmol) were added and the reaction mixture was stirred at room temperature for 2 h. After completion of the reaction, the reaction mixture was diluted with H_2O and CH_2Cl_2 layer was separated. The aqueous layer was extracted with CH_2Cl_2 (15 mL × 3). The combined organic layer was washed with water (15 mL × 1), brine (10 mL) and dried over Na_2SO_4. The solvent was removed under reduced pressure to obtain a brown residue which was purified by column chromatography over silica gel (Eluent: 20 % EtOAc in petroleum ether) to furnish the pure **81** (138 mg, 91 %) as brown solid. M.p.: 248 – 249 ^oC; HPLC Purity: 97.9%; IR (KBr): ν/cm^{-1} 3433, 3096, 2920, 1545, 1508, 1451, 1383, 1353, 1302, 1198, 1125; ^1H NMR (400 MHz, $CDCl_3$): δ 8.48 (s, 1H), 8.07 (dd, *J* = 8.6, 2.2 Hz, 1H), 7.72 (d, *J* = 8.7 Hz, 1H), 7.69 – 7.62 (m, 2H), 7.60 (dd, *J* = 4.6, 1.9 Hz, 2H), 7.41 – 7.33 (m, 1H), 7.42 – 7.30 (m, 4H), 6.69 (d, *J* = 5.2 Hz, 1H), 6.25 (d, *J* = 5.2 Hz, 1H), 6.23 (d, *J* = 3.8 Hz, 1H), 6.04 (d, *J* = 3.8 Hz, 1H), 3.89 – 3.79 (m, 8H); ^{13}C NMR (100 MHz, DMSO-D_6): δ 162.1, 150.8, 147.5, 146.9, 145.8, 135.6, 135.1, 134.6, 133.7, 132.9,

132.6, 132.4, 131.7, 128.9, 128.8, 128.3, 127.9, 127.8, 125.3, 122.0, 121.4, 118.4, 117.6, 115.8, 66.6, 51.2; HRMS (ESI): Calc. for $C_{31}H_{25}BF_2N_5O_8S^+$ $[M+H]^+$: 676.1485; Found: 676.1483.

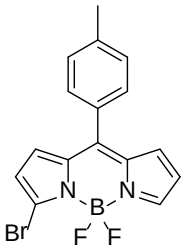

Synthesis of 7-bromo-5,5-difluoro-10-(p-tolyl)-5H-dipyrrolo[1,2-c:2',1'-f][1,3,2]diazaborinin-4-ium-5-uide (98): This compound was prepared in sequence of steps in one pot reaction. Meso-(p-tolyl) dipyrromethane **97** (500 mg, 2.12 mol) was treated with one equivalent of N bromosuccinimide (377 mg, 2.12 mmol) in dry THF (50 mL) at -78^oC under nitrogen for 1 h. The reaction mixture was warmed to room temperature and DDQ (483 mg, 2.12 mmol) was added. The solvent was removed on rotary evaporator under vacuum. The crude compound was subjected to flash column chromatography using CH_2Cl_2, concentrated on rotary evaporator, dissolved in CH_2Cl_2,, neutralized with triethylamine (10.5 mL, 75.4 mmol) and treated with $BF_3 \bullet Et_2O$ (13.5 mL, 107.0 mmol) at room temperature for additional 1 h. The reaction mixture was washed successively with 0.1 M NaOH solution and water. The organic layers were combined, dried over Na_2SO_4, filtered, and evaporated. The crude compound was subjected to silica gel column chromatography and the required 3-bromo derivative of BODIPY **98** was collected as second band using of petroleum ether/dichloromethane (90:10). The solvent was removed on rotary evaporator under vacuo and afforded pure **98** as red orange powder (495 mg, 65% yield). M.p. = 228 – 229 ^oC; IR (KBr): γ_{max}/cm^{-1} 3446, 2915, 2847, 1570, 1543, 1524, 1410, 1386, 1312, 1255, 1182, 1111; ^1H NMR (400 MHz, $CDCl_3$): δ 7.94 (s, 1H), 7.42 (d, *J* = 8.1 Hz, 2H), 7.33 (d, *J* = 8.1 Hz, 2H), 6.93 (d, *J* = 4.2 Hz, 1H), 6.84 (d, *J* = 4.2 Hz, 1H), 6.56 (d, *J* = 3.1 Hz, 1H), 6.51 (d, *J* = 4.3 Hz, 1H), 2.46 (s, 3H); ^{13}C NMR (100 MHz, $CDCl_3$): δ 145.5, 144.2, 141.3, 135.4, 134.6, 131.5, 131.4, 131.2, 130.4, 130.1, 129.1, 121.7, 118.8, 21.3.

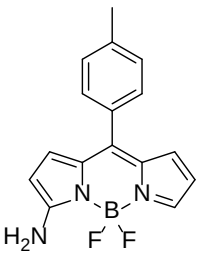

Synthesis of 7-amino-5,5-difluoro-10-(p-tolyl)-5H-dipyrrolo[1,2-c:2',1'-f][1,3,2]diazaborinin-4-ium-5-uide (91a): In a 25 ml round bottomed flask were added monobromo BODIPY **98** (104 mg, 0.29 mmol), aqueous NH_3 solution (2 mL) and dissolved in Acetonitrile 2 mL). The reaction mixture was stirred at room temperature for 2.5 h. After completion of the reaction, the reaction mixture was evaporated under reduced

pressure to remove acetonitrile and aqueous solution was extracted with Ethyl acetate (10 mL × 3). The combined organic layer was washed with water (10 mL × 3), brine (20 mL) and dried over Na_2SO_4. The solvent was removed under reduced pressure to obtain a brown residue which was purified by column chromatography over silica gel (Eluent: 20 % EtOAc in petroleum ether) to furnish the pure **91a** (82 mg, 96%) as a yellow solid. M.p. = 194 – 195 ^oC (decomposed); IR (KBr): γ_{max}/cm^{-1} 3450, 3367, 3279, 1665, 1595, 1573, 1522, 1474, 1408, 1394, 1376, 1257, 1217, 1170, 1156, 1098, 1059; ^1H NMR (400 MHz, $CDCl_3$): δ 7.44 (br s, 1H), 7.38 (d, *J* = 8.0 Hz, 2H), 7.26 – 7.24 (m, 2H), 6.92 (d, *J* = 4.88 Hz, 1H), 6.48 (d, *J* = 3.36 Hz, 1H), 6.34 – 6.32 (m, 1H), 6.07 (d, *J* = 4.80 Hz, 1H), 5.76 (br s, 2H), 2.42 (s, 3H); ^{13}C NMR (100 MHz, $CDCl_3$): δ 161.1, 139.5, 136.1, 134.8, 133.2, 132.7, 131.7, 131.6, 130.3, 129.0, 120.9, 21.5; HRMS (ESI): Calc. for $C_{16}H_{14}BF_2N_3Na$ $[M+Na]^+$: 320.1147; Found: 320.1144.

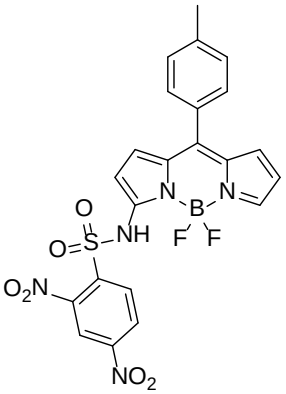

Synthesis of 7-(2,4-dinitrophenylsulfonamido)-5,5-difluoro-10-(p-tolyl)-5H-dipyrrolo[1,2-c:2',1'-f][1,3,2]diazaborinin-4-ium-5-uide (91): In a 25 ml round bottomed flask placed under nitrogen atmosphere amine **91a** (110 mg, 0.37 mmol) was dissolved in dry THF (10 mL) and cooled to 0°C in an ice bath. NaH (60 % suspension in mineral oil) (22 mg, 0.37 mmol) and 2,4-dinitrobenzene sulfonyl chloride (297 mg, 1.12 mmol) were added at 0°C and the reaction mixture was allowed to warm at room temperature over the period of 4 h. After completion of the reaction, the reaction mixture was quenched with satutated aqueous NH_4Cl solution and extracted with Ethyl acetate (20 mL × 3). The combined organic layer was washed with water (10 mL × 3), brine (20 mL) and dried over Na_2SO_4. The solvent was removed under reduced pressure to obtain a brown residue which was purified by column chromatography over silica gel (Eluent: 25% EtOAc in petroleum ether) to furnish the pure **91** (110 mg, 56%) as dark brown solid. M.p. = >250 ^oC (decomposed); IR (KBr): ν_{max}/cm^{-1} 3472, 2922, 2853, 1585, 1545, 1507, 1454, 1406, 1347, 1289, 1242, 1138, 1106, 1065, 1015; ^1H NMR (400 MHz, CD_3OD): δ 8.55 (d, *J* = 2.2 Hz, 1H), 8.51 (d, *J* = 8.7 Hz, 1H), 8.45 (d, *J* = 2.24 Hz, 1H), 7.33 – 7.24 (m, 5H), 6.83 (d, *J* = 5.08 Hz, 1H), 6.63 (d, *J* = 5.04 Hz, 1H), 6.26 – 6.21 (m, 2H), 2.39 (s, 3H); ^{13}C NMR (100 MHz, DMSO-d_6): δ 165.9, 149.2, 147.8, 142.5, 138.9,

134.8, 133.6, 132.3, 131.5, 130.5, 130.2, 129.9, 129.5, 119.9, 117.6, 117.0, 112.7, 21.4; HRMS (ESI): Calc. for $C_{22}H_{16}BF_2N_5O_6SNa$ $[M+Na]^+$: 550.0780; Found: 550.0778.

Synthesis of 3-phenyl-2*H*-chromen-2-imine (92a):

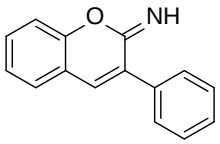

A solution of 2-hydroxybenzaldehyde (500 mg, 4.09 mmol), IRA 900 resin (500 mg, 4.09 mmol OH^-), and toluene (20 mL) was introduced into a 250-mL, three-neck flask equipped with a condenser and stirred for 3 h at 85 ^oC under a nitrogen atmosphere. After that, 2-phenylacetonitrile (20 mmol) was added, and the mixture was refluxed for 8 h. After completion of the reaction, the organic phase was separated from the solid catalyst and concentrated under reduced pressure. The solid phase was recrystallized from toluene to furnish the pure compound **92a** (500 mg, 55%). M.p.: 105–106 ^oC; IR (KBr) ν/cm^{-1}: 3565, 3051, 1643, 1586, 1109, 1055. ^1H NMR (400 MHz, $CDCl_3$) δ: 7.55 – 7.20 (m, 8H), 7.12 – 7.00 (m, 3H). ^{13}C NMR (100 MHz $CDCl_3$) δ: 153.2, 153.1, 136.2, 133.2, 130.5, 128.7, 128.6, 128.5, 127.4, 127.4, 123.4, 123.4, 119.9, 115.5; HRMS (ESI): Calc. for $[M+H]^+$: 222.0920, found: 222.0917. Obtained data was matched with the literature data.

2,4-dinitro-N-(3-phenyl-2H-chromen-2-ylidene) benzene sulfonamide (92): To a solution of 3-phenyl-2*H*-chromen-2-imine **92a** (200 mg, 0.9 mmol) in pyridine (10 mL) placed in a 100 mL two-neck round bottomed flask were added 2,4-dinitrobenzene-1-sulfonyl chloride (362 mg, 1.35 mmol) at 0 ^oC slowly with stirring. The reaction mixture was placed under nitrogen atmosphere and stirred at room temperature for 1 h. After completion of the reaction, the solvent was removed under reduced pressure. The residue was poured into H_2O (10 mL) and extracted with CH_2Cl_2 (15 mL × 3). The combined organic layer was washed with water (10 mL × 3), brine (10 mL) and dried over Na_2SO_4. The solvent was removed under reduced pressure to obtain a yellow residue which was purified by column chromatography over silica gel (Eluent: 45% EtOAc in petroleum ether) to furnish the pure compound **92** (169 mg, 35%) as yellow solid. M.p.: 242–243 ^oC; IR (KBr): ν_{max}/cm^{-1} 3367, 1624, 1607, 1557, 1535, 1481, 1446, 1384, 1366, 1333, 1313, 1159, 1105; ^1H NMR (400 MHz, DMSO-d_6): δ 8.95 – 8.75 (m, 1H), 8.67 (d, *J* = 1.6 Hz, 2H), 8.36 (s, 1H), 7.97 – 7.76 (m, 1H), 7.68 (dd, *J* = 7.9, 1.5 Hz, 3H), 7.56 – 7.19 (m, 5H); ^{13}C NMR (100 MHz, DMSO-d_6): δ 159.0, 152.0, 150.6, 148.4, 143.8, 139.0, 134.5, 133.6, 133.2, 129.9, 129.7

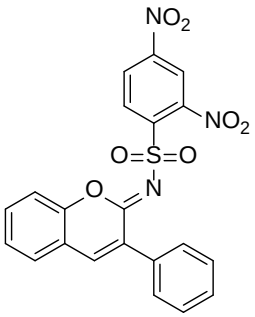

(2C), 129.5, 128.8 (2C), 128.5, 127.7, 127.1, 120.7, 120.4, 116.2; HRMS (ESI): Calc. for $C_{21}H_{14}N_3O_7S$ $[M+H]^+$: 452.0553; Found: 452.0554.

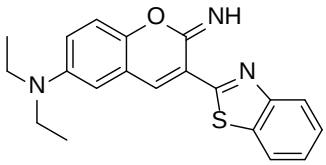

Synthesis of 3-(benzo[d]thiazol-2-yl)-*N*,*N*-diethyl-2-imino-2*H*-chromen-6-amine: (93a): To a solution of 2-benzothiazoleacetonitrile (150 mg, 0.86 mmol) in 15 mL of dry methanol was added piperidine (850 µL, 8.6 mmol) and the solution was stirred at room temperature for 3 min. Then 4-(diethylamino) salicylaldehyde (166 mg, 0.86 mmol) was added. The mixture was stirred for 5 h at room temperature, and the precipitate was collected by filtration, washed with dry methanol, and dried under high vacuum to afford **93a** (210 mg, 70%). M.p.: 192–193 ^oC; IR (KBr): ν/cm^{-1}: 3206, 2316, 1658, 1605, 1462, 1380, 1197; ^1H NMR (400 MHz, DMSO-d_6) δ: 8.47 (s, 1H), 8.02 (d, *J* = 7.8 Hz, 1H), 7.91 (d, *J* = 7.8 Hz, 1H), 7.54 – 7.39 (m, 2H), 7.33 (d, *J* = 7.2 Hz, 1H), 6.57 (dd, *J* = 8.9, 2.4 Hz, 1H), 6.34 (s, 1H), 3.47 – 3.33 (m, 4H), 1.35 – 0.91 (m, 6H); HRMS (ESI): Calc. for $[M+H]^+$: 350.1328, found: 350.1325. Obtained data was matched with the literature data.

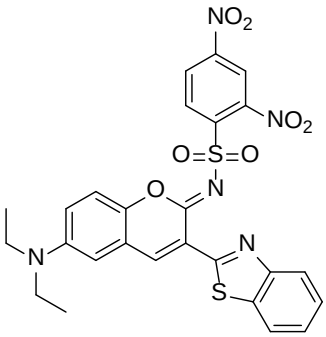

(Z)-N-(3-(benzo[d]thiazol-2-yl)-7-(diethylamino)-2H-chromen-2-ylidene)-2,4-dinitrobenzenesulfonamide (93): To a solution of 3-(benzo[*d*]thiazol-2-yl)-*N*,*N*-diethyl-2-imino-2*H*-chromen-7-amine **93a** (125 mg, 0.357 mmol) in pyridine (10 mL) placed in a 100 mL two-neck round bottomed flask were added 2,4-dinitrobenzene-1-sulfonyl chloride (362 mg, 1.35 mmol) at 0 ^oC slowly with stirring. The reaction mixture was placed under nitrogen atmosphere and stirred at room temperature for 1 h. After completion of the reaction, the solvent was removed under reduced pressure. The residue was poured into H_2O (10 mL) and extracted with CH_2Cl_2 (15 mL × 3). The combined organic layer was washed with water (10 mL × 3), brine (10 mL) and dried over Na_2SO_4. The solvent was removed under reduced pressure to obtain a yellow residue which was purified by column chromatography over silica gel (Eluent: 2% MeOH in Chloroform) to furnish the pure compound **93** (232 mg, 72%) as red solid. M.p.: 261–262 ^oC; IR (KBr): ν_{max}/cm^{-1} 3565, 1643, 1532, 1484, 1466, 1366, 1346, 1315, 1128, 1082; ^1H NMR (400 MHz, DMSO-d_6) δ 9.20 (s, 1H), 8.92 – 8.76 (m, 2H), 8.60 (dd, *J* = 8.7, 2.3 Hz, 1H), 8.13 (d, *J* = 7.9 Hz, 1H), 7.96 (d, *J* = 8.1 Hz, 1H), 7.85 (d, *J* = 9.1 Hz, 1H), 7.50 (t, *J* = 8.2 Hz, 1H), 7.39 (t, *J* = 7.5

Hz, 1H), 6.96 (dd, *J* = 9.1, 2.2 Hz, 1H), 6.45 (d, *J* = 1.7 Hz, 1H), 3.52 (d, *J* = 7.1 Hz, 4H), 1.11 (t, *J* = 7.0 Hz, 6H); ^{13}C NMR (100 MHz, DMSO-d_6): δ 159.3 (2C), 156.1, 155.1, 152.6, 151.2, 149.4, 147.4, 143.7, 143.7, 138.2, 135.5, 132.5, 132.0, 126.1, 125.9, 124.3, 121.5, 121.4, 119.4, 112.3, 109.9, 108.8, 94.4, 44.3 (2C), 11.7 (2C); HRMS (ESI): Calc. for $C_{26}H_{21}N_5O_7S_2$ $[M+H]^+$: 580.0961; Found: 580.0952.

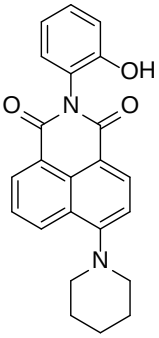

Synthesis of 2-(2-hydroxyphenyl)-6-(piperidin-1-yl)-1H-benzo[de]isoquinoline-1,3(2H)-dione (94a): To a solution of 6-bromo-2-(2-hydroxyphenyl)-1H-benzo[de]isoquinoline-1,3(2H)-dione **101a** (100 mg, 0.27 mmol) in 2-Methoxymethanol (10 mL) placed in 100 mL two-neck round bottomed flask were added Piperidine (160 µL 1.62 mmol) slowly with stirring. The reaction mixture was placed in nitrogen atmosphere and reflux at 125^{o}C for 24h. After completion of the reaction, the solvent was removed under reduced pressure to obtain a yellow residue which was purified by column chromatography over silica gel (Eluent: 40% EtOAc in petroleum ether) to furnish the pure compound 2-(2-hydroxyphenyl)-6-(piperidin-1-yl)-1H-benzo[de]isoquinoline-1,3(2H)-dione **94a** (60 mg, 60%) as yellow solid. M.p. = 248-249^{o}C IR (KBr): γ_{max}/cm^{-1} 3565, 1694, 1578, 1372, 1232; ^{1}H NMR (400 MHz, DMSO-d_6) δ 8.60 (dd, *J* = 7.3, 1.2 Hz, 1H), 8.52 (d, *J* = 8.2 Hz, 1H), 8.42 (dd, *J* = 8.4, 1.1 Hz, 1H), 7.68 (dd, *J* = 8.4, 7.3 Hz, 1H), 7.31 – 7.25 (m, 1H), 7.22 – 7.16 (m, 2H), 7.07 – 6.96 (m, 2H), 5.80 (s, 1H), 3.42 – 3.05 (m, 4H), 1.88 (p, *J* = 5.9 Hz, 4H), 1.77 – 1.68 (m, 2H). ^{13}C NMR (100 MHz DMSO-d_6): δ 164.0, 163.5, 157.2, 153.9, 132.6, 131.1, 131.0, 130.8, 130.2, 129.9, 126.3, 126.1, 123.7, 119.5, 116.8, 116.2, 115.4, 54.5, 26.2, 24.3; HRMS (ESI): Calc.for $C_{23}H_{20}N_2O_3$ $[M+H]^+$: 373.1553; Found: 373.1555.

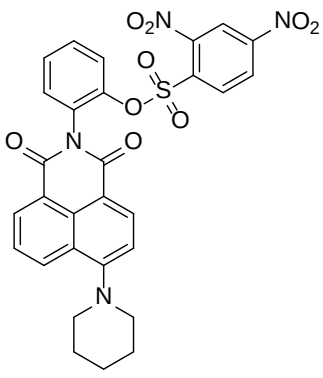

Synthesis of 2-(1,3-dioxo-6-(piperidin-1-yl)-1H-benzo[de]isoquinolin-2(3H)-yl)phenyl 2,4-dinitrobenzenesulfonate (94): To a solution of 2-(2-hydroxyphenyl)-6-(piperidin-1-yl)-1H-benzo[de]isoquinoline-1,3(2H)-dione **94a** (150 mg, 0.402 mmol) in dry DCM (10 mL) placed in 100 mL two neck round bottomed flask were added triethylamine (168 µL,1.206 mmol), 2, 4-dinitrobenzene-1-sulfonyl chloride (322 mg, 1.206 mmol).slowly with stirring. The reaction mixture was

placed under nitrogen atmosphere and stirred at room temperature for 3h. After completion of the reaction; the solvent was removed under reduced pressure. The residue was poured into H_2O (10 mL) and extracted with CH_2Cl_2 (15 mL × 3). The combined organic layer was washed with water (10 mL × 3), brine (10 mL) and dried over Na_2SO_4.The solvent was removed under reduced pressure to obtain a yellow residue which was purified by column chromatography over silica gel (Eluent: 45% EtOAc in petroleum ether) to furnish the pure compound 2-(1,3-dioxo-6-(piperidin-1-yl)-1H-benzo[de]isoquinolin-2(3H)-yl)phenyl 2,4-dinitrobenzenesulfonate **94** (200 mg, 83%) as yellow solid. M.p. = 283-284 ^oC IR (KBr): γ_{max}/cm^{-1} 1659, 1578, 1546, 1485, 1348, 1085; ^1H NMR (400 MHz, DMSO-d6) δ 8.34 (dd, *J* = 8.7, 2.4 Hz, 2H), 8.29 – 8.20 (m, 2H), 8.06 (d, *J* = 8.1 Hz, 1H), 7.99 (d, *J* = 8.7 Hz, 1H), 7.75 – 7.66 (m, 1H), 7.59 (d, *J* = 3.5 Hz, 1H), 7.51 (dt, *J* = 13.4, 6.1 Hz, 2H), 7.15 (d, *J* = 8.1 Hz, 1H), 3.20 (s, 4H), 1.80 (s, 4H), 1.65 (s, 2H).^{13}C NMR (100 MHz, DMSO-d_6):δ 163.3, 162.8, 157.6, 151.0, 147.3, 145.9, 133.9, 132.8, 132.4, 132.1, 131.7 131.2, 130.8, 129.8, 129.0, 128.6, 128.1, 126.1, 125.6, 124.4, 122.6, 120.3, 115.0, 114.6, 54.4, 26.2, 24.4;HRMS (ESI): Calc. for $C_{29}H_{22}N_4O_9S$ $[M+H]^+$: 603.1186; Found: 603.1196.

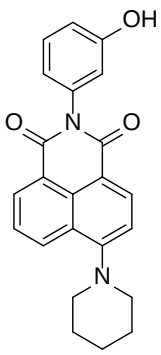

Synthesis of 2-(3-hydroxyphenyl)-6-(piperidin-1-yl)-1H-benzo[de]isoquinoline-1,3(2H)-dione (95a): To a solution of 6-bromo-2-(3-hydroxyphenyl)-1H-benzo[de]isoquinoline-1,3(2H)-dione **101b** (300 mg, 0.814 mmol) in 2-Methoxymethanol (10 mL) placed in 100 mL two-neck round bottomed flask were added Piperidine (162 µL 1.62 mmol) slowly with stirring. The reaction mixture was placed in nitrogen atmosphere and reflux at 125^oC for 24h. After completion of the reaction, the solvent was removed under reduced pressure to obtain a yellow residue which was purified by column chromatography over silica gel (Eluent: 40% EtOAc in petroleum ether) to furnish the pure compound. 2-(3-hydroxyphenyl)-6-(piperidin-1-yl)-1H-benzo[de]isoquinoline-1,3(2H)-dione **95a** (290 mg, 95%) as yellow solid M.p. = 283-284^oC IR (KBr): γ_{max}/cm^{-1} 3565, 1707, 1676, 1531, 1484, 1368, 1225; ^1H NMR (400 MHz, DMSO-d6) δ 9.58 (s, 1H), 8.47 – 8.26 (m, 3H), 7.77 (t, *J* = 7.8 Hz, 1H), 7.40 – 7.14 (m, 2H), 6.79 (d, *J* = 8.4 Hz, 1H), 6.68 (d, *J* = 8.7 Hz, 2H), 3.16 (s, 4H), 1.78 (s, 4H), 1.61 (s, 2H).^{13}C NMR (100 MHz DMSO-d_6): δ 164.2, 163.6, 158.3, 157.2, 137.6, 132.7, 131.2,

131.1, 130.1, 129.9, 126.3, 126.0, 123.5, 120.1, 116.7, 115.9, 115.5, 115.4, 54.5, 26.2, 24.3; HRMS (ESI): Calc.for $C_{23}H_{20}N_2O_3$ $[M+H]^+$: 373.1553; Found: 373.1554.

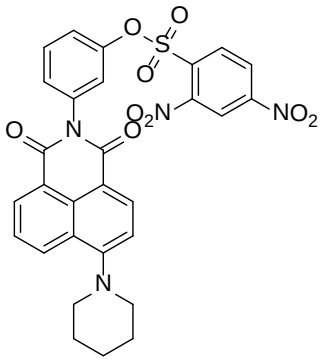

Synthesis of 3-(1,3-dioxo-6-(piperidin-1-yl)-1H-benzo[de]isoquinolin-2(3H)-yl)phenyl 2,4-dinitrobenzenesulfonate (95): To a solution of 2-(3-hydroxyphenyl)-6-(piperidin-1-yl)-1H-benzo[de]isoquinoline-1,3(2H)-dione **95a** (110 mg, 0.268 mmol) in dry DCM (10 mL) placed in 100 mL two neck round bottomed flask were added triethylamine (107 µL,0.805 mmol), 2, 4-dinitrobenzene-1-sulfonyl chloride (215 mg, 0.805 mmol).slowly with stirring. The reaction mixture was placed under nitrogen atmosphere and stirred at room temperature for 3h. After completion of the reaction; the solvent was removed under reduced pressure. The residue was poured into H_2O (10 mL) and extracted with CH_2Cl_2 (15 mL × 3). The combined organic layer was washed with water (10 mL × 3), brine (10 mL) and dried over Na_2SO_4.The solvent was removed under reduced pressure to obtain a yellow residue which was purified by column chromatography over silica gel (Eluent: 45% EtOAc in petroleum ether) to furnish the pure compound 3-(1,3-dioxo-6-(piperidin-1-yl)-1H-benzo[de]isoquinolin-2(3H)-yl)phenyl 2,4-dinitrobenzenesulfonate **95** (70 mg, 43%) as yellow solid. M.p. = 175-176 ^oC IR (KBr): γ_{max}/cm^{-1} 1657, 1547, 1478, 1359, 1073; ^1H NMR (400 MHz, DMSO-d6) δ 9.00 (s, 1H), 8.59 (d, *J* = 8.6 Hz, 1H), 8.40 (d, *J* = 8.4 Hz, 1H), 8.34 (d, *J* = 7.2 Hz, 1H), 8.26 (d, *J* = 8.1 Hz, 1H), 8.13 (d, *J* = 8.6 Hz, 1H), 7.78 (t, *J* = 7.8 Hz, 1H), 7.57 (t, *J* = 8.1 Hz, 1H), 7.42 – 7.25 (m, 1H), 7.13 (s, 3H), 3.17 (s, 4H), 1.79 (s, 4H), 1.62 (s, 2H).^{13}C NMR (100 MHz, DMSO-d_6): δ 164.0, 163.4, 157.4, 151.9, 148.8, 148.4, 138.2, 134.3, 132.6, 131.3, 130.9, 130.7, 130.0, 128.1, 126.2, 125.9, 123.8, 123.4, 122.5, 121.6, 115.7, 115.3, 54.4, 26.1, 24.3;HRMS (ESI): Calc. for $C_{29}H_{22}N_4O_9S$ $[M+H]^+$: 603.1186; Found: 603.1177.

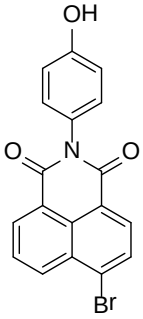

Synthesis of 6-bromo-2-(4-hydroxyphenyl)-1H-benzo[de]isoquinoline-1,3(2H)-dione (101c): To a solution of 4-Bromo-1, 8-napthalic anhydride **99** (500 mg, 1.80 mmol) in Pyridine (10mL) placed in a 100 mL two-neck round bottomed flask were added 4-aminophenol **100c** (196 mg, 1.80 mmol) slowly with stirring The reaction mixture was placed in nitrogen atmosphere and

reflux at 115^{o}C for 24h. After completion of the reaction, the solvent was removed under reduced pressure to obtain a yellow residue which was purified by column chromatography over silica gel (Eluent: 2% MeOH in chloroform) to furnish the pure compound 6-bromo-2-(4-hydroxyphenyl)-1H-benzo[de]isoquinoline-1,3(2H)-dione **101c** (350 mg, 53%) as white solid. M.p. = >294^{o}C IR (KBr): γ_{max}/cm^{-1} 3565,1676,1614,1484; ^{1}H NMR (400 MHz, DMSO-d6) δ 9.64 (s, 1H), 8.54 (q, *J* = 7.6 Hz, 2H), 8.29 (d, *J* = 7.8 Hz, 1H), 8.20 (d, *J* = 7.8 Hz, 1H), 7.98 (t, *J* = 7.9 Hz, 1H), 7.10 (d, *J* = 7.7 Hz, 2H), 6.82 (d, *J* = 8.6 Hz, 2H).^{13}C NMR (100 MHz DMSO-d_6): δ 163.9, 163.8, 157.7, 133.1, 132.0, 131.9, 131.4, 130.3, 129.5, 129.3, 129.2, 127.1, 123.9, 123.1, 115.9; HRMS (ESI): Calc.for $C_{18}H_{10}BrNO_3$ [M+H]$^{+}$: 367.9923; Found: 367.9915.

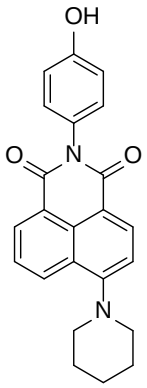

Synthesis of 2-(4-hydroxyphenyl)-6-(piperidin-1-yl)-1H-benzo[de]isoquinoline-1,3(2H)-dione (96a): To a solution of 6-bromo-2-(4-hydroxyphenyl)-1H-benzo[de]isoquinoline-1,3(2H)-dione **101c** (230 mg, 0.62 mmol) in 2-Methoxymethanol (10 mL) placed in 100 mL two-neck round bottomed flask were added Piperidine (124 µL 1.24 mmol) slowly with stirring. The reaction mixture was placed in nitrogen atmosphere and reflux at 125^{o}C for 24h. After completion of the reaction, the solvent was removed under reduced pressure to obtain a yellow residue which was purified by column chromatography over silica gel (Eluent: 40% EtOAc in petroleum ether) to furnish the pure compound. 2-(4-hydroxyphenyl)-6-(piperidin-1-yl)-1H-benzo[de]isoquinoline-1,3(2H)-dione **96a** (232 mg, 97%) as yellow solid. M.p. = 292-293^{o}C IR (KBr): γ_{max}/cm^{-1} 3418, 1692, 1580, 1376, 1231; ^{1}H NMR (400 MHz, DMSO-d6) δ 9.58 (s, 1H), 8.42 – 8.14 (m, 3H), 7.67 (s, 1H), 7.19 (d, *J* = 8.2 Hz, 1H), 6.94 (d, *J* = 8.6 Hz, 2H), 6.70 (d, *J* = 8.3 Hz, 2H), 3.06 (s, 4H), 1.69 (s,4H), 1.52 (s, 2H).^{13}C NMR (100 MHz DMSO-d_6): δ 164.5, 163.9, 157.6, 157.2, 132.7, 131.1, 130.4, 130.0, 127.4, 126.3, 126.0, 123.5, 116.0, 115.8, 115.4, 54.5, 26.2, 24.3;HRMS (ESI): Calc.for $C_{23}H_{20}N_2O_3$ [M+H]$^{+}$: 373.1553; Found: 373.1553.

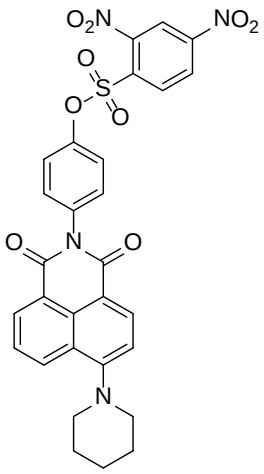

Synthesis of 4-(1,3-dioxo-6-(piperidin-1-yl)-1H-benzo[de]isoquinolin-2(3H)-yl)phenyl 2,4-dinitrobenzenesulfonate (96): To a solution of 2-(4-hydroxyphenyl)-6-(piperidin-1-yl)-1H-benzo[de]isoquinoline-1,3(2H)-dione **96a** (150 mg, 0.402 mmol) in dry DCM (10 mL) placed in 100 mL two neck round bottomed flask were added triethylamine (168 µL,1.206 mmol), 2, 4-dinitrobenzene-1-sulfonyl chloride (322 mg, 1.206 mmol).slowly with stirring. The reaction mixture was placed under nitrogen atmosphere and stirred at room temperature for 3h. After completion of the reaction; the solvent was removed under reduced pressure. The residue was poured into H_2O (10 mL) and extracted with CH_2Cl_2 (15 mL × 3). The combined organic layer was washed with water (10 mL × 3), brine (10 mL) and dried over Na_2SO_4.The solvent was removed under reduced pressure to obtain a yellow residue which was purified by column chromatography over silica gel (Eluent: 45% EtOAc in petroleum ether) to furnish the pure compound 4-(1,3-dioxo-6-(piperidin-1-yl)-1H-benzo[de]isoquinolin-2(3H)-yl)phenyl 2,4-dinitrobenzenesulfonate **96** (210 mg, 86%) as yellow solid. M.p. = 261-262^{0}C IR (KBr): γ_{max}/cm^{-1} 1693, 1579, 1370, 1141; ^{1}H NMR (400 MHz, DMSO-d6) δ 9.10 (d, *J* = 2.2 Hz, 1H), 8.63 (dd, *J* = 8.7, 2.3 Hz, 1H), 8.40 (d, *J* = 7.9 Hz, 4H), 8.33 (dd, *J* = 8.4, 7.0 Hz, 1H), 7.83 – 7.72 (m, 5H), 7.51 – 7.22 (m, 4H), 3.17 (s, 4H), 1.79 (s, 2H), 1.62 (s, 2H).^{13}C NMR (100 MHz, DMSO-d_6):δ 164.2, 163.6, 157.4, 152.0, 148.6, 148.4, 136.4, 133.9, 132.8, 132.0, 131.5, 131.3, 131.1, 130.1, 128.1, 126.3, 126.0, 123.4, 122.8, 121.7, 115.7, 115.4, 54.5, 26.2, 24.3;HRMS (ESI): Calc. for $C_{29}H_{22}N_4O_9S$ $[M+Na]^+$: 625.1004; Found: 625.1011.

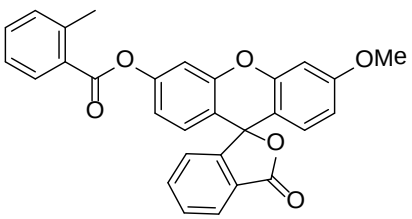

Synthesis of 3'-methoxy-3-oxo-3H-spiro[isobenzofuran-1,9'-xanthen]-6'-yl 2-methylbenzoate (103): In a 50 mL round bottom flask *ortho*-toluic acid (40 mg, 0.29 mmol) was dissolved in 10 mL CH_2Cl_2 and cooled to 0 ^{o}C. To this solution EDC·HCl (56 mg, 0.29 mmol), DMAP (4 mg, 0.03 mmol) and DIPEA (124 µL, 0.73 mmol) were added. The reaction mixture was stirred at 0 ^{o}C for 30 min and compound **102c**[3] (100 mg, 0.29 mmol) was added to it. The reaction mixture was warmed to room temperature and stirred for 16 h. After completion of the reaction, the reaction mixture

was diluted with H_2O and DCM layer was separated. The aqueous solution was extracted with DCM (10 mL × 3). The combined organic layer was washed with water (10 mL × 1), brine (20 mL) and dried over Na_2SO_4. The solvent was removed under reduced pressure to obtain a brown residue which was purified by column chromatography over silica gel (Eluent: 20 % EtOAc in petroleum ether) to furnish the pure **103** (67 mg, 50 %) as a white solid. M.p.: 107 – 108 ^oC; HPLC Purity: 98.3%; IR (KBr): ν/cm^{-1} 1766, 1746, 1630, 1611, 1576, 1497, 1465, 1421, 1287, 1247, 1166, 1149, 1107; ^1H NMR (400 MHz, $CDCl_3$): δ 8.13 (d, *J* = 7.6 Hz, 1H), 8.00 (d, *J* = 7.4 Hz, 1H), 7.58 – 7.67 (m, 2H), 7.46 (t, *J* = 7.4 Hz, 1H), 7.23 – 7.32 (m, 2H), 7.22 (s, 1H), 7.12 – 7.16 (m, 2H), 6.81 – 6.89 (m, 2H), 6.75 – 6.76 (m, 1H), 6.67 – 6.70 (m, 1H), 6.59 – 6.62 (m, 1H), 3.81 (s, 3H), 2.63 (s, 3H); ^{13}C NMR (100 MHz, $CDCl_3$): δ 169.3, 165.2, 161.5, 153.1, 152.3, 152.2, 152.0, 141.6, 135.1, 133.1, 132.1, 131.3, 129.9, 129.1, 129.0, 126.0, 125.1, 124.0, 117.7, 116.8, 112.0, 111.0, 110.6, 100.9, 82.5, 56.6, 22.0; HRMS (ESI): Calc. for $C_{29}H_{21}O_6^+$ $[M+H]^+$: 465.1278; Found: 465.1334.

Synthesis of 3'-methoxy-3-oxo-3H-spiro[isobenzofuran-1,9'-xanthen]-6'-yl 2-(bromomethyl)benzoate (102): In a 25 mL round bottomed flask were added compound **103** (150 mg, 0.32 mmol), AIBN (53 mg, 0.32 mmol) and N-bromosuccinimide (58 mg, 0.32 mmol) dissolved in CCl_4 (12 mL). The reaction mixture was stirred at reflux temperature for 12 h. After completion of the reaction, the reaction mixture was evaporated under reduced pressure to remove CCl_4 to obtain white residue which was purified by column chromatography over silica gel (Eluent: 20 % EtOAc in petroleum ether) to furnish the pure **102** (80 mg, 68%) as a white solid. Unreacted starting material (50 mg) was also recoverd from column purification. Reported yield for the product was based on the starting material recovered. M.p.: 186 – 187 ^oC; HPLC Purity: 98.3%; IR (KBr): ν/cm^{-1} 2925, 1756, 1736, 1653, 1618, 1577, 1463, 1424, 1384, 1284, 1256, 1174, 1151; ^1H NMR (400 MHz, $CDCl_3$): δ 8.17 (d, *J* = 7.8 Hz, 1H), 8.0 (d, *J* = 7.5 Hz, 1H), 7.65 (t, *J* = 7.5 Hz, 2H), 7.60 (d, *J* = 7.5 Hz, 1H), 7.56 (d, *J* = 7.4 Hz, 1H), 7.50 (d, *J* = 7.7 Hz, 1H), 7.44 (t, *J* = 7.6 Hz, 1H), 7.21 – 7.22 (m, 1H), 7.17 (d, *J* = 7.5 Hz, 1H), 6.93 (dd, *J* = 1.9 and 8.6 Hz, 1H), 6.85 (d, *J* = 8.6 Hz, 1H), 6.76 (d, *J* = 2.2 Hz, 1H), 6.69 (d, *J* = 8.8 Hz, 1H), 6.61 (dd, *J* = 2.1 and 8.8 Hz, 1H), 4.94 (s, 2H), 3.81 (s, 3H); ^{13}C NMR

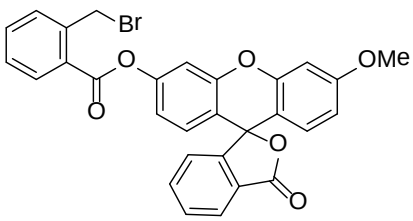

(100 MHz, $CDCl_3$): δ 169.3, 164.5, 161.5, 153.1, 152.3, 152.0, 151.9, 140.2, 135.2, 133.5, 131.9, 129.9, 129.2, 129.0, 128.8, 125.1, 124.0, 117.6, 117.1, 112.0, 110.9, 110.6, 100.9, 82.4, 55.6, 31.3; HRMS (ESI): Calc. for $C_{29}H_{20}BrO_6^+$ $[M+H]^+$: 543.0443; Found: 543.0446.

Synthesis of methyl 2-(bromomethyl) benzoate (105)[4]: In a 25 mL round bottomed flask were added methyl 2-methylbenzoate **104** (200 mg, 1.33 mmol), AIBN (218 mg, 1.33 mmol) and N-bromosuccinimide (237 mg, 1.33 mmol) dissolved in CCl_4 (8 mL). The reaction mixture was stirred at reflux temperature for 12 h. After completion of the reaction, the reaction mixture was evaporated under reduced pressure to remove CCl_4 to obtain white residue which was purified by column chromatography over silica gel (Eluent: 20 % EtOAc in petroleum ether) to furnish the pure **105** (275 mg, 90%) as a semisolid colorless compound. Obtained data was matched with the literature data.[4]

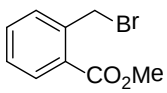

Synthesis of benzo[c]thiophen-1(3H)-one (54): In a 25 mL round bottomed flask methyl 2-(bromomethyl) benzoate **105** (200 mg, 0.87 mmol) was dissolved in methanol (5 mL). To this solution Na_2S (68 mg, 0.87 mmol) was added at rt. The reaction mixture was stirred at room temperature for 1 h. After completion of the reaction, the reaction mixture was evaporated under reduced pressure to remove methanol. White residue thus obtained was purified by column chromatography over silica gel (Eluent: 20 % EtOAc in petroleum ether) to furnish the pure **54** (115 mg, 88%) as a white solid. M.p.: 58 – 59 ^oC; ^1H NMR (400 MHz, $CDCl_3$): δ 7.83 (d, J = 7.8 Hz, 1H), 7.59 – 7.63 (m, 1H), 7.53 (d, J = 7.6 Hz, 1H), 7.46 (t, J = 7.4 Hz, 1H), 4.5 (s, 2H); ^{13}C NMR (100 MHz, $CDCl_3$): δ 192.2, 147.0, 135.9, 133.2, 128.1, 126.4, 123.9, 34.7; HRMS (ESI): Calc. for $C_8H_7OS^+$ $[M+H]^+$: 151.0218; Found: 151.0218.

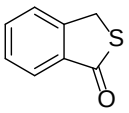

5.3 Crystal structure parameters

Crystal structure of probe 61 (CCDC 846909): $C_{24}H_{14}N_2O_3$; Compound **61** was crystallized from acetic anhydride at 4 ^oC. A yellow rectangular shaped crystal with approximate dimensions 0.11 x 0.10 x 0.10 mm gave an Orthorhombic with space group *P21/n*; a = 9.9766(8) b = 16.9632(13) c = 10.5391 (8) Å, α = 90^o β = 101.076(2)^o γ = 90^o; V = 1750.4(2) Å^3; T = 296 (2) K; Z = 4; ρ_{calc} = 1.440 Mgm^{-3}; $2\theta_{max}$ = 57.28^o; *MoKαλ* =

0.71073 Å. Fine-focus sealed tube source with graphite monochromator. *R* = 0.0569 (for 3740 reflection $I>2\sigma(I)$), *wR* = 0.1291 which was refined against |*F2*| and S = 1.0212 for 262 parameters and 4480 unique reflections. The structure was obtained by direct methods using SHELXS-97.[5] All non-hydrogen atoms were refined isotropically. The hydrogen atoms were fixed geometrically in the idealized position and refined in the final cycle of refinement as riding over the atoms to which they are bonded. μ = 0.096 mm^{-1}; Minimum/maximum residual electron density 0.000 / 0.000 $eÅ^{-3}$.

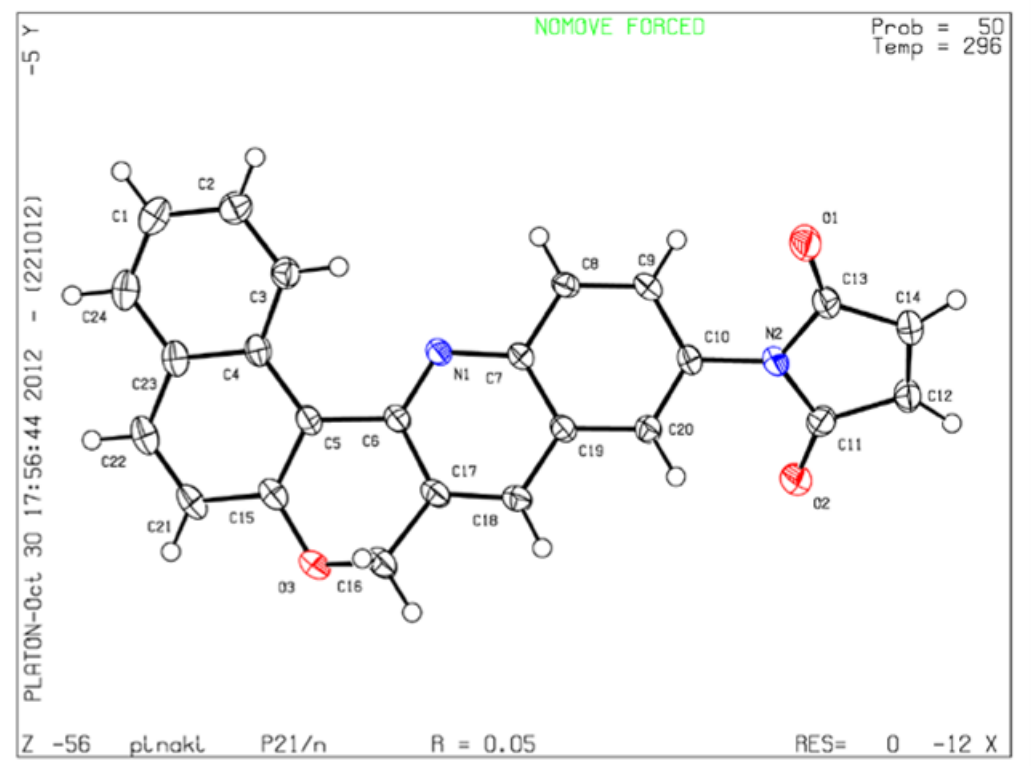

Figure 5.1: ORTEP diagram of probe **61**.

Crystal structure of compound 69 (CCDC 818213): $C_{25}H_{22}N_2O_3$; Compound **69** was crystallized from diethyl ether at 4 °C. A yellow rectangular shaped crystal with approximate dimensions 0.13 x 0.11 x 0.10 mm gave an Monoclinic with space group *P12(1)/c1*; *a* = 13.853(7) *b* = 9.965(5) *c* = 15.005(8) Å, α = 90° β = 90.891(10)° γ = 90°; *V* = 2071.1(19) $Å^3$; *T* = 296 (2) K; *Z* = 4; ρ_{calc} = 1.281 Mgm^{-3}; $2\theta_{max}$ = 49.54°; *MoKαλ* = 0.71073 Å. Fine-focus sealed tube source with graphite monochromator. *R* = 0.0495 (for 1798 reflection $I>2\sigma(I)$), *wR* = 0.1090 which was refined against |*F2*| and S = 0.922 for 274 parameters and 3548 unique reflections. The structure was obtained by direct methods using SHELXS-97. All non-hydrogen atoms were refined isotropically. The hydrogen atoms were fixed geometrically in the idealized position and refined in the final cycle of

refinement as riding over the atoms to which they are bonded. μ = 0.085 mm^{-1}; Minimum/maximum residual electron density -0.003 / 0.033 $eÅ^{-3}$.

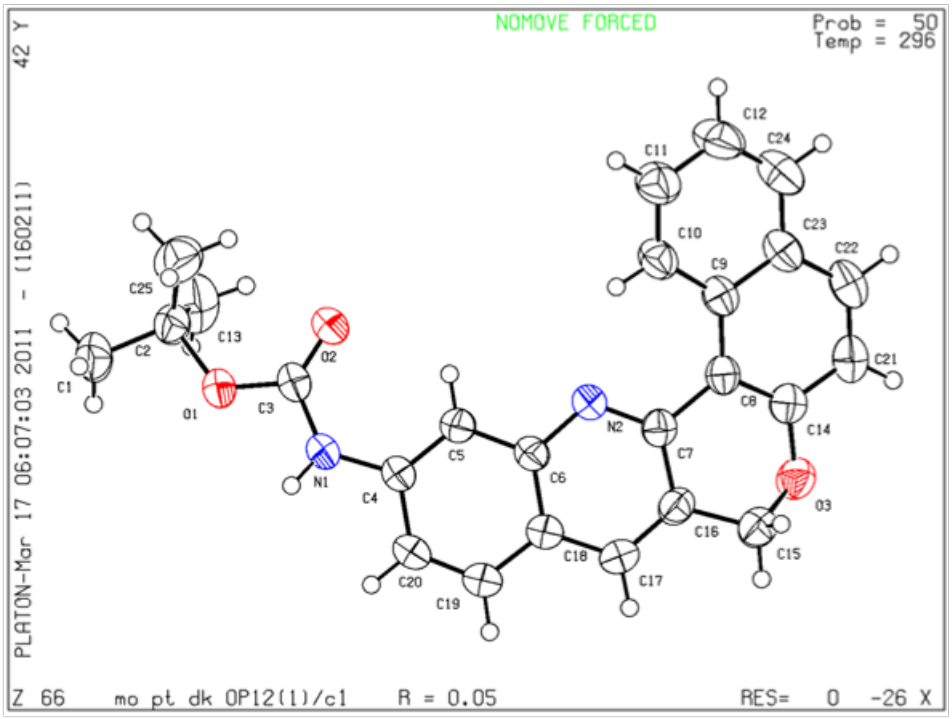

Figure 5.2: ORTEP diagram of chromenoquinoline **69**.

Crystal structure of probe 63 (CCDC 866226): Compound **63** was crystallized from acetic anhydride at 4 ^{o}C. A yellow rectangular shaped crystal with approximate dimensions 0.10 x 0.09 x 0.08 mm gave an Monoclinic with space group *C1c1*; *a* = 9.9766(8) *b* = 18.426(10) *c* = 9.036(5) Å, α = 90^{o} β = 122.238(9)^{o} γ = 90^{o}; *V* = 1791.4(17)$Å^{3}$; *T* = 296 K; *Z* = 4; ρ_{calc} = 1.403 Mgm^{-3}; $2\theta_{max}$ = 57.28^{o}; *MoKαλ* = 0.71073 Å. Fine-focus sealed tube source with graphite monochromator. *R* = 0.0453 (for 2911 reflection $I>2\sigma(I)$), *wR* = 0.1144 which was refined against |*F2*| and S = 0.991 for 263 parameters and 4050 unique reflections. The structure was obtained by direct methods using SHELXS-97. All non-hydrogen atoms were refined isotropically. The hydrogen atoms were fixed geometrically in the idealized position and refined in final cycle of refinement as riding over the atoms to which they are bonded. μ = 0.094 mm^{-1}.

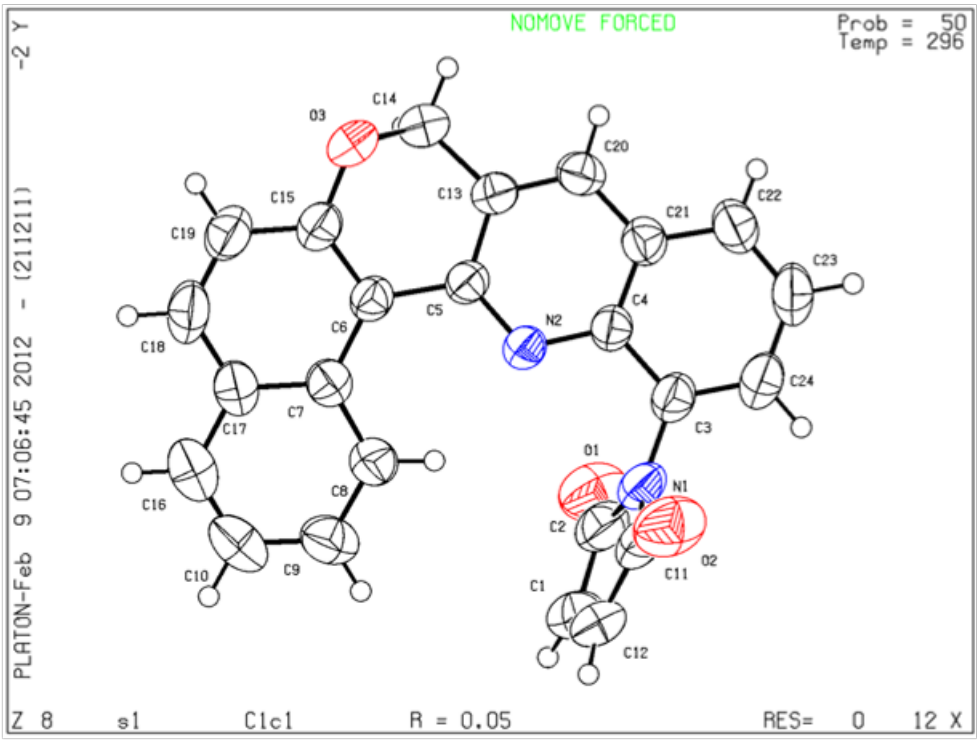

Figure 5.3: ORTEP diagram of probe **63**.

Crystal structure of 85 (CCDC 980654): Compound **85** was crystallized from methanol at room temperature. A red cube shaped crystal with approximate dimensions 0.300 × 0.250 × 0.130 mm gave an orthorhombic with space group *P b c n*; *a*=14.8291(4) *b*=12.6719(3) *c*=21.3493(6) Å, α = 90° β = 90° γ = 90°; *V* = 4011.81(18) Å^3; *T* = 100 K; *Z* = 8; ρ_{calc}= 1.537 Mgm^{-3}; $2\theta_{max}$= 72.325; *CuK*$_\alpha\lambda$ = 1.54178 Å. Fine-focus sealed tube source with graphite monochromator. *R* = 0.0784 (for 3551 reflection *I*>2σ(*I*)), *wR*= 0.2836 which was refined |*F2*| and S = 2.411 for 263 parameters and 3963 unique reflections. The structure was obtained by direct methods using SHELXS-97. All non-hydrogen atoms were refined anisotropically. The hydrogen atoms were fixed geometrically in the idealized position and refined in the final cycle of refinement as riding over the atoms to which they are bonded μ = 3.188^{-1}.

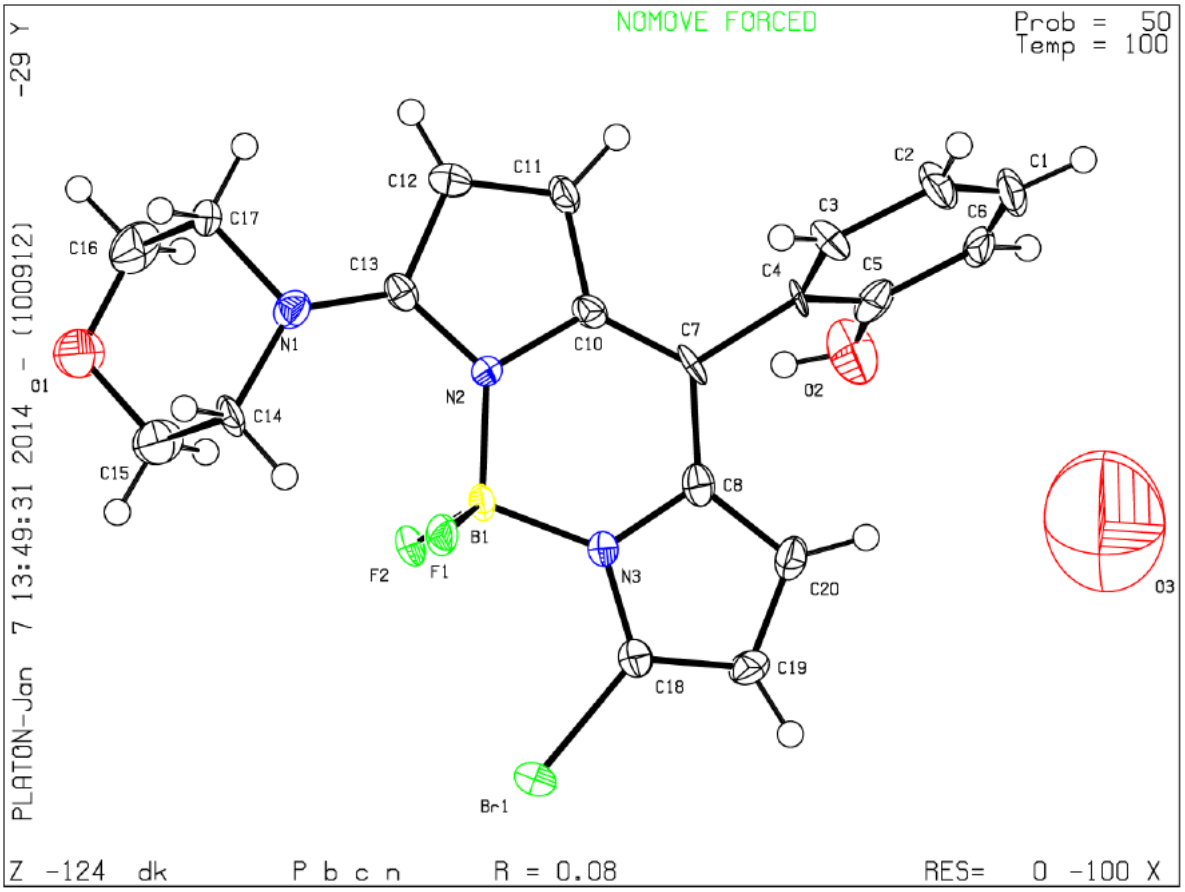

Figure 5.4: ORTEP diagram of compound **85**.

Crystal structure of 81 (CCDC 980654): Compound **81** was crystallized from chloroform at room temperature. A brown cube shaped crystal with approximate dimensions 0.195 × 0.170 × 0.090 mm gave an Monoclinic with space group *P2(1)/n*; *a* = 17.4761(5) *b* = 8.0976(2) *c* = 22.1564(7) Å, α = 90° β = 111.715(1)° γ = 90°; *V* = 2912.95(14)Å^3; *T* = 296 (2) K; *Z* = 4; ρ_{calc}= 1.540 Mgm^{-3}; $2\theta_{max}$= 64.980; $CuK_{\alpha}\lambda$ = 1.54178 Å. Fine-focus sealed tube source with graphite monochromator. *R* = 0.0434 (for 4530 reflection $I>2\sigma(I)$), *wR*= 0.1156 which was refined $|F2|$ and S = 1.045for 433 parameters and 4680 unique reflections. The structure was obtained by direct methods using SHELXS-97. All non-hydrogen atoms were refined anisotropically. The hydrogen atoms were fixed geometrically in the idealized position and refined in the final cycle of refinement as riding over the atoms to which they are bonded μ = 1.663 mm^{-1}.

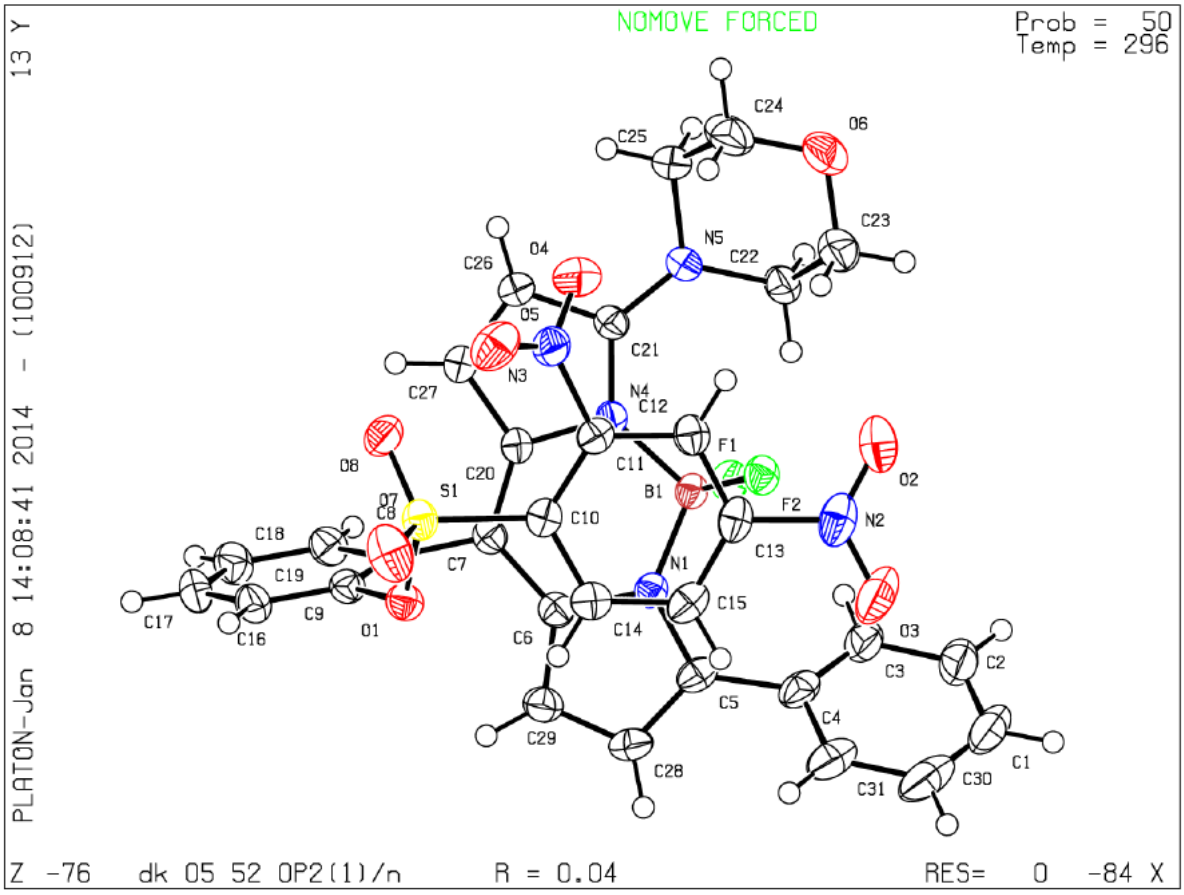

Figure 5.5: ORTEP diagram of probe **81**.

Crystal structure of compound 91a (CCDC 863628): $C_{16}H_{14}BF_2N_3$; Compound **91a** was crystallized from methanol at room temperature. A yellow rectangular shaped crystal with approximate dimensions 0.36 x 0.11 x 0.035 mm gave an Monoclinic with space group *P21/c*; *a* = 15.746(3) *b* = 8.9776(18) *c* = 10.2886(19) Å, α = 90° β = 99.120(4)° γ = 90°; *V* = 1436.1(5) Å^3; *T* = 296 (2) K; *Z* = 4; ρ_{calc} = 1.365 Mgm^{-3}; $2\theta_{max}$ = 56.98°; *MoKαλ* = 0.71073 Å. Fine-focus sealed tube source with graphite monochromator. *R* = 0.0589 (for 1835 reflection $I>2\sigma(I)$), *wR* = 0.1907 which was refined against |*F2*| and S = 0.990 for 201 parameters and 3567 unique reflections. The structure was obtained by direct methods using SHELXS-97. All non-hydrogen atoms were refined isotropically. The hydrogen atoms were fixed geometrically in the idealized position and refined in the final cycle of refinement as riding over the atoms to which they are bonded. μ = 0.100 mm^{-1}.

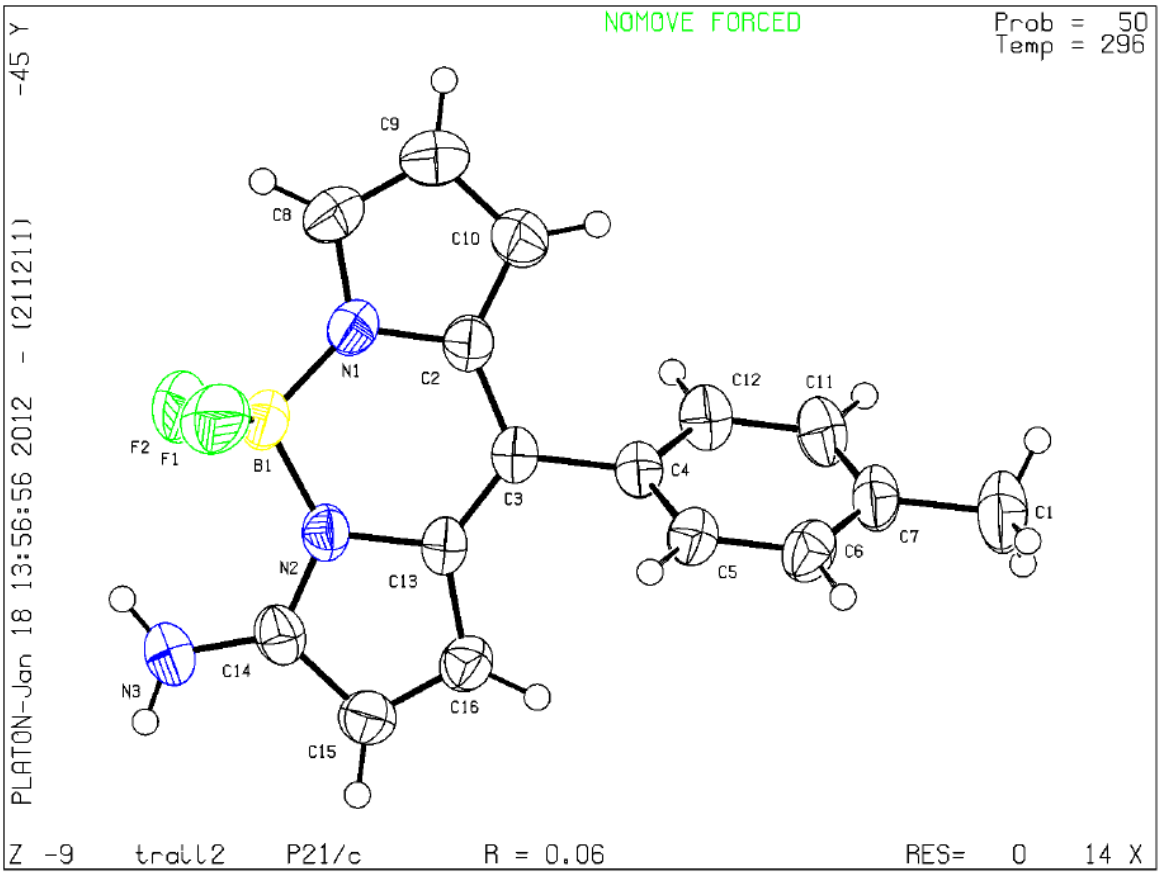

Figure 5.6: ORTEP diagram of probe **91a**.

2.5.1. 2,4-dinitro-N-(3-phenyl-2H-chromen-2-ylidene) benzene sulfonamide 92 (CCDC 940800)

$C_{21}H_{13}N_3O_7S$; Compound **92** was crystallized from dimethyl sulfoxide at room temperature. A yellow needle shaped crystal with approximate dimensions 0.286 × 0.090 × 0.037 mm gave an Orthorhombic with space group *P212121*; *a* = 7.2532(7) *b* = 14.6345(14) *c* = 18.2027(18) Å, α = 90° β = 90° γ = 90°; *V* = 1932.2(3) Å^3; *T* = 296 (2) K; *Z* = 4; ρ_{calc} = 1.504 g cm^{-3}; $2\theta_{max}$ = 48.24; $MoK_\alpha\lambda$ = 0.71073 Å. Fine-focus sealed tube source with graphite monochromator. *R* = 0.0300 (for 2826 reflection $I>2\sigma(I)$), *wR* = 0.0749 which was refined |*F2*| and S = 1.027 for 289 parameters and 3071 unique reflections. The structure was obtained by direct methods using SHELXS-97. All non-hydrogen atoms were refined anisotropically. The hydrogen atoms were fixed geometrically in the idealized position and refined in the final cycle of refinement as riding over the atoms to which they are bonded μ = 0.215 mm^{-1}.

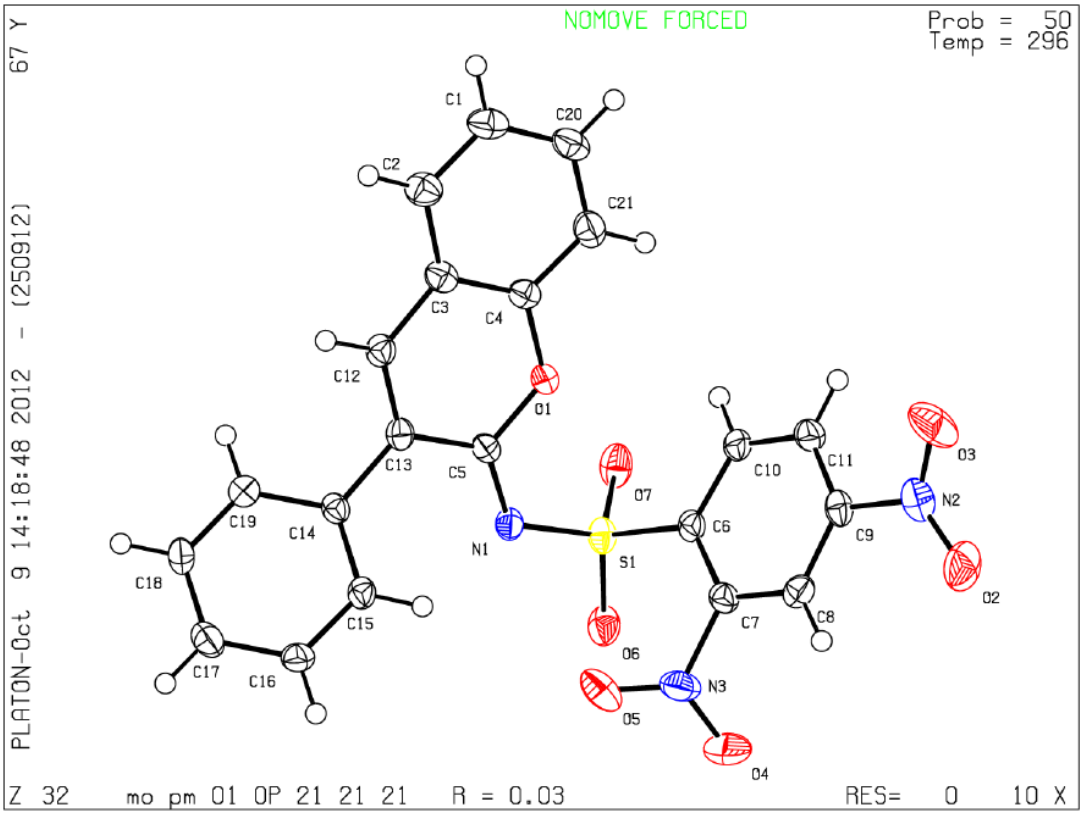

Figure 5.7: ORTEP diagram of probe **92**.

3-phenyl-2H-chromen-2-imine 92a (CCDC 940801)

$C_{15}H_{11}NO$; Compound **92a** was crystallized from toluene at room temperature. A colorless cube shaped crystal with approximate dimensions 0.210 × 0.117 × 0.065 mm gave an Monoclinic with space group *P21*; *a* = 6.247(5) *b* = 7.475(7) *c* = 12.177(10) Å, α = 90° β = 98.78(2)° γ = 90°; *V* = 561.9(9) Å^3; *T* = 296 (2) K; *Z* = 2; ρ_{calc} = 1.308 g cm^{-3}; $2\theta_{max}$ = 56.48; *MoK*$_\alpha\lambda$ = 0.71073 Å. Fine-focus sealed tube source with graphite monochromator. *R* = 0.0408 (for 1746 reflection *I*>2σ(*I*)), *wR*= 0.1040 which was refined |*F2*| and S = 1.056 for 158 parameters and 2212 unique reflections. The structure was obtained by direct methods using SHELXS-97. [6] All non-hydrogen atoms were refined anisotropically. The hydrogen atoms were fixed geometrically in the idealized position and refined in the final cycle of refinement as riding over the atoms to which they are bonded μ = 0.082 mm^{-1}.

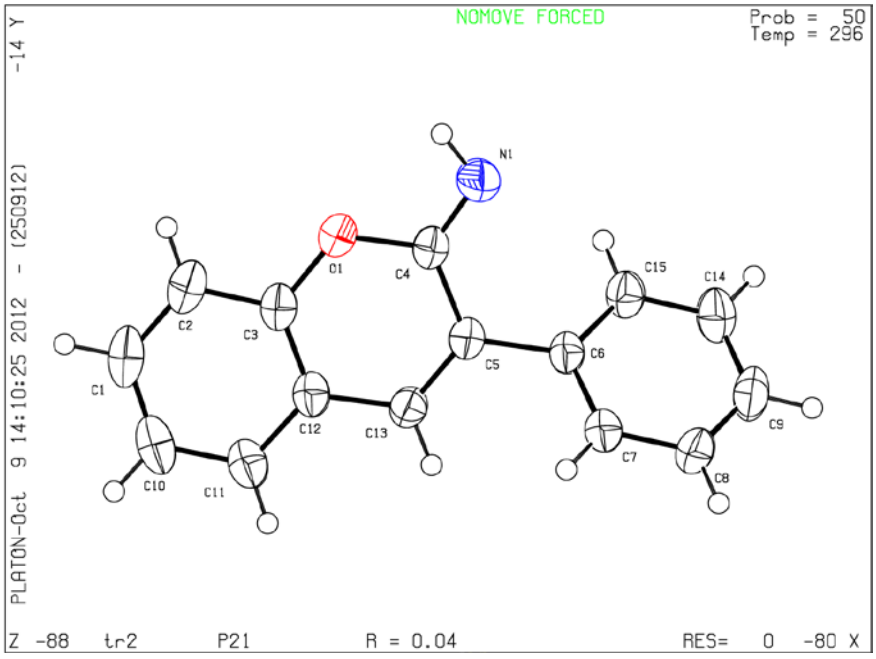

Figure 5.8: ORTEP diagram of compound **92a**.

5.4 NMR data

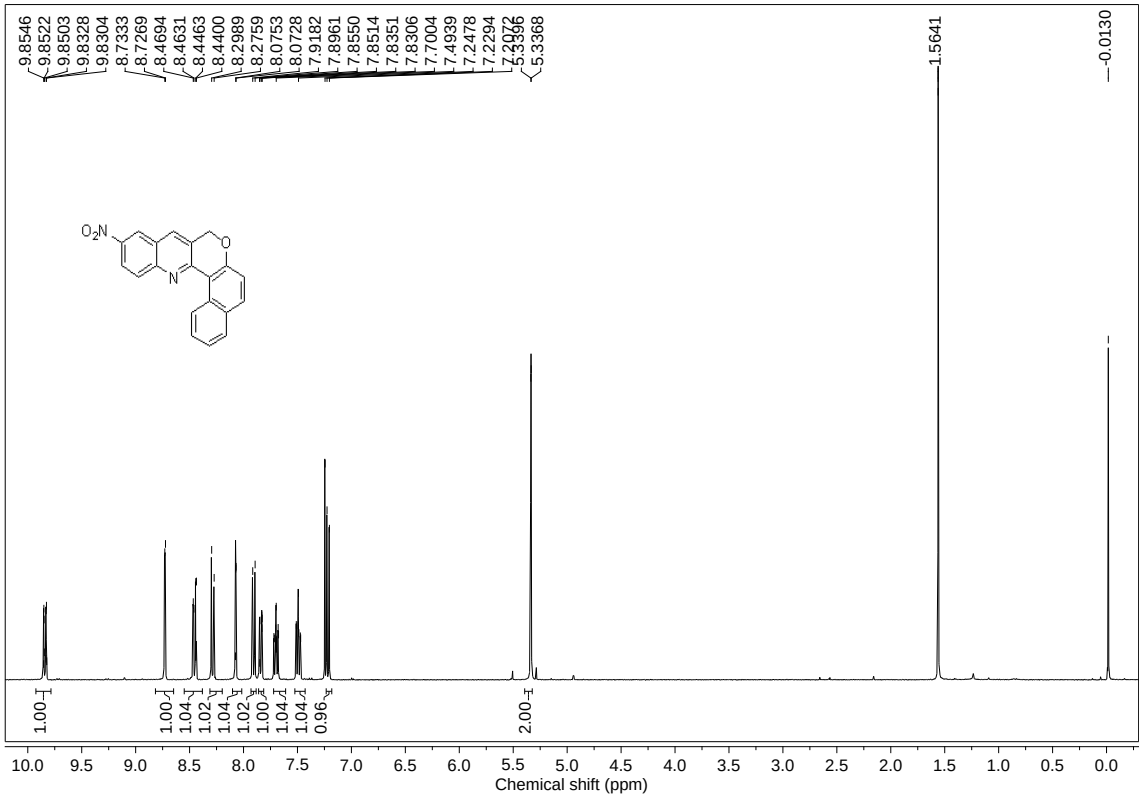

Figure 5.9: ^{1}H NMR spectra of **66** in $CDCl_3$.

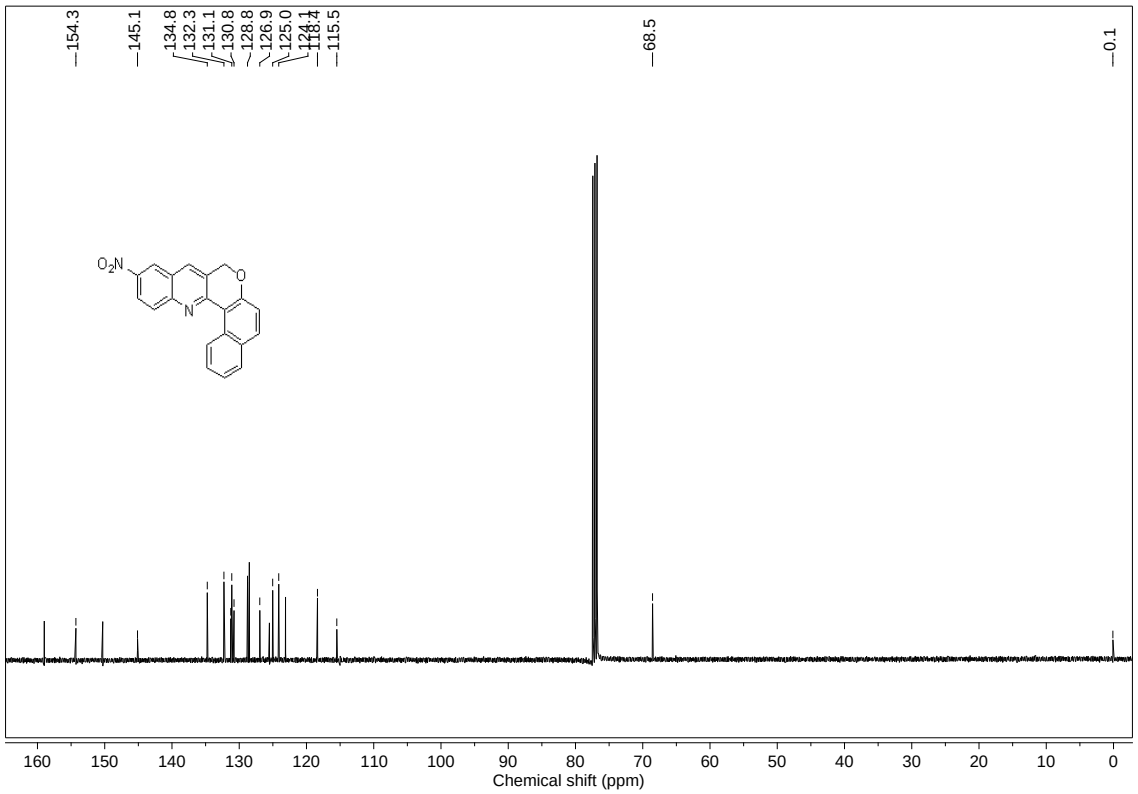

Figure 5.10: ^{13}C NMR spectra of **66** in $CDCl_3$.

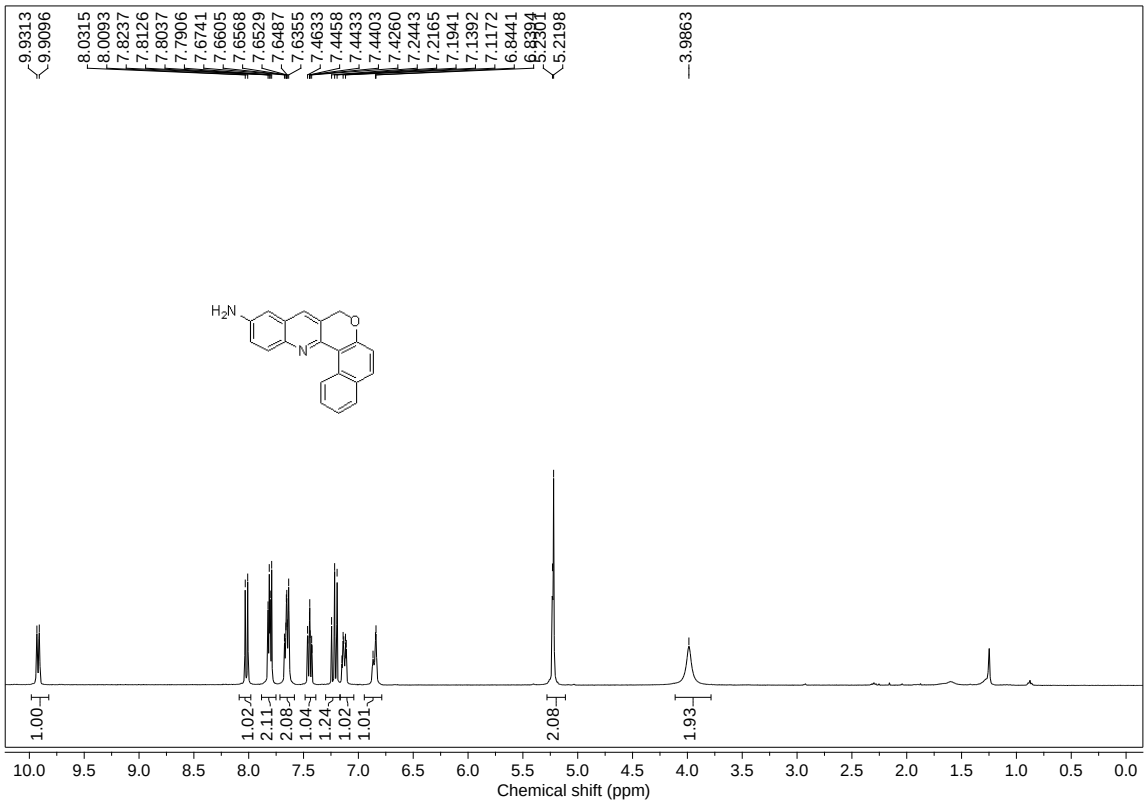

Figure 5.11: ^{1}H NMR spectra of **67** in $CDCl_3$.

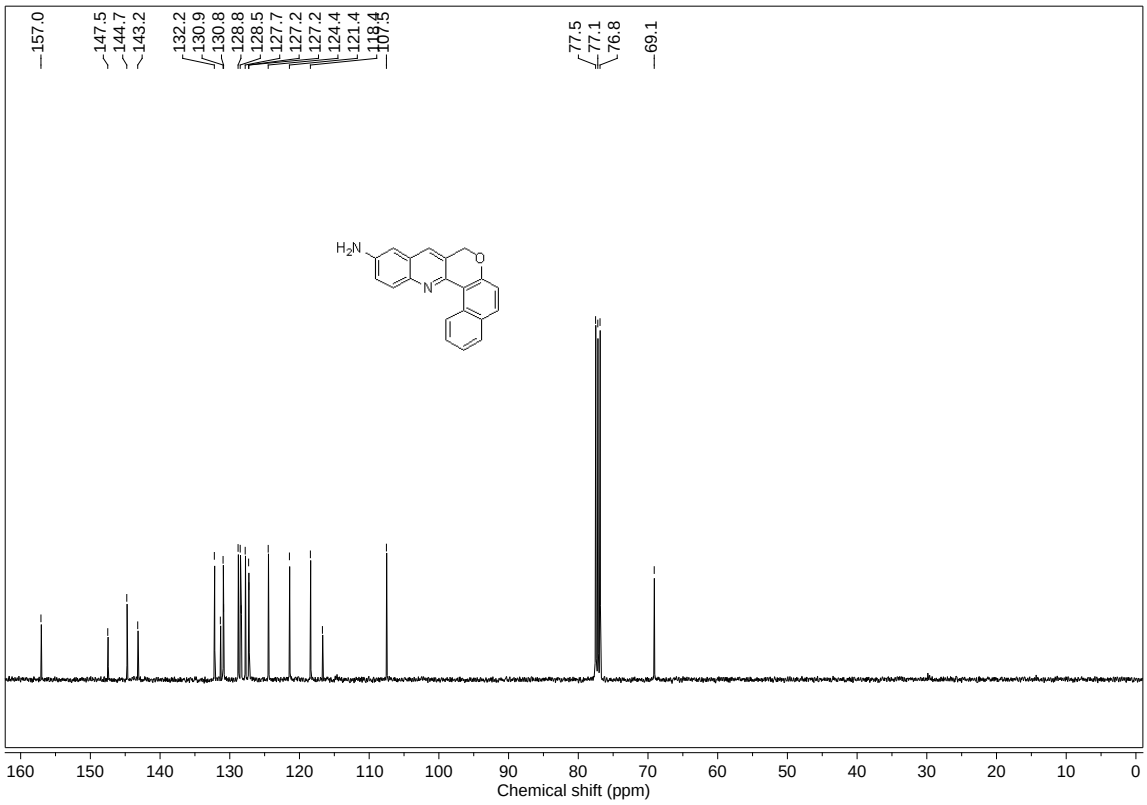

Figure 5.12: ^{13}C NMR spectra of **67** in $CDCl_3$.

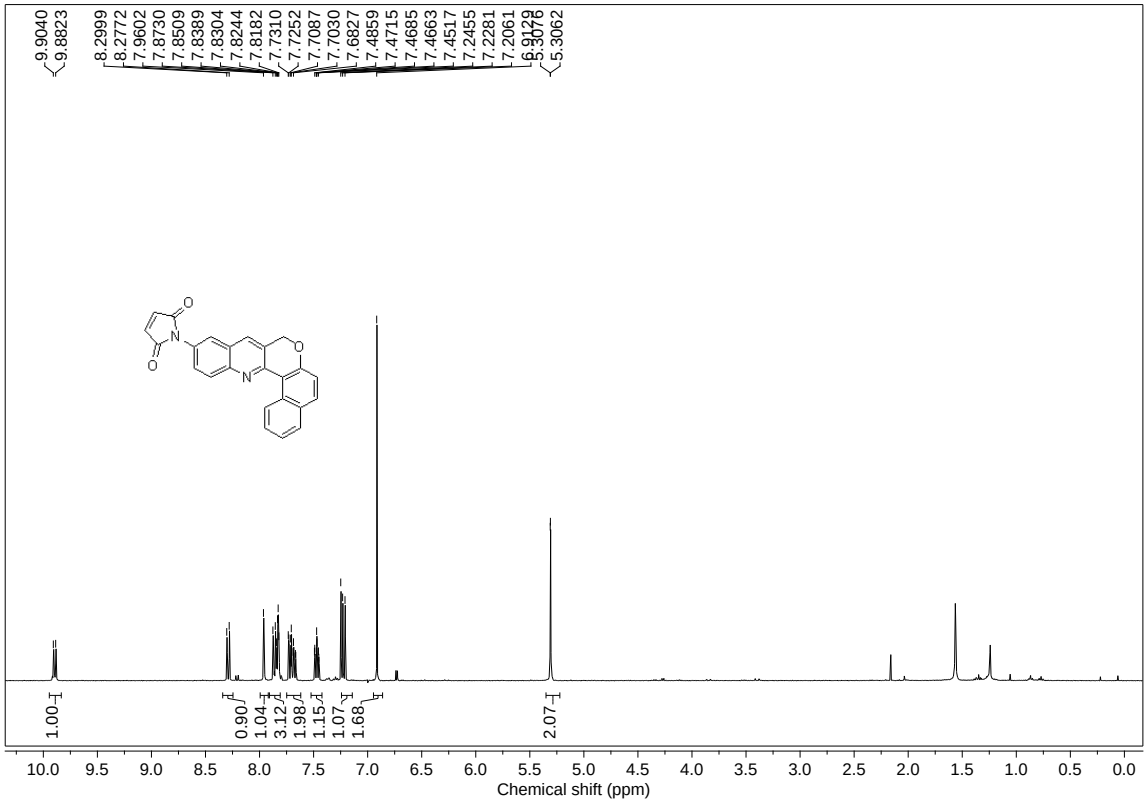

Figure 5.13: ^{1}H NMR spectra of **61** in $CDCl_3$.

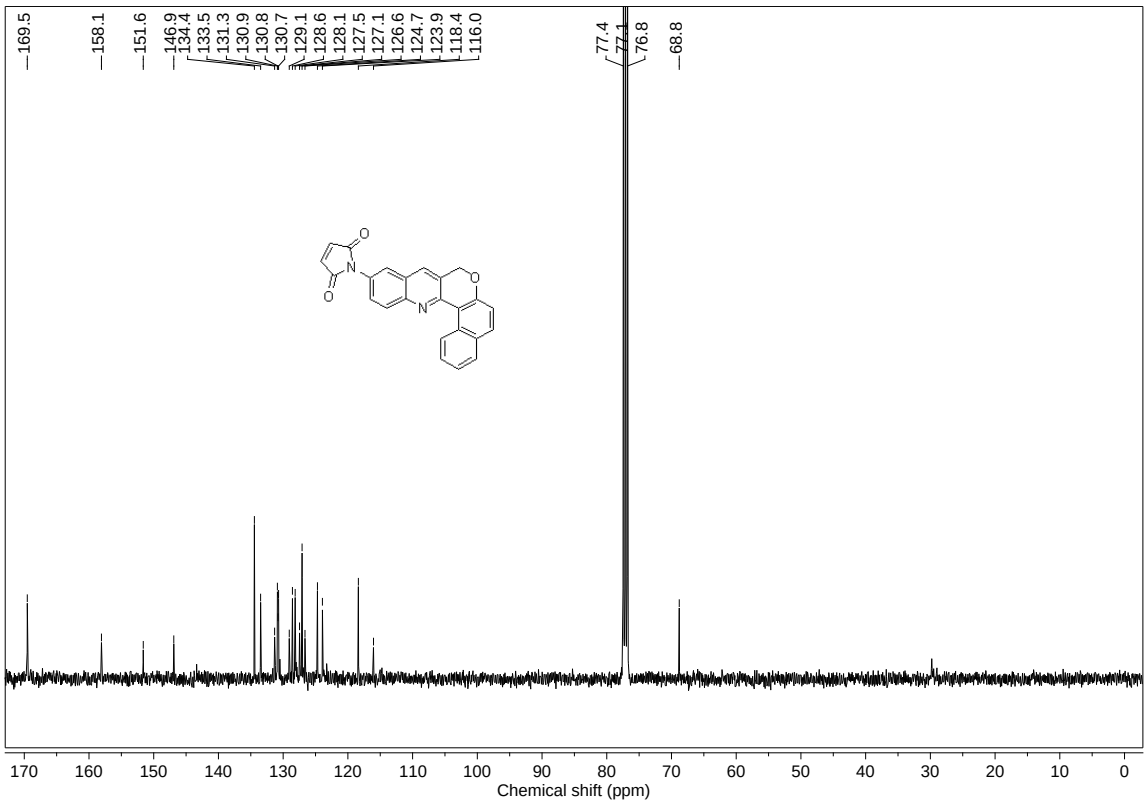

Figure 5.14: ^{13}C NMR spectra of **61** in $CDCl_3$.

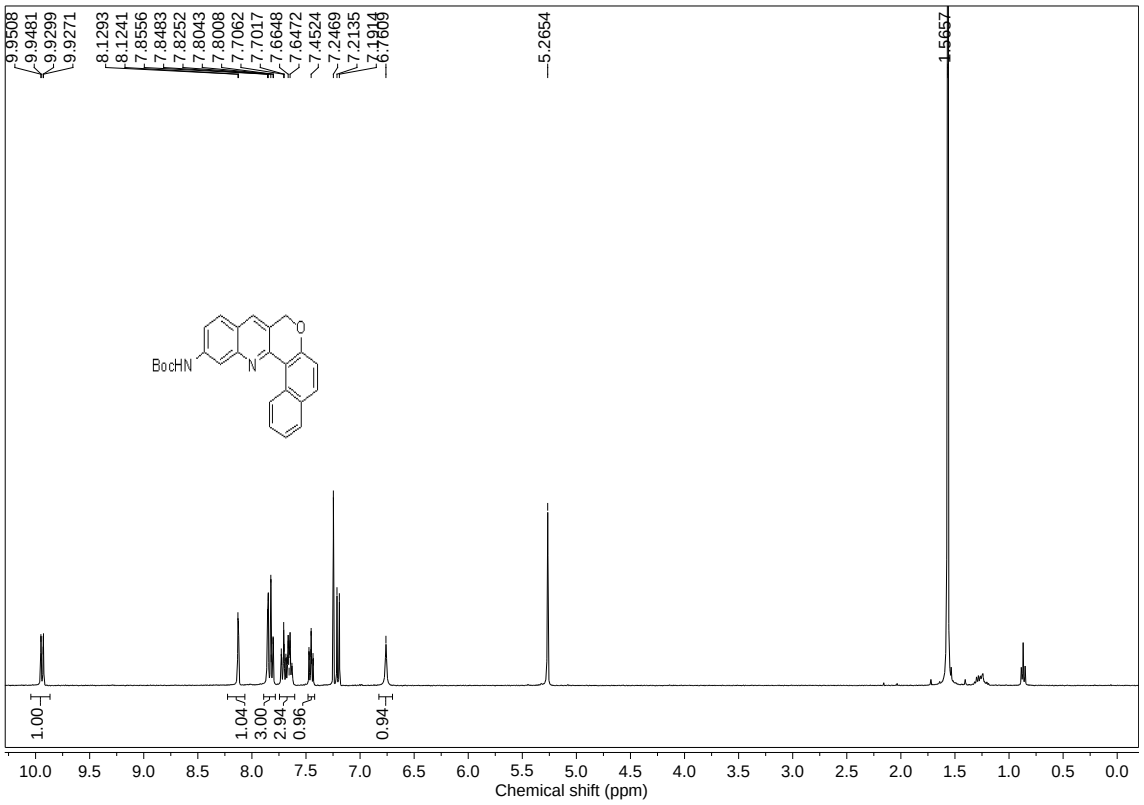

Figure 5.15: ^{1}H NMR spectra of **69** in $CDCl_3$.

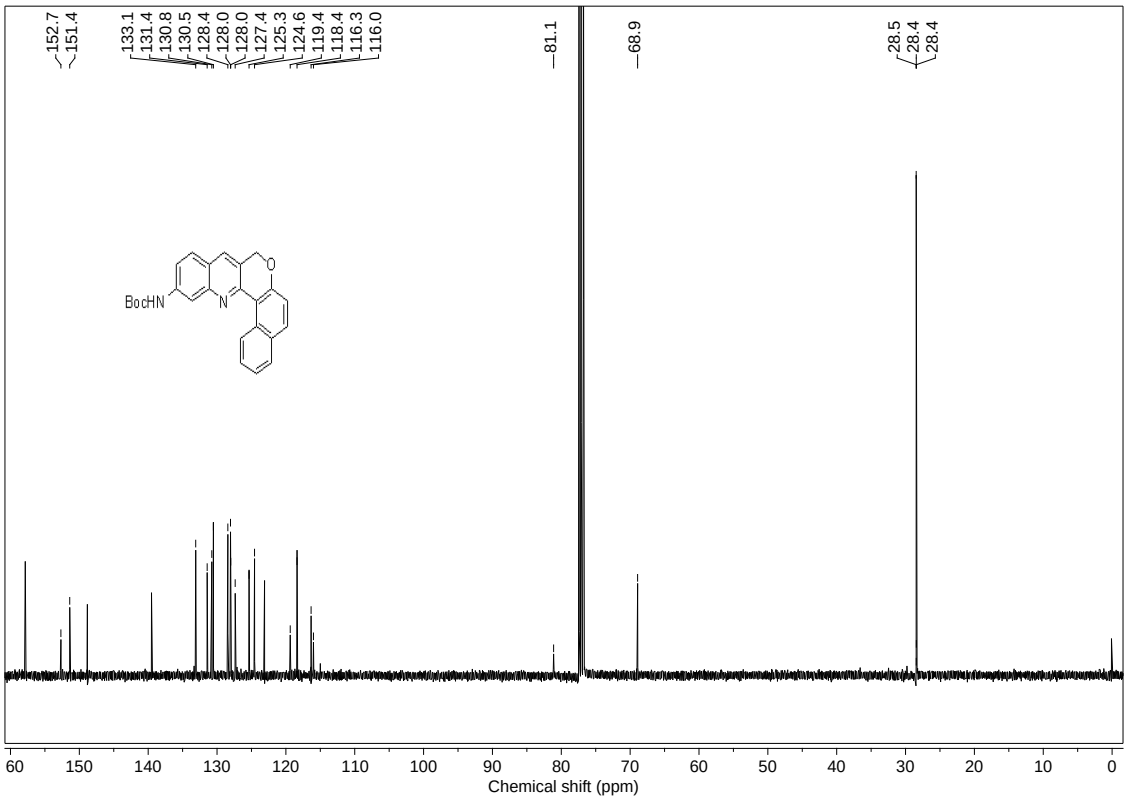

Figure 5.16: ^{13}C NMR spectra of **69** in $CDCl_3$.

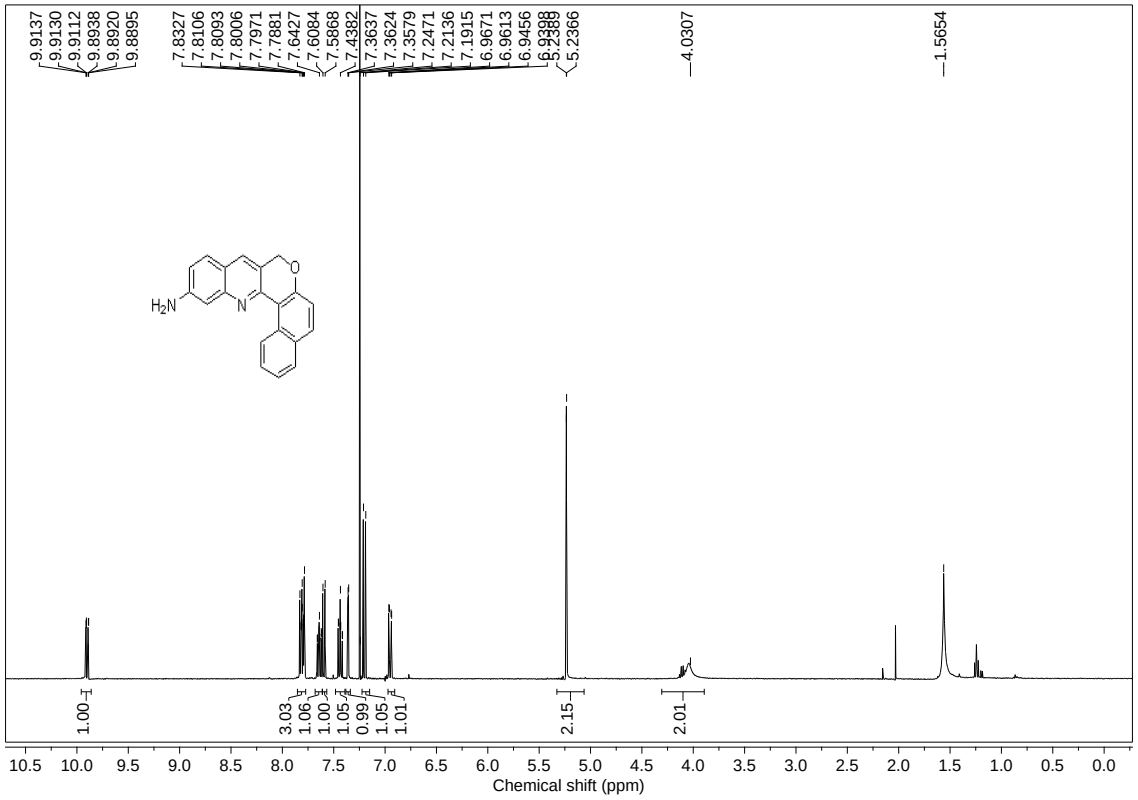

Figure 5.17: ^{1}H NMR spectra of **70** in $CDCl_3$.

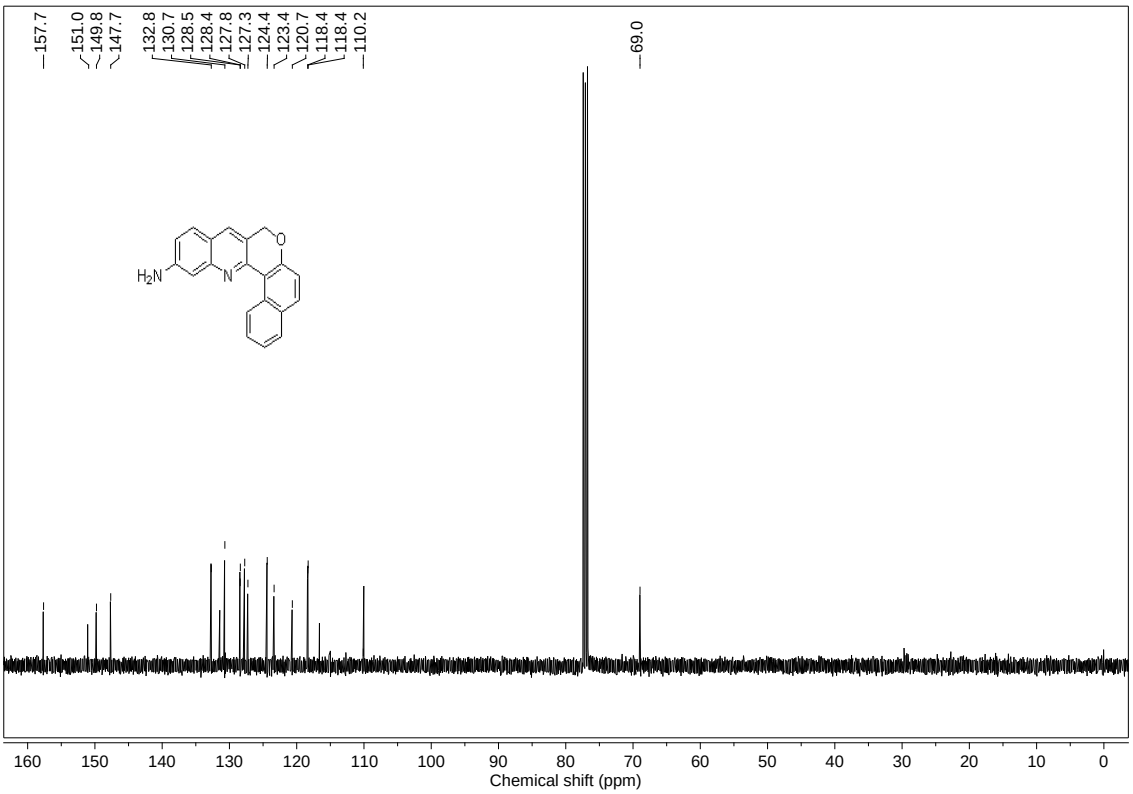

Figure 5.18: ^{13}C NMR spectra of **70** in $CDCl_3$.

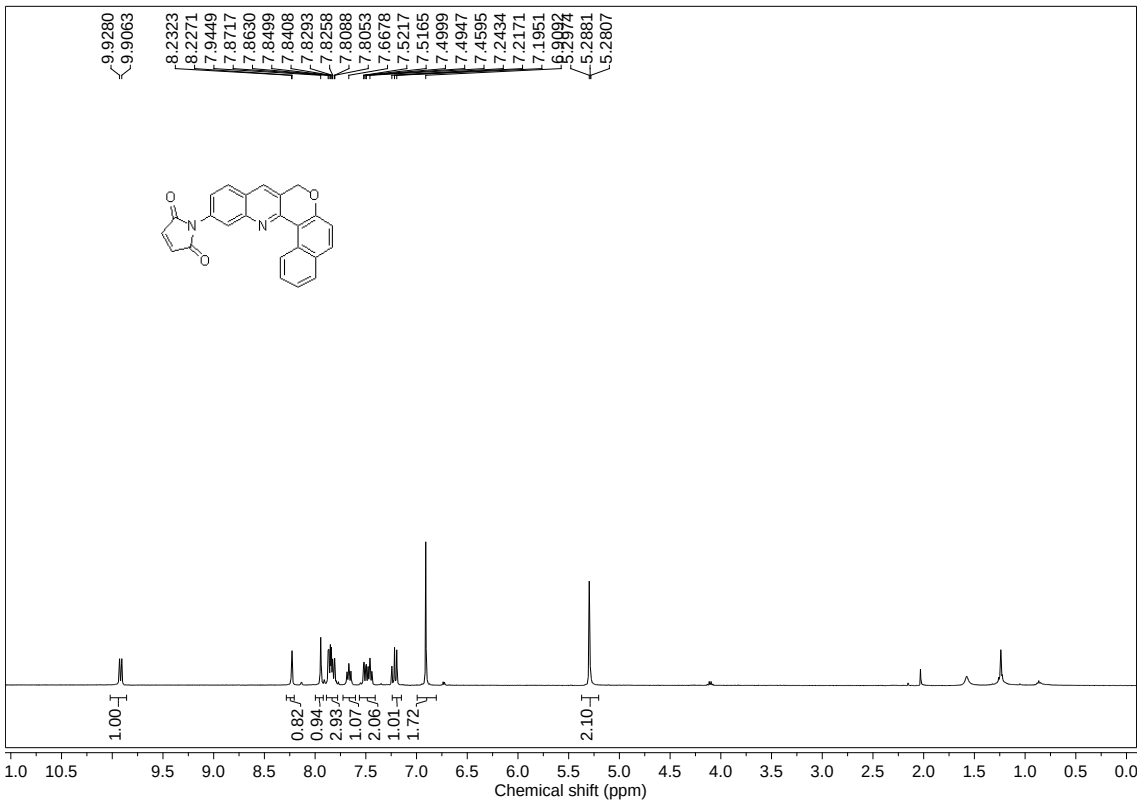

Figure 5.19: ^{1}H NMR spectra of **62** in $CDCl_3$.

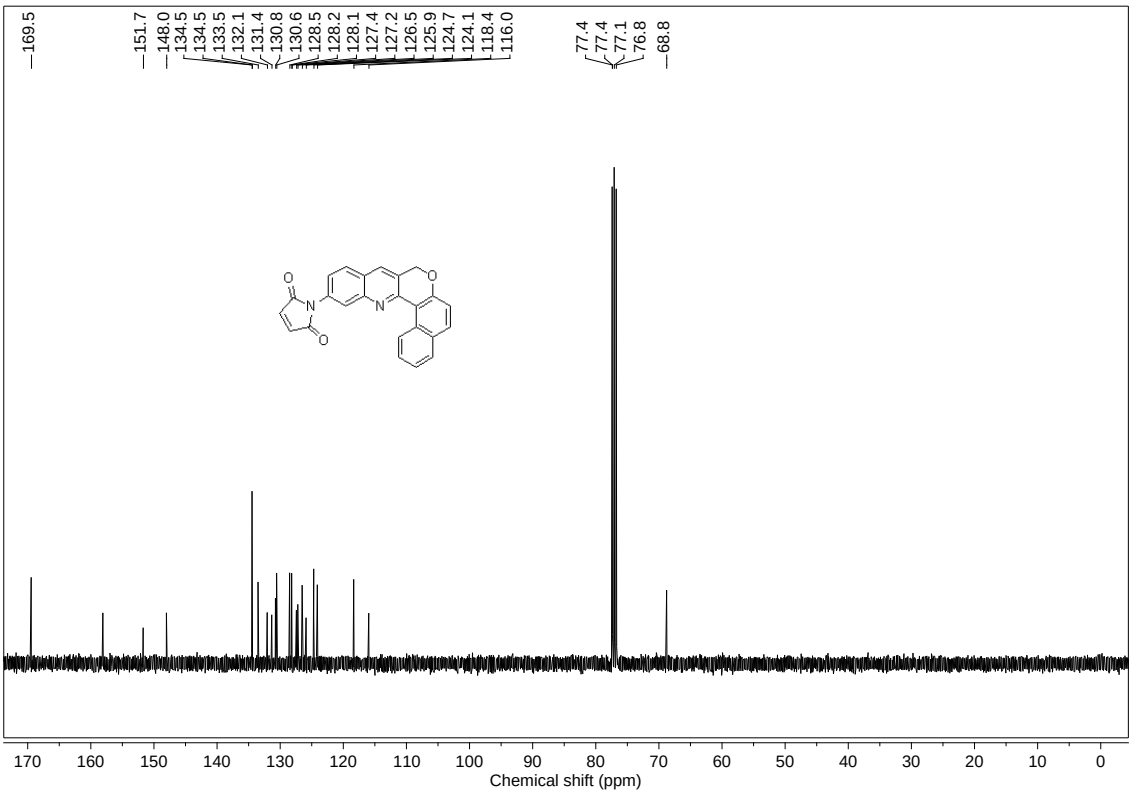

Figure 5.20: ^{13}C NMR spectra of **62** in $CDCl_3$.

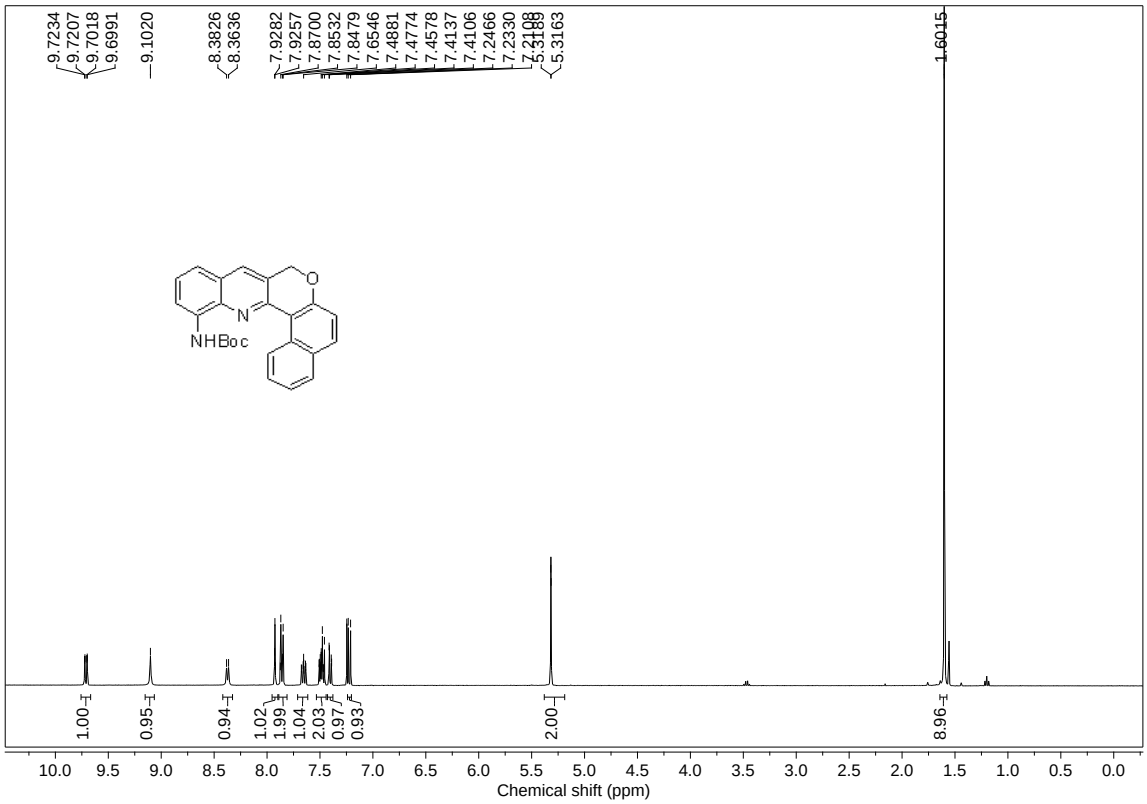

Figure 5.21: ^{1}H NMR spectra of **72** in $CDCl_3$.

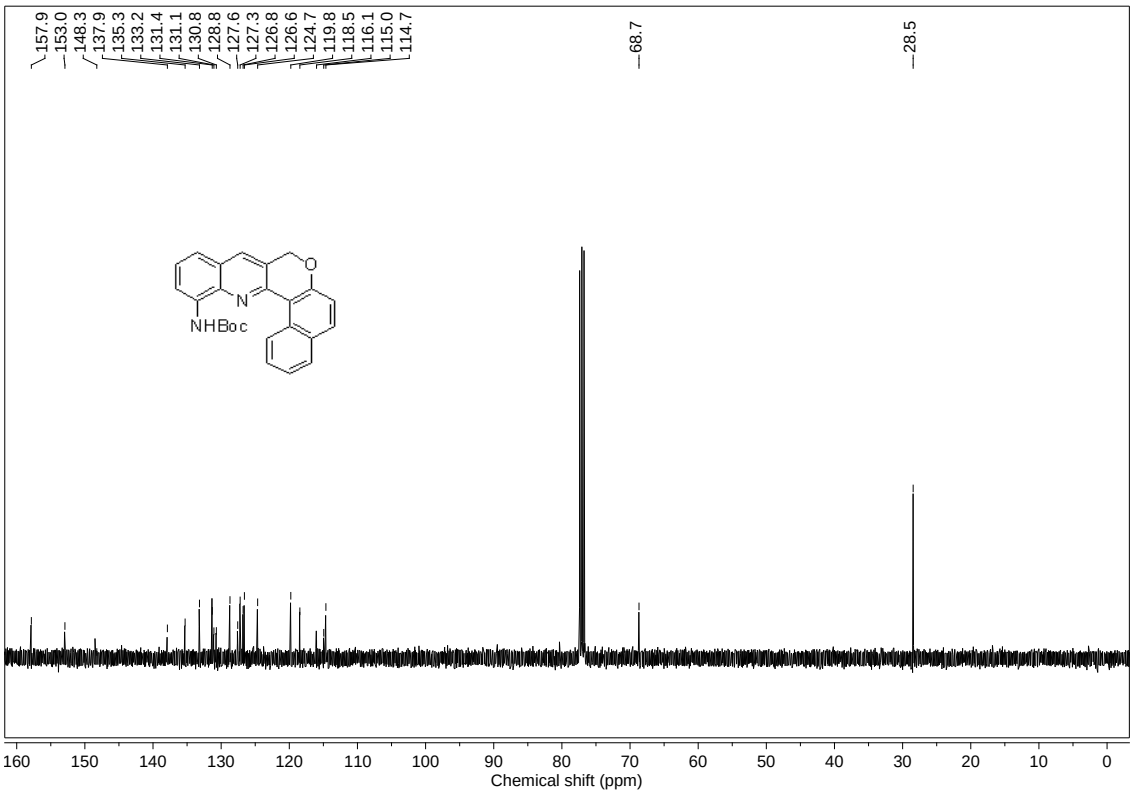

Figure 5.22: ^{13}C NMR spectra of **72** in $CDCl_3$.

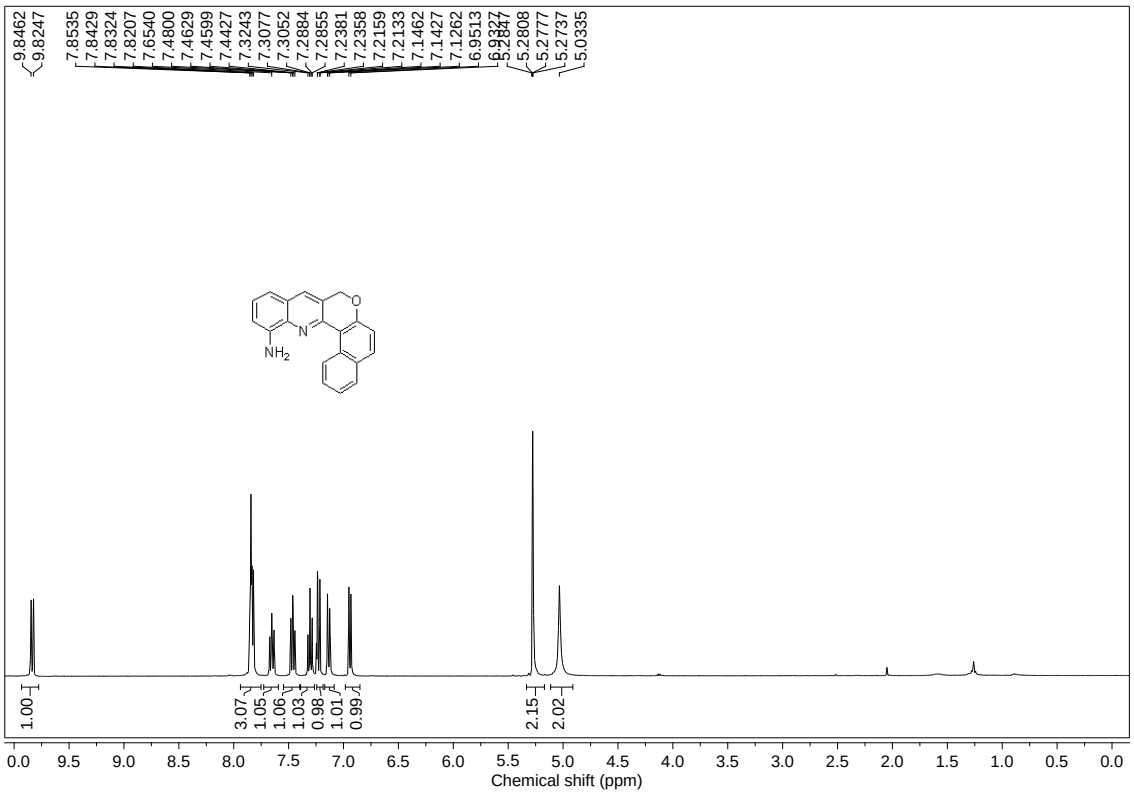

Figure 5.23: ^{1}H NMR spectra of **73** in $CDCl_3$.

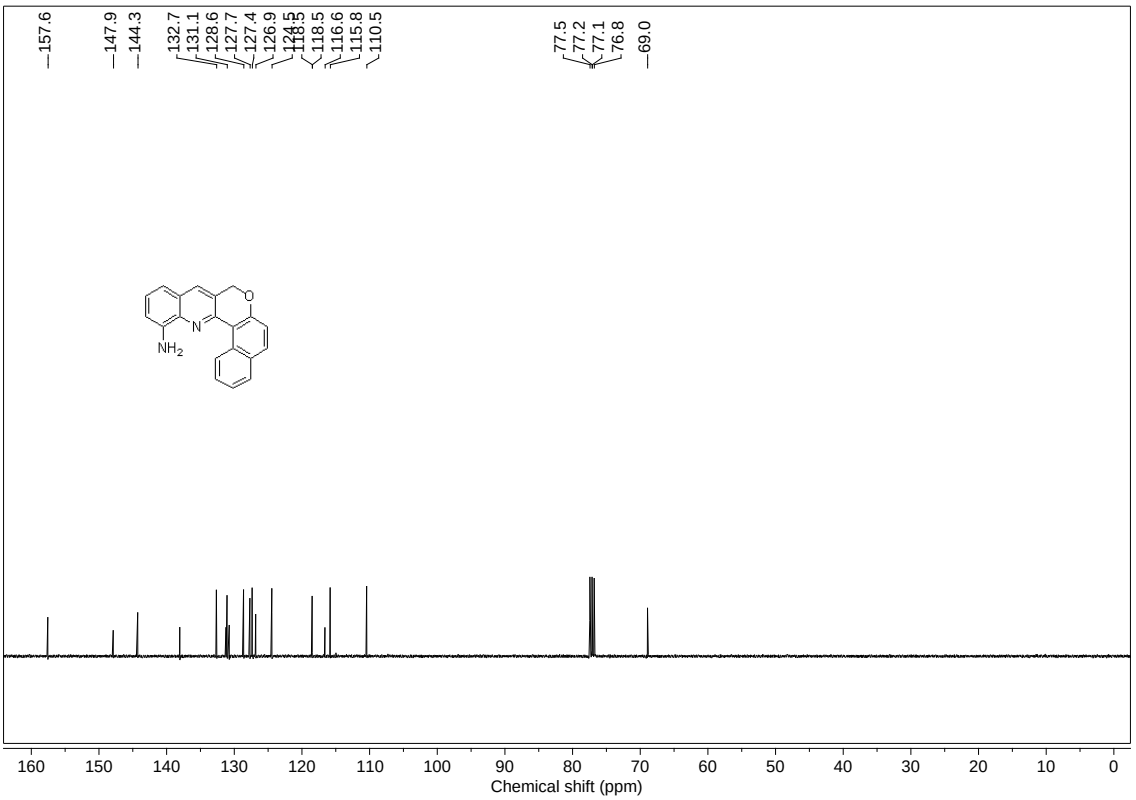

Figure 5.24: ^{13}C NMR spectra of **73** in $CDCl_3$.

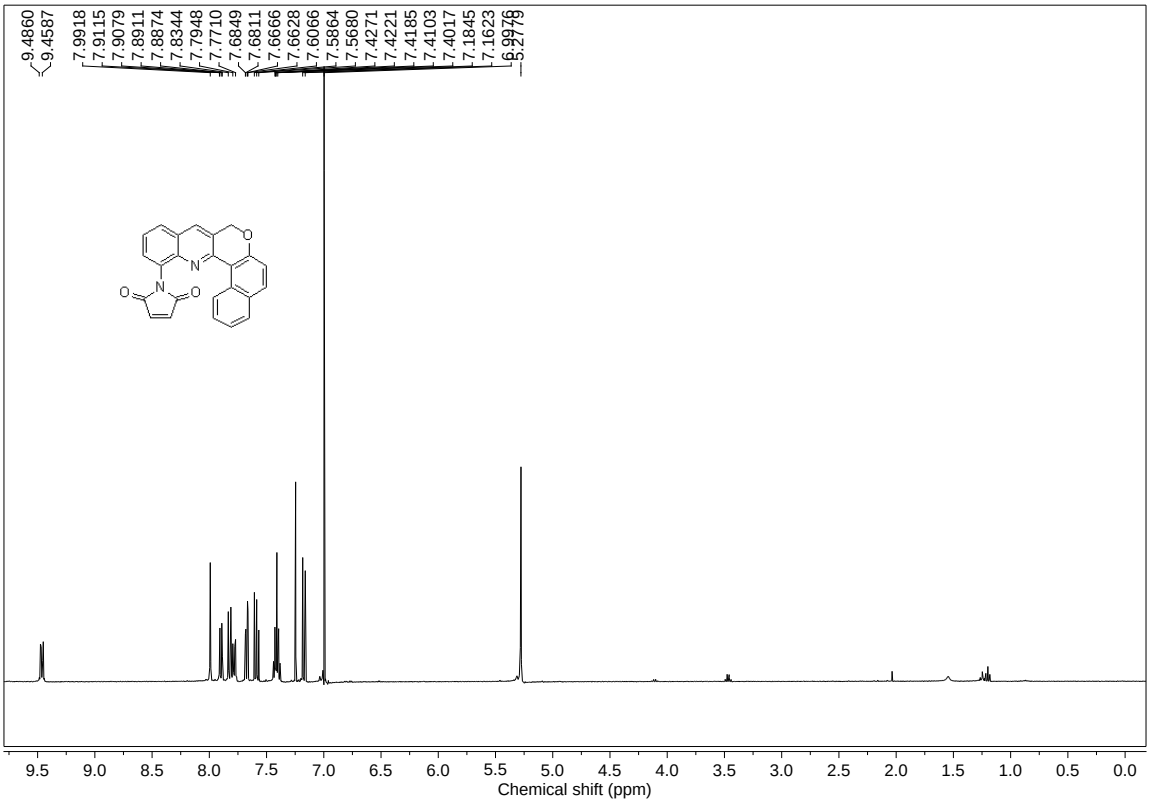

Figure 5.25: ^{1}H NMR spectra of **63** in $CDCl_3$.

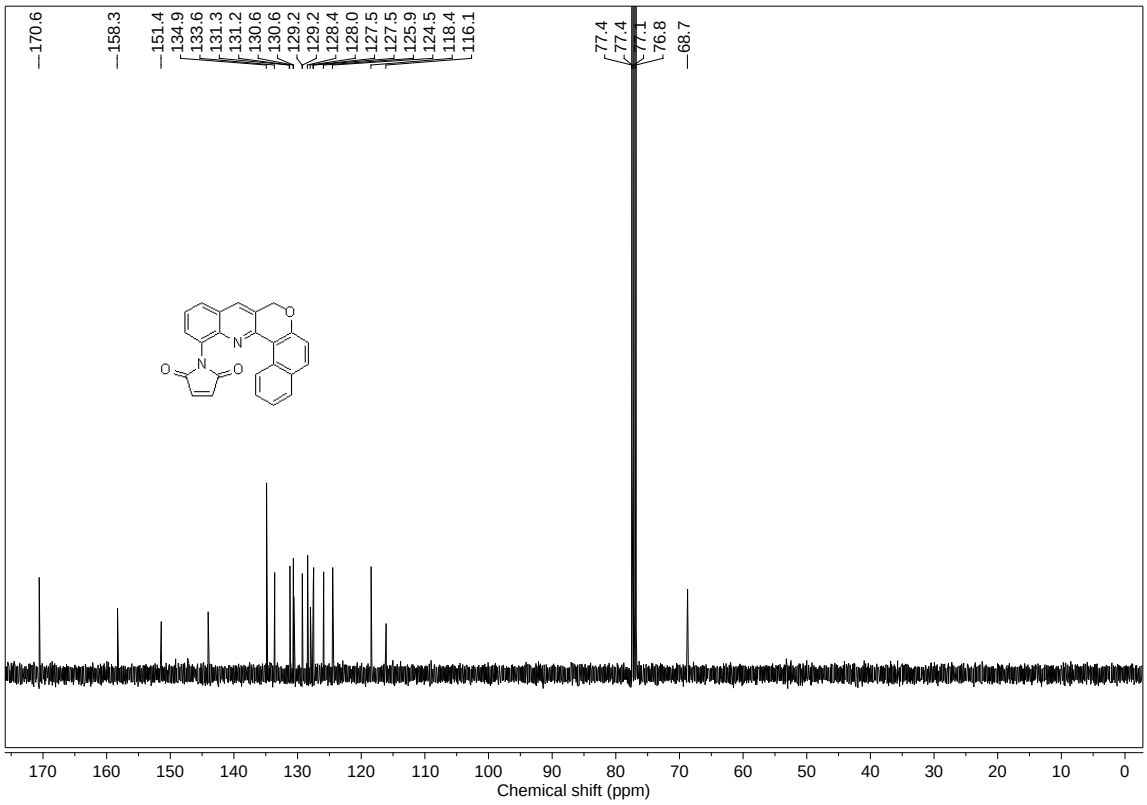

Figure 5.26: ^{13}C NMR spectra of **63** in $CDCl_3$.

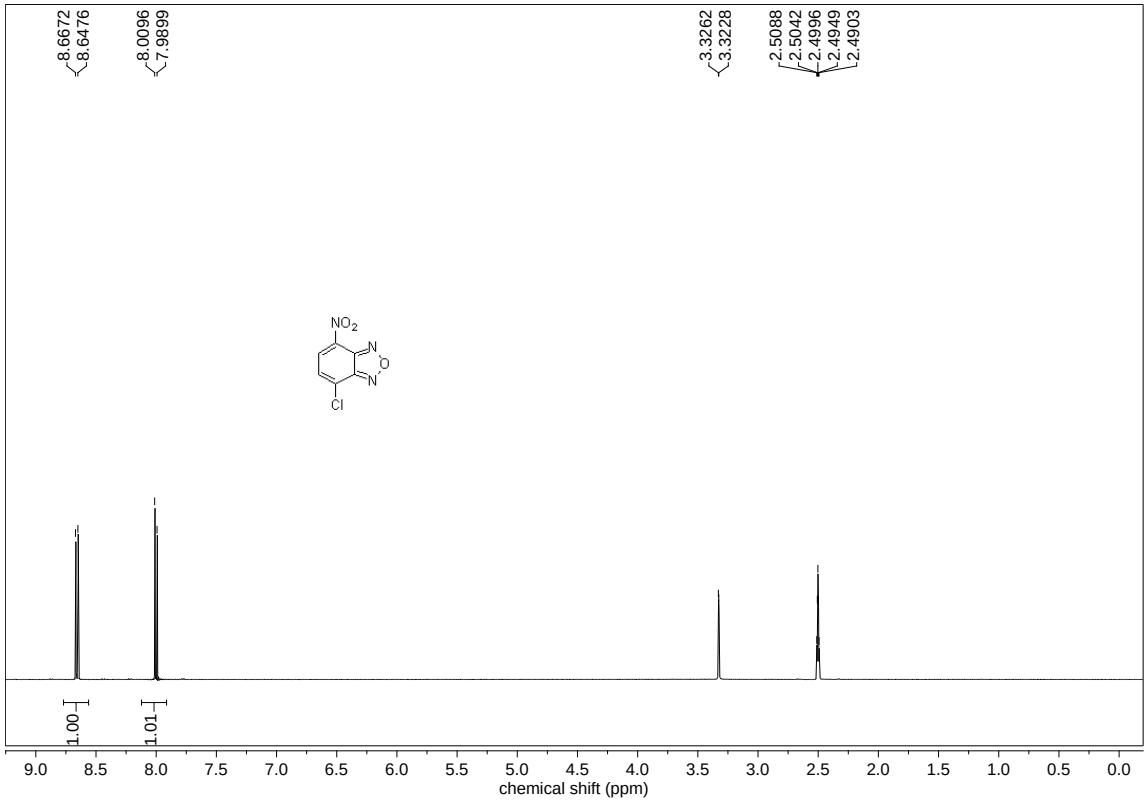

Figure 5.27: ^{1}H NMR spectra of **75** in DMSO-d_6.

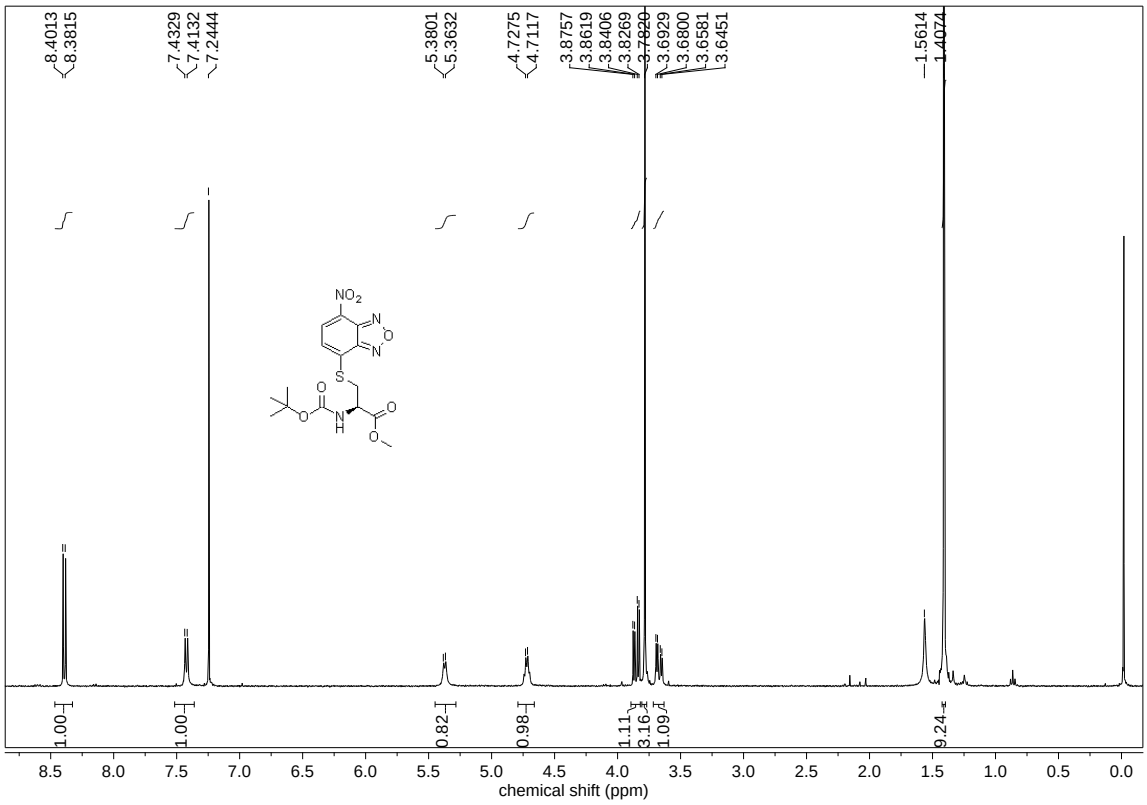

Figure 5.28: ^{1}H NMR spectra of **76** in $CDCl_3$.

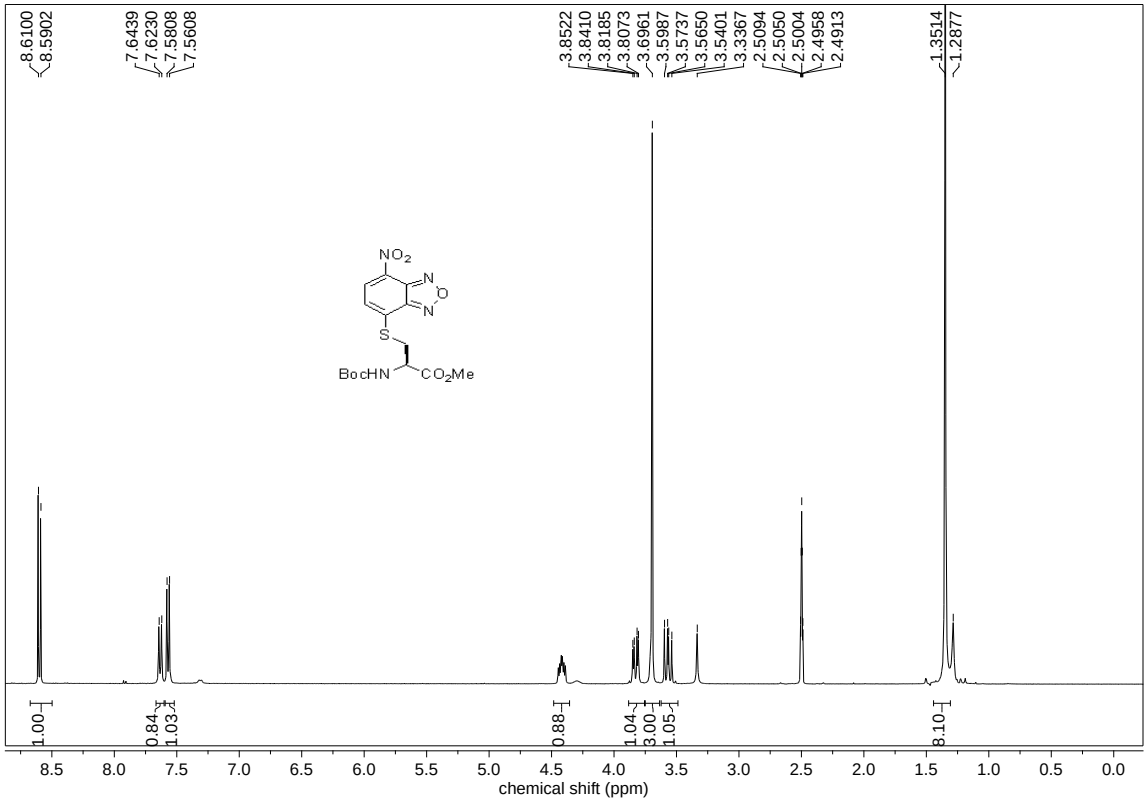

Figure 5.29: ^{1}H NMR spectra of **76** in DMSO-d_6.

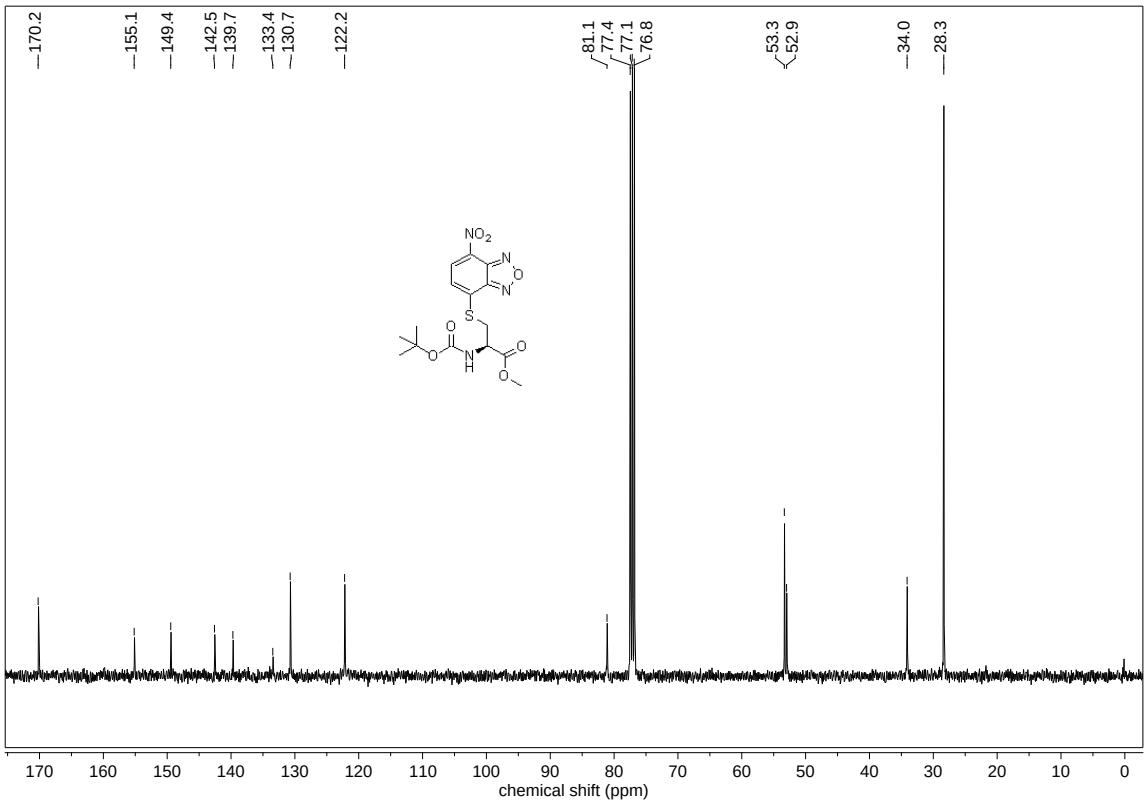

Figure 5.30: ^{13}C NMR spectra of **76** in $CDCl_3$.

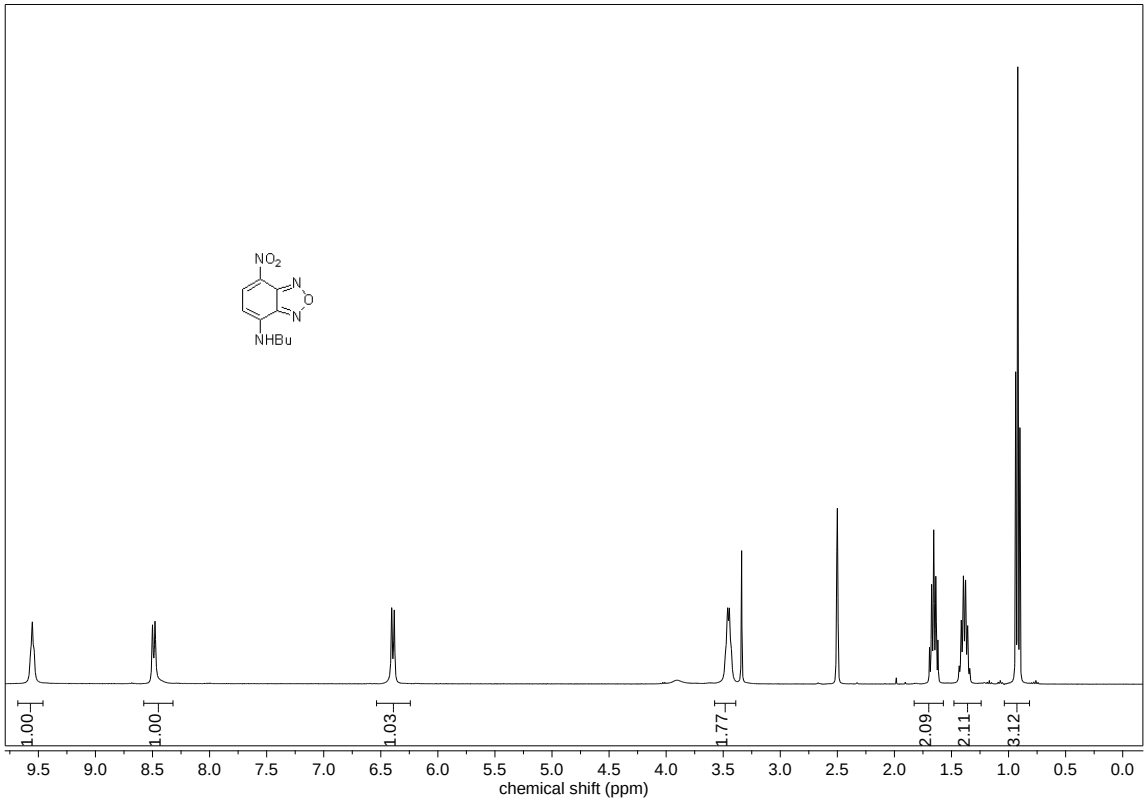

Figure 5.31: ^{1}H NMR spectra of **77** in DMSO-d_6.

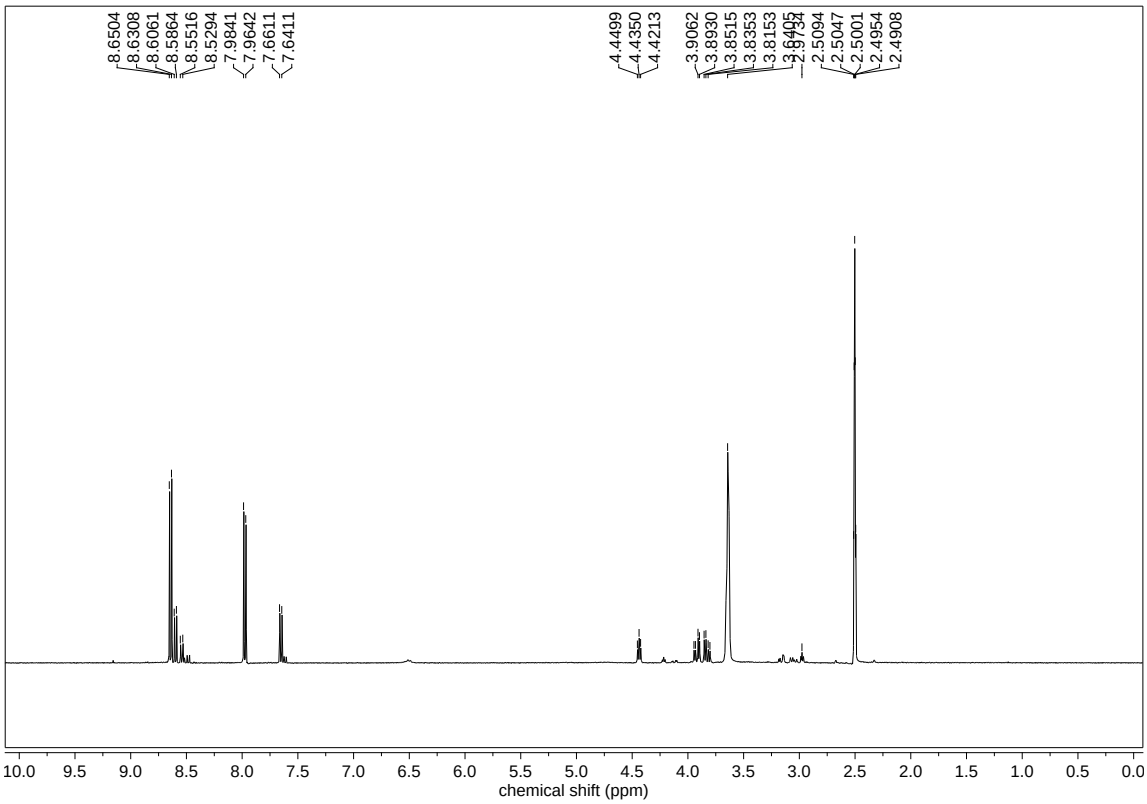

Figure 5.32: ^{1}H NMR spectra of **75+** Cys (2.0 equivalent) in DMSO-d_6.

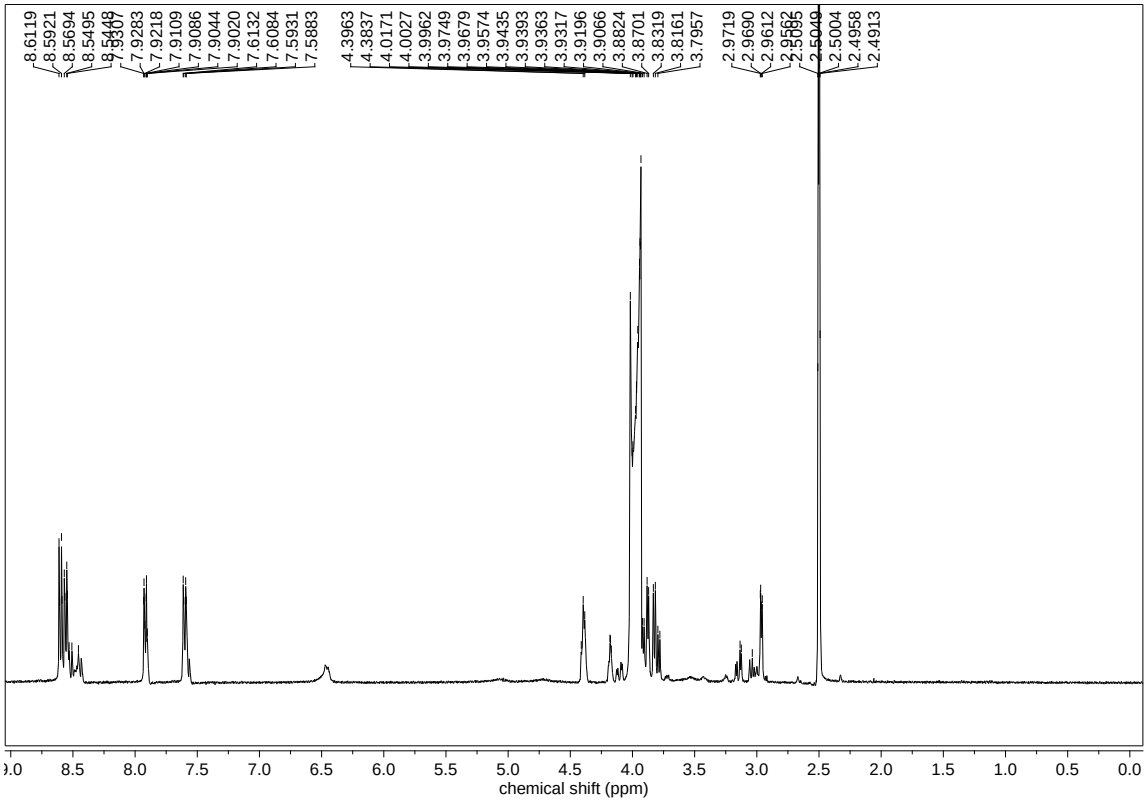

Figure 5.33: ^{1}H NMR spectra of **75+** Cys (4.0 equivalent) in DMSO-d_6.

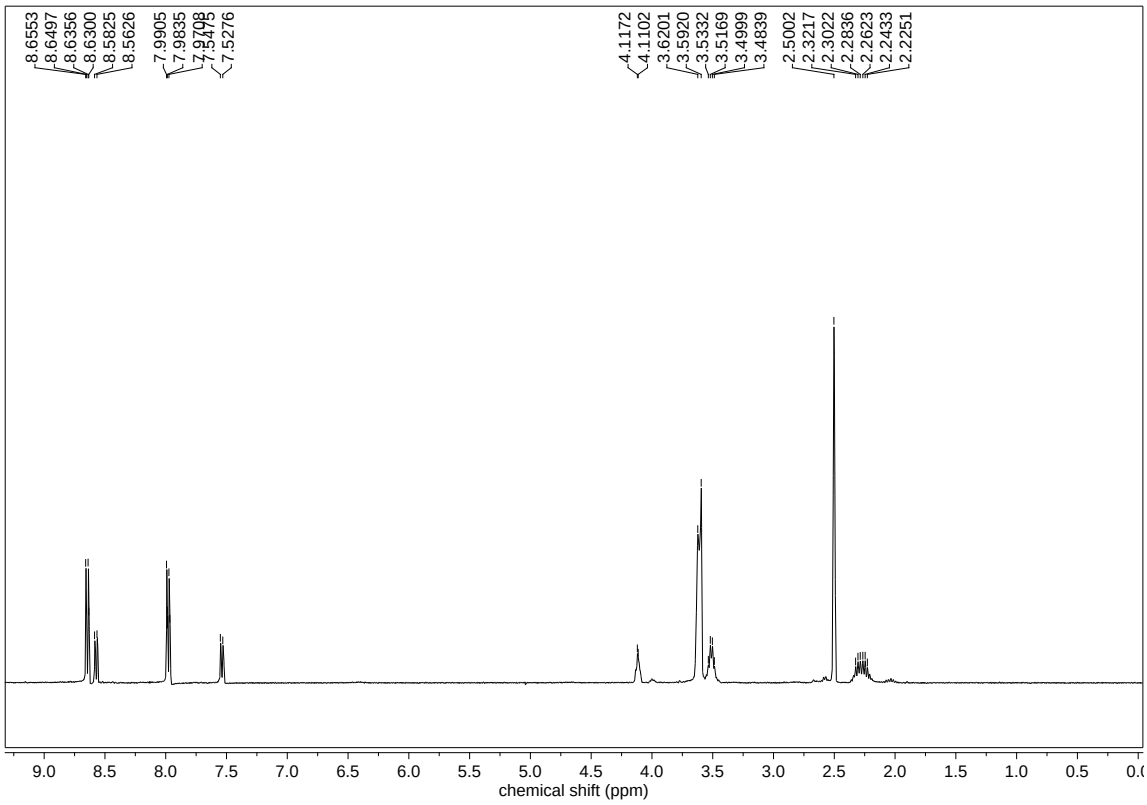

Figure 5.34: ^{1}H NMR spectra of **75+** Hcy (2.0 equivalent) in DMSO-d_6.

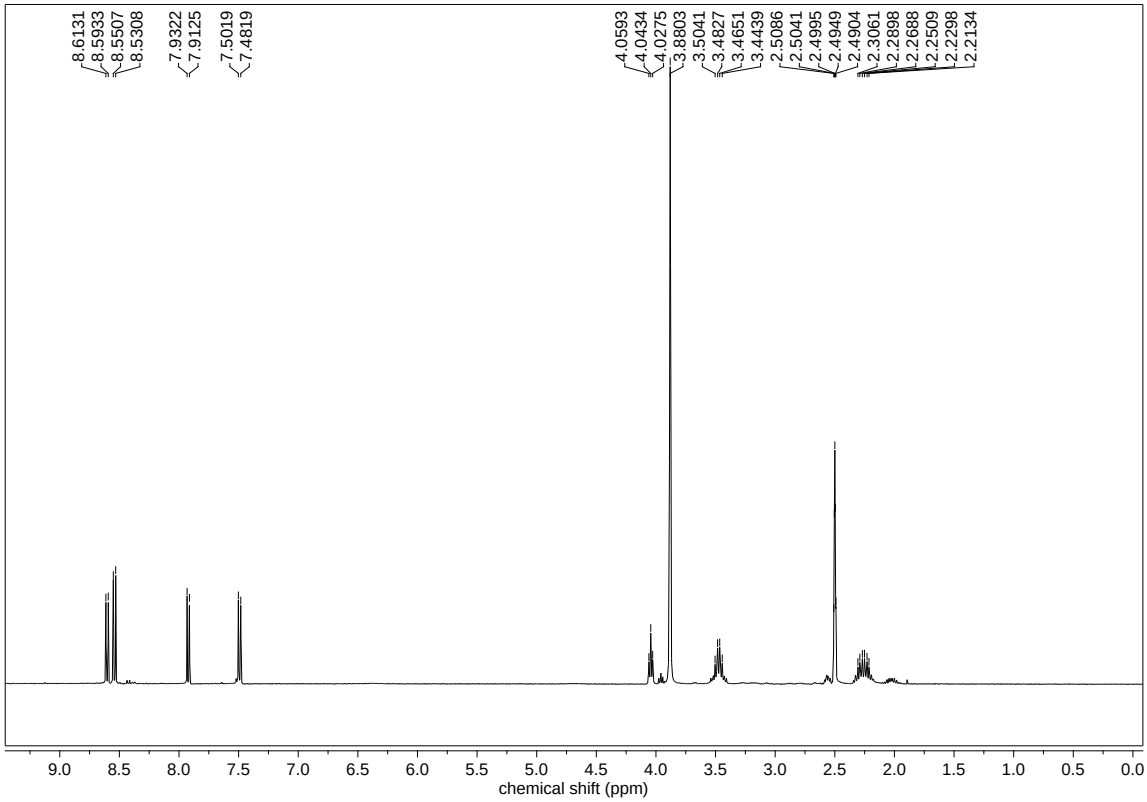

Figure 5.35: ^{1}H NMR spectra of **75+** Cys (4.0 equivalent) in DMSO-d_6.

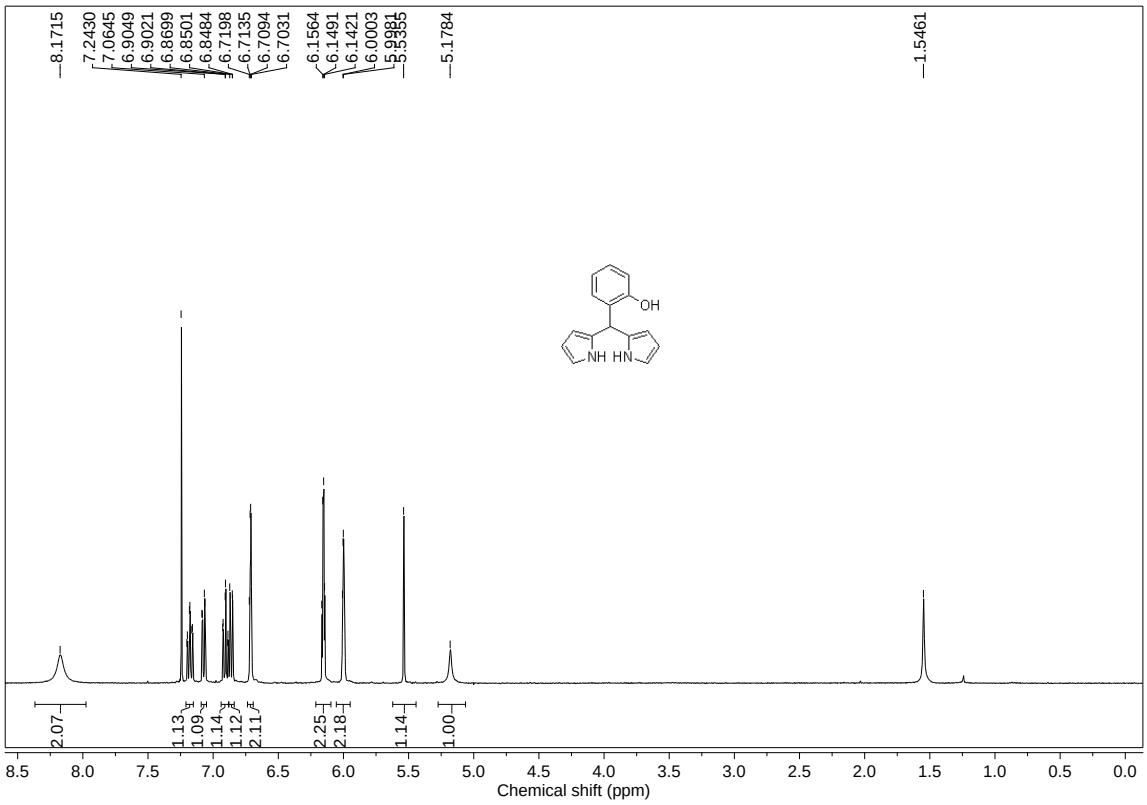

Figure 5.36: ^{1}H NMR spectra of **82** in $CDCl_3$.

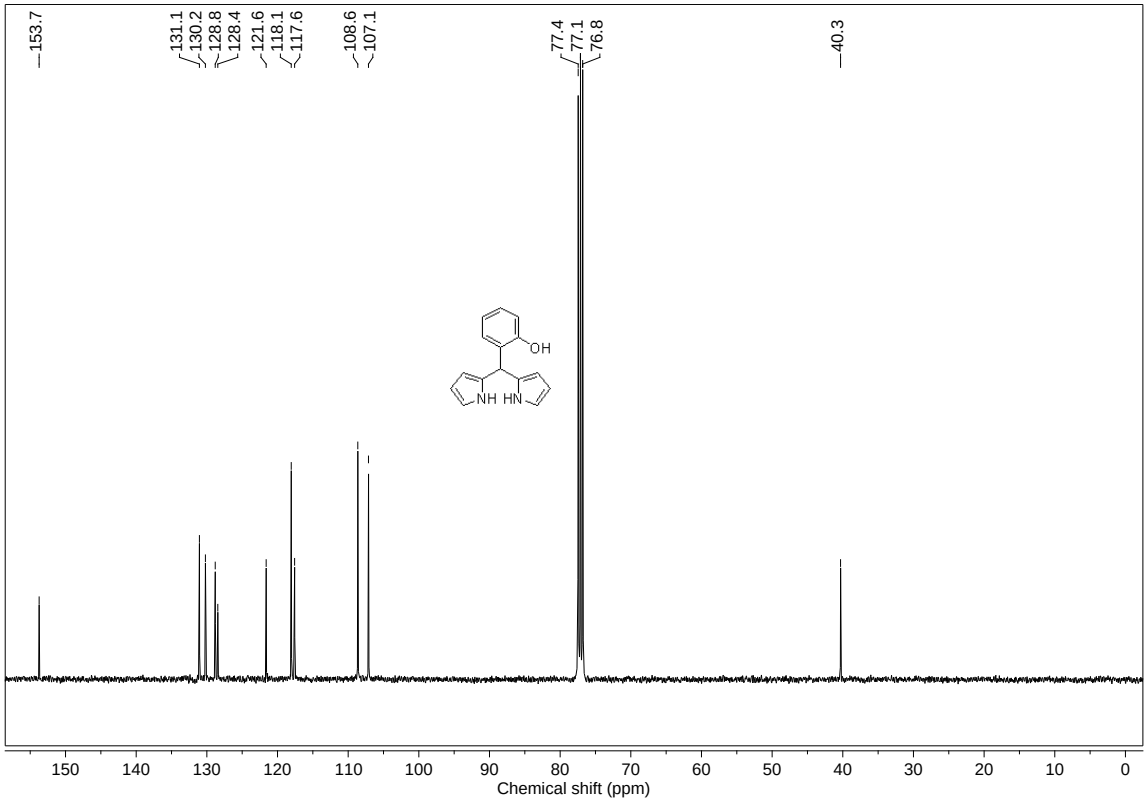

Figure 5.37: ^{13}C NMR spectra of **82** in $CDCl_3$.

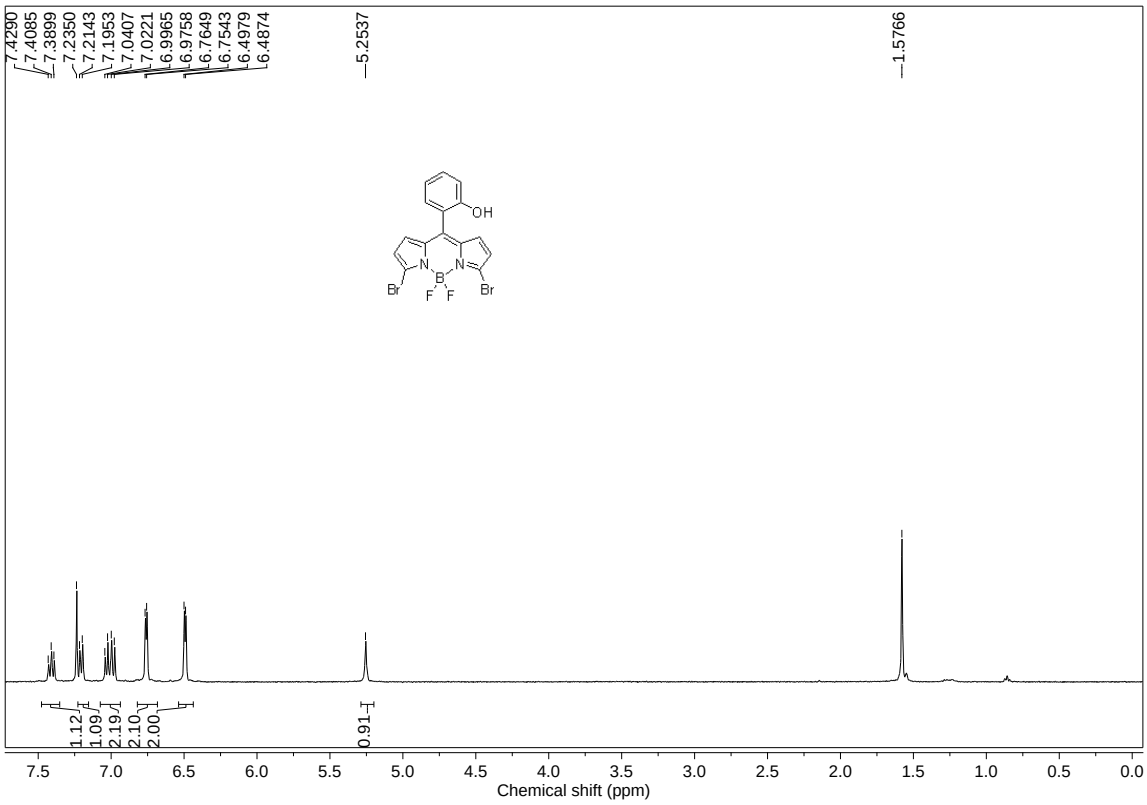

Figure 5.38: ^{1}H NMR spectra of **84** in $CDCl_3$.

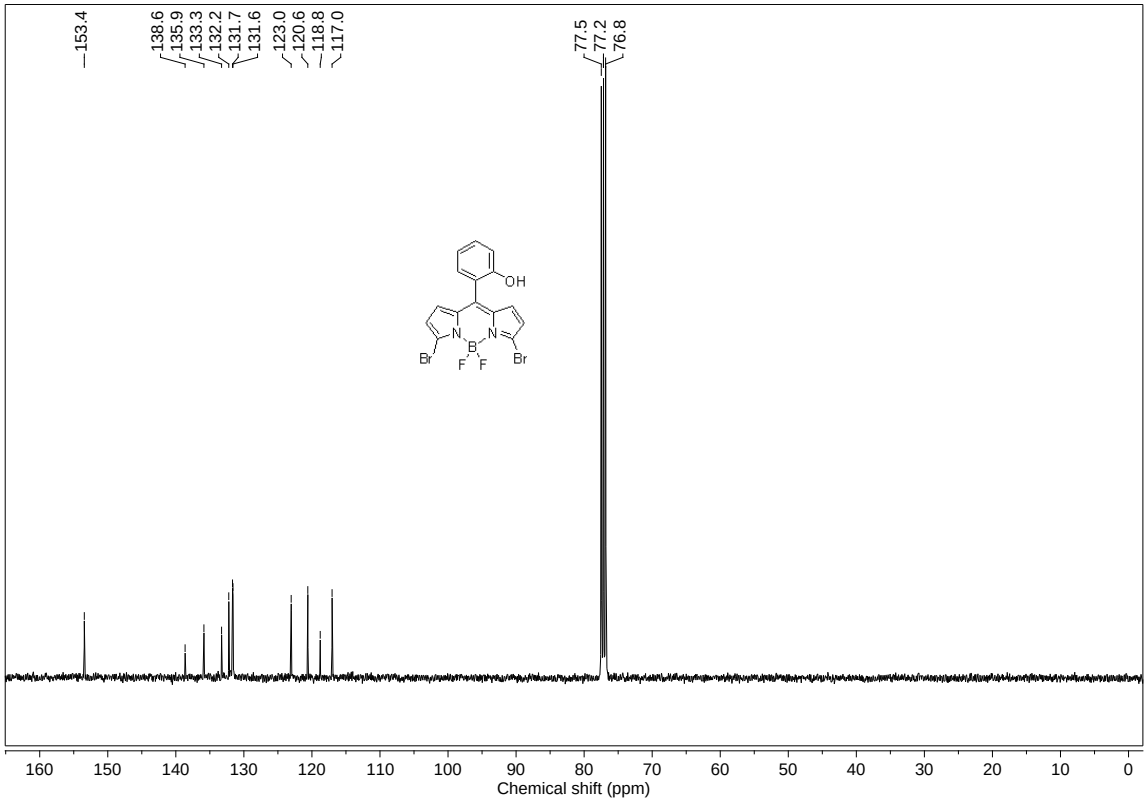

Figure 5.39: ^{1}H NMR spectra of **84** in $CDCl_3$.

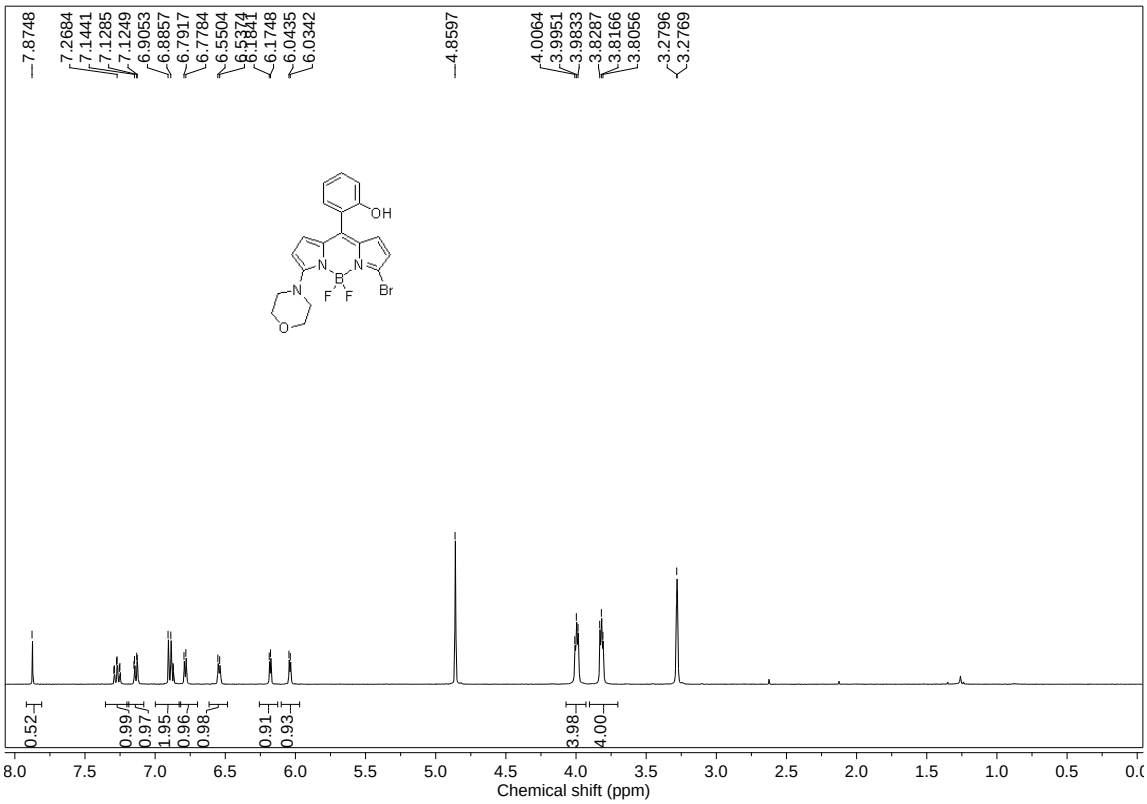

Figure 5.40: ^{1}H NMR spectra of **85** in CD_3OD.

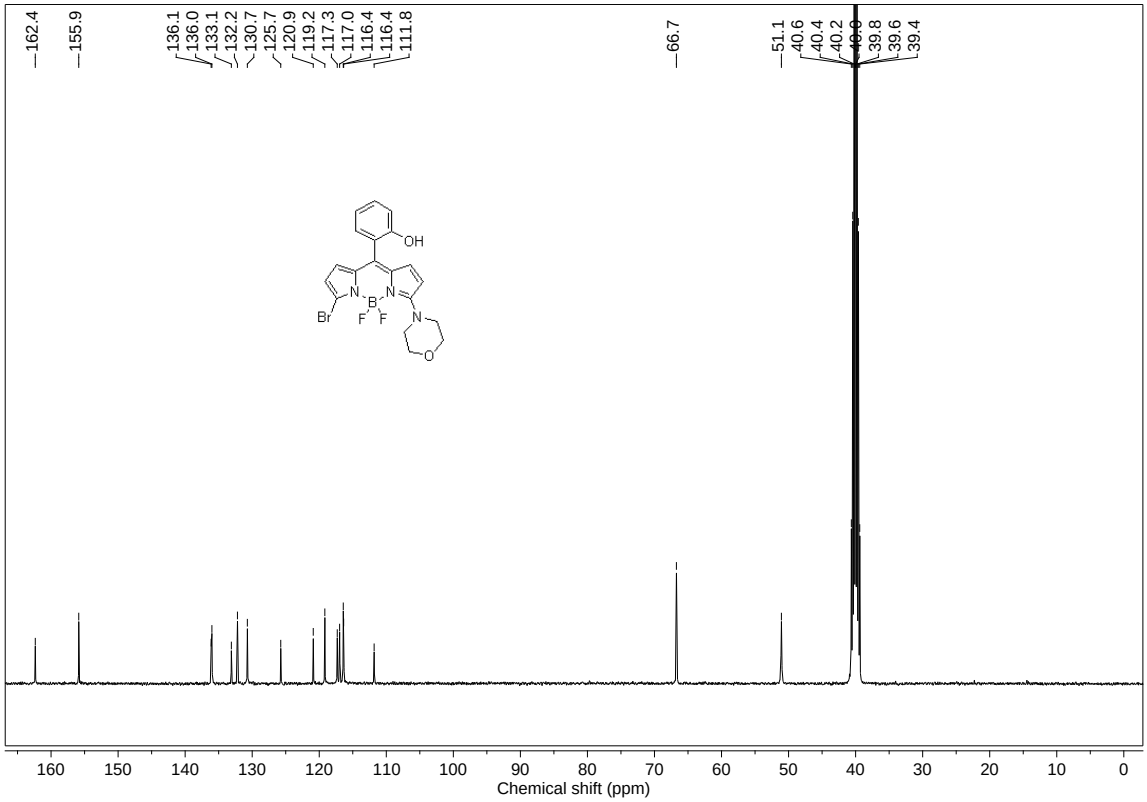

Figure 5.41: ^{13}C NMR spectra of **85** in DMSO-d_6.

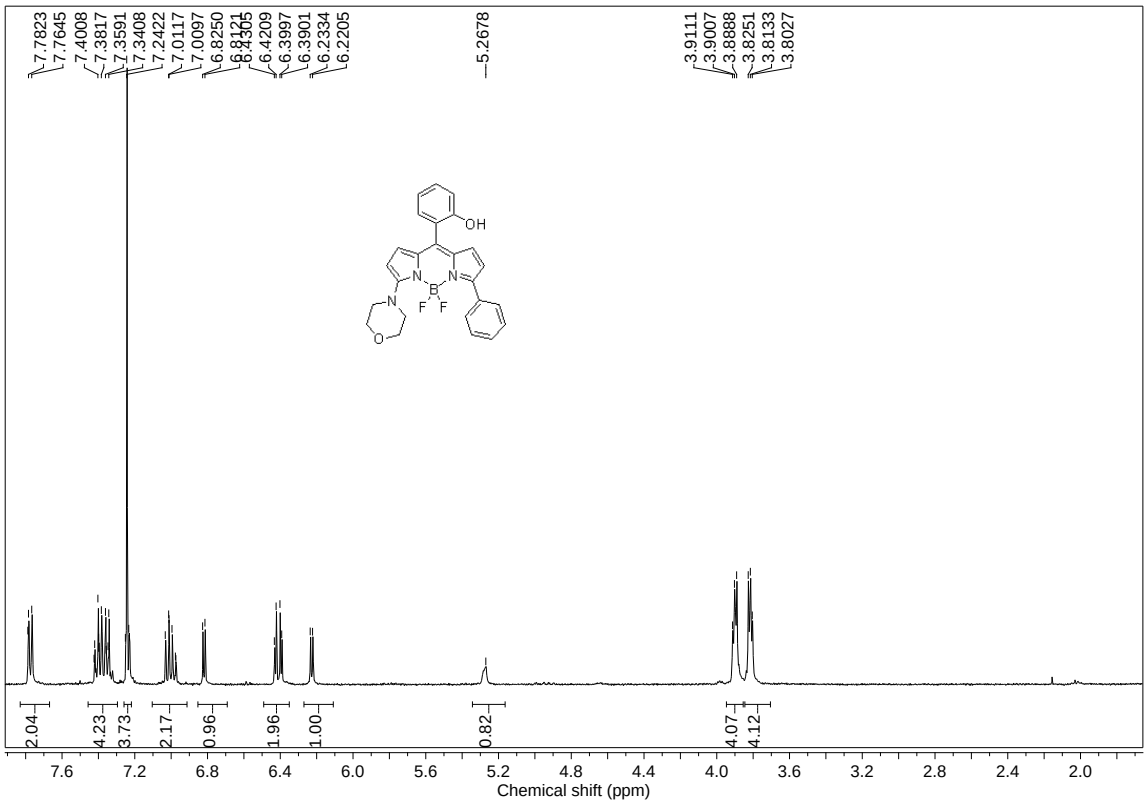

Figure 5.42: ^{1}H NMR spectra of **86** in $CDCl_3$.

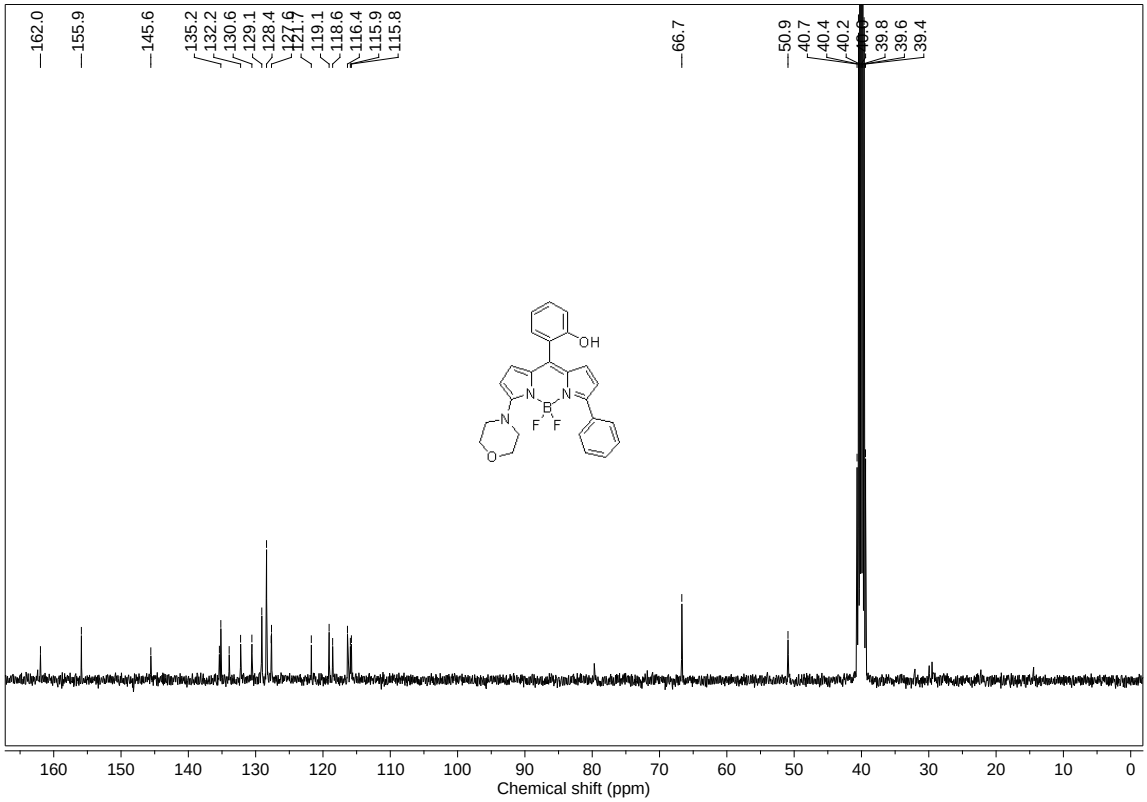

Figure 5.43: ^{1}H NMR spectra of **86** in DMSO-d_6.

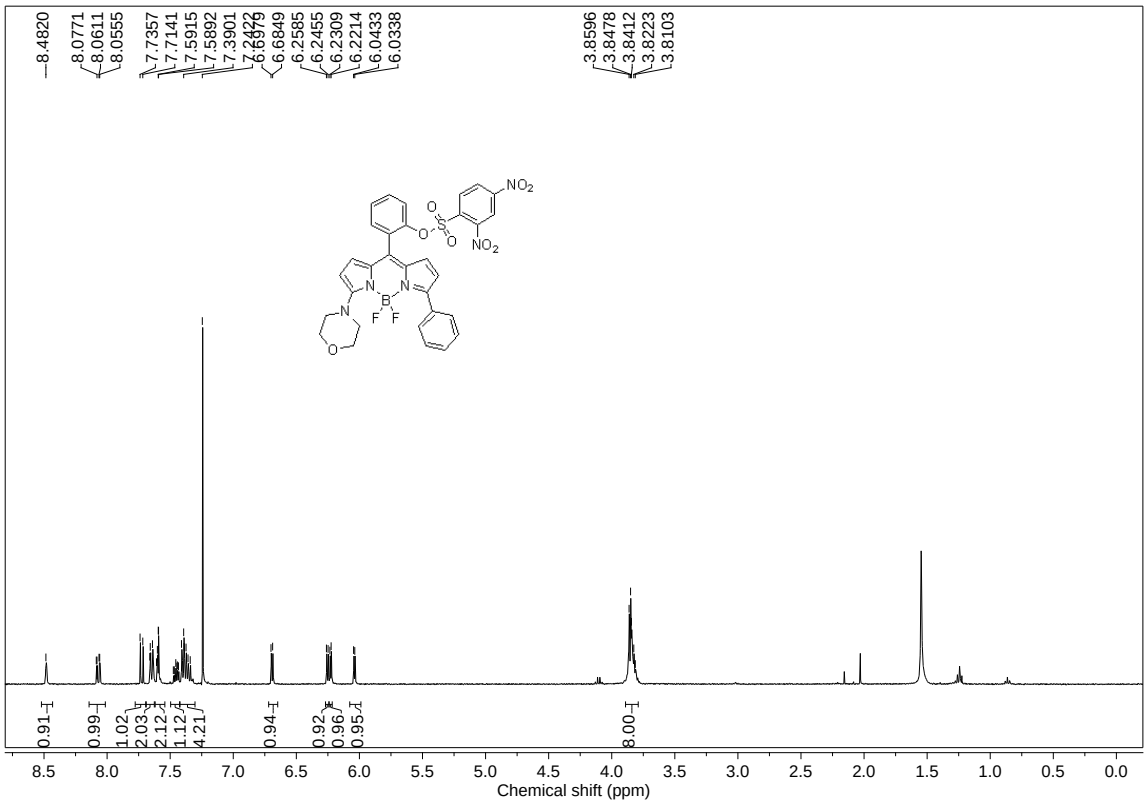

Figure 5.44: ^{1}H NMR spectra of **81** in $CDCl_3$.

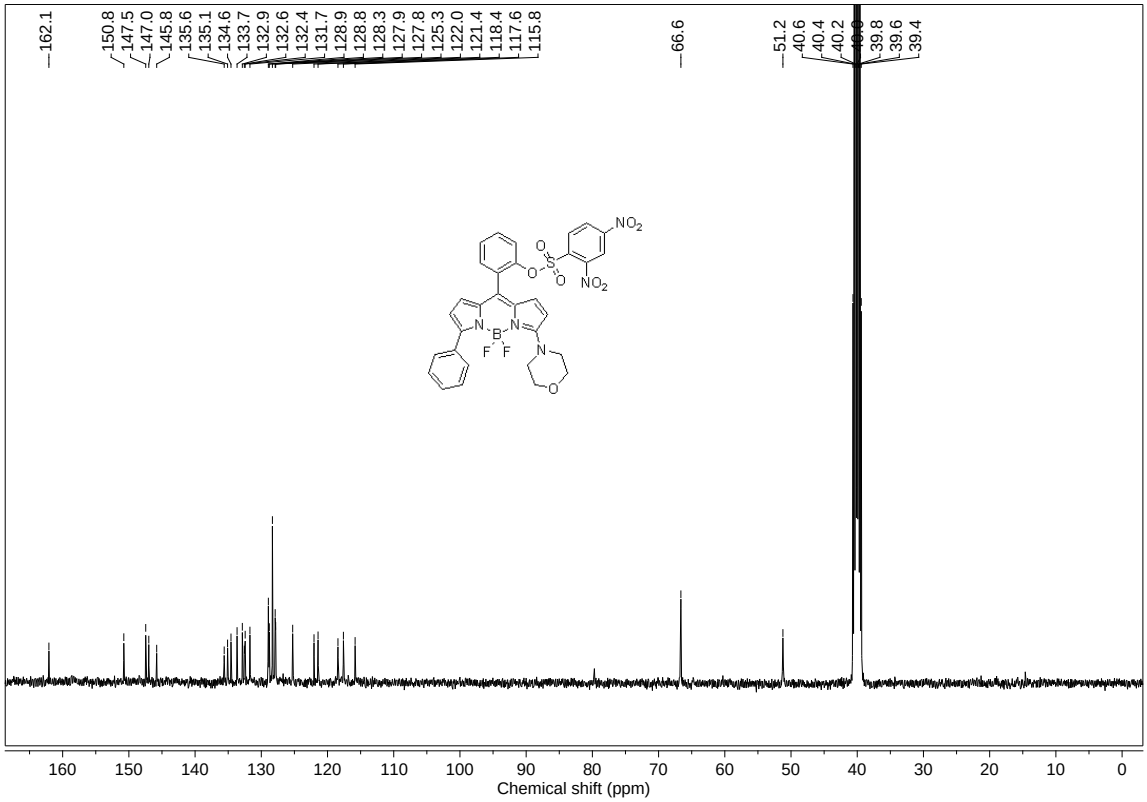

Figure 5.45: ^{13}C NMR spectra of **81** in DMSO-d_6.

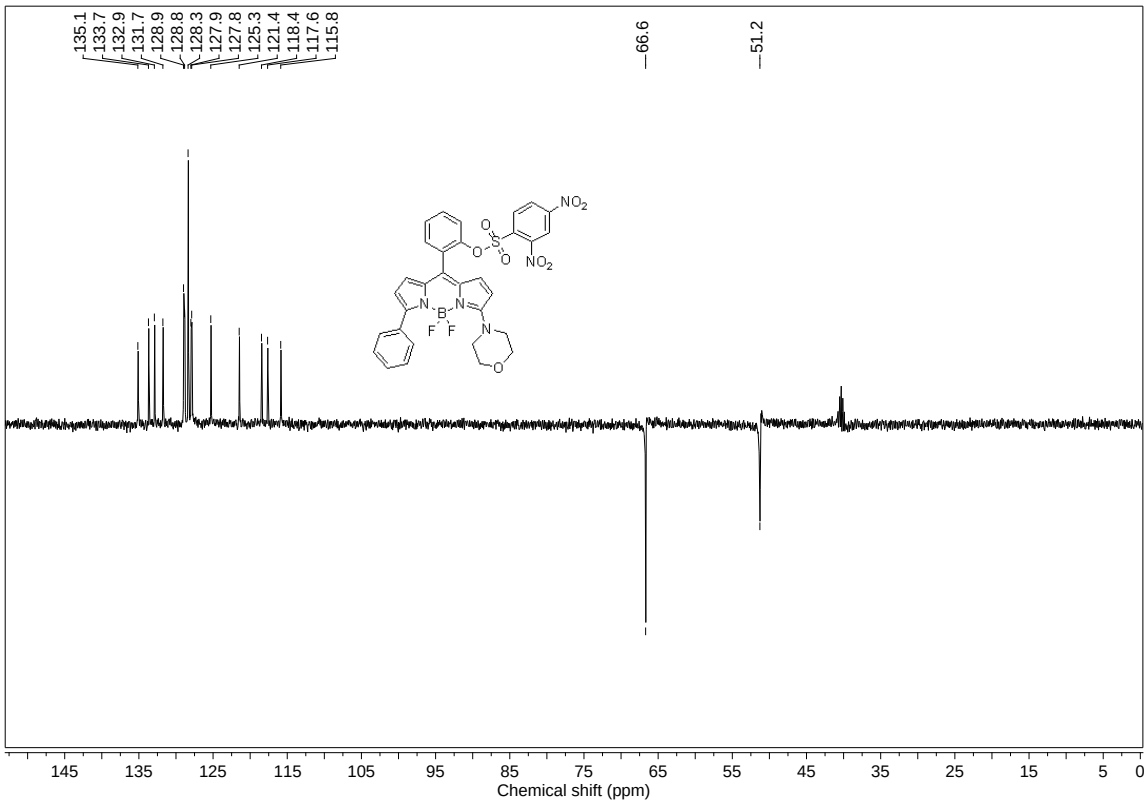

Figure 5.46: ^{13}C NMR spectra of **81** in DMSO-d_6.

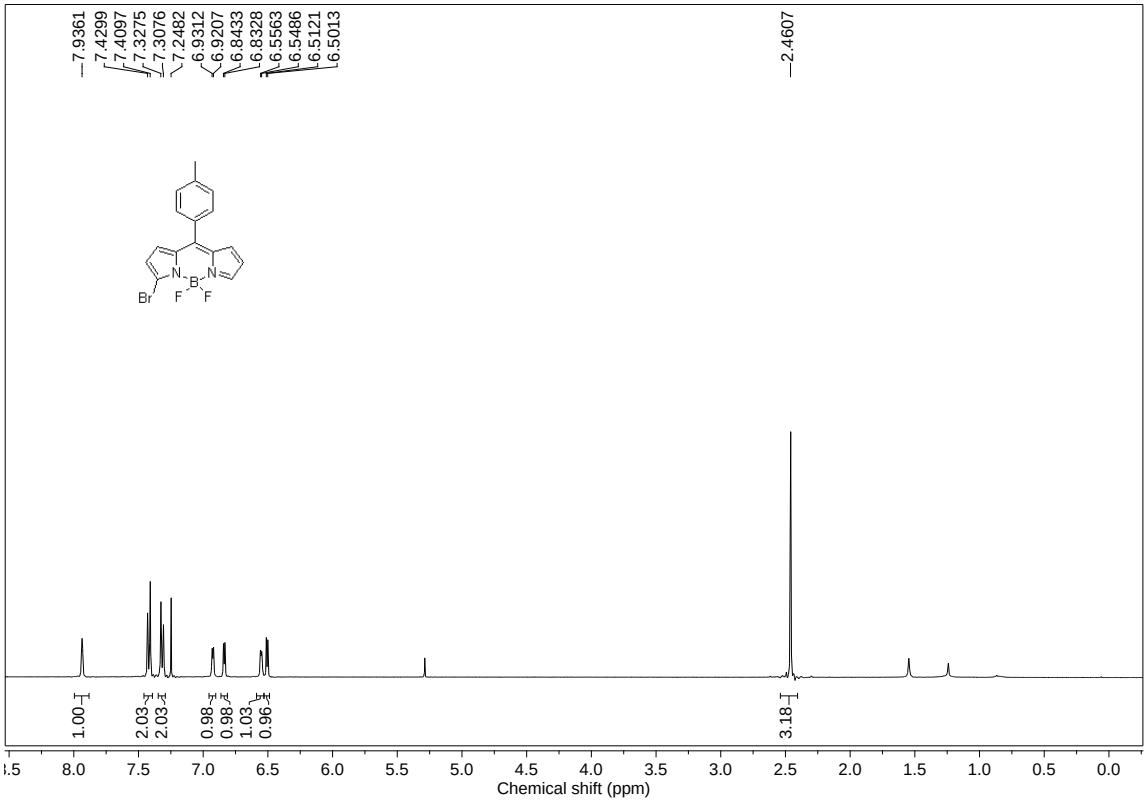

Figure 5.47: ^{1}H NMR spectra of **98** in $CDCl_3$.

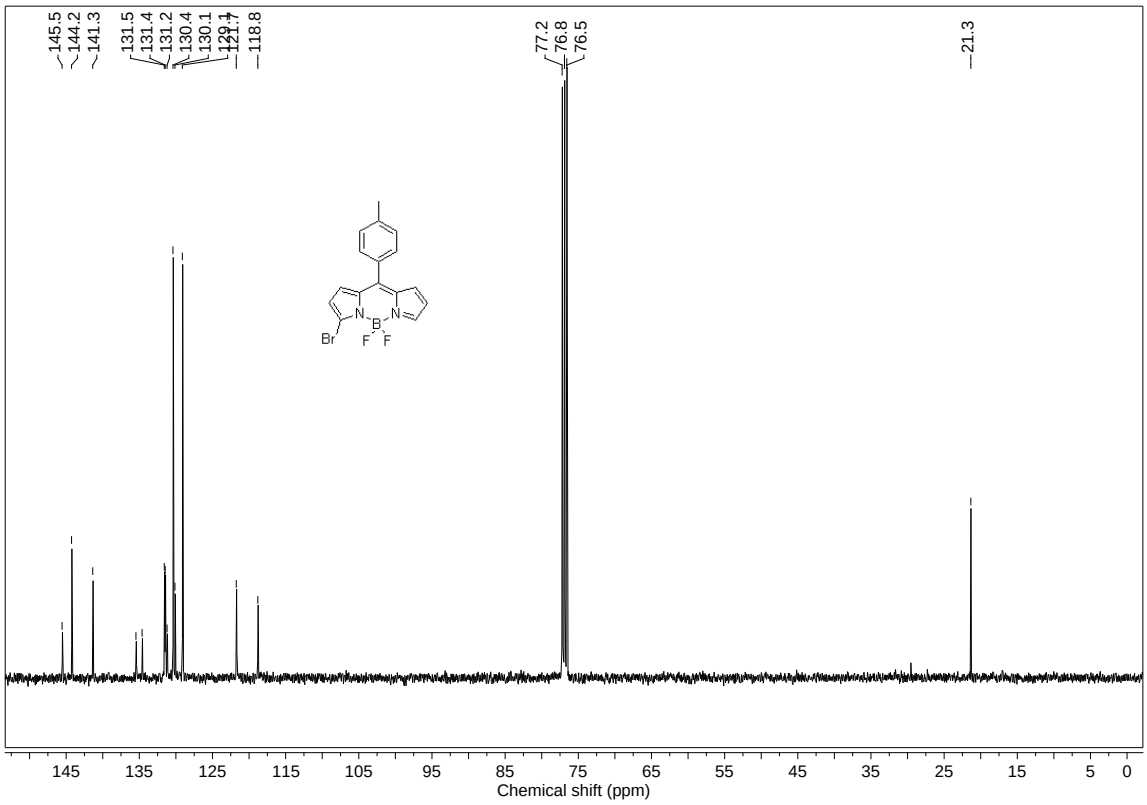

Figure 5.48: ^{13}C NMR spectra of **98** in $CDCl_3$.

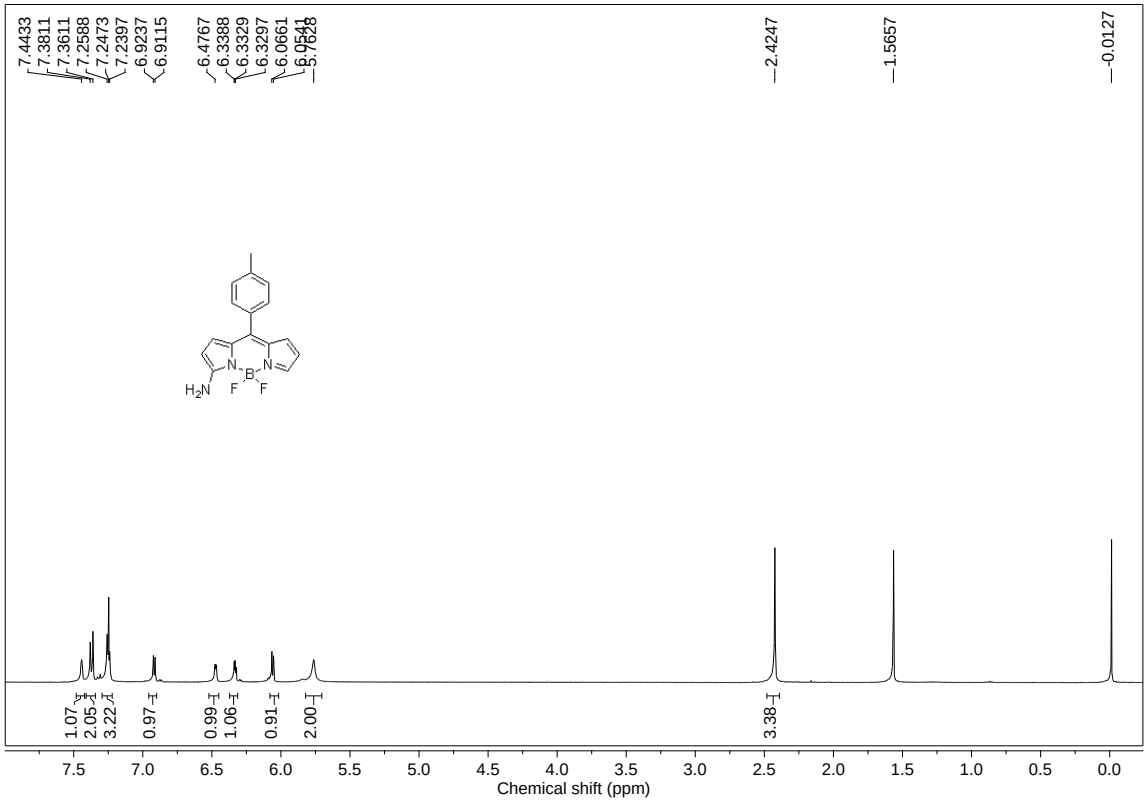

Figure 5.49: ^{1}H NMR spectra of **91a** in $CDCl_3$.

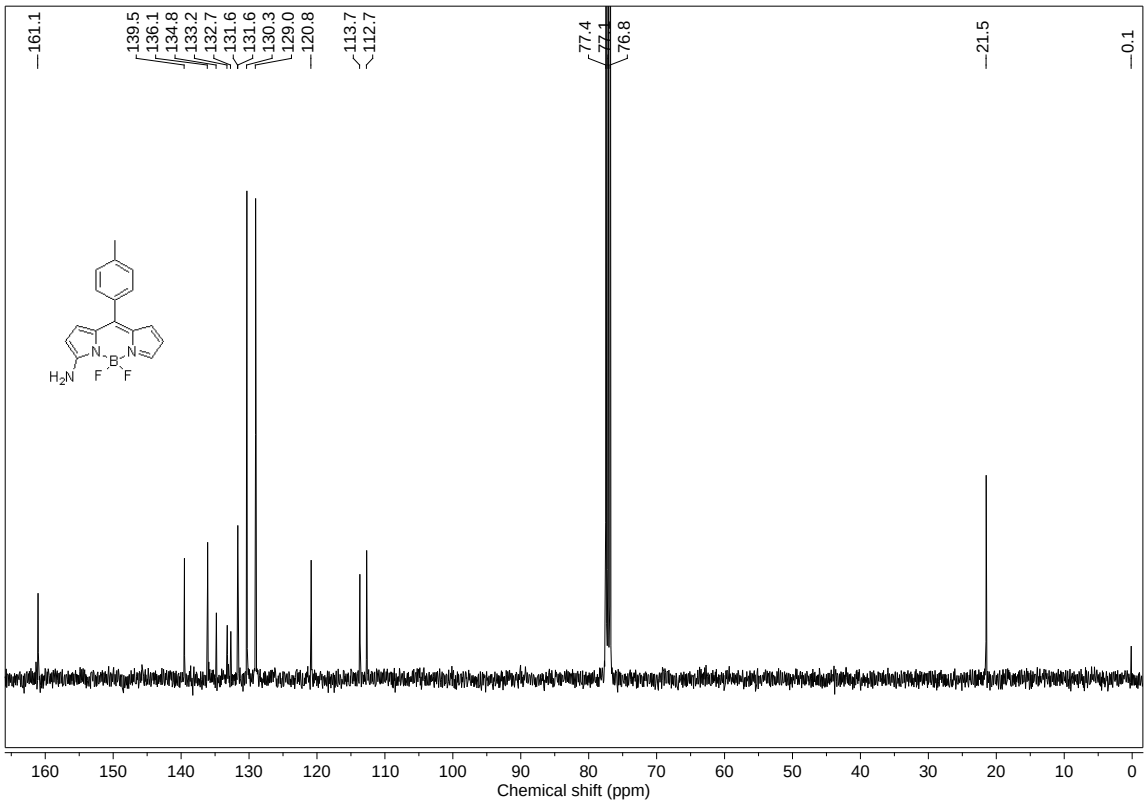

Figure 5.50: ^{13}C NMR spectra of **91a** in $CDCl_3$.

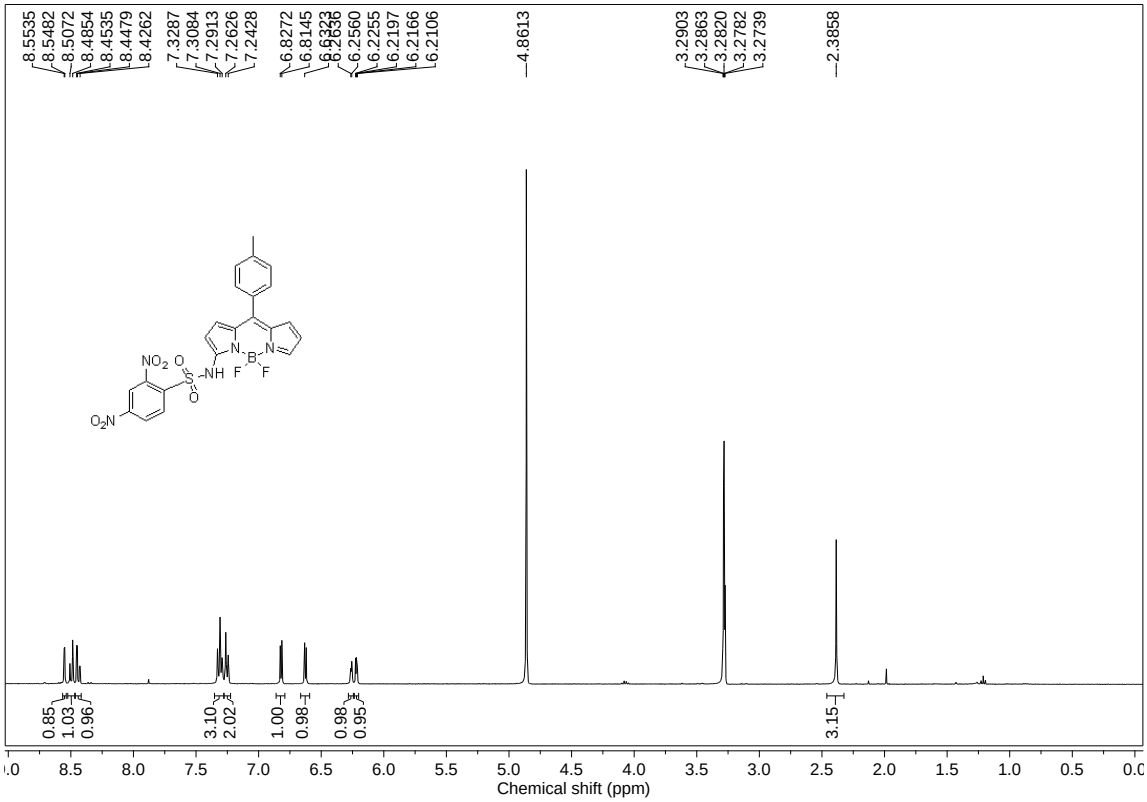

Figure 5.51: ^{1}H NMR spectra of **91** in CD_3OD.

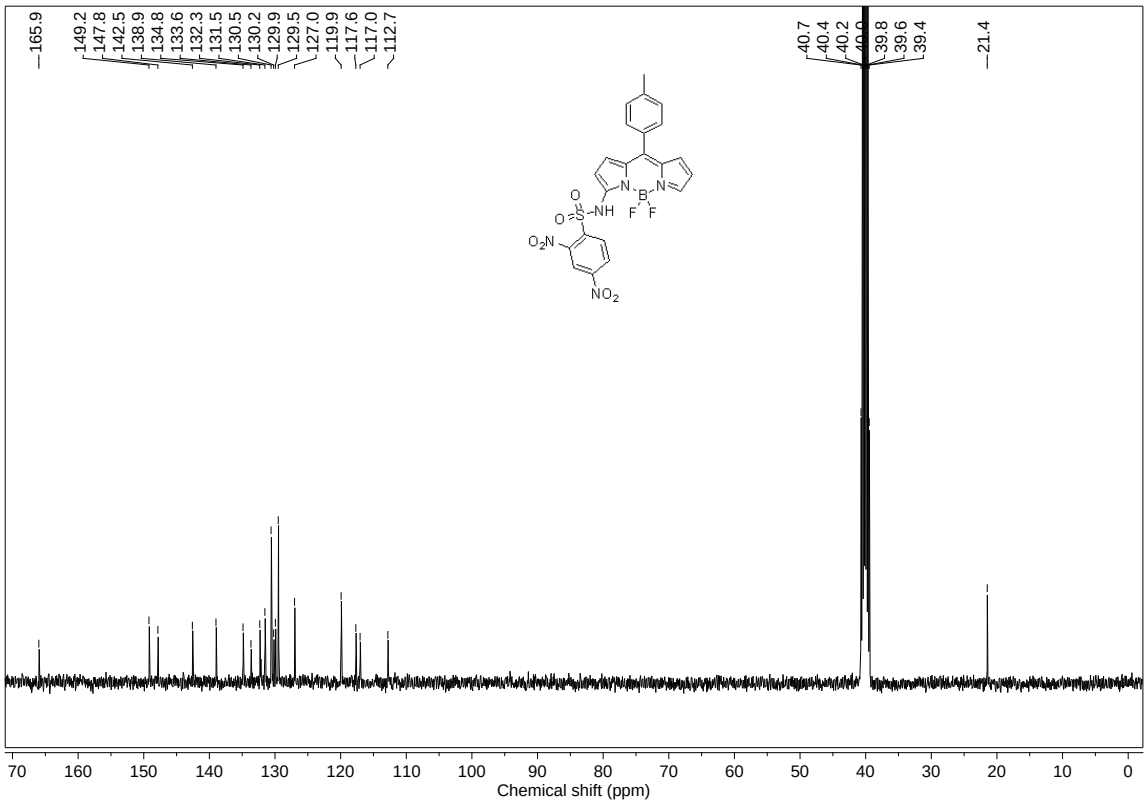

Figure 5.52: ^{13}C NMR spectra of **91** in DMSO-d_6.

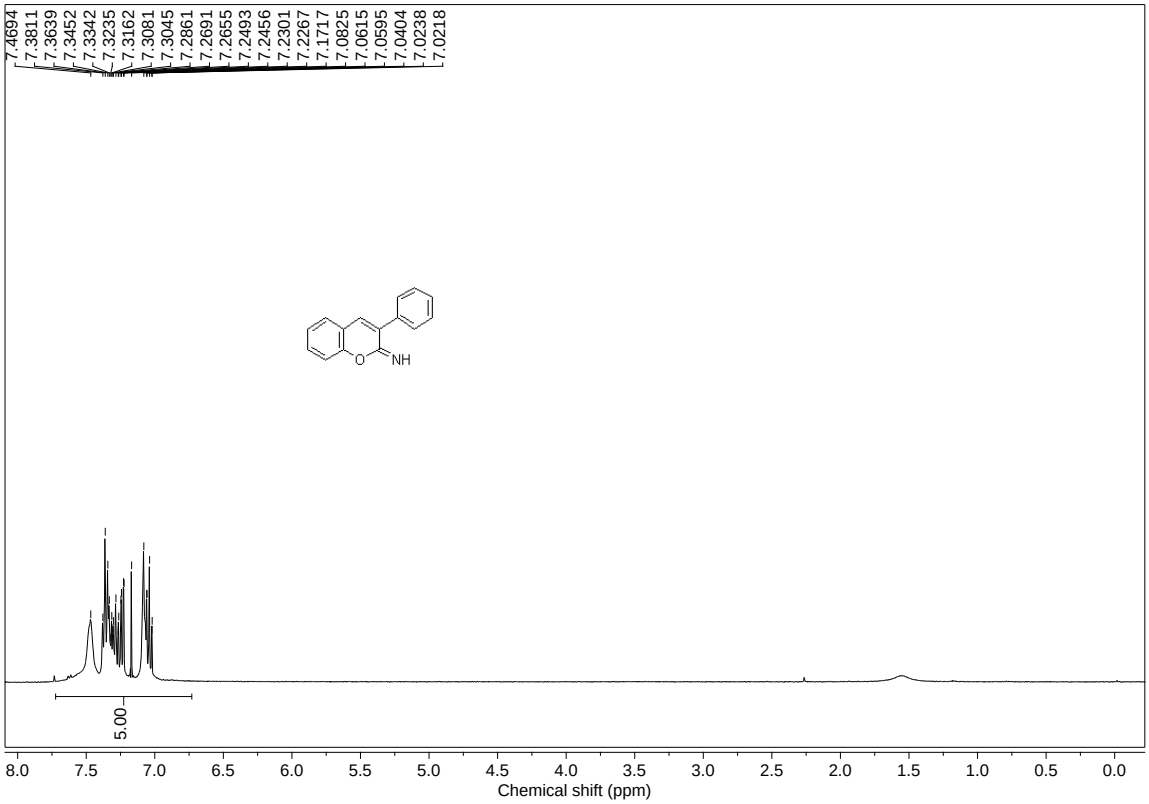

Figure 5.53: ^{1}H NMR spectra of **92a** in $CDCl_3$.

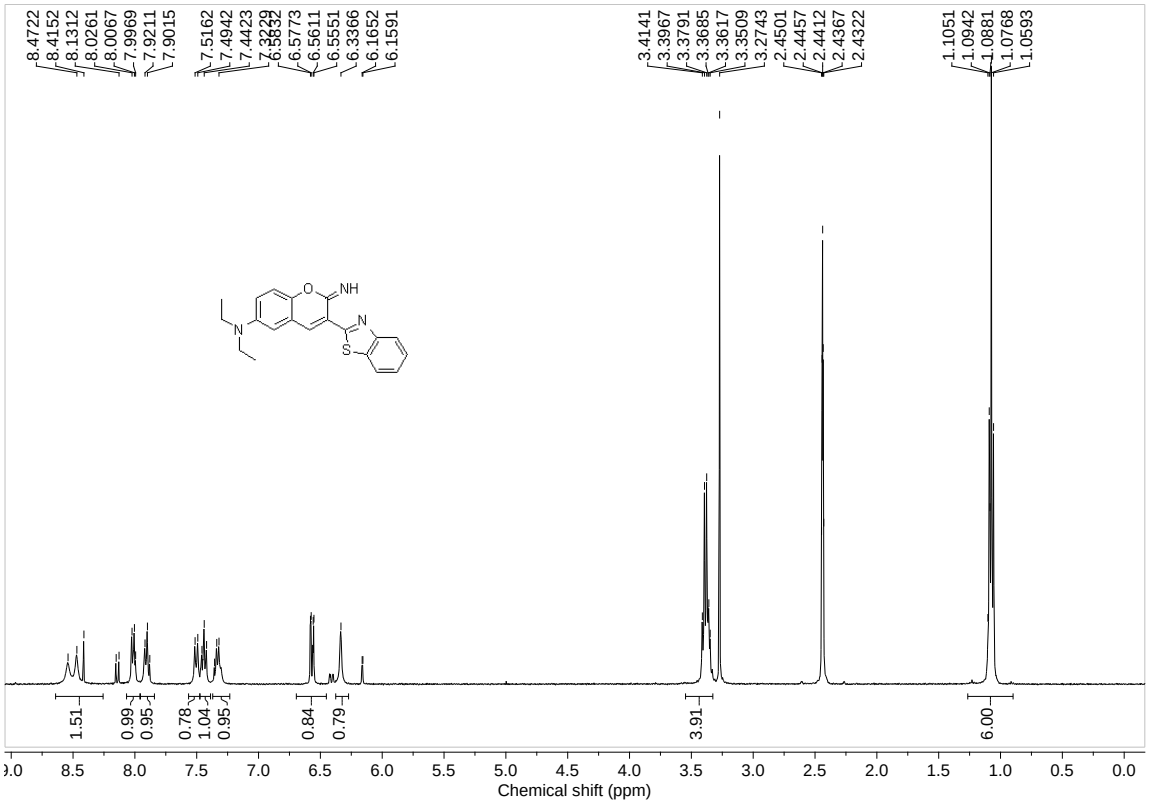

Figure 5.54: ^{1}H NMR spectra of **93a** in DMSO-d_6.

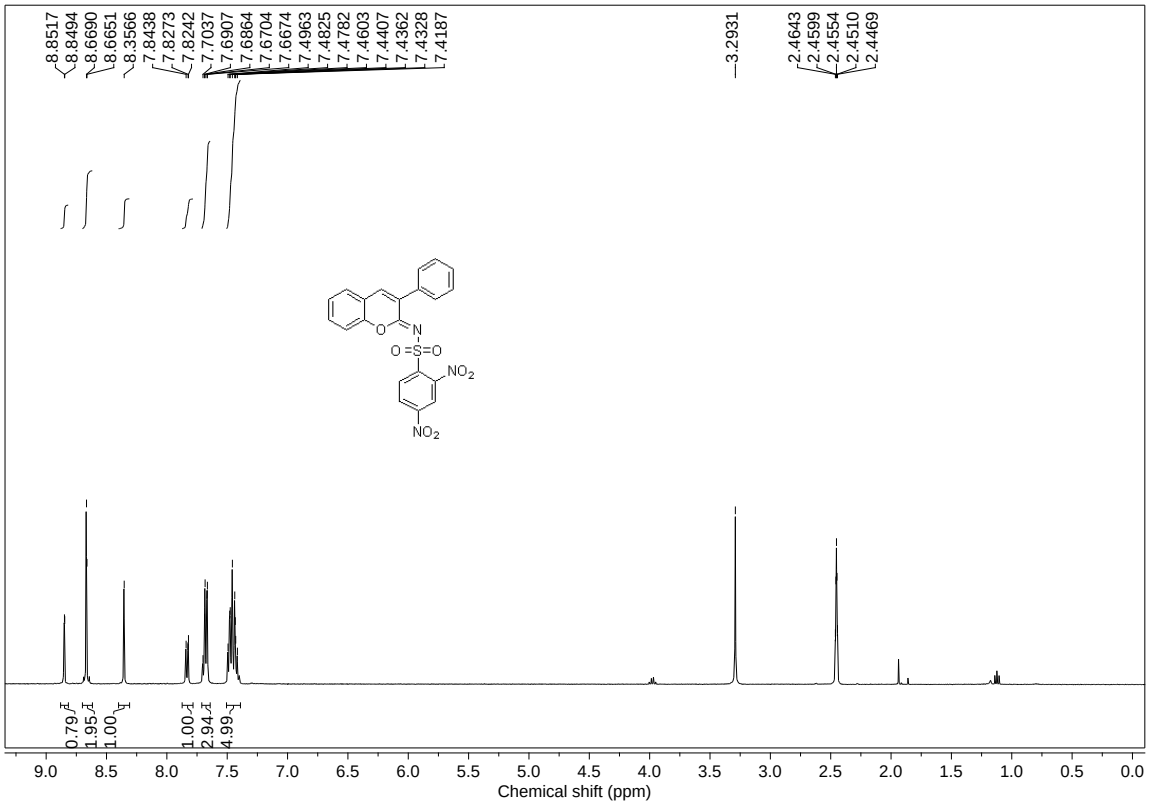

Figure 5.55: ^{1}H NMR spectra of **92** in DMSO-d_6.

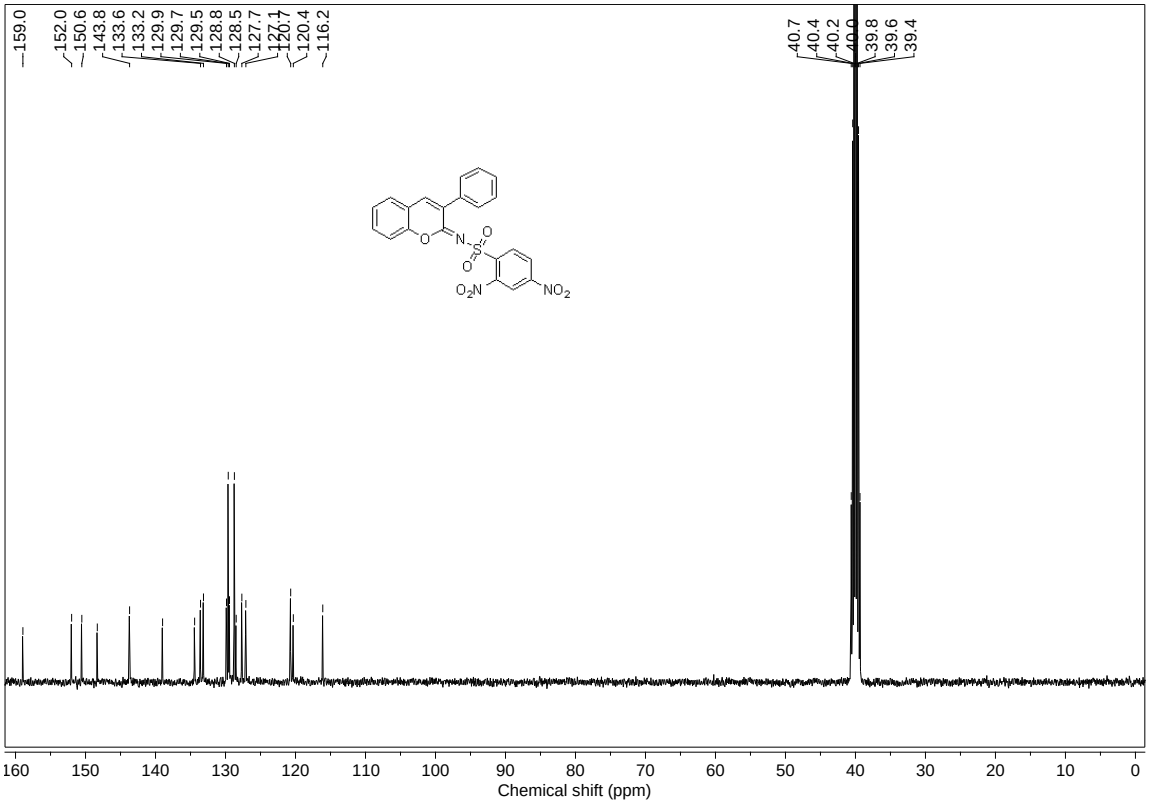

Figure 5.56: ^{13}C NMR spectra of **92** in DMSO-d_6

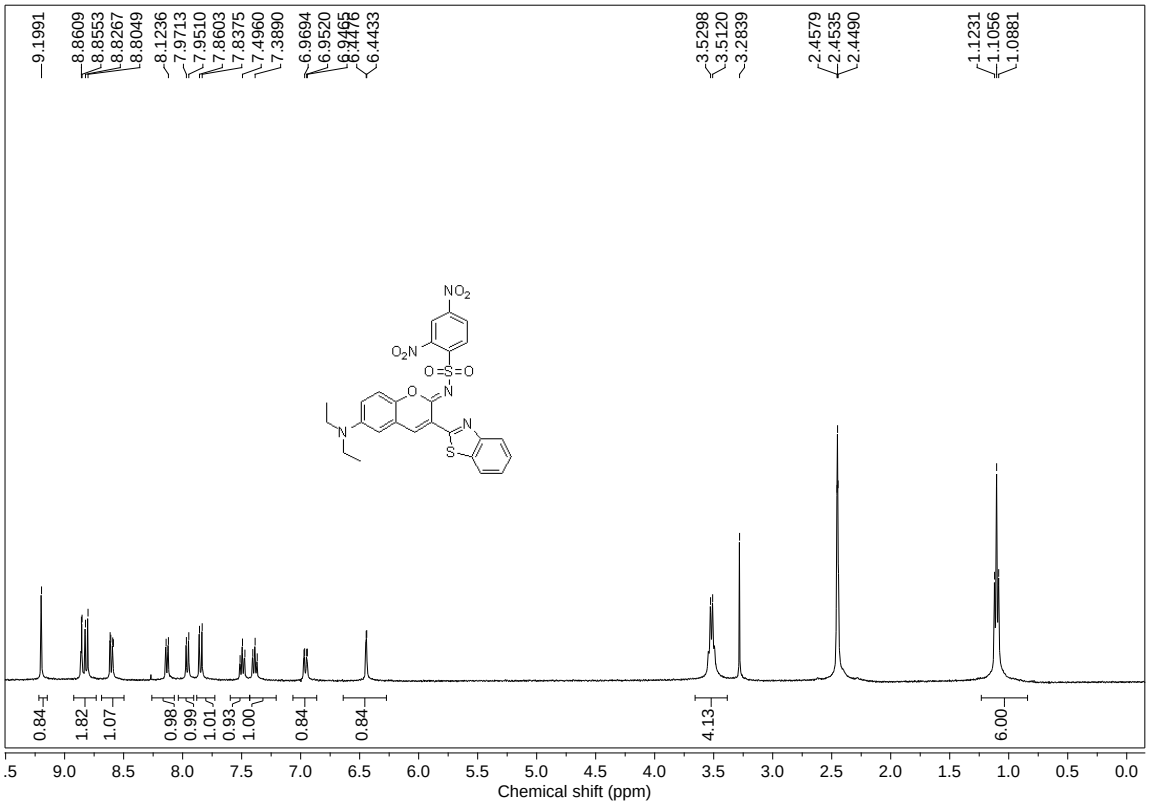

Figure 5.57: ^{1}H NMR spectra of **93** in DMSO-d_6.

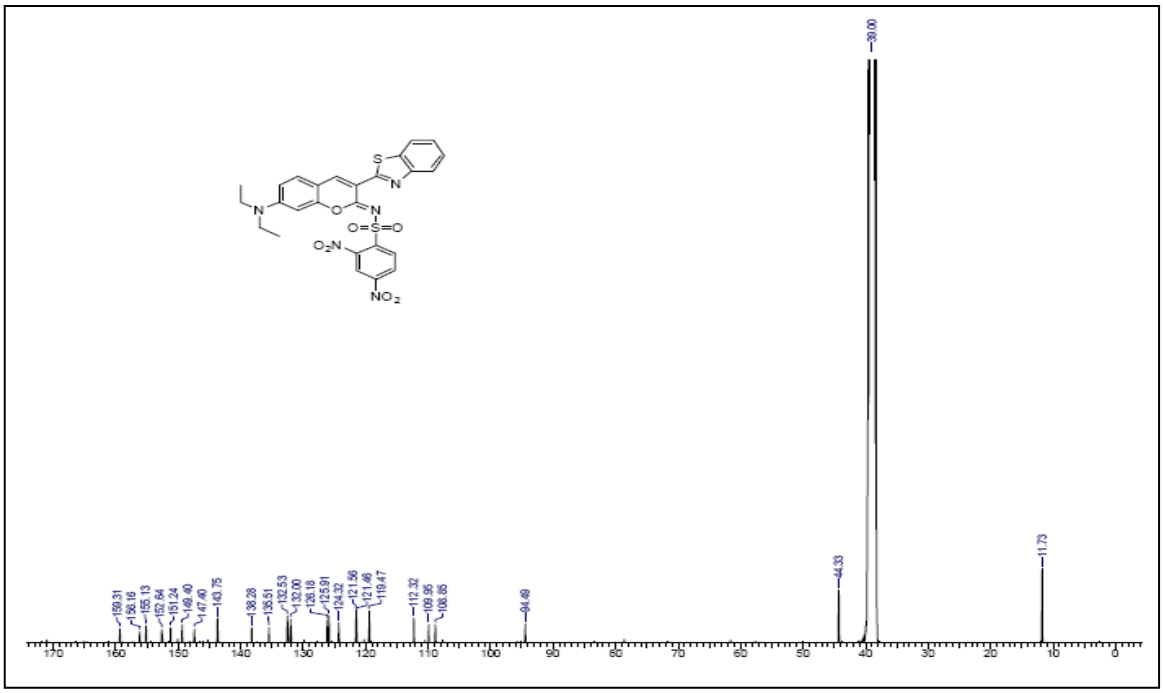

Figure 5.58: ^{13}C NMR spectra of **93** in DMSO-d_6.

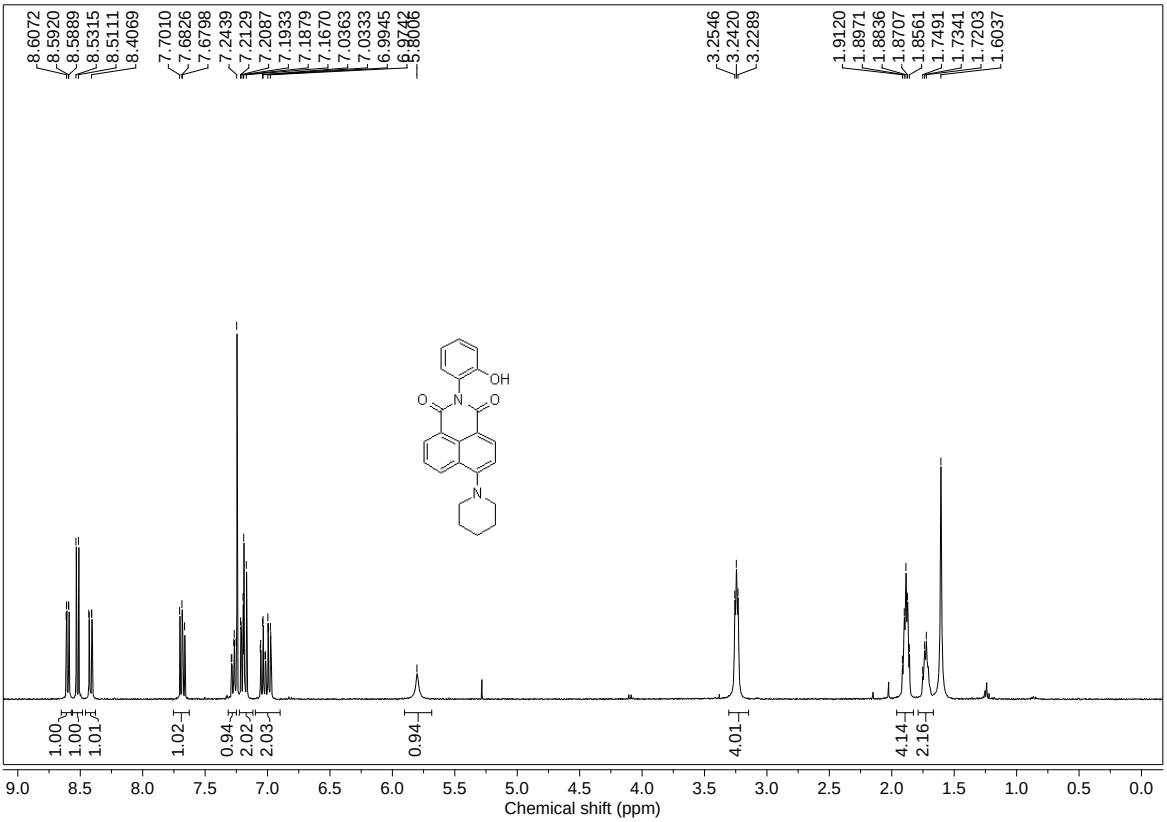

Figure 5.59: ^{1}H NMR spectra of **94a** in $CDCl_3$.

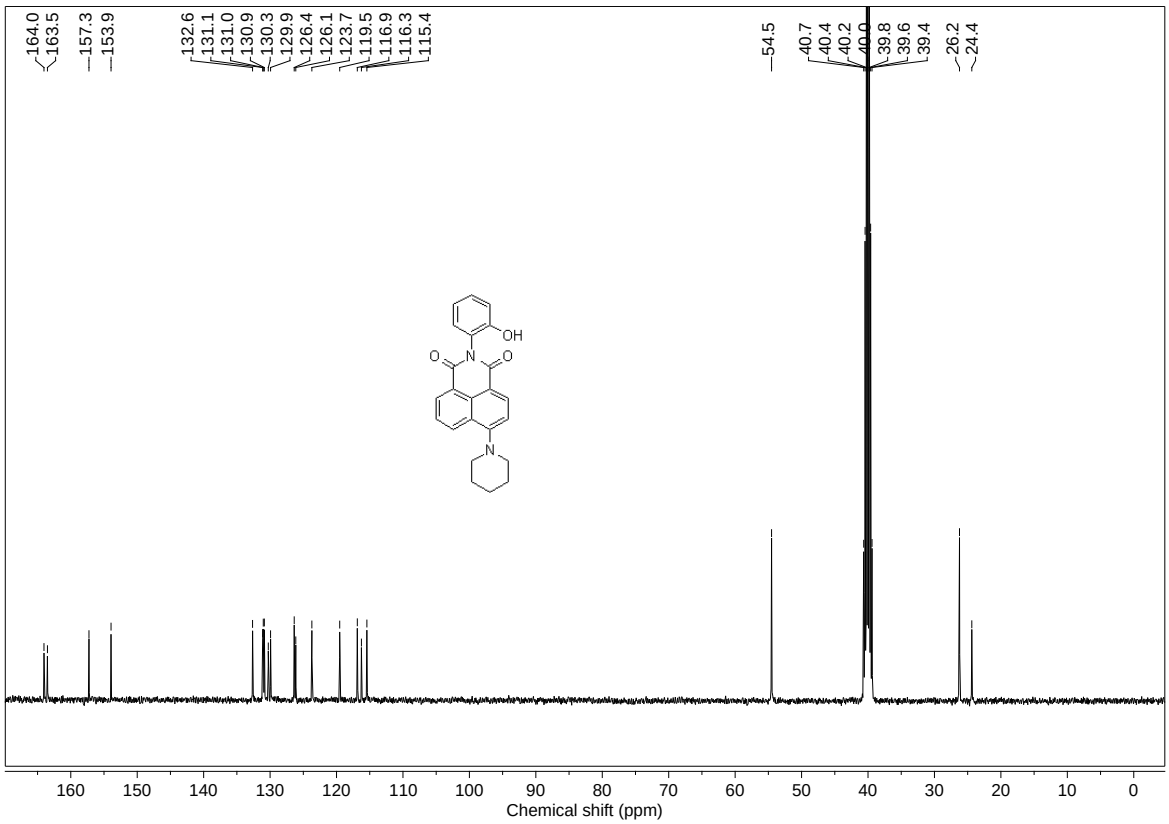

Figure 5.60: ^{13}C NMR spectra of **94a** in DMSO-d_6.

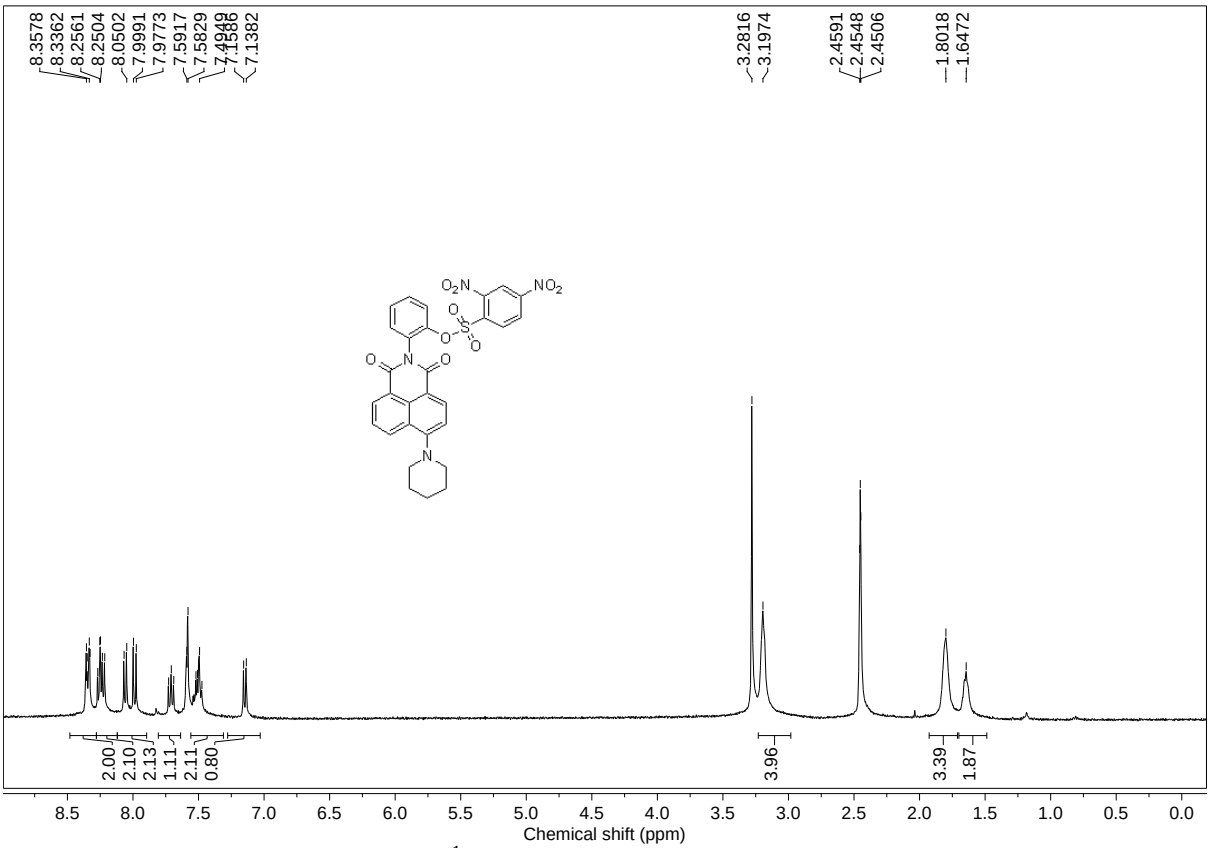

Figure 5.61: ^{1}H NMR spectra of **94** in DMSO-d_6.

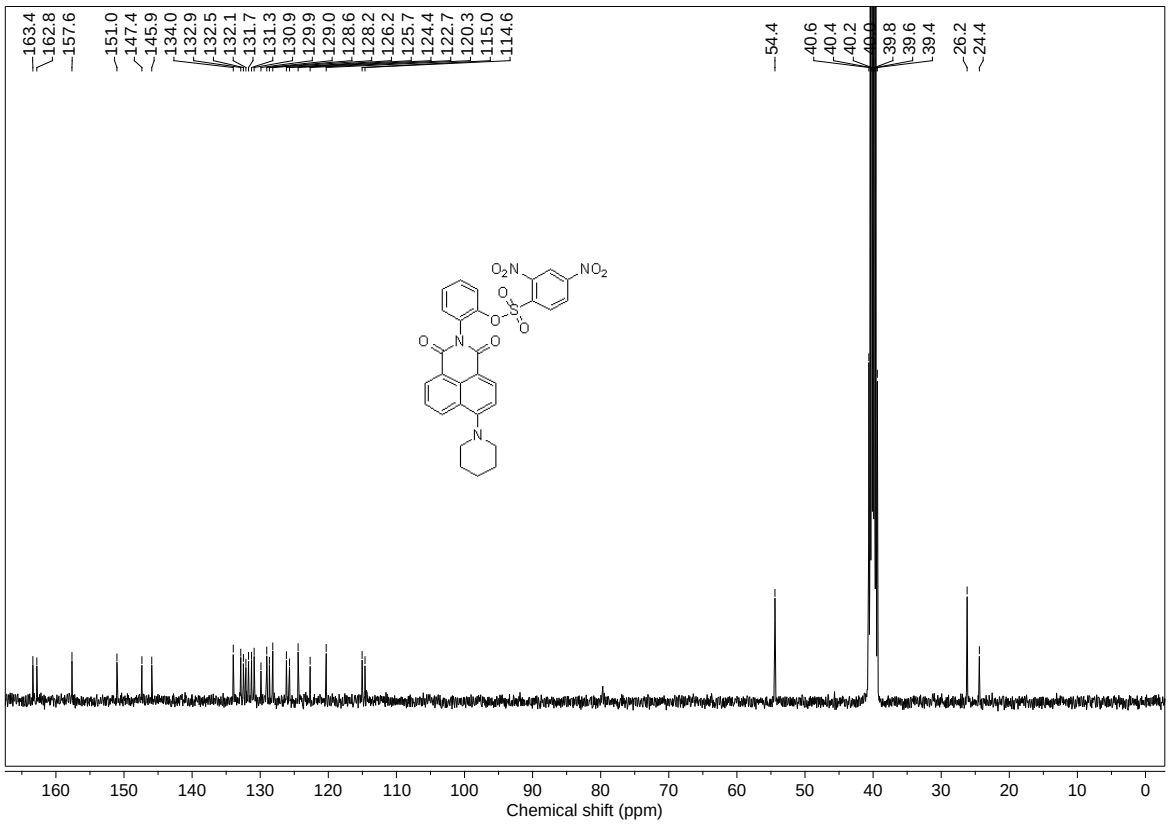

Figure 5.62: ^{13}C NMR spectra of **94** in DMSO-d_6.

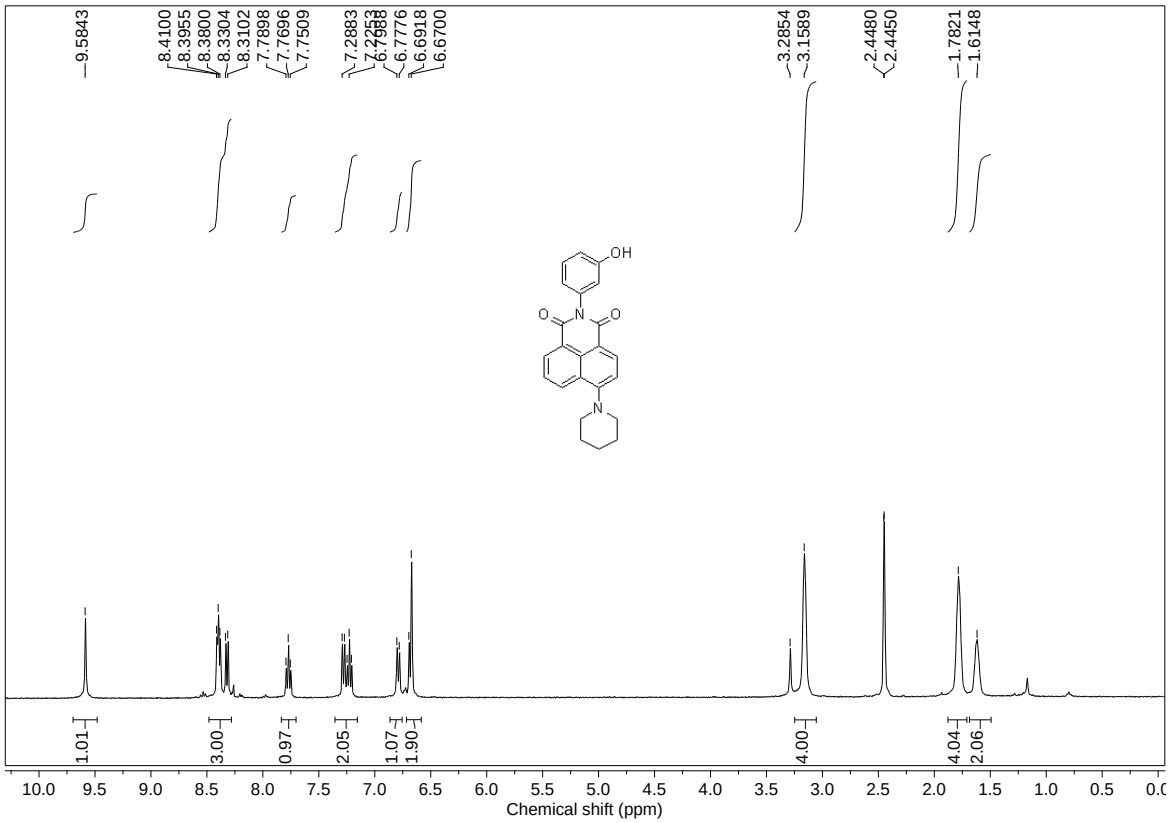

Figure 5.63: ^{1}H NMR spectra of **95a** in DMSO-d_6.

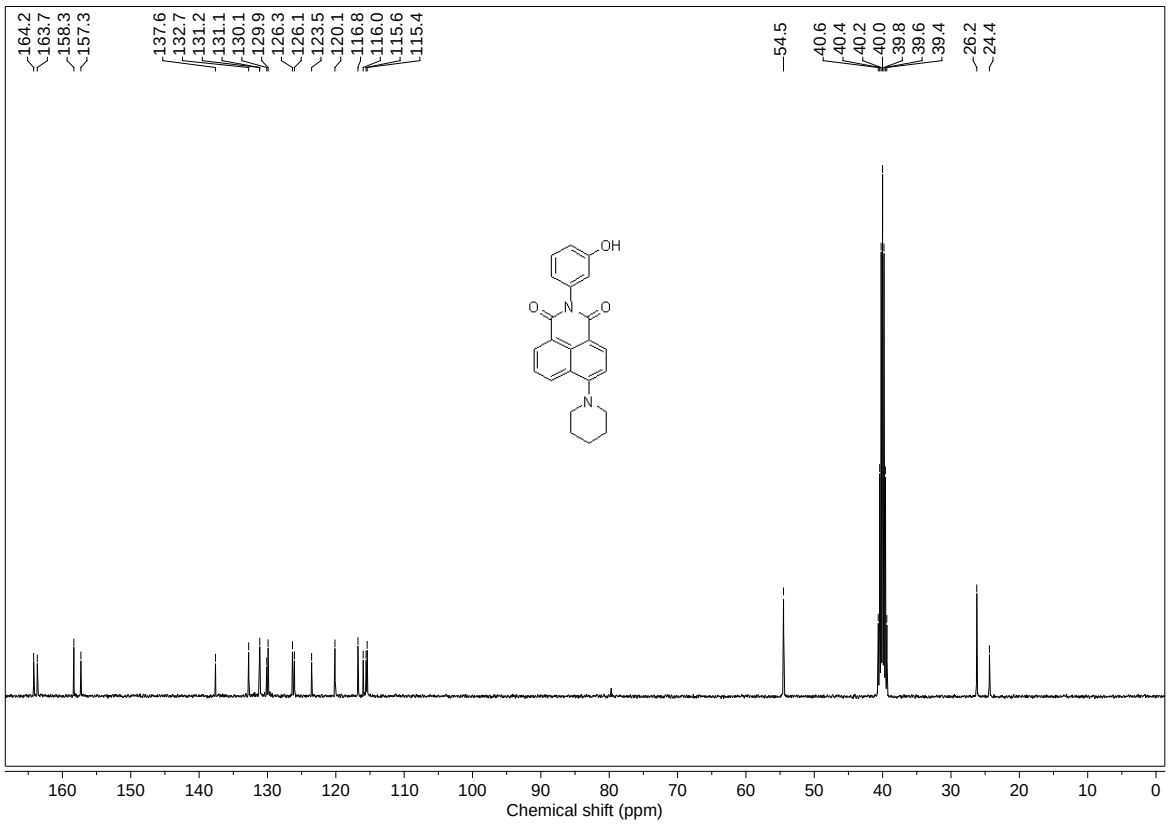

Figure 5.64: ^{13}C NMR spectra of **95a** in DMSO-d_6.

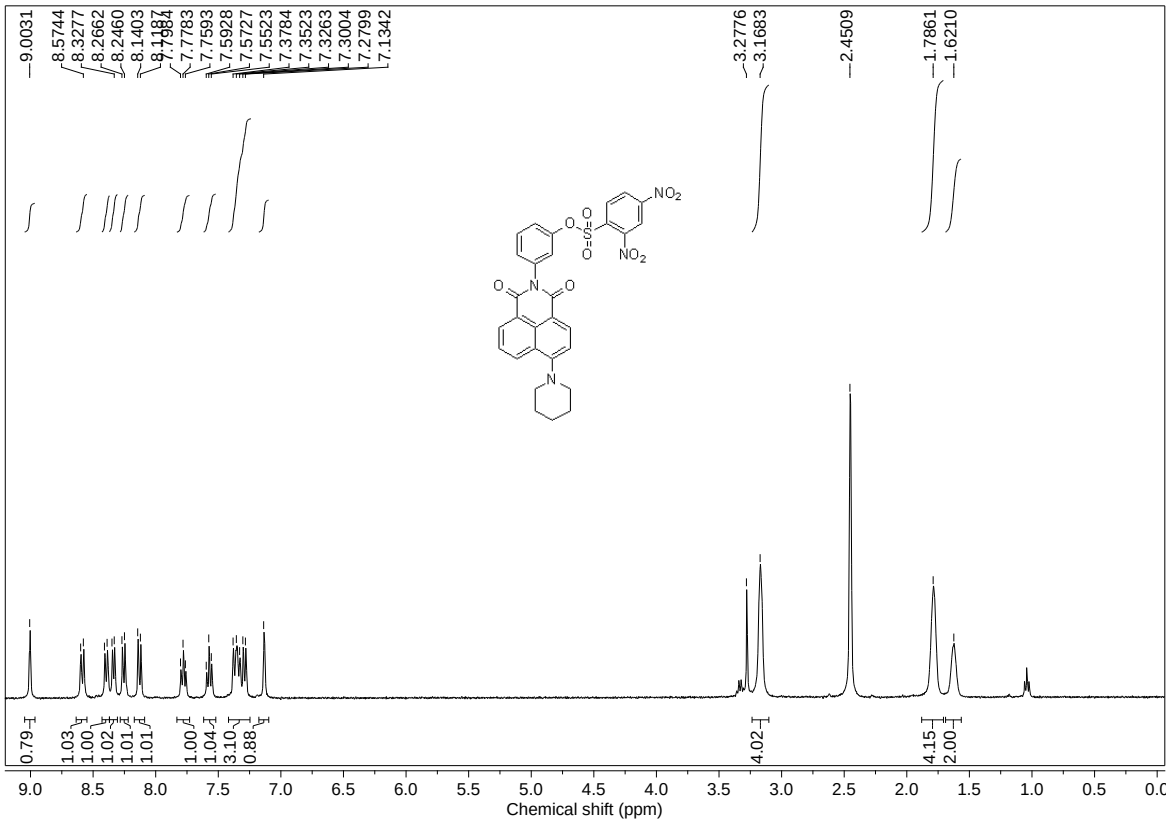

Figure 5.65: ^{1}H NMR spectra of **95** in DMSO-d_6.

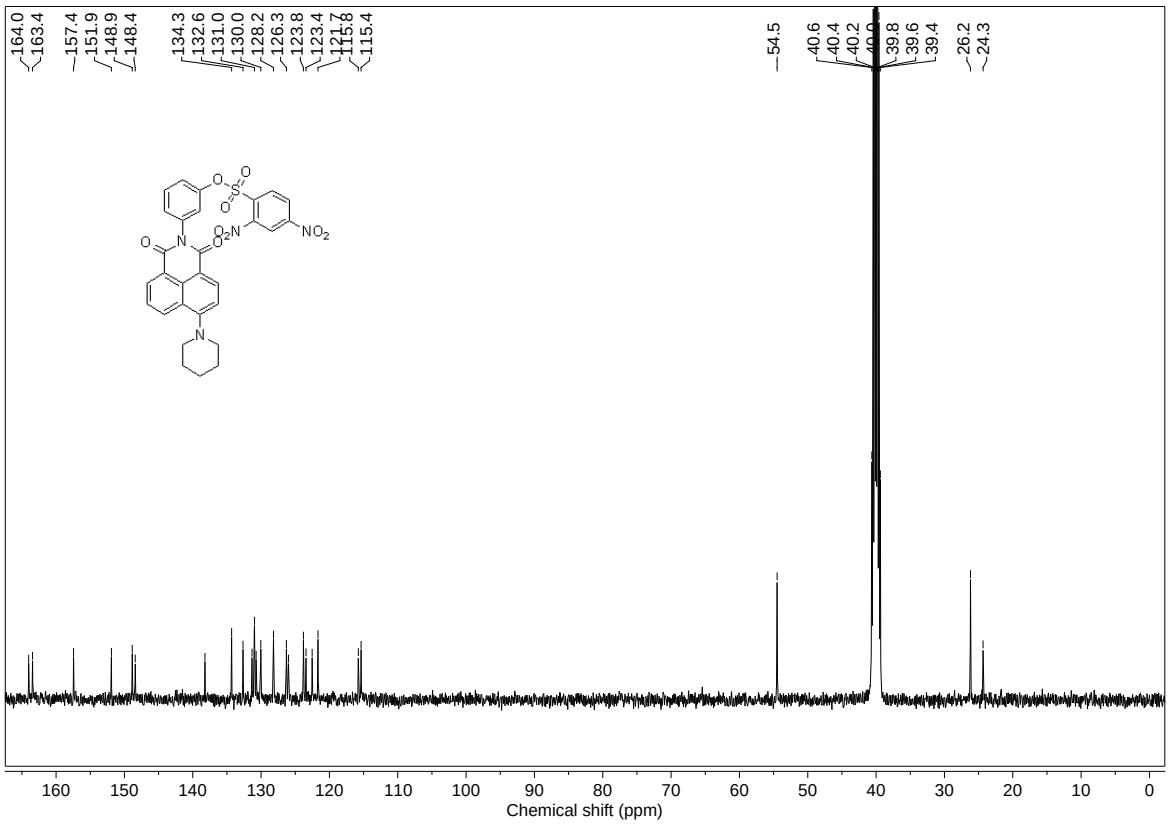

Figure 5.66: ^{13}C NMR spectra of **95** in DMSO-d_6.

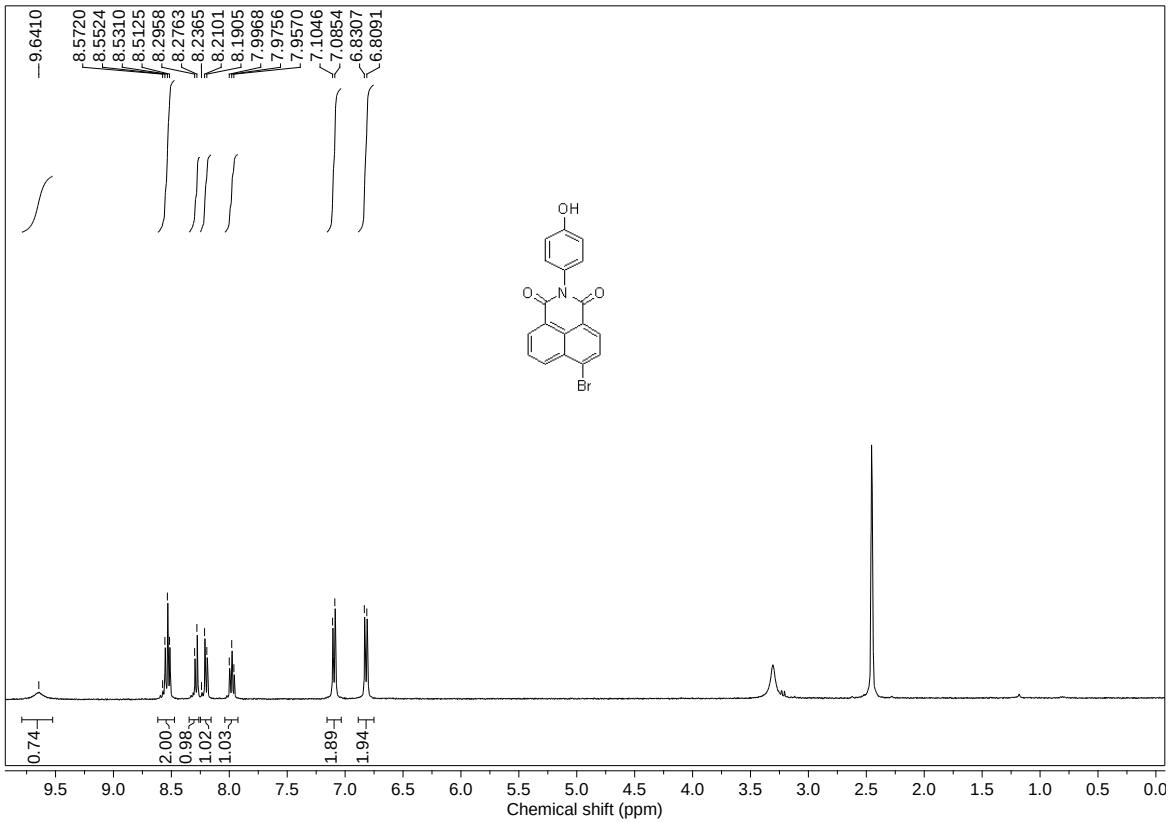

Figure 5.67: ^{1}H NMR spectra of **101c** in DMSO-d_6.

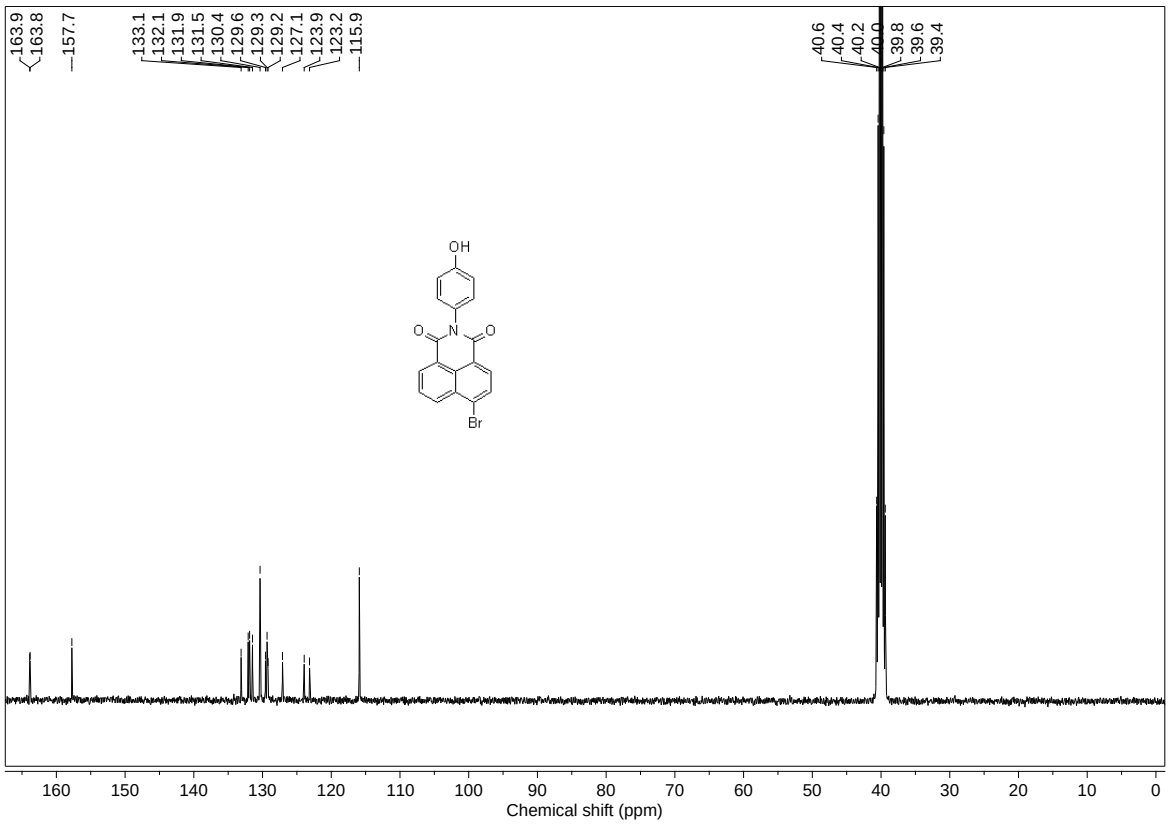

Figure 5.68: ^{13}C NMR spectra of **101c** in DMSO-d_6.

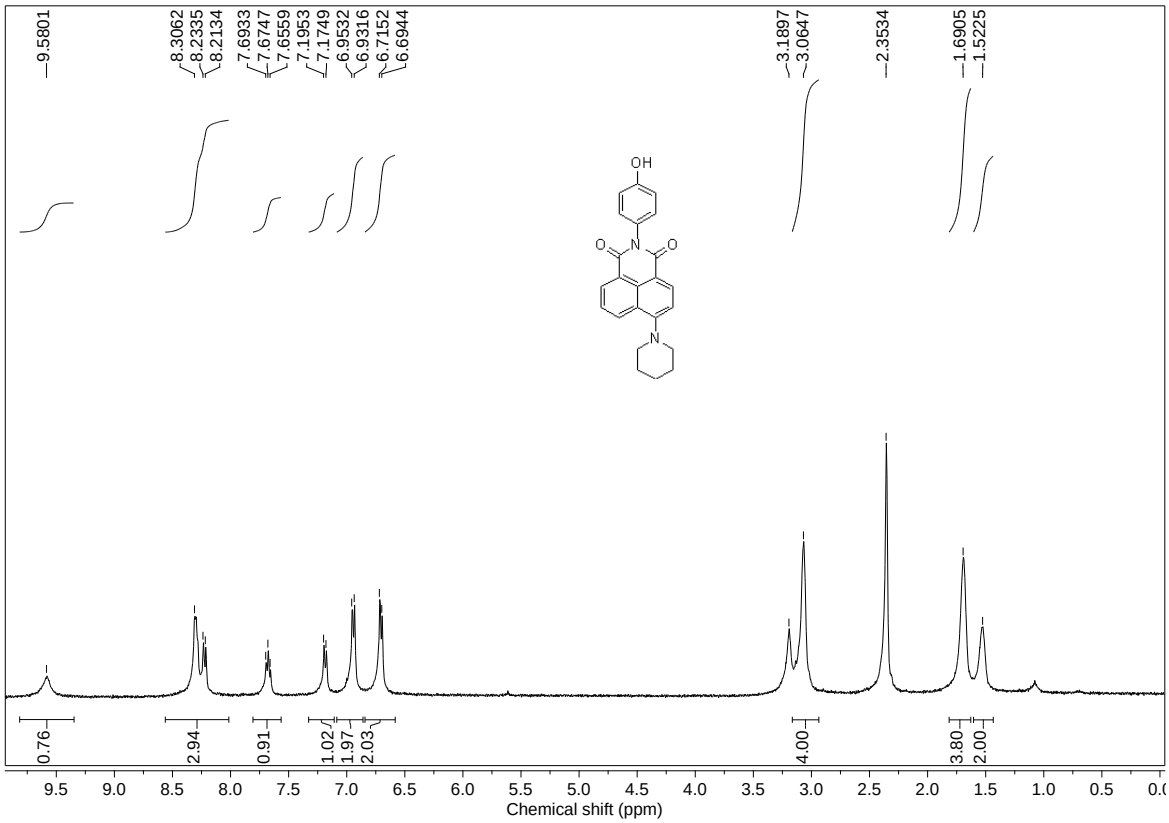

Figure 5.69: ^{1}H NMR spectra of **96a** in DMSO-d_6.

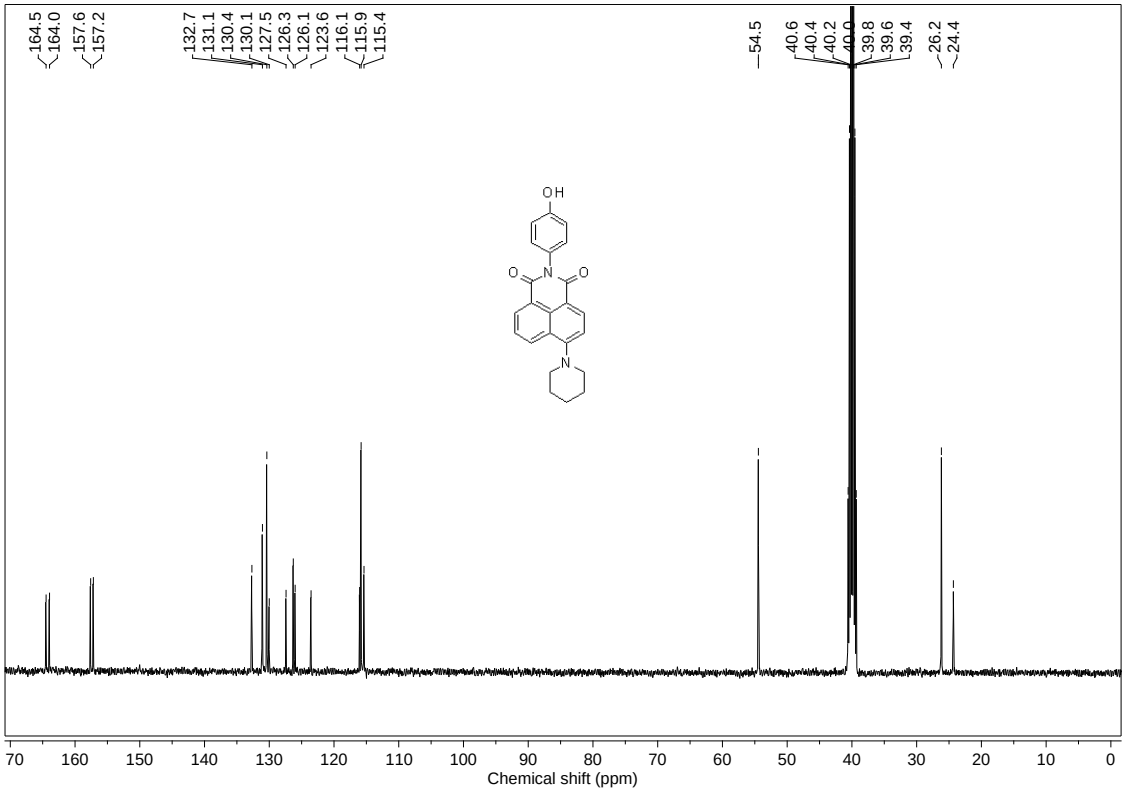

Figure 5.70: ^{13}C NMR spectra of **96a** in DMSO-d_6.

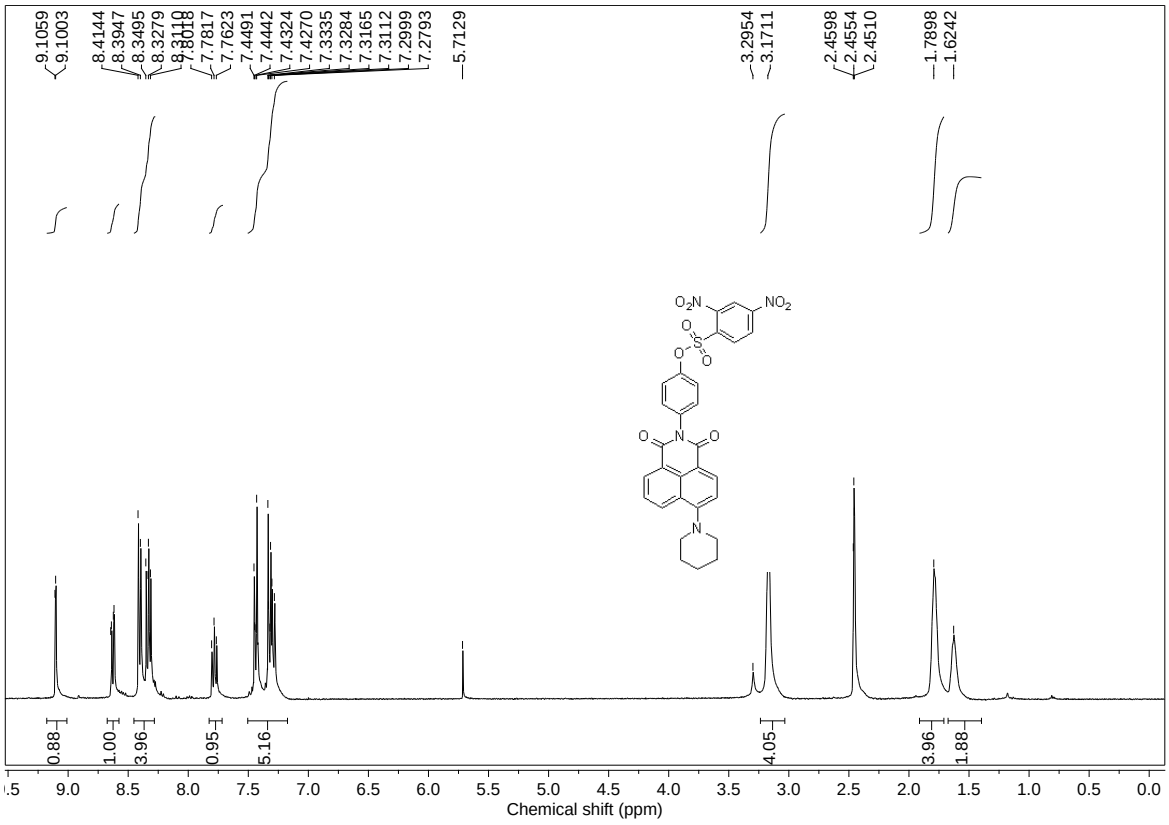

Figure 5.71: ^{1}H NMR spectra of **96** in DMSO-d_6.

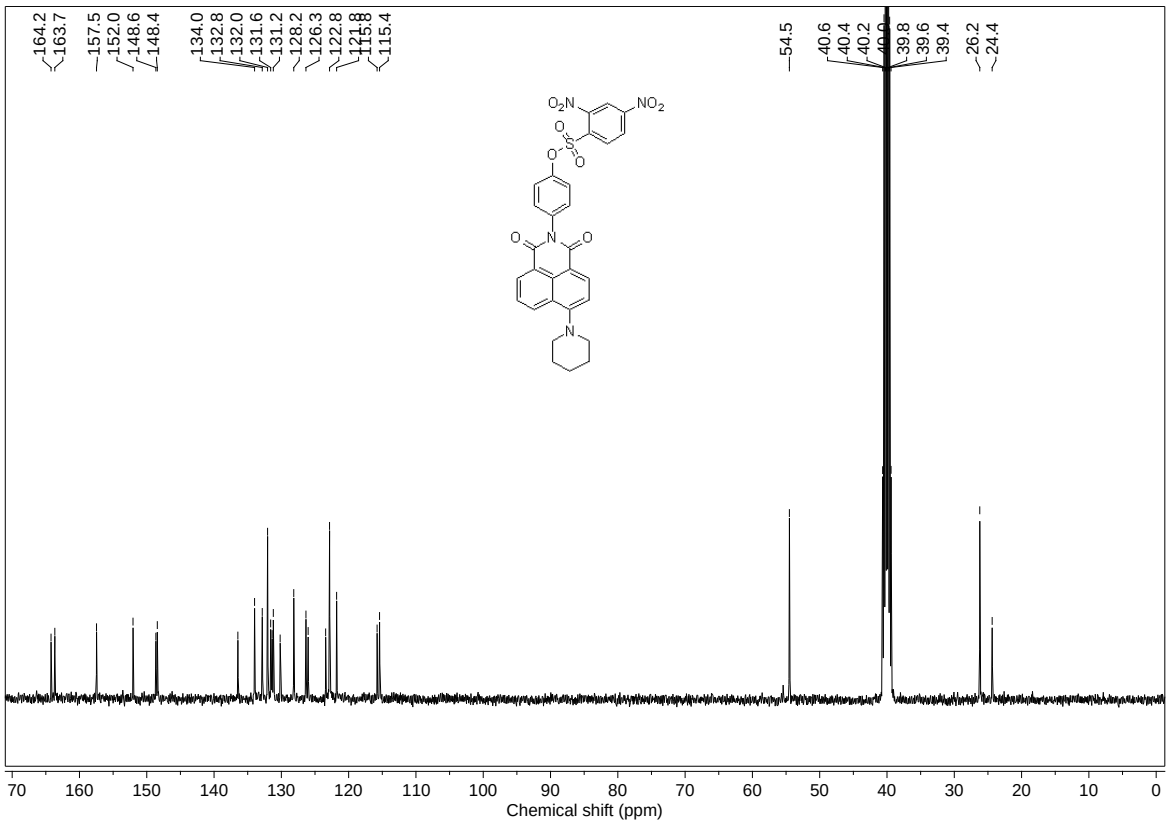

Figure 5.72: ^{13}C NMR spectra of **96** in DMSO-d_6.

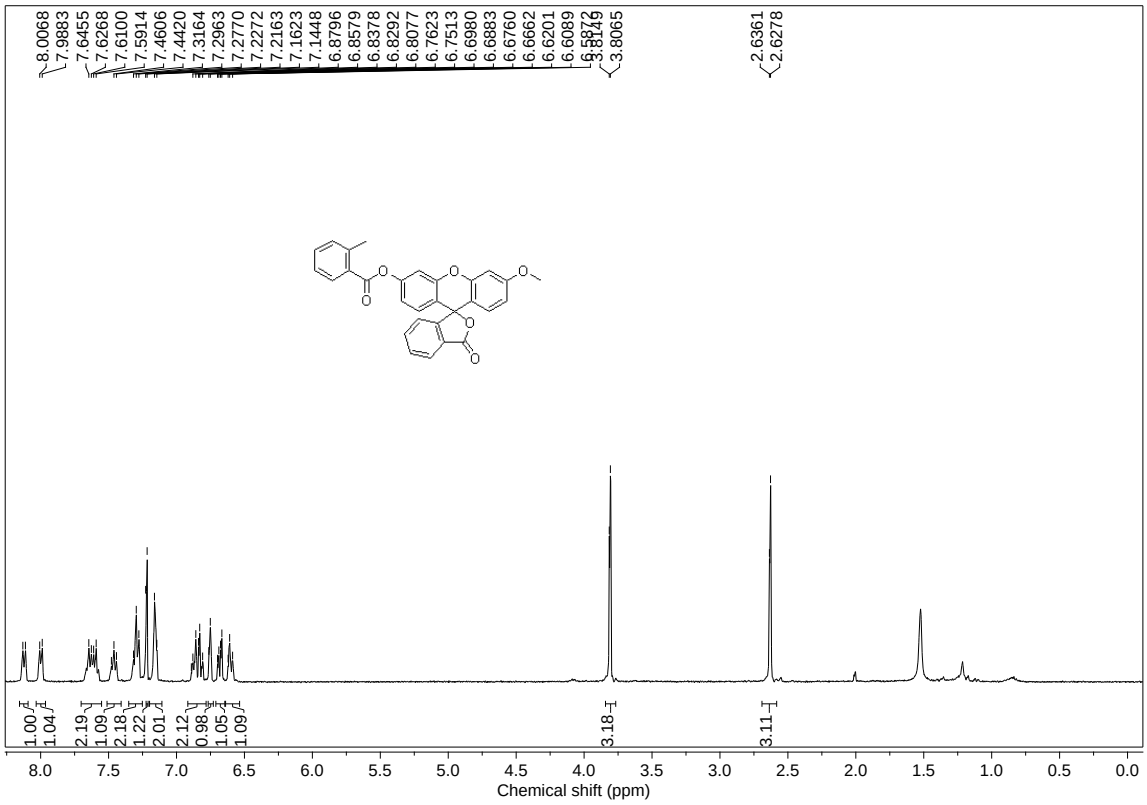

Figure 5.73: ^{1}H NMR spectra of **103** in $CDCl_3$.

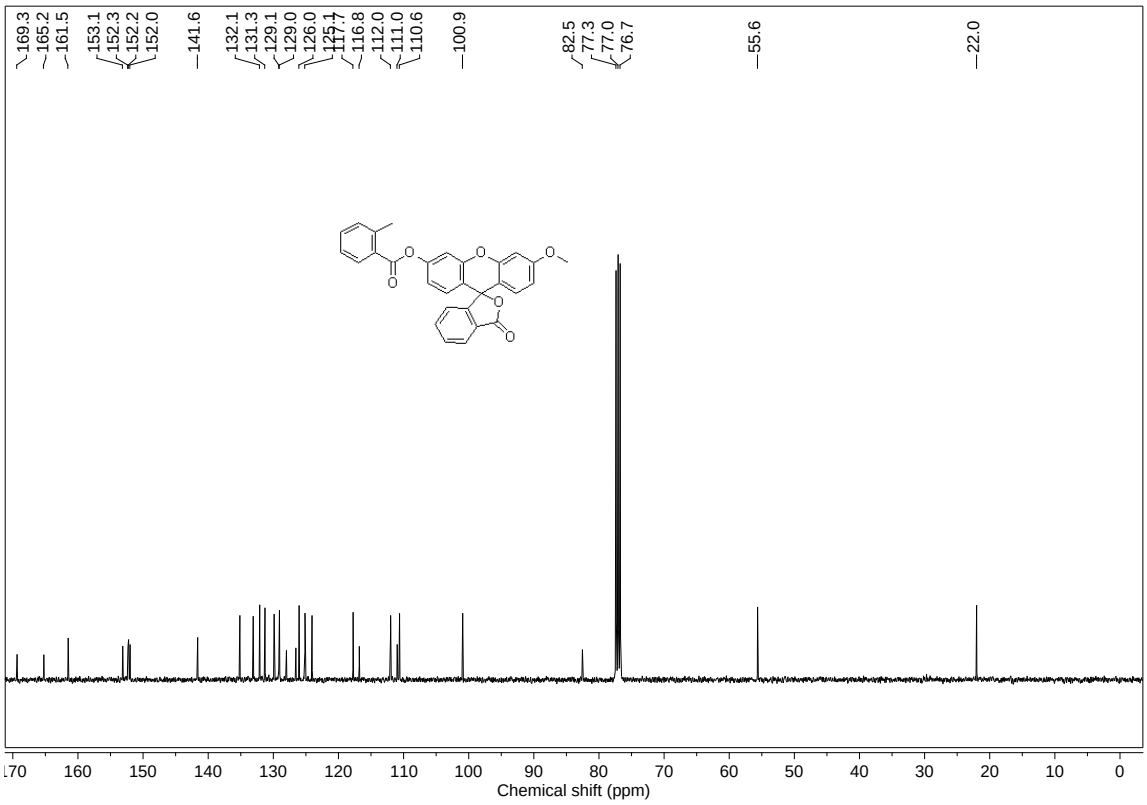

Figure 5.74: ^{13}C NMR spectra of **103** in $CDCl_3$.

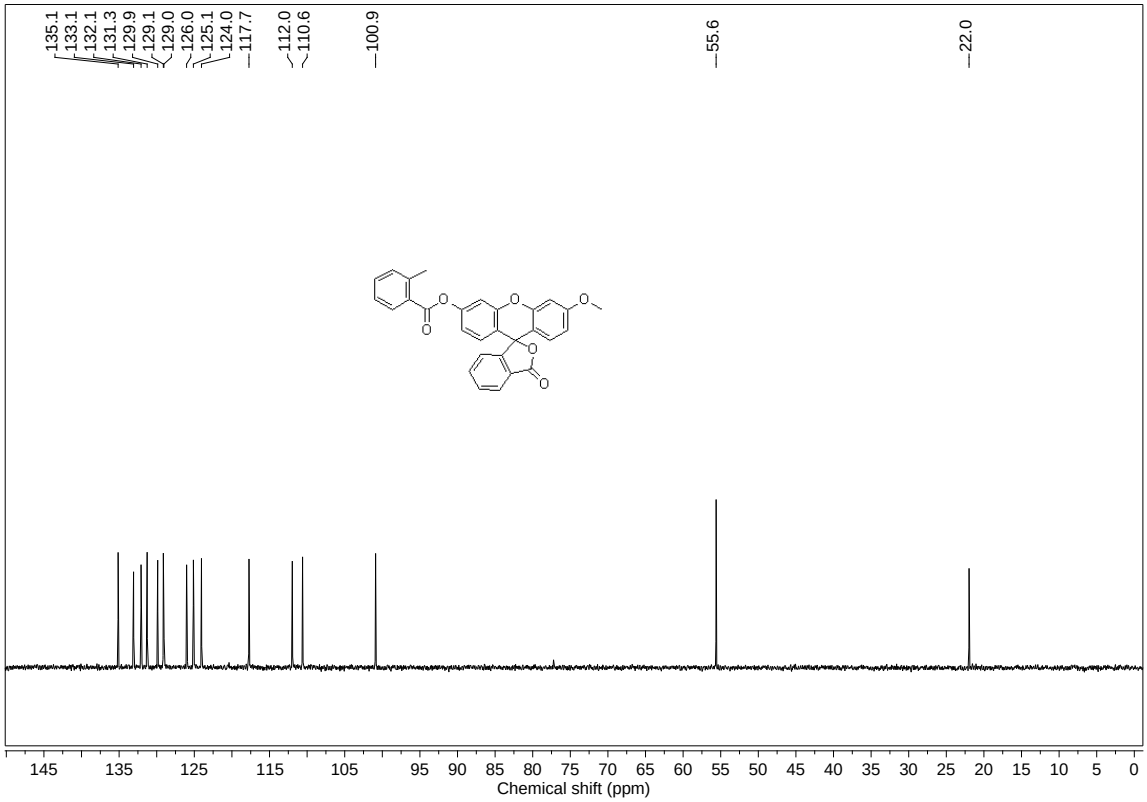

Figure 5.75: DEPT of **103** in $CDCl_3$.

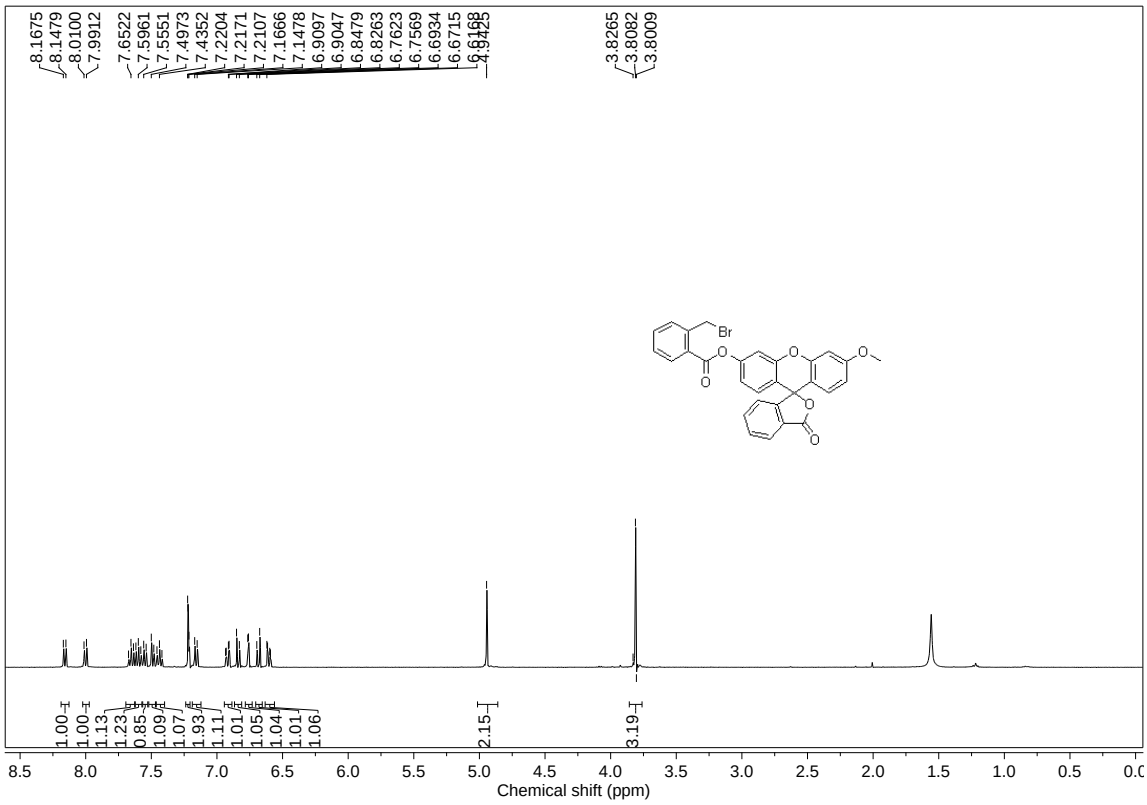

Figure 5.76: ^{1}H NMR spectra of **102** in $CDCl_3$.

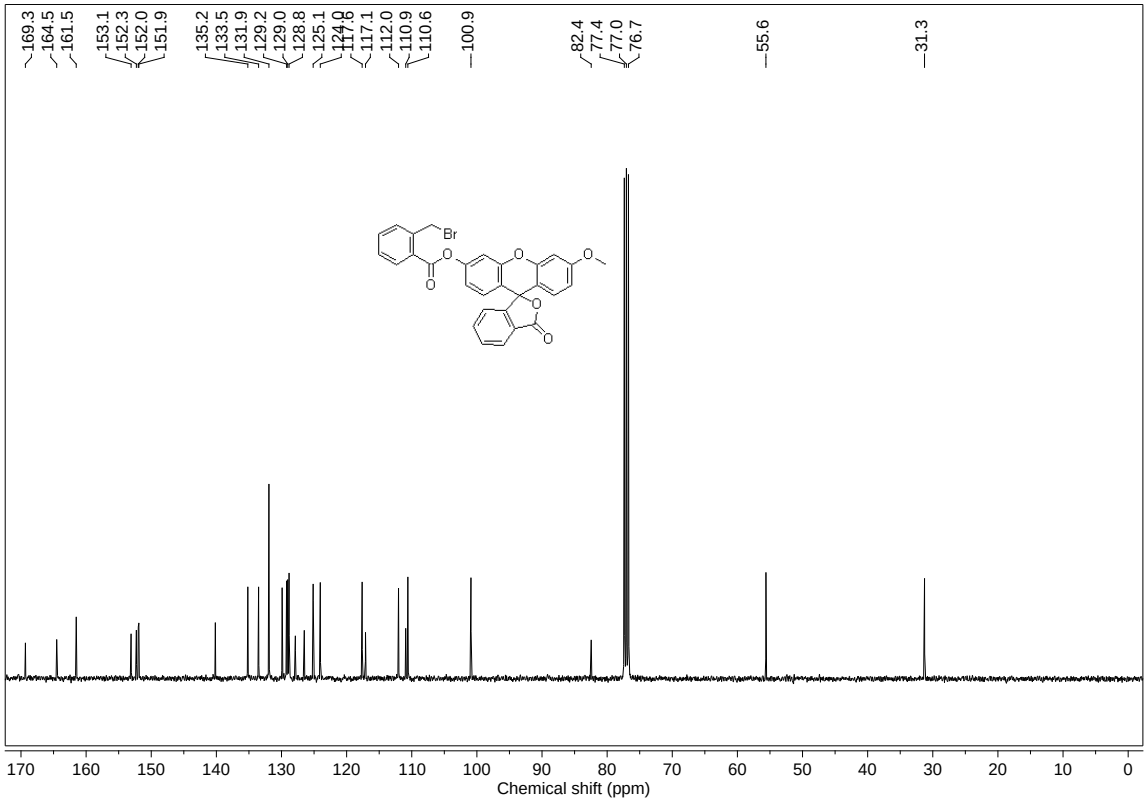

Figure 5.77: ^{13}C NMR spectra of **102** in $CDCl_3$.

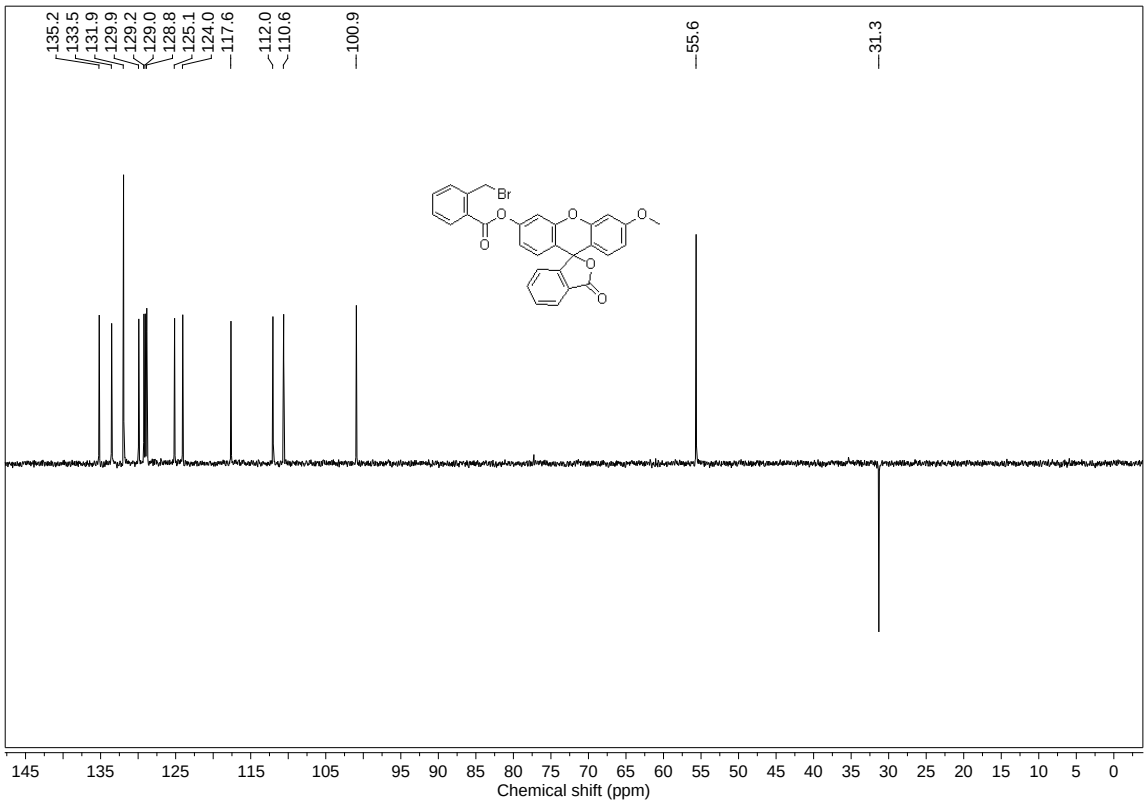

Figure 5.78: DEPT of **102** in $CDCl_3$.

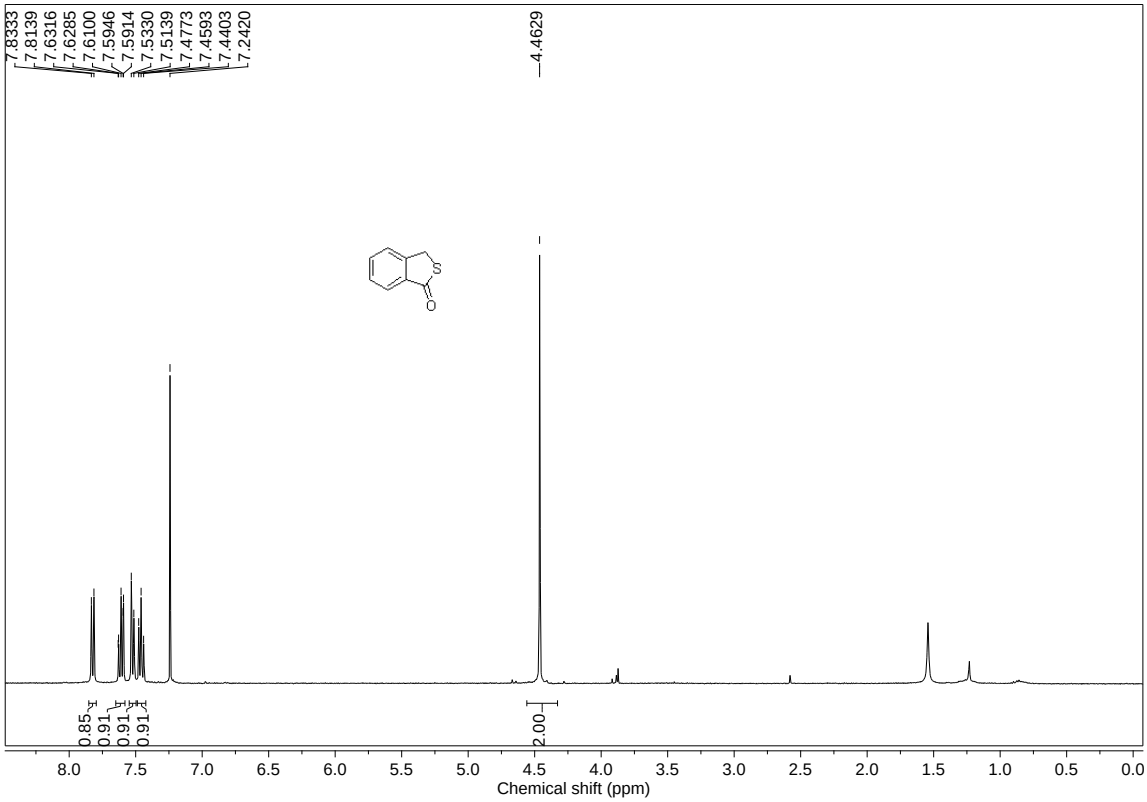

Figure 5.79: ^1H NMR spectra of **54** in $CDCl_3$.

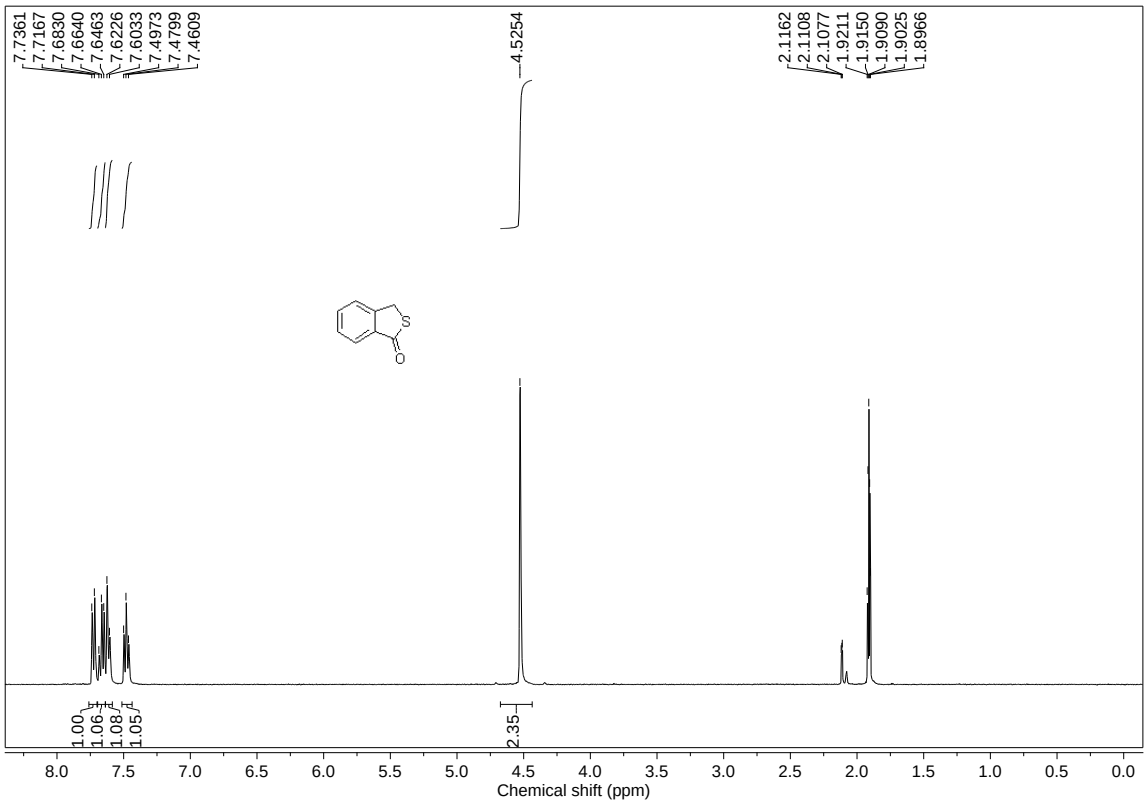

Figure 5.80: ^{1}H NMR spectra of **54** in CD_3CN.

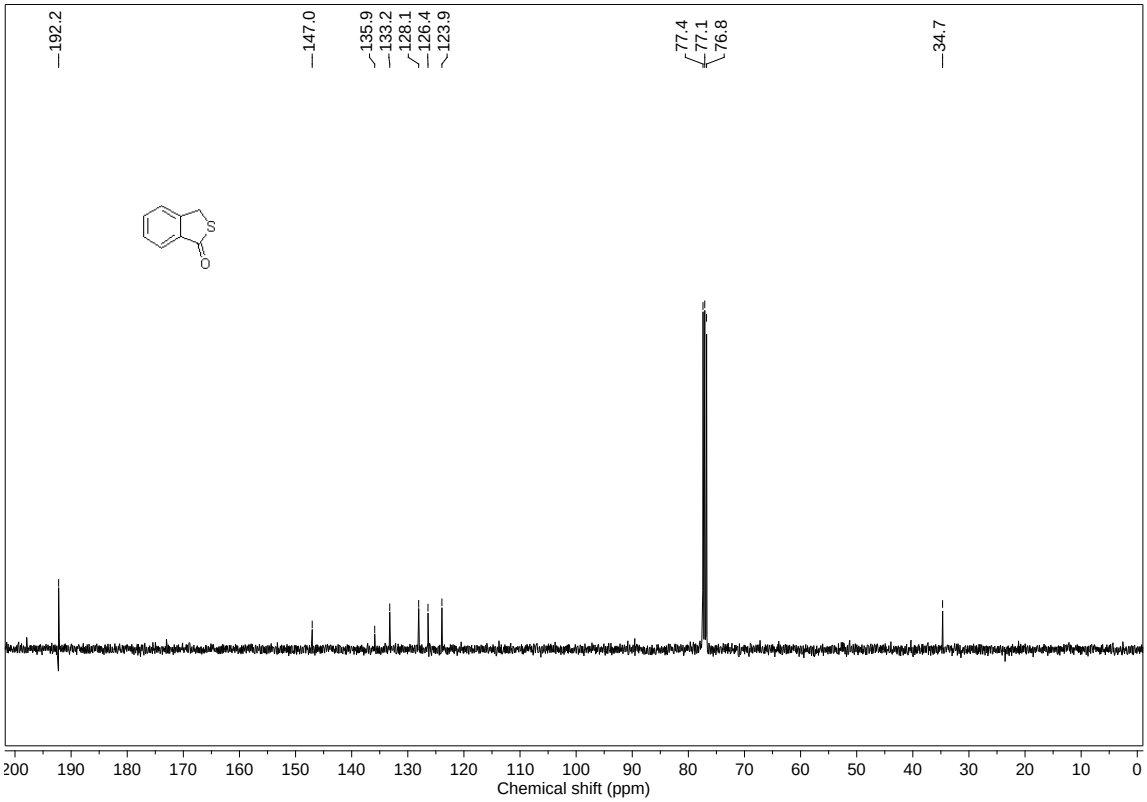

Figure 5.81: ^{13}C NMR spectra of **54** in $CDCl_3$.

5.5 HPLC Purity

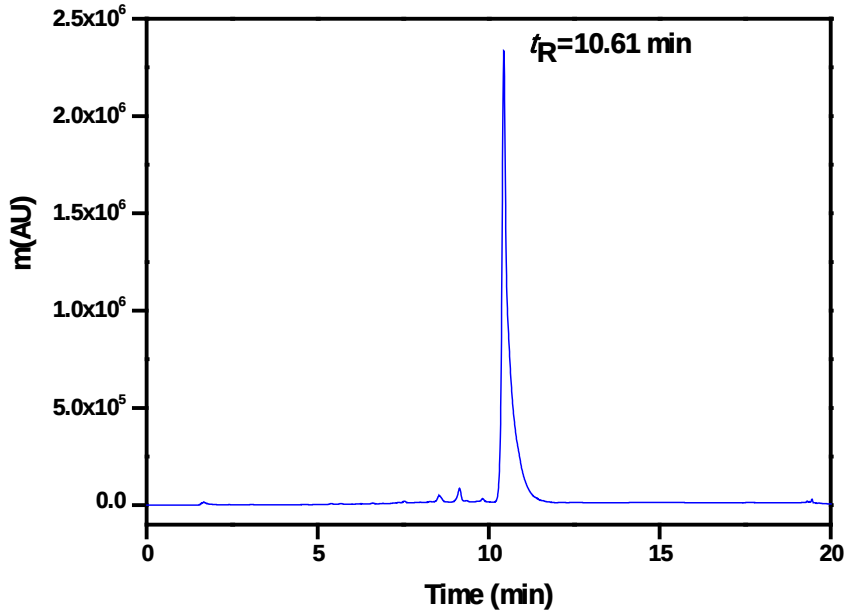

Figure 5.83. HPLC data of probe **81**.

HPLC conditions for assay: Reverse Phase HPLC analysis was performed to confirm that the reaction of probe **81** with Cys results in the Cys mediated cleavage of DNs to form compound **86**. HPLC chromatograms were obtained by treating probe **1** (10 μM) with increasing equivalents of Cys (0.5 eq, 1.0 eq and 2 eq) in mixture of acetonitrile/HEPES (10 mM, containing 1mM CTAB, pH = 7.4). HPLC gradient used for the analysis was as follows:

Column: Phenomenex (4.6 mm × 250 mm)

Flow: 1.0 mL/min

Method: Gradient

50 % Acetonitrile/water	0 min
100 % Acetonitrile	0 to10 min
100 % Acetonitrile	10 to 15 min
50 % Acetonitrile/water	15 to 20 min
50 % Acetonitrile/water	20 to 25 min

Wavelength: 254 nm.

Retention time (t_R) = 10.61 min.

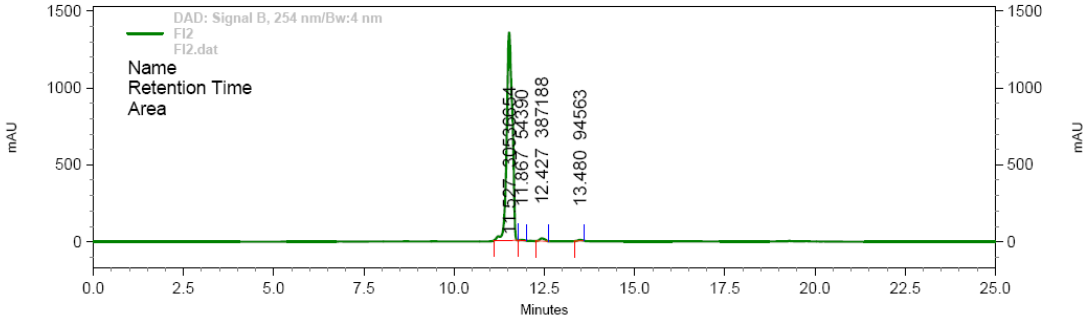

DAD: Signal B,
254 nm/Bw:4 nm
Results

Retention Time	Area	Area %	Height	Height %
11.527	30536654	98.27	2837061	97.97
11.867	54390	0.18	7581	0.26
12.427	387188	1.25	39352	1.36
13.480	94563	0.30	11993	0.41
Totals	31072795	100.00	2895987	100.00

Figure 5.84: HPLC data of probe **102**.

Column: Phenomenex (4.6 mm × 250 mm)

Flow: 1.0 mL/min

Method: Gradient

50 % Acetonitrile/water	0 min
100 % Acetonitrile	0 to10 min
100 % Acetonitrile	10 to 15 min
50 % Acetonitrile/water	15 to 20 min
50 % Acetonitrile/water	20 to 25 min

Wavelength: 250 nm.

Rentention time (t_R) = 11.52 min.

5.6 References

(1) Frisch, M. J.; Trucks, G. W.; Schlegel, H. B.; Scuseria, G. E.; Robb, M. A.; Cheeseman, J. R.; Scalmani, G.; Barone, V.; Mennucci, B.; Petersson, G. A.; Nakatsuji, H.; Caricato, M.; Li, X.; Hratchian, H. P.; Izmaylov, A. F.; Bloino, J.; Zheng, G.; Sonnenberg, J. L.; Hada, M.; Ehara, M.; Toyota, K.; Fukuda, R.; Hasegawa, J.; Ishida, M.; Nakajima, T.; Honda, Y.; Kitao, O.; Nakai, H.; Vreven, T.; Montgomery, J., J. A.; Peralta, J. E.; Ogliaro, F.; Bearpark, M.; Heyd, J. J.; Brothers, E.; Kudin, K. N.; Staroverov, V. N.; Kobayashi, R.; Normand, J.;

Raghavachari, K.; Rendell, A.; Burant, J. C.; Iyengar, S. S.; Tomasi, J.; Cossi, M.; Rega, N.; Millam, J. M.; Klene, M.; Knox, J. E.; Cross, J. B.; Bakken, V.; Adamo, C.; Jaramillo, J.; Gomperts, R.; Stratmann, R. E.; Yazyev, O.; Austin, A. J.; Cammi, R.; Pomelli, C.; Ochterski, J. W.; Martin, R. L.; Morokuma, K.; Zakrzewski, V. G.; Voth, G. A.; Salvador, P.; Dannenberg, J. J.; Dapprich, S.; Daniels, A. D.; Farkas, Ö.; Foresman, J. B.; Ortiz, J. V.; Cioslowski, J.; Fox, D. J. *Gaussian 09, Revision A.1*; Gaussian, Inc., Wallingford CT, **2009**.

(2) (a) Joshi, B. P.; Park, J.; Lee, W. I.; Lee, K.-H. *Talanta* **2009**, *78*, 903(b) Guo, H.; Jing, Y.; Yuan, X.; Ji, S.; Zhao, J.; Li, X.; Kan, Y. *Org. Biomol. Chem.* **2011**, *9*, 3844.

(3) Mugherli, L.; Burchak, O. N.; Chatelain, F.; Balakirev, M. Y. *Bioorg. Med. Chem. Lett.* **2006**, *16*, 4488.

(4) Pellicciari, R.; Camaioni, E.; Costantino, G.; Formentini, L.; Sabbatini, P.; Venturoni, F.; Eren, G.; Bellocchi, D.; Chiarugi, A.; Moroni, F. *ChemMedChem* **2008**, *3*, 914.

(5) (a) Sheldrick, G. M. *Acta Crystallographica Section A* **1990**, *46*, 467(b) G. M. Sheldrick *SHELXL-97, Universität Göttingen (Germany)* **1997**.